PRIFYSGOL ABERYSTWYTH UNIVERSITY

VIB-UGENT CENTER FOR PLANT SYSTEMS BIOLOGY

Self-Incompatibility induced Programmed Cell Death in plants

Identification of new physiological and molecular mechanisms

PhD. 2020

Marina Muñoz Triviño

Abstract

Papaver rhoeas uses a self-incompatibility (SI) system to specifically arrest the growth of "self" pollen, which later undergoes programmed cell death (PCD). The SI response is triggered by the interaction between the male S-determinant (PrpS) localised to the pollen tube plasma-membrane and its cognate female S-determinant (PrsS) secreted by the stigma. It has been demonstrated that the expression of both *Papaver* S determinants is sufficient to make normally self-compatible *Arabidopsis thaliana* plants SI. Moreover, when SI is induced in transgenic *A. thaliana* pollen, remarkably similar responses to those observed in incompatible *P. rhoeas* pollen are obtained. Using SI *Arabidopsis* plants and the tools now available, in this thesis we identify and analyse key molecular mechanisms involved in regulating SI-PCD and new genes possibly implicated in this response.

The SI response was triggered *in vitro* in SI *A. thaliana* pollen grains and pollen tubes for live-cell imaging with confocal microscopy. Five physiological changes were analysed, finding that immediately after SI induction, the cytosolic calcium concentration increases in incompatible pollen tubes followed by the arrest of pollen tube elongation. The vacuolar and mitochondria structure after SI diverges from the observed in compatible tubes. In *A. thaliana* pollen grains late events, related to SI-triggered PCD were also registered: The disruption of the nuclear envelope and an increase of caspase-3-like activity, which are hallmarks for PCD, were detected hours after the SI induction.

On the other hand, advanced genetic approaches available for *Arabidopsis* were applied to identify novel genes possibly involved in SI-PCD. Using reverse genetic approaches, we observed that the mutation of relevant genes described in the *Papaver*SI system is not enough to revert the SI response. Specifically, genes codifying for actin-binding proteins, cathepsin b and the elongation factor 1α.

However, the absence of the candidate gene highlander1 (HLD1) obtained from a forward genetic screening presented here can significantly reduce the SI. This is considered a promising candidate to play a critical role in this response. It was spotted from a self-compatible phenotype screening after an EMS mutagenesis of self-incompatible *Arabidopsis* seeds. We tested its pollen-specific action and an SC seed-set even in the presence of both SI determinants. In addition, a pool of genes was identified to potentially have a role in SI-PCD with the analysis of the SI transcriptome profile.

The results from all those experiments, demonstrates that innovative techniques can be applied to the heterologous *Arabidopsis* SI system for a better understanding of SI-PCD in *Papaver*, allowing further investigations of molecular mechanisms and genes involved in this response.

I dedicate this thesis in loving memory of my grandparents,
who bravely emigrated to Novelda del Guadiana
so that we can have this beautiful life.

Acknowledgements

Firstly, I would like to express my enormous and sincere gratitude to my supervisors Maurice Bosch, Moritz Nowack and Zongcheng Lin. I really feel like I was the luckiest person for being part of your research groups. Thank you very much for believing in my capacities, for the patience you always showed with me and the strong support. I never would have imagined myself involved in such an amazing project. I am also very thankful to Noni Franklin-Tong for her leading advice and for instilling her love for this topic.

Working in Ghent and Aberystwyth allowed me to meet a lot of wonderful people. I want to thank the PCD group at the VIB for the beautiful times we spent during my first year. I found a great plantmate in Marta Cubría, gràc' for always brightening the days with your creativity. The flamingos will always bond me with Roman Hudeck, it was great having him as a lab-flatmate and the times sharing our fears as new PhD students. I would also like to thank our guardian angel Freya De Winter, Ambra De Simone, Anna Daneva, Marie Pfeiffer, Marlies Huysmans, Maria Simaskova, Matthias Van Durme, Rafael Buono and Zhen Gao for being so fantastic colleagues. For always finding the funny side to the hard part of being a scientist, I also thank Jorge Palaci, Laura Dolero and Álvaro Fernández.

The next two years I spent in Aberystwyth, I was also surrounded by excellent people. First of all, I would like to say thanks Ludi Wang for being that supportive and inspiring me with her know-how and her kind advice. Special thanks to Krikika Bhardwaj for always being there in the worst and best moments. I am also very grateful to my excellent colleagues Lucy Abosede, Jose Carli, Agnieszka Gladala-Kostarz, Rebecca Hindhaugh, Rosario Iacono, Marius Rohner and to Emma Timms, Simon Betts and Samantha Gill. The more enriching moments in Aber were also shared with Cristina Monterrubio, Noelia Villarroel, Jorge Martinez, Pilar Martínez, Odín Morón, Álvaro García and Lord Fabio subjects.

Finally, a huge thanks to my family and friends in Spain and Dublin. I am especially grateful to my parents, for all the love and support I constantly receive from them. Thanks for instilling me a creative curiosity. The last massive thank is to Jose, for being my rock. You were an inspirational boyfriend and husband throughout the PhD. Thanks for every number we counted together and your warm encouragement.

Thank you, Dank u, Danke, 谢谢, Gràcies, Děkuju, Grazie, Obrigada, Ďakujem, Благодаря ти, Dziękuję Ci, Diolch, धन्यवाद, Gracias

Table of contents

List of figures and tables

Chapter one. Introduction

Chapter two. Cellular characterization of SI-PCD in Arabidopsis PrpS-expressing pollen

Chapter three. SI-PCD transcriptome profiling

Chapter four. Reverse genetics approaches to analyse candidate genes to be suppressors of SI-PCD

Chapter five. Forward genetics analysis: Mutant screen for SI-PCD suppressors

Abbreviations

$[Ca^{2+}]_{cyt}$: Cytosolic calcium concentration

A: Adenine

ABP: Actin-binding protein

Ac-DEVD-AMC: Caspase-3 activity specific probe

Ac-DEVD-CHO: Caspase-3 activity inhibitor

ADF: Actin-depolymerizing factor

Agrobacterium: *Agrobacterium tumefaciens*

Arabidopsis: *Arabidopsis thaliana*

AtGM: Liquid *Arabidopsis* germination medium

At-SI: Transgenic *Arabidopsis* expressing the *Papaver S*-determinants

BAR: BASTA herbicide resistance gene

BC1: First backcross

BC2: Second backcross

BSA: Bovine serum albumin

C: Cytosine

Ca^{2+}: Calcium ions

CAP: Cyclase-associated protein

carboxy-DCFDA: carboxy-5-(and-6)-carboxy-2',7'-dichlorofluorescein diacetate

CathB: Cathepsin B

CFP: Cyan fluorescent protein

Col: *Arabidopsis* Columbia ecotype

Col-0: Wild type *Arabidopsis* Colombia ecotype

$CR(DEVD)_2$: Caspase-3 activity specific probe

CRISPR: Clustered regularly interspaced short palindromic repeats

CRISPR-TSKO: (CRISPR)-based tissue-specific knockout system

DEVDase: Caspase-3 activity

DGPP: Phospholipid diacylglycerol pyrophosphatase

DNA: Deoxyribonucleic acid

e.g.: *exempli gratia*, for example

EF1α: Eukaryotic translation elongation factor 1α

EMS: Ethyl metanesulfonate

et al.: alia, and others

F-actin: Filamentous actin

FAM-YVAD-FMK: Caspase-1 specific probe

FDR: False discovery rate

FragEL: Fragment end labelling

FRET: Fluorescence resonance energy transfer

G: Guanine

GFP: Green fluorescent protein

gRNA: Guide RNA

GSI: Gametophytic self-incompatibility

HAP: Hours after pollination

HetSI: Heteromorphic sporophytic self-incompatibility

HM: Homozygous

HZ: Heterozygous

IETDase: Caspase-8 activity

LasX: Leica Application Suite X software

Lb: Left border primer

LEHDase: Caspase-9 activity

Ler: *Arabidopsis* Landsberg *erecta* ecotype

Ler-0: Wild type *Arabidopsis* Landsberg *erecta* ecotype

LEVDase: Caspase-4 activity

LogCMP: Log counts per million

LP: Left primer

LSI: Late-acting self-incompatibility

MAPK: mitogen-activated protein kinase

MGU: Male germ unit (vegetative nucleus and sperm cells)

Mito: Expressed in the mitochondria

MS: Murashige and Skoog basal medium

MT-CMXRos: Mitotracker Red CMXRos mitochondrial probe

mTFP: Monomeric teal fluorescent protein

NA: Numerical aperture

NGS: Next-generation sequencing

NLS: Nuclear-localised signal

NO: Nitric oxide

PA: Phosphatidic acid

Papaver: *Papaver rhoeas*

PCD: Programmed cell death

PIP: Phosphatidylinositol monophosphate

PLD: Phospholipase D

PrpS: *Papaver rhoeas* pollen *S*

PrsS: *Papaver rhoeas* stigma *S*

RNA: Ribonucleic acid

RNAseq: Ribonucleic acid sequencing

ROI: region of interest

ROS: Reactive oxygen species

RP: Right primer

SC: Self-compatibility, Self-compatible

SI: Self-incompatibility, Self-incompatible

SNP: Single-Nucleotide Polymorphisms

sPPase: Soluble inorganic pyrophosphatase

SRM: SNP-Ratio Mapping

S-RNase: Glycoprotein with ribonuclease activity

SSI: Homomorphic sporophytic self-incompatibility

T: Thymine

TATDase: Caspase-9 activity

TEM: Transmission electron microscopy

TFP: teal fluorescent protein

TIP: δ-Tonoplast Intrinsic Protein

TUNEL: Technique transferase UTP-nick end labelling

UT: Untreated

UV: Ultraviolet

VAMP711: Vesicle-associated membrane protein 711

VEIDase: Caspase-6 activity

vs.: versus, against

WAVE9R: Tonoplast marker line

Ws: *Arabidopsis* Wassilewskija ecotype

Wt: Wild type

YC3.6: Genetically encoded fluorescent Ca^{2+} sensor

YFP: Yellow fluorescent protein

YVADase: Caspase-1 activity

Unit abbreviations

µm: Micrometre

bp: Base pair

cm: Centimetre

g: Grams

h: Hour

Hz: Hertz

L: Litre

LogFC: Log fold change

M: Molar

min: Minute

mL: Millilitre

mm: Millimetre

nm: Nanometre

ºC: Centigrade

rpm: Revolutions per minute

sec: Second

v/v: Volume per volume

w/v: Weight per volumen

Chapter one. Introduction

1.1. Introduction

Sexual reproduction is a process for the multiplication of living beings that implies the fusion of two gametes for the development of a new individual. In contrast to asexual reproduction, it increases genetic variability and helps to mitigate the effect of harmful mutations (Curtis, 1900; Crow, 1994). In sexual reproduction, there are two types of breeding systems: inbreeding and outbreeding. Outbreeding happens when both gametes are generated in two genetically different individuals, commonly differentiated as a male and a female individual. On the other hand, inbreeding or selfing occurs when the gametes are derived from a single organism. In the *Plantae* kingdom, both types of systems are present (Simpson, 2010). However, some plants that produce female and male gametes cannot fertilise themselves, which is called self-incompatibility (SI). Self-incompatibility is a genetically controlled system present in flowering plants. The families containing SI species present different molecular basis to inhibit selfing (Igic *et al.*, 2008). In all cases, it involves the recognition and rejection of self or genetically identical pollen to prevent self-fertilization and enhance outbreeding and genetic diversity (Franklin-Tong, 2013).

A better understanding of SI-PCD processes in *Papaver rhoeas* can be used to develop new hybrid breeding methods. Hybrid breeding is applied in the majority of the crops nowadays even if causal factors and genetic mechanisms of heterosis are still not fully understood (Govindaraju, 2019). It was in 1716 when the first plant hybrid was described and it was stated that from certain crosses, between unrelated individual plants and animals, greater productivity, vigour, disease resistance, viability and fertility was obtained (reviewed in Clark, 1961). In modern crops, the production of an F1 hybrid variety requires several putative parental lines from heterozygous sources obtained by the cross of homozygous lines obtained by consecutive generations of inbreeding from a genetically heterogeneous gene pool. Due to its complexity and the time-consuming procedures required, new methods are constantly being sought to generate F1 hybrids more efficiently and a new protocols based on the *Papaver* SI system could facilitate this process.

1.2. Consequences of becoming self-compatible

Evolution has led a large number of plant species to take similar drifts. Although it is well known that SI mechanisms have a diverse origin according to different families, many of them coincide in the loss of this capacity, being transformed over time into self-compatible (SC) plants which means they can fertilize themselves (Reviewed in Igic *et al.*, 2008). The intensity in the pollen tube selection was observed to be related to the pollen received in the stigma. Plants that tend to receive a large pollen load are more severe in their selection to guarantee successful fertilizations. However, plants that need foreign pollen, because they are self-incompatible, are dependent on their pollinators (either biotic or abiotic) to form seeds. Those may suffer a dramatic decrease in genetic variability if there is a low variety of plants providing pollen nearby or the quantity of pollen arriving at the stigma is very low due to inefficient pollinations (Levin, 1970). In order to guarantee a high success in fecundation and speed the colonization of spaces, the self-incompatible system is atrophied in some species, becoming self-compatible plants. The SC capacity provides the benefit of virtually guaranteed foundations, but the least favourable consequence is the decrease in gene flow in the population, which may result in the formation of new species allopatrically (Baker, 1953). To clarify this drift, the challenge of reconstructing the ancestral and estimate the transition rates between the SI and SC states is still open. So far, the phylogenetic record allows us to deduce a frequent, complete and irreversible loss of SI. It has been shown that SC plants harbor multiple mutations, which results in a loss of function, difficulting the reversion to SI (Igic *et al.*, 2008).

1.3. Compatible pollen-stigma interaction in *A. thaliana*

Arabidopsis thaliana (*Arabidopsis*) is a self-pollinated plant species (Bergelson *et al.*, 1998). To obtain successful fertilization, compatible pollen-stigma interaction is required, followed by a pollen tube formation to fertilise the ovule located in the embryo sac (Simpson, 2010). The dehiscence of anthers releases mature dry pollen grains that need to reach the female reproductive organ (Figure 1.1). The stigma is the upper part of the pistil that presents papillae cells on its surface. After pollen has landed on papilla cells, they undergo a hydration process regulated by factors expressed on the stigmatic surfaces (Ma *et al.*, 2012). After hydration, the pollen grain forms a foot structure, made

with pollen coat material, that keeps it attached to the papilla surface (Kandasamy *et al.*, 1994). After the foot formation, the pollen grain germinates and a pollen tube grows down the papilla's length between the outer and inner layers of the papilla cell wall. In around 45 to 50 minutes after pollination, the pollen tube reaches the intercellular matrix between the papillar cells and the subepidermal cells of the stigma. It is crucial that compatible pollen continues growing forward in the transmitting tissue of the style and ovary to reach the embryo sac and effect fertilization (Kandasamy *et al.*, 1994). The growth orientation is guided by attractant proteins secreted from the synergid cells (Punwani *et al.*, 2007). In the pollen tube, together with the vegetative nucleus, which is the nucleus of the pollen tube, there are two sperm cells encharged to perform double fertilization (Weterings and Russell, 2004).

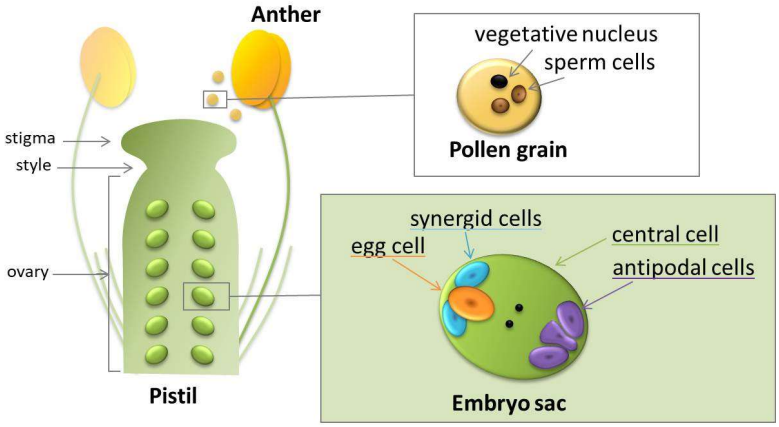

Figure 1.1. Scheme of the female and male sexual structures in *Arabidopsis*. The female structure (Pistil) is divided into three main regions: stigma, style and ovary. The ovary contains the embryo sacs, formed by seven cells and containing a total of eight nuclei. The pollen grains develop in the male organ (anther) and are released after anther dehiscence. In the lumen of *Arabidopsis* pollen grains, there is a vegetative nucleus and two sperm cells, encharged of double fertilization.

1.4. Self-incompatibility systems to prevent self-fertilization

Plants developed strategies to promote genetic diversity and avoid self-fertilization. According to morphological differences, flowering plants are classically divided into heteromorphic, when one plant species presents polymorphism in its flowers, and homomorphic, when the flowers are indistinguishable (reviewed in Charlesworth, 2010). The heteromorphic systems based their success on the differences in location, morphology or maturation time of the reproductive structures. On the other hand, in homomorphic species, the self-incompatible system is based on the pollen rejection after pollen-stigma interaction. This genetically encoded system discriminates

the self-pollen avoiding its pollen tube development (reviewed in Stone and Goring, 2001). The molecules that mediate SI are the *S*-locus gene products which can vary between families (Thompson and Kirch, 1992). The specificity of the SI response is determined by the haplotypes of the *S*-locus, which contains at least two separate multiallelic genes. These genes are commonly defined as the female and the male determinant genes, according to the location of their expression the tissue or cell in which they are expressed (reviewed in Takayama and Isogai, 2005).

Recently, the terminology for angiosperm reproductive systems defined the different self-incompatibility responses in four main types: homomorphic sporophytic (SSI), heteromorphic sporophytic (HetSI), the late-acting (LSI) and gametophytic self-incompatibility (GSI) (Cardoso *et al.*, 2018). The SSI and HetSI have in common the prompt rejection as the reactions occur in the stigma (Figure 1.2). In those two cases, as the *S* gene is activated in the sporophyte, before meiosis, the proteins derived from *S* alleles reside in the pollen exine. If the dominant allele is expressed in the parental plant, the SI reaction is triggered immediately after the pollination regardless of which allele is in the genome of the pollen grain itself (Figure 1.2). SSI and HetSI mainly differ in the type of flower as the plants presenting SSI have only one type of flower while the ones presenting HetSI have flowers with different structures (Gibbs, 2014; Cardoso *et al.*, 2018). The third type of SI corresponds to LSI however, according to Cardoso *et al.* 2018, still little is known about it. This type of self-incompatible reaction is considered post-zygotic as it is effective after the fecundation takes place but before the embryogenesis initiates (Bittencourt Júnior, 2017).

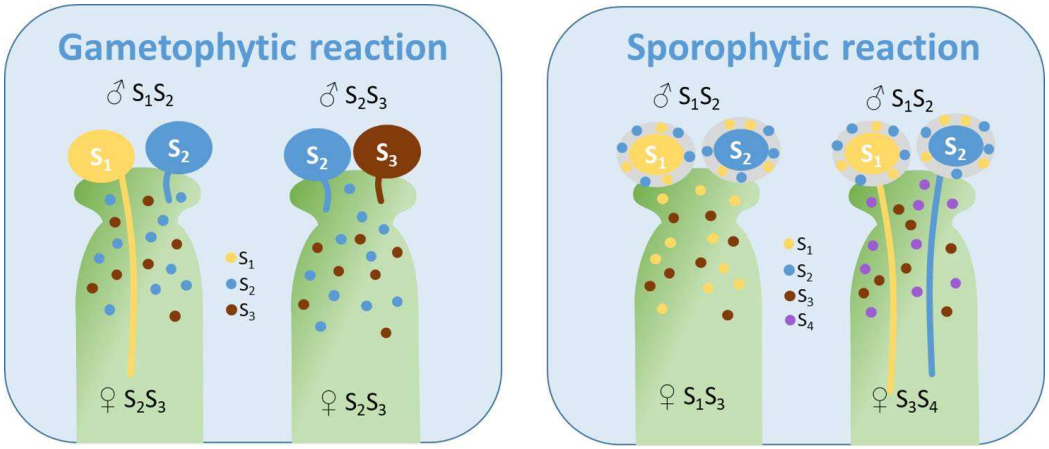

Figure 1.2. Scheme of gametophytic and sporophytic SI reactions. Since the pistils (represented in green) are diploid organs, it can express two different alleles, as it does in the scheme where a heterozygous plant is represented. In gametophytic reactions, the haploid pollen grain genotype is encharged of triggering the SI reaction when the S-haplotype is cognate with one of the expressed S-haplotypes in the pistil. The sporophytic reaction depends on the diploid genotype of the tissue from the anthers that get adhered to the released pollen grains. Due to this, the pollen grains in sporophytic SI are blocked before they start developing the pollen tube when there is a cognate interaction.

To date, 105 flowering plant families have been reported containing SI species whose systems evolved independently in some cases presenting different molecular basis to inhibit selfing (Figure 1.3) (Igic *et al.*, 2008). Widely divergent families (*i.e.*, Rosaceae, Solanaceae, Scrophulariaceae, Rubiaceae) present one gene that encodes pistil-expressed glycoproteins with ribonuclease activity (S-RNases) that cause rejection of pollen when its haploid *S*-haplotype matches either of the two S-haplotypes in the diploid pistil. The different taxa having S-RNAse based GSI use similar genes for the pollen rejection but the mechanisms show differences. In all those cases, the incompatible pollen tubes can initially grow and later be arrested when they reach about one-third of the way through the style (Muñoz-Sanz *et al.*, 2020). Differently from the RNAse system, the SI response in Papaveraceae plants causes rapid pollen tube inhibition and cell death (Franklin-Tong and Franklin, 2003).

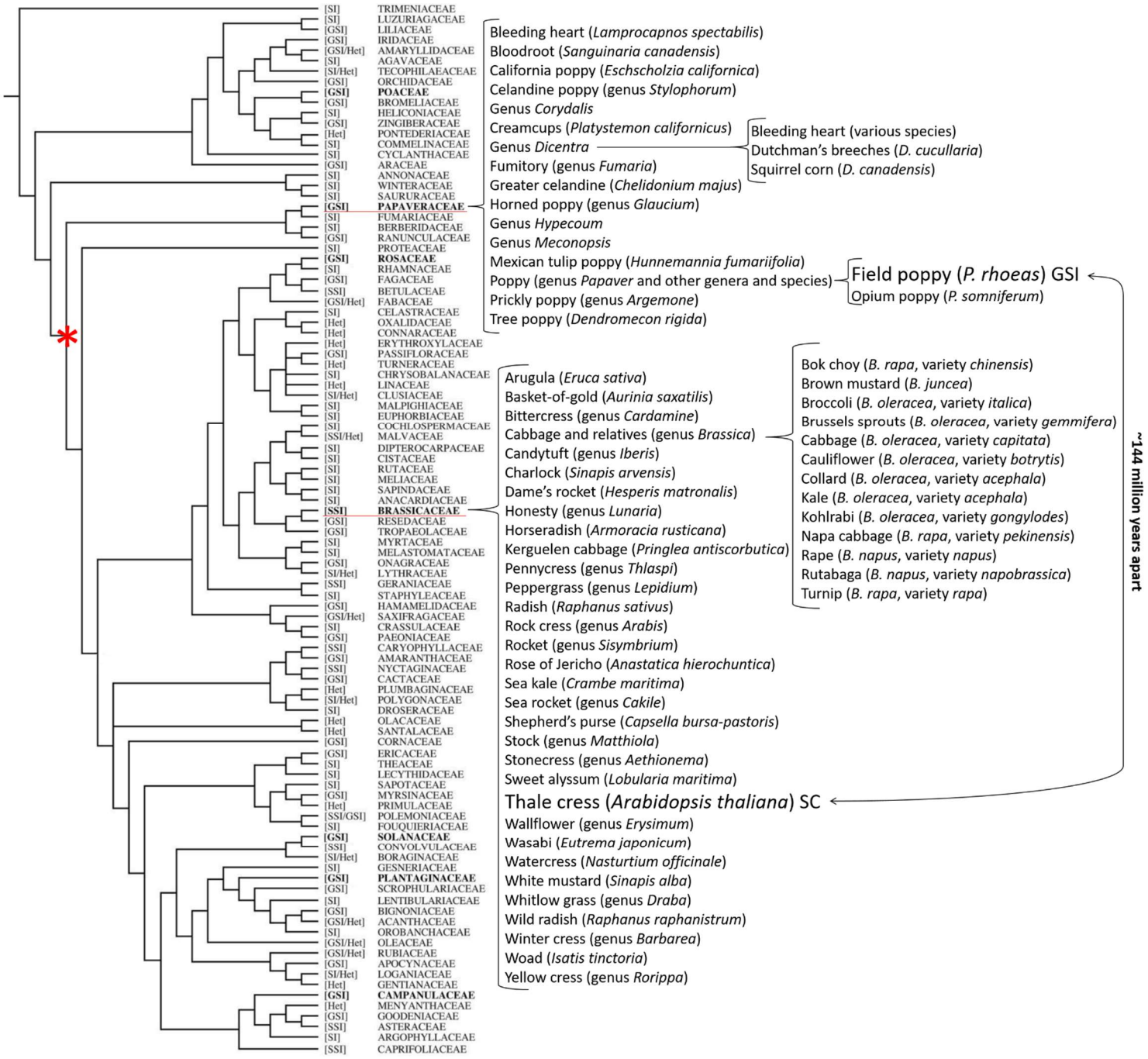

Figure 1.3. Phylogenetic hypothesis for the relationships among families containing SI species. The families with SI systems whose genetic and molecular basis are at least partially characterised are in bold. [GSI] indicates homomorphic gametophytic SI, [SSI] homomorphic sporophytic SI, [Het] heteromorphic SI, [SI] that the SI mode of action is uncharacterised and SC self-compatible. The families including *Papaver rhoeas* and *Arabidopsis thaliana* are underlined in red, Paveraceae and Brassicaceae respectively. The asterisk indicates their ancestral node. (Image adapted from: Igic *et al.*, 2008; Britannica, 2017; Petruzzello, 2020).

1.5. SI-PCD *Papaver* system

P. rhoeas presents a gametophytic self-incompatibility triggered by the proteins *Papaver rhoeas* pollen *S* (PrpS) and *Papaver rhoeas* stigma *S* (PrsS), which are the male and female determinants respectively.

PrpS is a ~20 kDa protein that is predicted to be a transmembrane protein with three to five putative membrane-spanning domains. The knockdown of PrpS by antisense oligonucleotides resulted in the alleviation of pollen tube growth inhibition in an S-specific manner (Wheeler *et al.*, 2009). It indicates that PrpS has a role as a male determinant in *Papaver* SI.

On the other hand, the female determinant PrsS is a ~14 kDa protein secreted by the stigma papilla cells. PrsS binds to the predicted extracellular loop of PrpS in a ligand-receptor type interaction (Wheeler *et al.*, 2009). Sequence alignment of PrsS with the other two S-genes families in S-RNase-based SI and Brassicaceae SI systems showed the uniqueness of PrsS (Foote *et al.*, 1994). It confirmed that the *Papaver* SI system differs from the other SI systems. In addition, to confirm that PrsS is a biologically active and functional S determinant, the nucleotide sequence encoding the predicted mature polypeptide was cloned and expressed in *E. coli*. The recombinant PrsS was tested *in vitro* and it confirmed to be sufficient to inhibit the pollen tube growth in an S-specific manner (Walker *et al.*, 1996; Kurup *et al.*, 1998), triggering a chain of reactions resulting in inhibition of the pollen tube growth and programmed cell death (PCD) (Figure 1.4) (Thomas and Franklin-Tong, 2004).

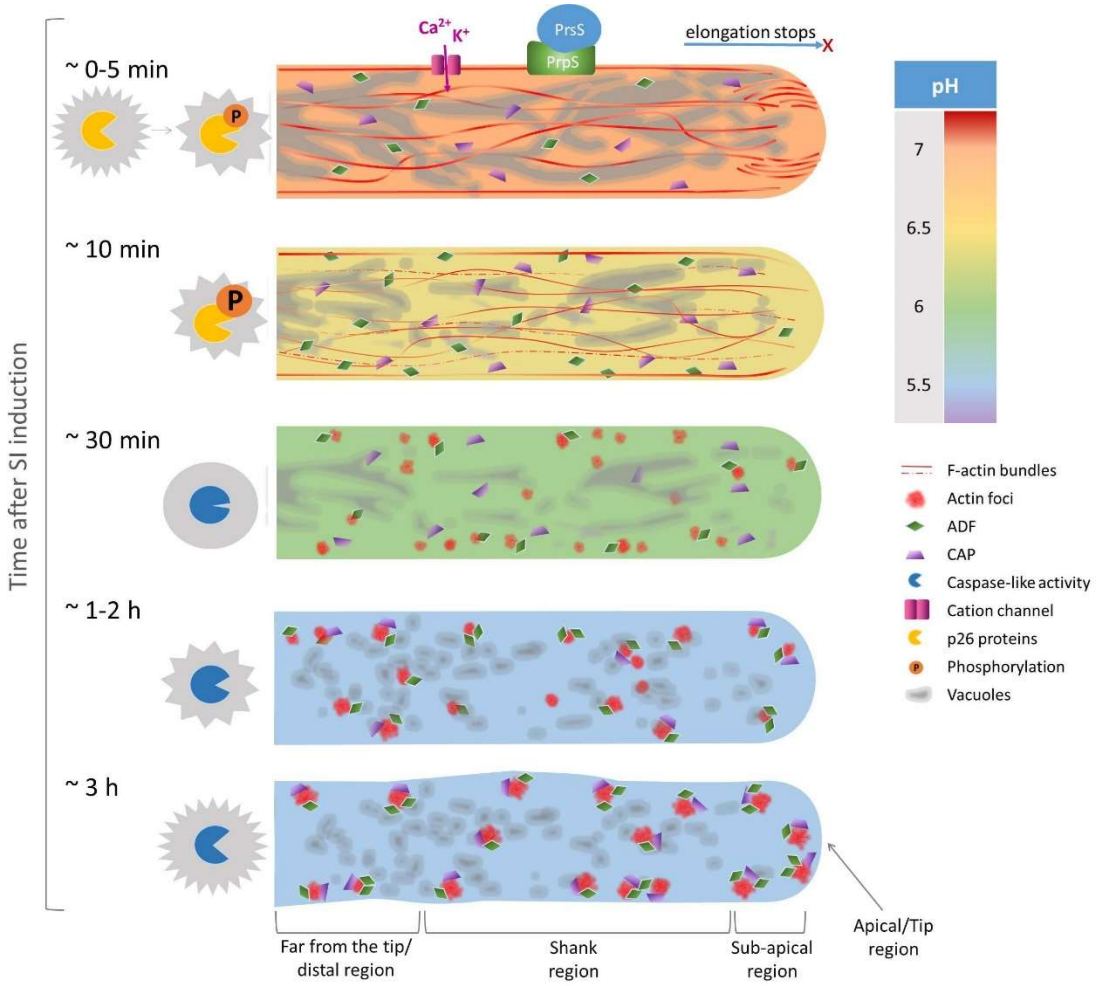

Figure 1.4. Scheme of some of the changes observed in *Papaver* pollen during the SI response. The pH drop, a calcium and potassium influx, the phosphorylation of p26 and the stop of the elongation are the earliest events represented. From 10 min after SI induction the F-actin bundles are observed disrupted and subsequently it form actin foci growing in size in time. ADF and CAP are actin-binding proteins that present colocalization with the mature actin foci. Two late events are represented: the activation of caspase-like activity and the disruption of the reticular structure that the vacuoles present initially.

The reactions triggered by PrpS-PrsS interaction has been studied for decades with the technology available for *Papaver* (Figure 1.5). One of the earliest events in incompatible pollen tubes is the alterations in channel activity that stimulate the ion conductance (Juyou Wu *et al.*, 2011) and the activation of a calcium-dependant signalling network (Franklin-Tong *et al.*, 1996; Wilkins *et al.*, 2015). The sudden SI-induced increase in $[Ca^{2+}]_{cyt}$ triggers the phosphorylation and inactivation of the soluble inorganic pyrophosphatase p26 (De Graaf *et al.*, 2006) and a dramatic alteration in the filamentous actin (F-actin) cytoskeleton (Geitmann *et al.*, 2000a). The main change in the cytoskeleton is the fast depolymerization of F-actin and its subsequent reorganization to form stable "punctate foci" that increase in size over time (Geitmann

et al., 2000; Snowman *et al.*, 2002; Poulter *et al.*, 2010). SI-induced changes in $[Ca^{2+}]_{cyt}$ are upstream of cytosolic acidification and the artificial acidification of *Papaver* pollen tubes *in vitro* with propionic acid also triggers the formation of F-actin foci (Wilkins *et al.*, 2015). Those changes in the cytoskeleton structure seem to be directly related to the network leading to PCD (Thomas *et al.*, 2006). Furthermore, the involvement of reactive oxygen species (ROS) in *Papaver* SI-PCD has also been demonstrated, peaking ~3 to 6 min in the SI response and returning to basal levels by 10 to 15 min (Wilkins *et al.*, 2011). After the ROS starts decreasing, there is also a decrease in the phospholipid phosphatidylinositol monophosphate (PIP). Even if the responsible of this decrease and the possible implications it may have in the SI response are still unknown, it is considered that is implicated in the regulation of the pollen tube growth (Franklin-Tong *et al.*, 1996). Another early event that occurs ~10 min after SI induction is the activation of p56, a mitogen-activated protein kinase (MAPK). It is linked to late events like the increase in DEVDase/caspase-3-like activity and DNA fragmentation (Li *et al.*, 2007). At that time point, a rapid decrease of the cytosolic pH is observed, which is enough to trigger the generation of DEVDase/caspase-3-like activity (Bosch and Franklin-Tong, 2007; Wilkins *et al.*, 2015). The pH decrease was thought to be related to the vacuole breakdown. However, there is no evidence about the vacuoles participating as a source of protons responsible for this acidification. In addition, also ~10 min after SI induction, the mitochondrial morphology present alterations and there are cytochrome *c* leakage (Thomas and Franklin-Tong, 2004; Bosch *et al.*, 2010). Later in time, ~15 min after SI induction, it has been observed an increase in the signalling messenger nitric oxide (NO) which has like pH a link with the formation of punctate actin foci that colocalise with actin-binding proteins and the increase of DEVDase/caspase-3-like activity (Poulter *et al.*, 2010; Wilkins *et al.*, 2011). It was observed that ~20 to 30 min after SI induction, there are significant increases in the phospholipid diacylglycerol pyrophosphatase (DGPP) which is suspected to act as a signalling molecule during plant stress, and an increases in phospholipase D (PLD) activities probably linked to phosphatidic acid (PA) production (Wilkins *et al.*, unpublished). From ~2 h after induction, there is an increase in the DEVDase/caspase-3-like activity that reach its maximum 5 h after SI (Bosch and Franklin-Tong, 2007). Late in the response there is also DNA fragmentation that starts

from 4 h after SI induction and continued for 10 hours fragmentation has been documented after 4 hrs of SI-induction, and continued to increase for 10 hrs (Jordan *et al.*, 2000; Bosch and Franklin-Tong, 2008).

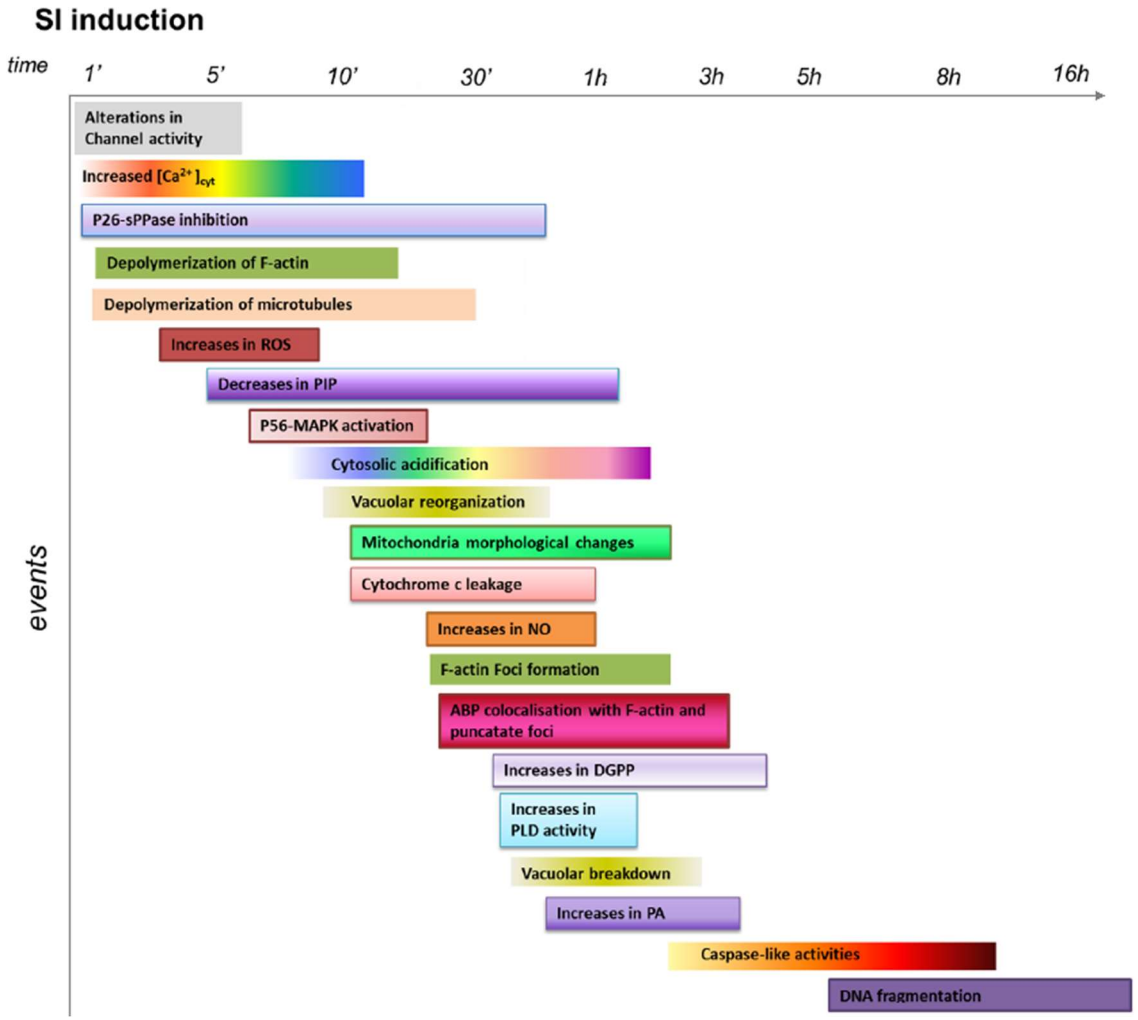

Figure 1.5. SI induced events characterised in *Papaver*. Timeline representing the time points in which the different events were observed and its length in time. Details are described in the text. The colours are only used to separate different events. The abbreviations indicate: concentration of cytosolic calcium ($[Ca^{2+}]_{cyt}$), means soluble inorganic pyrophosphatase (sPPase), reactive oxygen species (ROS), phosphatidylinositol monophosphate(PIP), mitogen-activated protein kinase (MAPK), Nitric oxide (NO), diacylglycerol pyrophosphatase (DGPP), phospholipase D (PLD) and phosphatidic acid (PA). (Source: Wilkins, 2013).

1.6. *Arabidopsis thaliana* expressing *Arabidopsis lyrata S*-locus become self-incompatible

The self-incompatible system present in *Brassicaceae* species is sporophytic, which makes the pollen grain be recognized and rejected during the interaction of the pollen grain with the epidermal cell of the stigma surface. When cognate, this interaction rapidly blocks early events like hydration and metabolic activation leading to the pollen tube growth inhibition (Heslop-Harrison, 1975). In this system, an *S* locus receptor protein kinase (SRK) gene that is expressed in the stigma epidermis resulting in a receptor protein SRK located as an integral component in the plasma membrane (reviewed in Kachroo *et al.*, 2002). The SI response is triggered when the SRK in the stigma interacts with the small peptide of 50 to 59 amino acids that participates as a male determinant in Brassica: S locus Cys-rich protein (SCR). SCR is expressed in the anther and is necessary and sufficient to activate the SI response (Schopfer *et al.*, 1999). There is a third gene, *S*-locus glycoprotein (SLG), found in most *Brassica* S haplotypes that is encharged to encode a protein that enhances the activity and stability of SRK (Takasaki *et al.*, 2000). As sowed in figure 1.3, *Arabidopsis thaliana* belongs to the Brassicaceae family, but it is a self-compatible species. However, the closely related species *Arabidopsis lyrata*, which diverged from *A. thaliana* only ~5 million years ago, is self-incompatible (Koch *et al.*, 2000). Apart from the proximity in the evolution tree, another characteristic makes the *A. lyrata* SI system especially interesting to be the one selected when attempting to transfer an SI system to *A. thaliana*. That is the absence of the SLG gene, which simplifies the system to only two determinants: SRK and SCR (Kusaba *et al.*, 2001). Both determinants were transferred to *A. thaliana,* obtaining a transformed Columbia ecotype presenting a robust SI response rejecting self-pollen. It demonstrates that the expression of SRK and SCR genes is enough to reverse the self-compatibility of *A. thaliana* to the ancestral state of SI (Nasrallah *et al.*, 2002) and opened a new possibility of studying the SI systems by using the model plant *A. thaliana*.

1.7. *Papaver* SI system engineered in *Arabidopsis*

Arabidopsis is a self-compatible *Brassicaceae* used as a model plant with a high potential for molecular biology research since it was the first plant whose genome was sequenced. In addition, it has a small size and a rapid life cycle that facilitates its genetic transformation (Liepman *et al.*, 2010; Sawada *et al.*, 2014). In the *Arabidopsis* family, there is a self-incompatible model species which is *Arabidopsis lyrata*. The *Brassicaceae* SI determinants present in *A. lyrata*, SRK and SCR, were successfully transferred to *Arabidopsis* resulting in self-incompatible *Arabidopsis* plants (Boggs *et al.*, 2009). A similar process was attempted for the transfer of the *Papaver* SI determinants to *Arabidopsis*. Wild type *Arabidopsis* Colombia ecotype (Col-0) was transformed to express PrpS with a green fluorescent protein (GFP) as a reporter tag. It generated the called At-PrpS lines, whose pollen tube growth was shown to be inhibited when treated with cognate PrsS *in vitro* (De Graaf *et al.*, 2012). These results supported the idea of successfully obtaining *Arabidopsis* plants expressing both the *Papaver* SI determinants, PrpS and PrsS. To achieve this, again Col-0 plants were used to get the female determinant PrsS transferred generating At-PrsS plants. The stigma of At-PrsS plants were pollinated with At-PrpS pollen resulting in no seeds which indicated self-incompatibility. When pollinated pistils were stained with aniline blue at different time points, the same phenotype as observed in *Papaver* was present. The At-PrpS pollen tubes stopped growing when reaching the stigma suggesting it to be a consequence of the PrsS-PrpS interaction. The transgenic *Arabidopsis* lines expressing the *Papaver* determinants were called “At-SI” (Lin *et al.*, 2015). Even if both species have an evolutionary distance greater than 140 million years and their families independently evolved different SI systems (Bell *et al.*, 2010), the results observed in At-SI indicates that PrsS-PrpS interaction in *Arabidopsis* is able to recruit elements that are shared between *Papaver* and *Arabidopsis* pollen tubes. Initial observations showed that in both species the interaction of the SI determinants results in the arrest of pollen tube growth and induction of PCD (Lin *et al.*, 2015; Wang *et al.*, 2020).

1.8. Aims of this project

The overall objective of the research presented in this thesis is to exploit the availability of the heterologous *Arabidopsis* SI system taking advantage of the variety of powerful genetic tools and technologies to advance our knowledge of *Papaver* SI-PCD. To address this, three different research strategies have been used (Figure 1.6). First, we characterised the cellular events induced by the SI response in the poppydopsis system using cell biological approaches (Figure 1.6A). Secondly, we followed a transcriptome profiling approach to identify new molecular components involved in the SI response (Figure 1.6B). Thirdly, we used forward and reverse genetic approaches to identify genes involved in the SI-PCD response (Figure 1.6C).

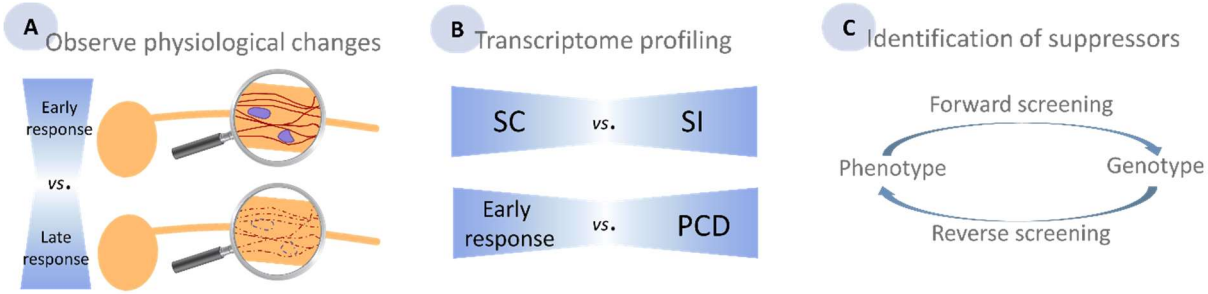

Figure 1.6. Scheme of the experiments carried out with poppydopsis. A) Cellular characterization of the self-incompatible (SI) response observing the physiological changes in the pollen tubes or pollen grains during the SI response. B) The comparison of the self-compatible (SC) and SI transcriptome to identify the differences between the transcriptome profile in early stages of SI and late stages when programmed cell death (PCD) starts. C) Identification of genes involved in SI-PCD unknown to date using forward and reverse genetic approaches.

For the cellular characterization of SI-PCD in *Arabidopsis* PrpS-expressing pollen (Chapter one), we will be using probes and genetically encoded markers. The *in vitro* pollen germination assays combined with confocal microscopy let us obtain detailed information about events of interest already identified in *Papaver* during the SI response. The *in vitro* germination of transgenic SI *Arabidopsis* pollen will enable us to obtain life cell images before and during the SI response, to record changes in cellular events or specific organelles. From this data, we can compare SI-induced events in the heterologous *Arabidopsis* SI system with the endogenous *Papaver* system and obtain more detailed spatio-temporal information about certain SI-induced events.

Transcriptome profiling will be used to identify new candidate genes involved in the SI-PCD response (Chapter two). The SI-PCD response transcript will be profiled and compared with compatible pollinations. In addition, the comparison between the transcriptome at the early stage after the SI induction and the late one, will provide us with information about genes possibly related to PCD.

In addition to transcriptome profiling, more direct genetic approaches will be carried out to identify genes involved in SI-PCD. Starting with reverse genetics analysis of candidate genes potentially involved in the SI-PCD response (Chapter three), the aim was to target genes potentially involved in the SI response and test the fertility and seed-set of their corresponding mutants. On the other hand, a forward genetic approach will be followed to identify genes involved in SI-PCD response (Chapter four). This approach will comprise a mutant screen to find genes whose mutation suppresses the sterile SI-PCD phenotype.

The work presented here expands our understanding of the SI-induced programmed cell death in plants, with the characterization of the cellular and subcellular processes occurring during the SI-PCD response and the new identification of genes involved.

Chapter two.

Cellular characterization of SI-PCD in *Arabidopsis* PrpS-expressing pollen

2.1. Introduction

To understand the processes taking place during the SI response in the *Papaver* system, the approach of using genetically encoded probes, stably expressed in the pollen, was not available in *Papaver rhoeas* (*Papaver*). *Papaver* plants cannot yet be transformed, and the only means of expressing genetically encoded probes in *Papaver* pollen is by transient expression through the particle bombardment of the pollen (Chen *et al.*, 2002). Transgenic *Arabidopsis* lines expressing genetically encoded probes were used to elucidate the details of five different cellular events related to SI-PCD: changes in cytosolic calcium concentration ($[Ca^{2+}]_{cyt}$), vacuolar morphology, nuclear disintegration, mitochondrial morphology and caspase-like activities.

Life cell imaging allows us to track cell biological changes of organelles in the pollen tube as a consequence of the interaction of the SI determinants in real-time. We focused on the organization of the vacuole and the mitochondria

Besides these early events, we also examined SI-induced changes in the nuclear integrity and increases of caspase-3-activity in *Arabidopsis* pollen grains expressing PrpS.

Furthermore, we looked for information related to the caspase-3-like activity.

The results obtained from the *Arabidopsis* SI response in this thesis provide information about the events triggered by the PrpS-PrsS interaction and the role these events may have in this SI pathway in the endogenous *Papaver* system. Therefore, results will always be compared with those already published for *Papaver* SI. Considering *Papaver* as the reference, one of the questions we want to answer is in how far the engineered SI-response in *Arabidopsis* recapitulates the native system in *Papaver*. Beyond that, the possibility of using a bioassay in which the SI response can be triggered *in vitro* in growing *Arabidopsis* pollen tubes (similar to the bioassay used for *Papaver*) combined with live-cell confocal imaging allows us to obtain new details about the SI-PCD response.

2.1.1. Cytosolic calcium increase

Two types of tendencies related to Ca^{2+} have been observed in compatible *Papaver* pollen tubes growing *in vitro*: an oscillating influx directed at the tip and significant influxes at the shank region (Franklin-Tong *et al.*, 2002). Changes in $[Ca^{2+}]_{cyt}$ have also been tested in *Papaver* pollen tubes following the triggering of SI *in vitro* (Franklin-Tong *et al.*, 1993). The results are similar to the calcium influx present as an early step of the pathogen defence response signal cascade in plant innate immunity (Ma and Berkowitz, 2007). With the microinjection of fura-2 dextran, which is a calcium indicator dye, the presence of the tip-focused $[Ca^{2+}]_{cyt}$ gradient was altered when cognate PrsS was added to PrpS expressing pollen, and the gradient in the sub-apical region also suffered alterations. A dramatic $[Ca^{2+}]_{cyt}$ reduction at the tip was observed 70 seconds after SI induction and it was irreversibly lost from ~1 min after SI (Franklin-Tong *et al.*, 1997). In the sub-apical region, there was a large increase in $[Ca^{2+}]_{cyt}$ and it moved further back in the tube at ~30 sec after SI. These findings support the idea of calcium to be playing a role as a second messenger in *Papaver* SI (Franklin-Tong *et al.*, 1993). The Ca^{2+} transient was established to last ~6-10 minutes (Franklin-Tong *et al.*, 1993).

In addition, considering that *in vivo* the SI reaction occurs in the pollen grain shortly after germination, not in mature pollen tubes, it was imitated using *Papaver* pollen protoplasts. When SI is triggered *in vitro*, this stimulates the activation of voltage-sensitive channels in the plasma membrane that conduct Ca^{2+} and K^{+}. However, this response is reversible since washing out PrsS after the induction reverses the inward Ca^{2+} current back to prestimulus levels (Juyou Wu *et al.*, 2011).

It has been decades since the discovery that calcium ions (Ca^{2+}) have signalling functions in both prokaryotes and eukaryotes. Ca^{2+} is involved in a variety of cellular and physiological processes, including development, as well as biotic and abiotic stress responses (Hepler, 2005; Saito and Uozumi, 2020). The $[Ca^{2+}]_{cyt}$ also plays an essential role in pollen germination and pollen tube growth (Taylor and Hepler, 1997; Iwano *et al.*, 2009), presenting a tip-focused gradient (Hepler *et al.*, 2001), which is also common in other tip growing cells such as root hairs (Wymer *et al.*, 1997). In both pollen tubes

and root hairs, it was found that an elevated $[Ca^{2+}]_{cyt}$ at the tip is essential for growth in normal conditions.

In *Papaver* pollen tubes, microinjections of the free Ca^{2+} dye Calcium Green-1 were used to confirm *in vitro* the increase of $[Ca^{2+}]_{cyt}$ after incompatible PrsS protein treatment, suggesting a role of $[Ca^{2+}]_{cyt}$ as a second messenger in SI. It was shown how the addition of PrsS to pollen tubes expressing the cognate PrpS caused an increase in $[Ca^{2+}]_{cyt}$ and stopped the growth. Furthermore, pollen tube growth was also inhibited when intracellular calcium levels were artificially elevated with caged Ca^{2+} (Franklin-Tong *et al.*, 1993). Later studies revealed localised $[Ca^{2+}]_{cyt}$ waves related to the SI response. The Ca^{2+} signal after PrpS-PrsS interaction seems to initiate in the shank and travel to the subapical region, decreasing the high Ca^{2+} gradient ordinarily present in the apex while the tube is growing (Franklin-Tong *et al.*, 1997).

More has been discovered about the mode of action of $[Ca^{2+}]_{cyt}$ in *Papaver* during the SI-PCD response, which leads to defining it as a possible link with pH changes in the cytosol (Wilkins *et al.*, 2015). Besides the increase in the $[Ca^{2+}]_{cyt}$, one of the fastest events during SI is dramatic cytosolic acidification in *Papaver* and *Arabidopsis* incompatible pollen tubes (Wilkins *et al.*, 2015; Wang *et al.*, 2020). A recent discovery has shown that an increase in $[Ca^{2+}]_{cyt}$ can affect the pH, due to Ca^{2+}/H^{+} antiport exchange that takes place when injured leaf and root cells were observed. A reduction in the Ca^{2+} influx in the cytosol occurs simultaneously with a reduction in the cytosol acidification. The ATPases that generate the H^{+} gradients are localised in the plasma membrane and tonoplast, and the Ca^{2+} seems to be exported by Ca^{2+}-ATPases at the plasma membrane, tonoplast, endoplasmic reticulum and Golgi. The increase in the cytosolic proton concentration was suggested to be the consequence of the mechanisms in charge of maintaining the low level of $[Ca^{2+}]_{cyt}$ (Behera *et al.*, 2018). It indicates that the increase of $[Ca^{2+}]_{cyt}$ that we observe at the beginning of the SI response could be directly linked to the pH reduction, ultimately leading to PCD.

Nonetheless, an increase of $[Ca^{2+}]_{cyt}$ does not seem to be related only to changes in pH, but can also be a stimulus of degradative processes in PCD, for instance by activation of endonuclease activity in animals (Nicotera *et al.*, 1994; Clapham, 1995).

Calcium signals have also been implicated in PCD-like changes in protists (Koutsogiannis *et al.*, 2019), and in plants an increase in $[Ca^{2+}]_{cyt}$ before PCD has been described during ceramide-induced cell death and developmentally controlled PCD (Fraser *et al.*, 2020; Zhang *et al.*, 2020). Indeed, calcium was the first signalling molecule found to play a role in PCD in *Aponogeton madagascariensis* (lace plant) which is a model system for developmental PCD research, showing a significant decrease of leaves perforations produced by PCD when blocking the calcium channels (Gunawardena and McCabe, 2015). All these data make calcium an interesting molecule to be studied concerning SI-PCD.

In order to get information about the changes induced by an elevation of $[Ca^{2+}]_{cyt}$, the ionophore A23187 can be used to cause an increase of $[Ca^{2+}]_{cyt}$ in plants. When applied to *Zinnia elegans* xylogenic cell cultures, a model plant for PCD research, A23187 treatment-induced premature cell death of tracheary elements (Groover and Jones, 1999). The ionophore A23187 was also used to study the role of calcium in the *Papaver* SI-PCD response, showing that the increase in $[Ca^{2+}]_{cyt}$ activate the formation of F-actin foci (Zhao *et al.*, 2020), which is enough to trigger PCD in SI pollen (Thomas *et al.*, 2006). However, the alterations in $[Ca^{2+}]_{cyt}$ were not yet investigated in the heterologous *Arabidopsis* SI system. To investigate if calcium signalling occurs during the heterologous SI-response in PrpS-expressing *Arabidopsis* pollen, we monitored alterations in $[Ca^{2+}]_{cyt}$ with the genetically encoded fluorescent Ca^{2+} sensor YC3.6 (Nagai *et al.*, 2004; Wang *et al.*, 2020). This sensor is a fusion of a calmodulin-binding peptide which is a cyan fluorescent protein (CFP) and a circularly permuted form of the yellow fluorescent protein cpVenus (Figure 2.1). When Ca^{2+} binds to calmodulin, it results in a conformational change that enhances the fluorescence resonance energy transfer (FRET) between the two fluorescent proteins. Due to this, the ratio of cpVenus/CFP is proportional to the concentration of free $[Ca^{2+}]_{cyt}$ in such that the ratio value increases with rising Ca^{2+} levels (Krebs *et al.*, 2012).

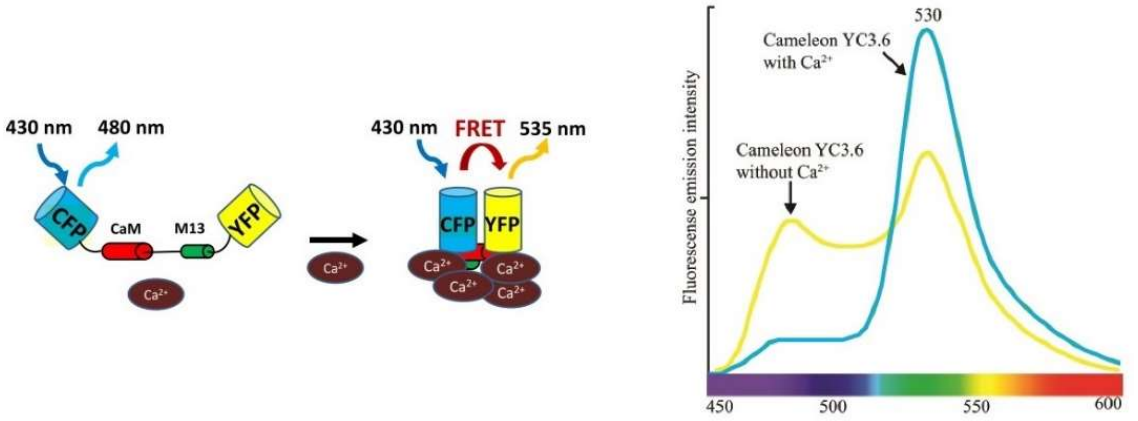

Figure 2.1. Fluorescent Ca2+ sensor YC3.6 mode of action. The sensor is composed of two mutated forms of the green fluorescent protein that absorb and emit light at matching wavelengths: Yellow cpVenus and Cyan Fluorescent Proteins (YFP and CFP). In the absence of Ca^{2+}, CFP releases the absorbed energy as fluorescence at 480 nm. In the presence of Ca^{2+}, the Ca^{2+}-binding protein Calmodulin (CaM) and a calmodulin-binding peptide (M13) change their conformation bringing YFP and CFP closer, resulting in enhanced fluorescence resonance energy transfer (FRET). In this case, we observe YFP with light emission at 530-535 nm, generating an increase of the YFP/CFP ratio (Source: Kanchiswamy *et al.*, 2014; Vaz Martins and Livina, 2019).

2.1.2. Vacuolar disorganisation

As previously mentioned, the vacuole presents a low pH and it was contemplated to be responsible for the pH decrease after SI. In addition, it was considered that the vacuolar disruption could promote SI-induced PCD, since the vacuolar breakdown is responsible for PCD when the cells suffer the differentiation to the tracheary element in plants (Groover and Jones, 1999; Obar *et al.*, 2001). One of the events taking place early in the SI response is a cytosolic pH drop directly related to PCD (Wilkins *et al.*, 2015). The vacuole presents a low pH but it is still unknown if protons derived from the vacuole are involved in this cytoplasmic pollen tube acidification. To measure the vacuolar pH, a plant-solubility-modified ratiometric pHluorin was used, revealing a pH of 5.2±0.2 in *Arabidopsis* protoplasts (Shen *et al.*, 2013a). Using the vacuolar marker carboxy-5-(and-6)-carboxy-2',7'-dichlorofluorescein diacetate (carboxy-DCFDA) in *Papaver* pollen tubes, the vacuole presented a reticular organization that was disorganised during the SI reaction. When SI was triggered, small vacuolar aggregations were observed 15 min after induction and the reticulate structure was lost from this time point on (Wilkins *et al.*, 2015). Using another reporter, the "δ-Tonoplast Intrinsic Protein -Green Fluorescent Protein", that labels the vacuolar membrane, the same reticulate pattern was observed

before SI followed by little intact vacuolar signal at 89 min after SI induction (Wilkins *et al.*, 2015). Furthermore, the SI response was simulated with the Ca^{2+} ionophore A23187 and 25 min after the addition, a major vacuolar reorganization with the appearance of collapse/aggregation was observed. Aggregations were observed 46 min after the addition of A23187, while after 77 min the signal was reduced, suggesting an extensive breakdown of the vacuole (Wilkins *et al.*, 2015).

The role that the vacuole may have in the SI response is still unknown. However, the changes in its structure suggest that this organelle could have a functional role in SI-induced PCD.

Vacuoles are organelles with a large volume in most differentiated plant cells, although, in the pollen tubes vacuolar morphology is reticular (Hicks *et al.*, 2004). The vacuolar content presents an acidic pH reaching 5.2 ± 0.2 when tested with PRpHluorin-based sensor, which is a plant-solubility-modified genetically encoded pH-sensitive GFP variant, optimised for *Arabidopsis* (Shen *et al.*, 2013b). Vacuoles are the most acidic organelles known, followed by the multivesicular bodies and trans-Golgi network with pH 6.2 and 6.3 respectively (Shen *et al.*, 2013b). Vacuoles and vacuolar contents in plants can be used for destructive purposes, contributing to cellular degradation by liberating vacuolar hydrolytic enzymes into the cytoplasm (Hara-Nishimura and Hatsugai, 2011). A cytoplasmic pH decrease and vacuolar rupture are events observed when PCD in *Arabidopsis* root cap and *Papaver* SI-induced PCD were analysed (Fendrych *et al.*, 2014; Wilkins *et al.*, 2015). The morphologies observed in *Papaver* pollen tubes when SI is induced, treated with the indicator Carboxy-DCFDA, were defined as vacuolar reorganization or breakdown (Wilkins *et al.*, 2015). The typical reticulate structure that vacuoles present in untreated pollen tubes is lost within 15 minutes after SI induction and instead small aggregations are observed. In samples observed 1 h after SI induction, the vacuolar structure appears disintegrated with additional aggregations and a reduction in vacuolar labelling, which suggests breakdown (Wilkins *et al.*, 2015). This process may have a functional or signalling role as it has been suggested that lipids (in particular phosphatidic acid) can act as pH biosensors leading cells to rapidly respond to changes in pH (Shin and Loewen, 2011). Because of its low pH, changes to vacuolar integrity have been considered as a candidate for being involved in the SI-induced

cytosolic acidification. Although the SI response in *Papaver* triggers a rapid vacuolar reorganization, the tonoplast appears to be intact in *Papaver* SI when the cytosolic pH already starts to drop (Wilkins *et al.*, 2015). Labelled with the vacuole marker Carboxy-DCFDA, a vacuolar breakdown is observed significantly later than the onset of cytosolic acidification, which in principle indicates that the vacuoles may not be involved in the initial cytosolic pH drop. In addition, when *Papaver* pollen tubes were pre-treated with propionic acid pH7 to maintain physiological pH and prevent acidification during SI, the vacuole reorganization was reduced and a low number of tubes presented caspase-3/DEVDase activity. This indicates that the cytosolic pH is linked to the PCD initiation. To conclude, the experiments with *Papaver* pollen tubes suggest that the SI-induced cytosolic acidification precedes the vacuole disintegration, therefore is unlikely that this desintegration is causing the pH drop. However, the changes in tonoplast permeability for protons play a role in the acidification process (Wilkins *et al.*, 2015).

The aim here was to determine if SI induction in the heterologous *Arabidopsis* SI system leads to changes in the vacuolar organization similar to those previously observed in *Papaver* pollen tubes. We used the vesicle-associated membrane protein 711 (VAMP711) localised in the tonoplast, targeted with a fluorescent protein, as a reporter for the vacuolar structure (Geldner *et al.*, 2009; Löfke *et al.*, 2015; Feng *et al.*, 2017). In this case, we worked with the fluorescent protein mCherry as a tag fused to VAMP711 (Figure 2.2). With this genetically encoded indicator, the SI-induced changes in vacuolar morphology could be monitored with enhanced spatio-temporal precision compared to the use of the fluorescent carboxy-DCFDA probe or transient expression of the δ-Tonoplast Intrinsic Protein (TIP)-GFP (Hicks *et al.*, 2004) previously used to follow changes in vacuolar organization in *Papaver* SI (Wilkins *et al.*, 2015).

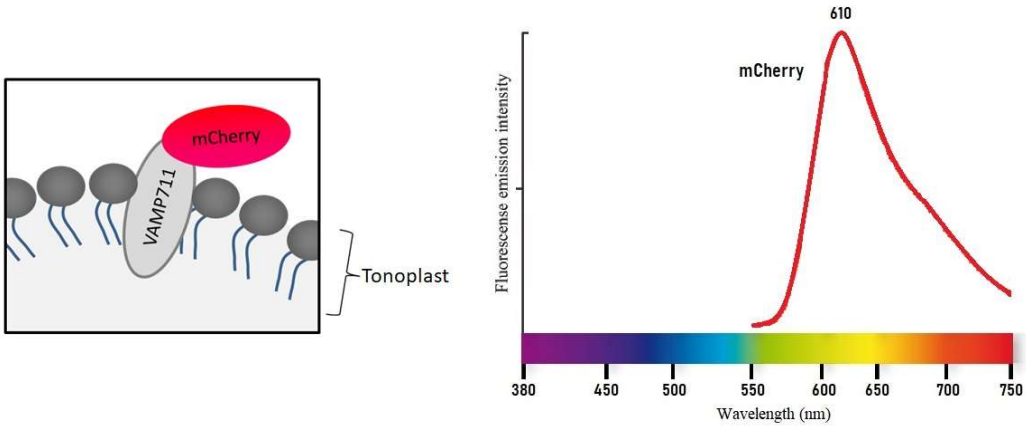

Figure 2.2. The marker used to observe the vacuolar structure is VAMP711 tagged with mCherry. The membrane protein VAMP711, localized in the tonoplast, was tagged with mCherry fluorescent protein. When excited, it presents a red colour emission revealing the vacuolar phenotype.

2.1.3. Mitochondria

Another interesting organelle due to its possible relation to PCD during SI is the mitochondrion. It has been reported that the leaking of the cytochrome *c* from the mitochondria induces PCD in animal cells tested *in vitro* (Adrain and Martin, 2001). Besides, this organelle has also been suggested to be involved in plant PCD since its intermembrane space contains DNAase activity in *Arabidopsis* cell suspension cultures (Balk *et al.*, 2003). The release of cytochrome *c* was shown in SI-induced *Papaver* pollen extracts, reaching its maximum 120 min after induction, considering it as a possible indicator of the time point in which PCD is triggered following SI (Thomas and Franklin-Tong, 2004). The presence of cytochrome *c* indicates the loss of mitochondrial integrity. However, it may not be related to PCD since only small amounts of cytochrome *c* were observed in extracts of incompatible pollen compared with the compatible (Thomas and Franklin-Tong, 2004).

In an experiment to obtain information about the possible relation of the mitochondria with SI-induced caspase-activities, normally growing *Papaver* pollen tubes were treated with the mitochondrial probe Mitotracker MT-CMXRos®. In addition, they were labelled with FAM-YVAD-FMK, which is a caspase-1 specific probe. Using the confocal microscopy a colocalization, even if not complete, of the two probes for the mitochondria and YVAD was observed in normally growing pollen tubes without SI induction, suggesting that the mitochondria contain caspase-1-like activity (Bosch *et al.*,

2010). Further analysis of the changes in mitochondrial morphology may give us some information about the role that the mitochondria have in the SI-PCD response.

The denotation of animal apoptosis can be defined based on specific hallmarks. One of them is the cytochrome c leakage from the mitochondria into the cytosol, which induces apoptosis (reviewed in Martínez-Fábregas *et al.*, 2013). Not only in plants but also animal PCD cytochrome c leakage can be initiated by cellular stress signals (Lam *et al.*, 2000).

Besides, mitochondria seem to be also related to PCD due to their electron transport chain that can result in diminished ATP production. According to studies in human cells grown *in vitro*, mitochondrial dysfunction can generate a perturbation of the cell's bioenergetic state, which can be a signal to indicate the necessity of cell death (Izyumov *et al.*, 2004).

The characterization of the mitochondria in incompatible pollen tubes has been carried out using *Papaver* pollen (Geitmann *et al*., 2004). Fixed samples were observed with transmission electron microscopy (TEM) after SI induction. This investigation revealed two conformations that differ from the mitochondria in normal conditions. One of them is defined as “extreme swelling” with a reduction or loss of cristae and fuse with each other. The other one manifests as “blebbing” with a spherical shape and presenting a local ballooning of the cristae. Both types of conformations could be found in the same cell and further biochemical studies are needed to elucidate if the mitochondria are functional at the different time points (Geitmann *et al.*, 2004). The swelling phenotype was also observed in plant cells during PCD (Yaqing and Keming, 1998). In this thesis, *Arabidopsis* SI pollen assays were performed to observe the mitochondrial structure's phenotype when SI is triggered *in vitro* using the genetically encoded mitochondrial (mito) teal fluorescent protein (TFP) contained a mitochondrial leader sequence fused with TFP.

2.1.4. Nuclear disruption

Since DNA fragmentation is one of the characteristic features of PCD (Thornberry and Lazebnik, 1998), it was tested how this event could be caused in an *S*-specific manner during the SI in *Papaver*. It was initially tested using the DNA fragmentation detection Klenow-FragEL kit for fixed samples. This essay showed that it takes 4 h to obtain evidence for nuclear DNA fragmentation in incompatible pollen tubes. However, the percentage of FragEL positive nuclei presenting DNA fragmentation continued to increase in time up to 14 h after induction (Jordan *et al.*, 2000). The proportion of pollen tubes with permeable membranes increased after SI induction, showing significant differences compared to the control from 30 min after SI. This observation was possible by pretreating incompatible *Papaver* pollen tubes with DAPI, that indicates the location of the nuclei and Texas Red that labels DNA fragmentation (Jordan *et al.*, 2000). Interestingly, the DNA fragmentation is inhibited when the tubes are pretreated with the caspase-3 inhibitor Ac-DEVD-CHO suggesting the implication of caspases and therefore PCD in this process (Thomas and Franklin-Tong, 2004; Bosch and Franklin-Tong, 2007).

The mature pollen grain of *Arabidopsis* is tricellular, differing from *Papaver* bicellular pollen containing the vegetative nucleus and the generative cell. In *Arabidopsis*, the generative cell undergoes the second mitotic division forming two sperm cells before anthesis (Liu and Qu, 2008), while this mitotic division only happens after pollen tube germination in *Papaver* (Mccue *et al.*, 2011). The functional assembly that the sperm cells perform associated with the vegetative nucleus is called the male germ unit (MGU). The three cells forming the MGU are physically bounded by a transverse cell wall and evaginations of their plasma membranes (Lalanne and Twell, 2002).

The dismantling of the nuclear envelope and the fragmentation of DNA is a hallmark feature of the PCD process occurring in plants, and also in animal apoptosis (Taylor and Hepler, 1997; Gunawardena and McCabe, 2015). Experiments with *Z. elegans* cell cultures suggest a relation between the vacuole rupture and nuclear degradation. In this case, the nucleus begins being degraded from its central region and it starts immediately after the vacuolar disruption (Obara *et al.*, 2001). Nevertheless,

this conclusion cannot be considered standard for all plant tissues since they present a great variation compared to animals whose changes in the nuclear structure related to PCD have been well defined due to their homogeneity (Gunawardena and McCabe, 2015). In plants, the nuclear breakdown is led by the process of PCD that has been divided into three main phases: signalling, execution and nuclear dismantling itself (Latrasse *et al.*, 2016). In addition, nuclear disruption can be related to cytoplasmic events taking place in plant cells (Table 2.1). Despite the differences, in both animal and plant cells, the nuclei undergo breakdown of the envelope, chromatin condensation, DNA fragmentation (reviewed in Domínguez and Cejudo, 2012).

Table 2.1 Cytoplasmic events that may be related to plant nuclear disruption. The changes in the cytoplasm produced by the individual action or combination of these events seem to be involved in triggering the nuclear disturbance in plants cells (Source: Domínguez and Cejudo, 2012)

Organelle	Event
ER-derived compartments	Accumulation and release of cysteine proteases and nucleases in the onset of PCD
ER-Golgi	Chaperoning and inhibition of cysteine proteases by protein disulfide isomerase-5 during trafficking to vacuole before PCD
Vacuole (PSV and Lytic Vacuole)	-Self-processing of vacuolar processing enzyme at acid pH -Maturation of precursors of PR proteins and hydrolases by vacuolar processing enzyme -Accumulation of aspartate proteases, cysteine proteases and nucleases until their release in PCD -Tonoplast disruption
Mitochondria	Release of endonucleases, cytochrome c and other apoptogenic factors
Chloroplast	Release of ROS
Cytoskeleton	Depolymerization of microtubule and reorganization of actin network providing a skeleton to trigger autophagosome formation and promoting autophagic movements for cell content engulfment
Autophagosomes and autophagic vacuoles	Digestion of remnants of membrane-less nuclear fragments

Related to SI-PCD, *Papaver* pollen tubes undergoing the SI response were observed following the fragment end labelling (FragEL) *in situ* technique to detect fragmentation of nuclear DNA. The pollen tubes were treated with the Klenow-FragEL kit supplied by Calbiochem and the nuclear morphology was detected by Texas Red staining. It confirmed that only in incompatible tubes the DNA is degraded in the presence of the female S-determinant. The DNA fragmentation was first detected 4 h after the SI induction and continued to increase thereafter (Jordan *et al.*, 2000). These findings are in agreement with results obtained using electron microscopy showing that

the MGU becomes more electron-dense 4 h after SI induction and it starts to appear less homogenous (Geitmann *et al.*, 2004).

In this thesis, we use the genetically encoded fluorescent protein tdTomato presenting nuclear-localised signal (NLS), which is optimal to detect the nuclear morphology and position in plants (Kong *et al.*, 2015). TdTomato emits its maximum at 581 nm in a bright red colour that does not interfere with the detection of GFP-tagged $PrpS_1$ in *Arabidopsis*, since it is optimally detected at 510 nm (Lambert, 2019).

2.1.5. Caspase activity

The use of caspase activity inhibitors in *Papaver* pollen extracts evidenced that SI triggers PCD by the induction of caspase activity (Thomas and Franklin-Tong, 2004a).

Using AMC-based fluorogenic indicators for caspase activities, a number of caspase activities were detected in *Papaver* pollen extracts after SI induction: YVADase/caspase-1, DEVDase/caspase-3, LEVDase/caspase-4 and VEIDase/caspase-6. In this experiment, significant caspase-3 and caspase-6-like activities were detected in SI-induced pollen extracts while increases in caspase-1 and caspase-4 activities were much lower, suggesting these activity may not be involved in SI-mediated PCD (Bosch and Franklin-Tong, 2007). The activation of those caspase-like activities was followed in time also using pollen extracts. It was concluded that the profile of DEVDase and VEIDase activity are very similar, presenting an increase at 3 h after SI induction with peak activity 5 h after induction. Both present a significant decrease at 8 h after induction. The detected caspase-3 activities were higher than caspase-6 activities (Bosch and Franklin-Tong, 2007). Furthermore, SI-induced *Papaver* pollen tubes were pretreated with caspase inhibitors. Only when pretreated with the caspase-3 inhibitor, Ac-DEVD-CHO, the SI-induced DEVDase activity was reduced, showing a high specificity (Bosch and Franklin-Tong, 2007).

The use of the live-cell probe NucView 488 confirmed that there is DEVDase activity in incompatible pollen tubes. In order to measure its activity in live cells, SI was induced in pollen tubes germinated *in vitro* and incubated with the caspase-3 indicator probe $CR(DEVD)_2$. It revealed that untreated normally growing pollen tubes do not

present DEVDase activity. However, when treated with cognate PrsS to induce SI, DEVDase activity is detected 2 and 4 h after induction (Bosch and Franklin-Tong, 2007)

The activity of caspases is key in animal PCD. Comparedto animals, it was discovered that the genomes of plants do not encode true homologs of this family of protease enzymes. However, the suppression of PCD in plants is possible when caspase inhibitors are applied. Due to this, there is a group of activities in plants described as "caspase-like activity" that are carried out by proteases with a similar role to animal caspases (Sueldo and van der Hoorn, 2017). To date, there have been identified eight distinct caspase-like activities in plants denoted by their preferred tetrad of amino-acid sequence: YVADase, DEVDase, VEIDase, IETDase, VKMDase, LEHDase, TATDase and LEVDase (reviewed in Xu and Zhang, 2009). We focussed on caspase-3 like activity (DEVDase), which has been implicated in *Papaver* SI (Thomas and Franklin-Tong, 2004). This activity participates in SI-induced PCD and the DEVDase activity is alleviated when incompatible *Papaver* tubes are pre-treated with the caspase-3 inhibitor Ac-DEVD-CHO (Bosch and Franklin-Tong, 2007).

The fluorogenic probe Ac-DEVD-AMC allows us to measure the caspase-3 like-activity in plants (Korthout *et al.*, 2000). It is a synthetic tetrapeptide fluorogenic probe that works as a substrate for caspase-3-activity. The activity can be measured as caspase-3 cleaves the tetrapeptide releasing the fluorescent AMC which can be quantified with a fluorescent microscope (Figure 2.3). The presence or absence of this activity in *Arabidopsis* will give more information about how similar *Papaver* and *Arabidopsis* SI systems are.

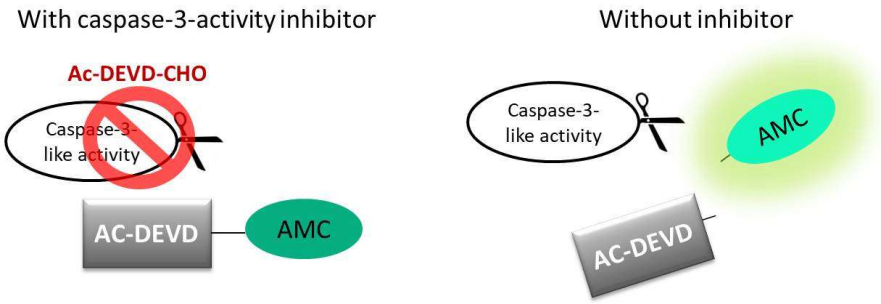

Figure 2.3. Interaction between caspase-3-inhibitor and Ac-DEVD-AMC probe. In the presence of the inhibitor, the Ac-DEVD-AMC probe is not cleaved by the DEVDase activity and the probe does not emit any signal when excited. But in the absence of Ac-DEVD-CHO, the DEVDase activity is not inhibited and can thus cleave the Ac-DEVD-AMC substrate, releasing AMC. AMC emission can be captured and quantified, being directly proportional to the caspase-3-like activity.

2.2. Material and Methods

2.2.1. *Arabidopsis* lines used for life imaging

For the visualization of these five events of interest, the followed lines were used:

To observe the changes in $[Ca^{2+}]_{cyt}$, an *Arabidopsis* line coexpressing $PrpS_1$-GFP and YC3.6 Ca^{2+} sensor (Nagai *et al*., 2004) generated at the VIB-UGent Center for Plant Systems Biology department was used.

Arabidopsis coexpressing $PrpS_1$-GFP and VAMP711-mCherry was used to observe the morphology that vacuoles present during the SI response. To obtain this line, At-SI stigmas were pollinated with pollen expressing the tonoplast fluorescent marker WAVE9R which carries pUBQ10::VAMP711-mCherry (Geldner *et al*., 2009). This genetically encoded vacuolar marker facilitates the visualization of the tonoplast.

To characterise the mitochondria phenotype during the SI-PCD response, the line pntp303::mito-mTFP_pntp303::$PrpS_1$ generated at the VIB-UGent Center for Plant Systems Biology department was used. The mito-TFP tags N-terminal domains present in the outer mitochondrial membrane being exposed to the cytoplasm outside of the mitochondria (Vigano *et al.*, 2018). This line also expresses $PrpS_1$ without any fluorescent tag.

For the experiments following the nuclear integrity, the line used is pUBQ10-NLS-Tdtomato_$PrpS_1$-GFP. To obtain this, two lines that express SLR1p::$PrsS_1$_ ntp303p::$PrpS_1$-GFP (At-SI) and pUBQ10::Tdtomato-NLS were crossed manually and the next generation plants were selected until it was obtained a line homozygous for both indicators.

For other experiment carried out, mimicking the procedures in *Papaver* (Bosch and Franklin-Tong, 2007) the probe Ac-DEVD-AMC was used to observe the DEVDase/caspase-3 activity. Since the spectrum for imaging this probe overlaps with GFP, we could not use the line At-$PrpS_1$-GFP. A more suitable At-$PrpS_1$ line, expressing $PrpS_1$ without any fluorescent tag, was generated. To obtain this line, wild-type *Arabidopsis* plants were transformed with *Agrobacterium* carrying the plasmid pORE3.pNTP303::$PrpS_1$.

2.2.2. Pollen *in vitro* hydration and samples set up

Hydrated pollen grains were used to imaging the nuclear disruption and caspase activity after SI induction. However, for the samples used to observe changes in $[Ca^{2+}]_{cyt}$, vacuolar disorganisation and mitochondria, it was required to grow appropriate pollen tubes *in vitro*.

In both types of experiments, 35 mm glass-bottom microwell culture dishes (MatTek Corporation) were used. *Arabidopsis* pollen grains from the correspondent line were placed on the 10 mm No. 1.5 coverglass (MatTek Corporation) that was coated with 0.01% (w/v) poly-L-lysine. The positive charges of the poly-L-lysine help to maintain the pollen grains attached to the bottom and attract the tubes to grow near to the bottom glass. To hydrate pollen, a wet chamber was created placing wet filter papers in the lid of the culture dishes, and it was sealed with parafilm and placed in a 25 ^{o}C room for 60 min. After hydration, 150 µl liquid germination medium (AtGM) was added. The composition of the AtGM is 15% (w/v) sucrose, 0.01% (w/v) H_3BO_3, 5 mM KCl, 1 mM $MgSO_4$, 2.5 mM $CaCl_2$ and 2.5 mM $Ca(NO_3)_2$ (De Graaf *et al.*, 2012; Wang *et al.*, 2020). In all cases, the pollen grains were incubated 60 minutes under continuous light at 25 ^{o}C, before further manipulations.

Since the SI response is equally triggered in pollen grains before and after germination, using pollen grains before germination facilitates the research on nuclear integrity and caspase activity. Imaging pollen grains we could follow big groups of them in time, increasing the number of samples tested considerably. Furthermore, maintaining the microscope focus on the sample before and after SI induction by the addition of the cognate PrsS is not that arduous when working with grains instead of tubes.

2.2.3. Confocal microscope adjustments for image capture

In all cases, a Leica SP8 confocal microscope was used. Confocal microscopy has been used for the majority of flower development studies for decades, as it allows us to get high-quality images reducing the out-of-focus noise comparing with conventional microscopy (White *et al*., 1987; Prunet and Duncan, 2020).

For $[Ca^{2+}]_{cyt}$ in the pollen tubes, images were taken 1 frame/sec. The Z-axis had 1.99 µm total length, divided into 3 sections, with 6 line average. Argon laser 5% was used to excite at 458nm, with the shutter on and a 7% of intensity. The magnification objective used was x63, zoom 2x. Detectors HyD Gain 200 in both cases (PMT Trans Bright field gain 360). Emissions of cyan fluorescent protein (CFP, 470-500 nm) and Venus (YFP, 530-580nm) were collected simultaneously.

In the experiment performed to capture the changes in the vacuolar organisation, an x63 CS2 objective NA 1.20 was used focussing on the mid-plane of the pollen tubes. The fluorescent protein mCherry was captured with excitation 561 nm, emission 576–680 nm (Wang *et al*., 2020). Even if not captured, the emission of GFP was always checked before imaging to ensure the presence of $PrpS_1$.

For obtaining images with the signal of mTFP tagged to mitochondria, the captures were made with x63 CS2 objective, NA 1.20. The protein mTFP was excited at 458 nm with an Argon laser at 14,2% (emission 480-550 nm). With 8 line average, 10 layers were captured in a total of 10 µm to obtain information from not only the middle plane but all the tube area, including the cortex. Images were captured from the tip till 35 µm from the tip.

To image SI induced changes in the nuclear integrity, after hydration, tdTomato signal was captured with excitation 561 nm, emission 596–665 nm (×63 CS2 objective, NA 1.20). The Z-axis was readjusted for each group of pollen grains defining the top and bottom plane of the group. The z-stack was set to 10 µm, to capture all the MGUs, avoiding blind spots and capturing all the signal, independently of the nucleus location in each pollen grain. All the MGUs of pollen grains were assessed for the presence of an NLS-tdTomato signal. Pollen exhibiting either a positive or negative fluorescent signal were counted on images taken every 20 minutes. MGUs were considered disrupted when they lost the fluorescent signal previously observed. The experiment was carried out 8 times, obtaining a total number of 170 pollen grains followed for 8 hours after SI induction.

In order to capture the caspase-3-activity, 150 µl of AtGM containing 0.9 mM final concentration of Ac-DEVD-AMC was added to the pollen grains after hydration. We let it settle for 30 min and after that, the confocal imaging was started capturing images every 1 hour for 8 hours from the SI induction. The fluorescent probe Ac-DEVD-AMC signal was captured with excitation 405 nm, emission 451–496 nm. The objective used for this experiment was ×63 CS2 NA 1.20. In addition, to verify the specificity of the fluorescent signal derived from Ac-DEVD-AMC, the samples were pre-treated with the caspase-3/7 inhibitor Ac-DEVD-CHO. For this, 1.49 µM final concentration of Ac-DEVD-CHO was added to the AtGM solution containing the Ac-DEVD-AMC probe.

2.2.4. SI induction and image capture

In all the experiments carried out in this chapter, the final concentration of $PrsS_1$ used to induce SI is 20 µg/ml. Since the proteins were stored at 4 ^{o}C, for controls cold AtGM at 4 ^{o}C was added to pollen samples. The time-point zero corresponds to the exact moment in which $PrsS_1$, or extra AtGM when control, was added to the sample.

There were differences in the time points in which the images were captured. For testing $[Ca^{2+}]_{cyt}$ the frames were captured every second for up to 20 minutes following single tubes.

On the contrary, to image the vacuolar structure, continuous images were obtained all around the sample from different tubes. Captures were made before the SI induction up to four hours after SI. All the images obtained were clustered in 30 minutes intervals to characterise the vacuolar phenotypes.

For the mitochondria analysis, single tubes were followed, capturing an image every 30 or 60 minutes up to five hours after SI induction in order to get sequences of images showing if and how the mitochondria changes. The same procedure was carried out when checking the nuclear disruption and caspase-3-like activity, but following groups of pollen grains instead of pollen tubes. In these two cases, the frames were taken every 20 minutes and every 60 minutes respectively up to 8 hours after SI induction.

2.3. Results

2.3.1. Image analysis

In all cases, the images obtained with the microscope required a specific treatment to obtain information from them. The procedures in each experiment were as follows: Images obtained from pollen tubes expressing the Ca^{2+} sensor YC3.6, were processed using Leica Application Suite X (LAS X). The region of interest (ROI) was delimited in LAS X, capturing in all channels the same area (Figure 2.4). The criteria for the width x length of the ROI was variable, according to the necessities for each analysis, but the height x length was in all cases as tight as possible considering that the tube position changes from frame to frame. Those changes are produced due to the tube motion due to tip growth or waves in the liquid medium that slightly displaces the tube when it is not properly attached to the bottom of the glass slide. Due to this, we checked the area in which the tube is located in every time frame before calculations. When measuring the increase of the tube length, the LAS X software was also used. The tip location was measured considering its position at time point 0 as a reference.

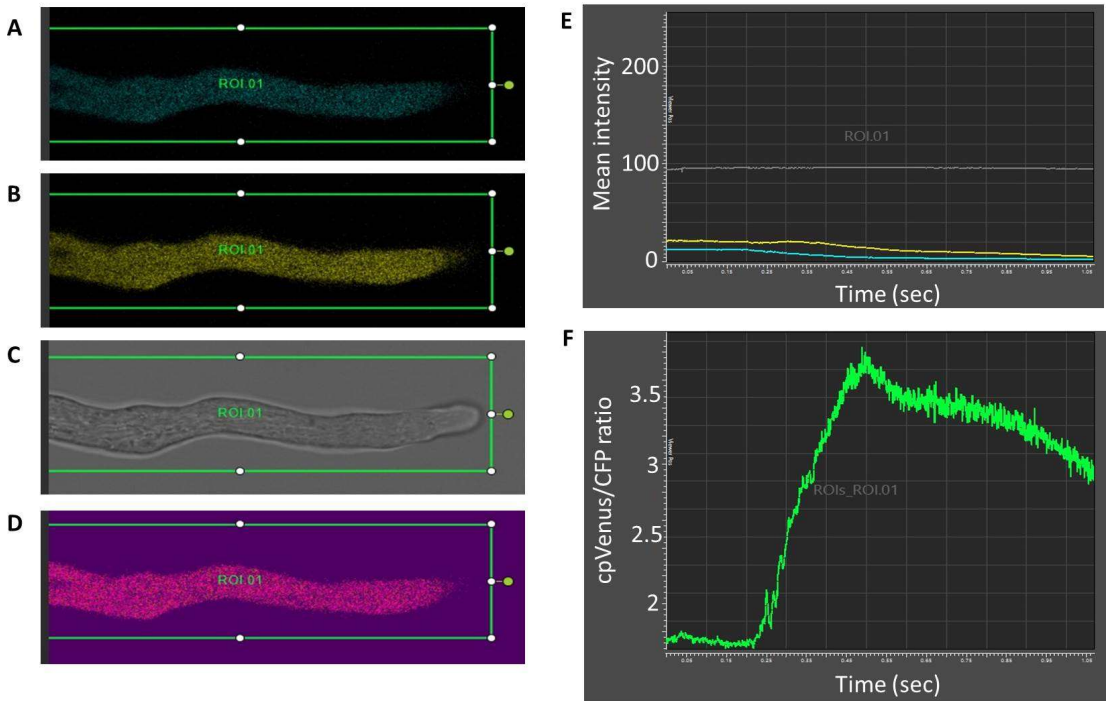

Figure 2.4. Representative example of multi-channel setup in LAS X. (A) CFP channel. (B) cpVenus YFP channel. (C) Bright field channel. (D) Ratio cpVenus/CFP channel. (E) Mean intensity of bright field (grey), cpVenus YFP (yellow) and CFP (blue) channels in time. (F) Representation of the values obtained at consecutive time points when calculated the cpVenus/CFP ratio.

The LAS X software was also used for defining the phenotype of the vacuole during SI-PCD. In each observation, the tube length considered was till 35-40 µm from the tip. The ROIs were drawn with this length and with the width required to include the entire tube diameter. To define the different morphologies, we considered the shape and density of the structures present in the tube and the number of them. To evaluate the density, the channel in which the signal of $PrpS_1$-GFP is captured was taken into account as it presents differences in its intensity that colocalise the VAMP711-mCherry signal.

To record the presence or absence of mTFP tagged to mitochondria organelles the z-stack layers were merged. The software LAS X allows us to create a 3D reconstruction with the images obtained that helps to better understand where the signal is localised in the tube.

Also for analysing the images from the line expressing TdTomato tagged to the nuclear envelope, the images were observed in maximum projection to merge all the z-stack layers. We considered the nucleus disrupted when losing the signal presented in previous time points. The percentage of nuclei lost was calculated from the total number of nuclei observed before SI induction.

For the images showing the signal emitted by the fluorogenic caspase-3 probe, the LasX software was used to obtain the mean fluorescent value of the AMC signal. It was calculated based on a 15 µm diameter region of interest drawn over every individual pollen grain. For each time point, 100–300 pollen grains were scored in three independent experiments. The variation in fluorescent intensity between grains was colour-coded using the ImageJ Fire LUT plugin (Geissbuehler and Lasser, 2013). For statistical analysis, the values obtained for each time-point were compared with the control. In this case, the data for the DEVDase/Caspase-3-like activity did not present a normal distribution according to the Lilliefors (Kolmogorov-Smirnov) normality test. Due to this, the p-values were calculated using the Wilcoxon test.

2.3.2. Cytosolic calcium increase

In order to profile the dynamics of calcium signatures of *Arabidopsis* pollen expressing PrpS during the SI response, we monitored the YC3.6 signal of $PrpS_1$-expressing pollen after cognate $PrsS_1$ protein treatment. As various stimuli can trigger calcium signature changes, to make sure that our experimental setup did not introduce additional calcium responses, we started our experiments by treating *Arabidopsis* $PrpS_1$-expressing pollen with AtGM germination medium (see section 2.2 Material and Methods) alone as a control. The YC3.6 signal was recorded from 1.5 min before the addition of AtGM up to 5 min after that, capturing 1 frame per second. The data obtained shows a constant ratio between cpVenus and CFP in the defined ROI (Figure 2.5A and 2.5B), indicating that treatment with AtGM alone does not trigger a change in $[Ca^{2+}]_{cyt}$. In agreement with this, a continuous elongation of the pollen tube, which showed no significant difference before and after AtGM treatment, was observed (Figure 2.5A and 2.5C). These data demonstrate that our experimental setup did not introduce any artificial calcium signature or disturbances in the tube growth, and was suitable to perform further investigations.

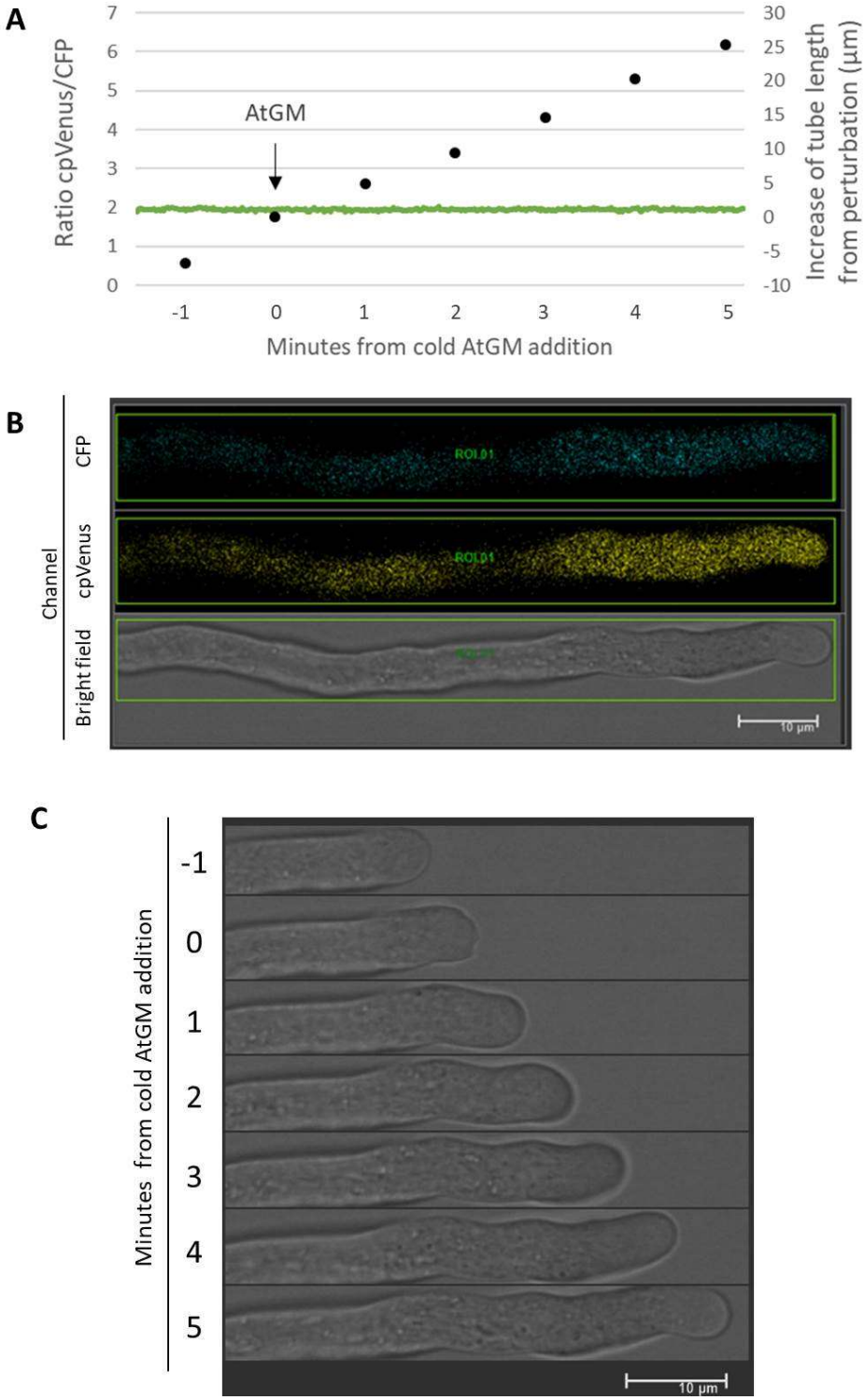

Figure 2.5. A typical example of cytosolic calcium in normal conditions (A) 1 frame/second data representation of the fluorescence intensity λ cpVenus/CFP ratio before and after the addition of growth medium (green). The length variation of the tube compared to the time point 0 is represented with black dots, it shows a continuous increase not affected by the addition of cold AtGM, added at time 0 as indicated with a black arrow. (B) Region of interest (ROI.01: green box 1000 x 11.5 µm) in the three channels captured, defined for obtaining data represented in A. CFP signal: blue, cpVenus signal: yellow. (C) Bright field channel showing that changes in the tube length are constant, not being affected by the addition of cold AtGM. At time point 0 the image is slightly deformed due to the wave that the addition of AtGM causes in the medium.

When the SI response was induced by adding $PrsS_1$ to the germination medium, the $[Ca^{2+}]_{cyt}$ concentration showed an increase, with levels continuing to rise even after the pollen tube elongation had stopped. Before the elongation stops, in all cases a slight and short transient increase of calcium was observed before the onset of the curve depicting the large increase in $[Ca^{2+}]_{cyt}$ (Figure 2.6A). When comparing different tubes, the same pattern of events related with the SI response was always observed in all of the tubes analysed: firstly the elongation stops, followed by the calcium concentration reaching the maximum point and finally cytoplasmic streaming stops (Figure 2.6B). Although the same pattern was observed in all cases, the speed in the execution of these events differed between individual tubes.

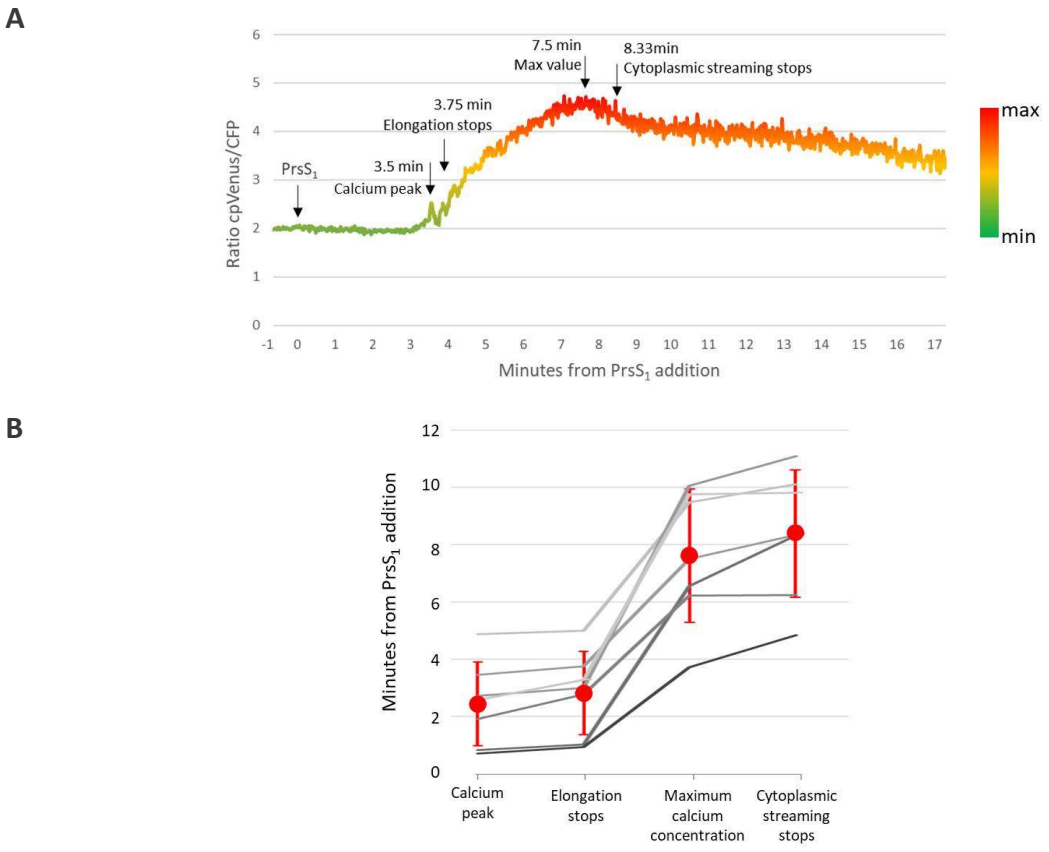

Figure 2.6. Cytosolic calcium after SI induction. Cytosolic calcium after SI induction. (A) 1-second data representation of cpVenus/CFP ratio in an individual pollen tube. Before and immediately after SI induction, the ratio values obtained are the lowest (green). The ratio increases reaching its maximum 7.5 min after SI induction (red). Together with the addition of $PrsS_1$, the time point of four remarkable events is indicated with a black arrow: The early calcium peak is always observed before the tube stops growing, when the elongation stops, when the maximum value is obtained and when the cytoplasmic streaming stops. (B) The defining events as a function of the time from $PrsS_1$ addition in individual pollen tubes (n = 7 greyscale). The samples present differences in their speed when particular events occur but in all cases, the four events are equally consecutive. The average value and standard deviation are represented in red (dots and bars respectively).

Two ROIs were defined to determine potential differences of SI-induced calcium signatures within different areas of the same pollen tube. Firstly, the tip area (including apex and the subapical region, ROI.01 in Figure 2.7A) and the whole pollen tube (ROI.02 in Figure 2.7A). Comparing the cpVenus/CFP ratios of the two ROIs showed that both exhibited very similar temporal calcium concentration profiles (Figure 2.7B). A slightly higher ratio is observed in the tip before elongation stops, which most likely results from the tip-focused calcium gradient at the pollen tube apex. However, as we can see in all further cases, there is a calcium peak that preceded the arrest of pollen tube elongation and is always more predominant in the tip or apical area (Figure 2.7B).

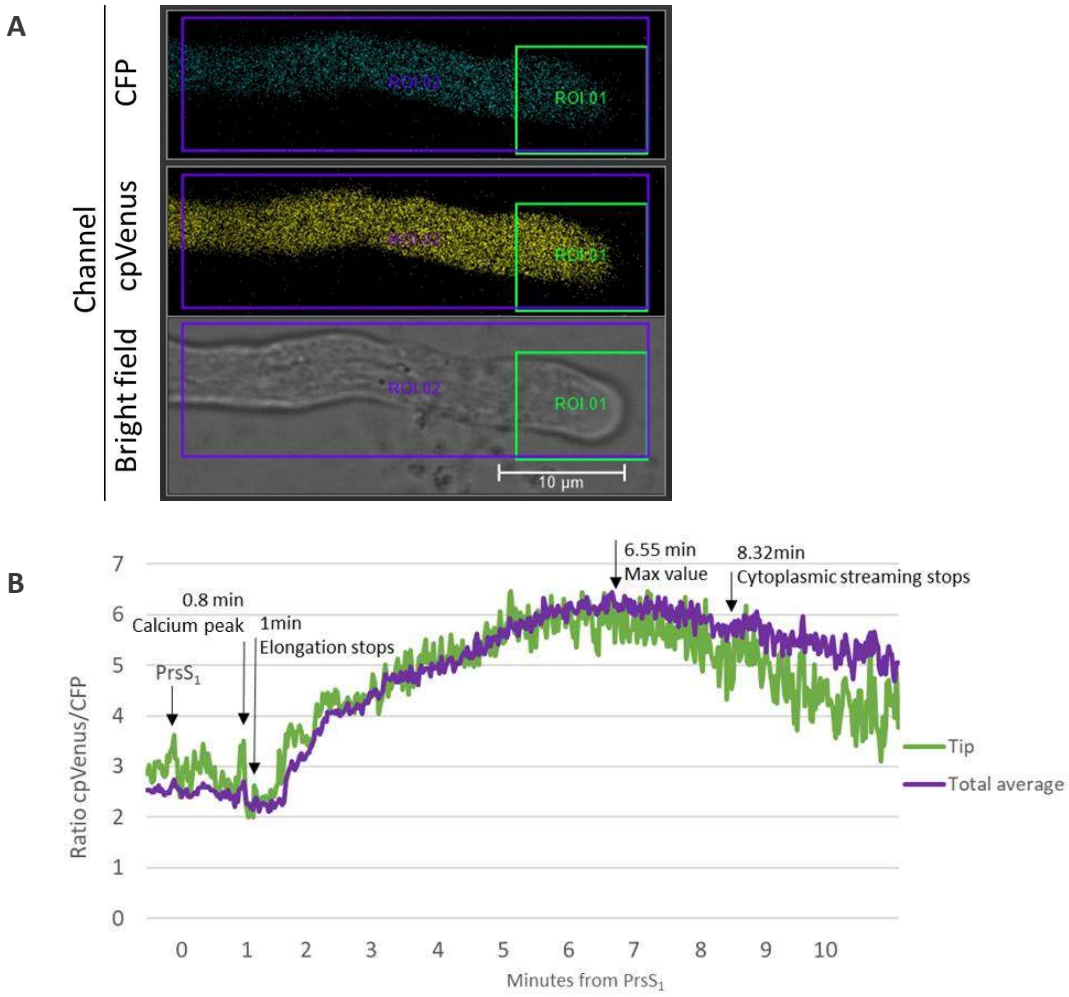

Figure 2.7. Comparison of cytosolic calcium in the tip and total areas after SI induction. (A) Regions of interest defined for this calculation (ROI.01: green box 10.5 x 8.5 µm, ROI.02: purple box 37 x 10.5 µm) in the three channels captured. CFP signal in blue, cpVenus signal in yellow. (B) 1 second/frame data representation of cpVenus/CFP ratio in each region of interest before and after the addition of the female S-determinant.

To determine if the SI-induced increases in calcium at the tip could also be observed in more distal areas of the pollen tube, two further sections were defined: ~50 µm and ~100 µm distal from the tip (Figure 2.8A and 2.8C). In both samples, an earlier increase of $[Ca^{2+}]_{cyt}$ is observed in the tip compared with the more distal areas. While the timing of the peak cpVenus/CFP ratio is very similar between the examined regions, calcium levels drop after that in the tip region while the concentration remains high in the more distal areas (Figure 2.8B and 2.8D).

A

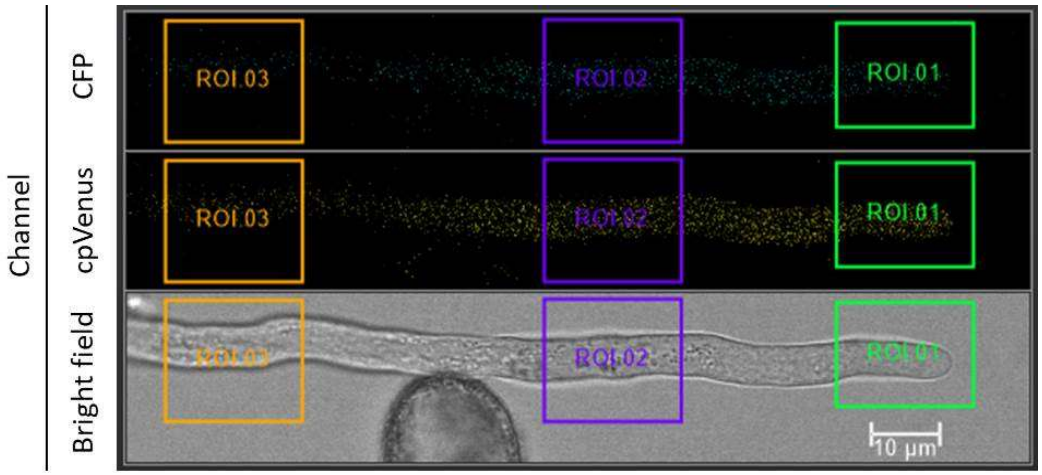

B

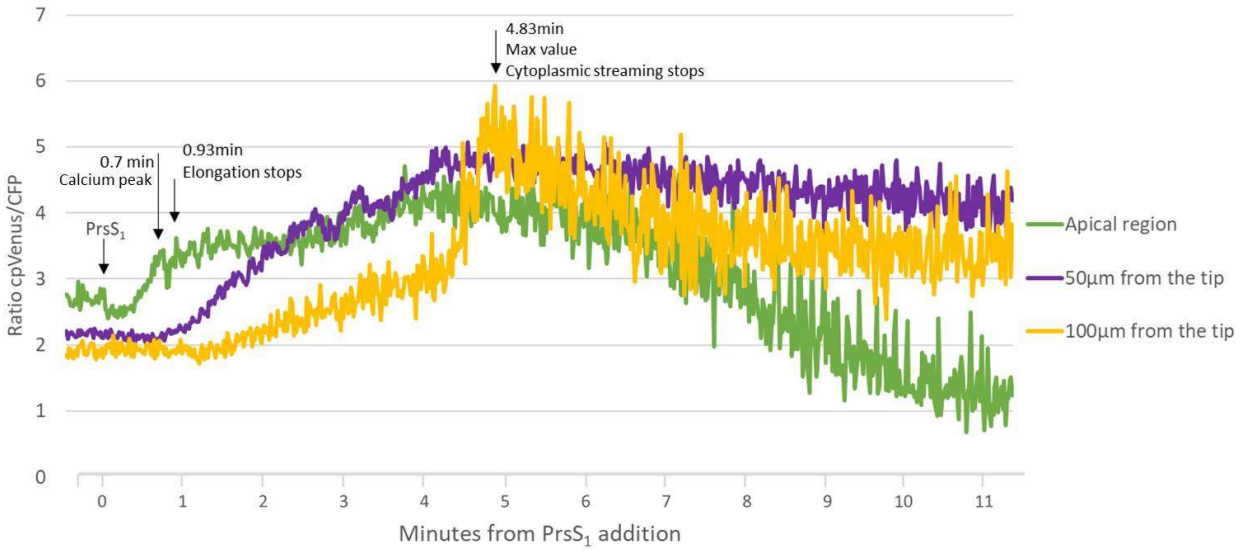

C

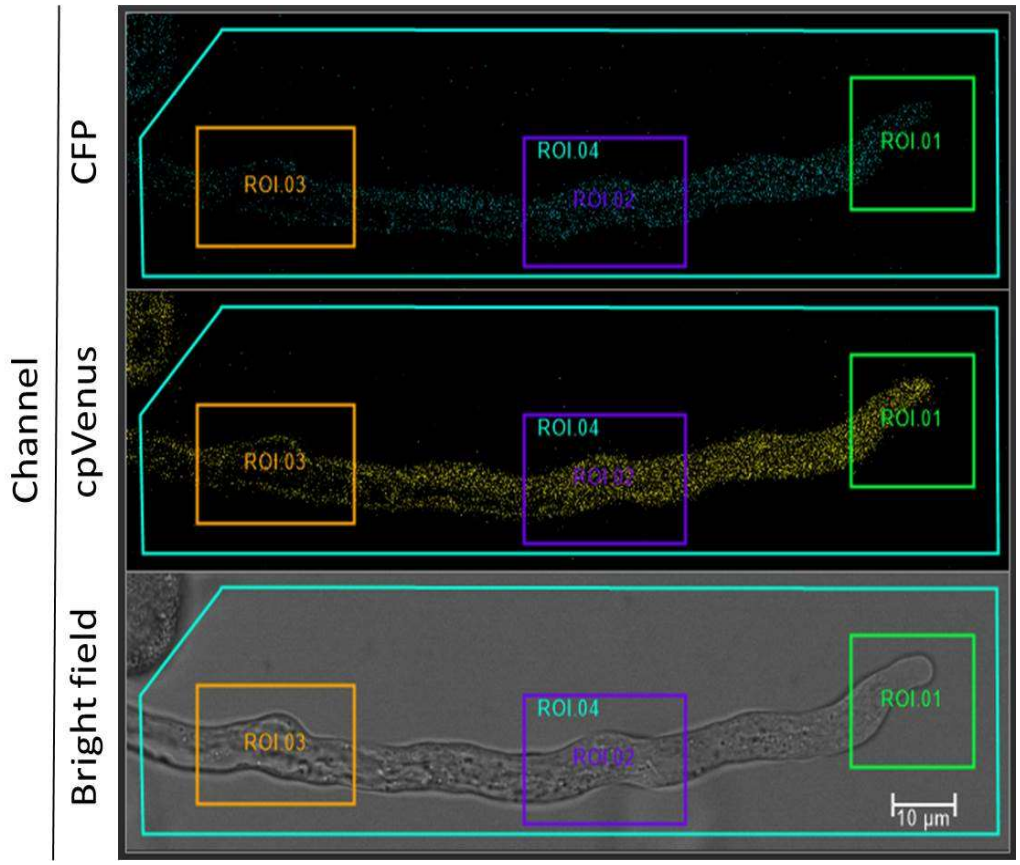

D

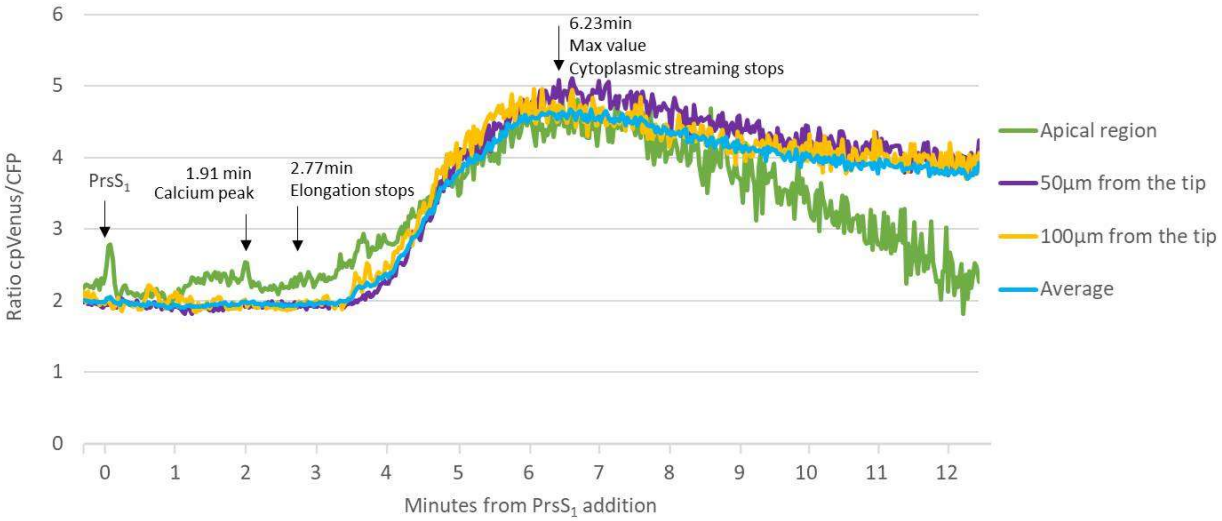

Figure 2.8. Comparison of cytosolic calcium in the apical region and areas more distal from the tip after SI induction. (A and C) Areas of interest defined for the analysis represented in B and D respectively (ROI.01: green box, ROI.02: purple box, ROI.03: orange box, ROI.04: blue box) defined in the three channels captured. CFP and cpVenus signal are shown in blue and yellow respectively. (B and D) 1 second/frame data representing the fluorescence intensity of cpVenus/CFP ratio before and after the addition of $PrsS_1$. Up to one minute after the elongation stops, the cpVenus/CFP ratio is higher in the apical region compared to the rest of the ROIs, as well as the calcium peak that is more predominant in the ROI that includes the tip. In these both cases, the maximum value obtained coincides with the time point in which the cytoplasmic streaming stops.

To conclude, in all the cases observed we found a pattern starting with an increase of $[Ca^{2+}]_{cyt}$ for the first minutes after the SI induction. A calcium peak was detected immediately before the pollen tube elongation stops and it will be interesting to investigate if there is a causative relation between these two events. Also, the fact that the calcium keeps increasing until the cytoplasmic streaming stops when it starts decreasing constantly, suggests a possible functional relationship between changes in $[Ca^{2+}]_{cyt}$ and physiological events in pollen tubes.

2.3.3. Vacuolar disorganisation

To profile changes in vacuolar organization induced by SI we used *Arabidopsis* pollen coexpressing $PrpS_1$-GFP and the tonoplast marker VAMP711-mCherry. According to their appearance and size, the vacuoles present in the observed pollen tubes were clustered in seven different morphologies. Untreated pollen tubes presented a reticulated vacuole structure throughout the pollen tube shank until the subapical area, which was defined as Morphology A (Figure 2.9A). Morphology A was also the most predominant during the first 30 min after SI induction with cognate $PrsS_1$ protein treatment, as 60.2 % of the tubes observed (n = 98) presented this reticulated structure (Figure 2.9B).

A key characteristic was taken into account for the rest of the morphologies which involved the presence of globular structures, even when in some cases remains of the reticular structure was still present. Globular structures were observed in two different forms. When the tonoplast-associated mCherry signal was observed as aggregates, we defined it as globular compact. In contrast, when only a perimeter was defined by this fluorescent protein, creating an empty space, the globular structures were defined as globular empty (Figure 2.10).

When in addition to the reticulated morphology, globular compact structures were observed with a diameter of 1 µm, two different morphologies were distinguished according to the number of them present in the ROI. The presence of 1 to 3 of distinct globular compact structures was defined as Morphology B. Detection of this morphology was the scarcest during the SI response, with maximum occurrence in the first 30 min period after SI induction with only presented in 13.3 % of the tubes observed (n=98).

The tubes showing more than three 1 µm compact structures were grouped in Morphology C, representing the predominant morphology observed in the 31 – 60 min interval with 29.6 % of the tubes (n=71) followed closely by Morphology D with 28.2%. Morphology D was considered the one presenting 1 to 3 bigger globular and compact structures, each with a diameter greater than 4 µm. It was the predominant morphology for all the stages from 61 min onwards (Figure 2.9A, 2.9B).

When globular empty structures were present, as defined before, their diameter always was greater than 4 µm. Morphology E was defined as the one where three or more of these structures were present while Morphology F contains less than three of them. Both these morphologies became more prevalent over time, with Morphology E apparent in 35.7 % of the tubes observed in the 211 – 240 min (n=14) time-interval and Morphology F in 23.8% of tubes in the 181-210 interval (n=21) (Figure 2.9A, 2.9B).

The final morphology identified is G, presenting a central empty structure occupying more than 50 % of the total area in the pollen tube. This morphology was observed from the first 30 min after SI, even if at a very low number, only 1 % of the tubes for this period. Its maximum presence was during the 30 minutes before the 3 hours of observations when 16.7 % of the tubes observed (n=24) presented this big vacuolar structure with no mCherry signal within (Figure 2.9G).

The detailed examination of the vacuolar changes induced by SI in our *Arabidopsis* system showed a range of different morphologies that exhibit a distinct progression over time. From 1h after SI induction onwards, most of the vacuoles can be described as large globular compact (Morphology D) and large empty structures (Morphologies E and F). Further studies are required to examine the dynamic formation of these morphologies from the standard reticulate structure in more detail and to evaluate if these vacuolar morphologies play a functional role in the later stages of the SI-PCD process.

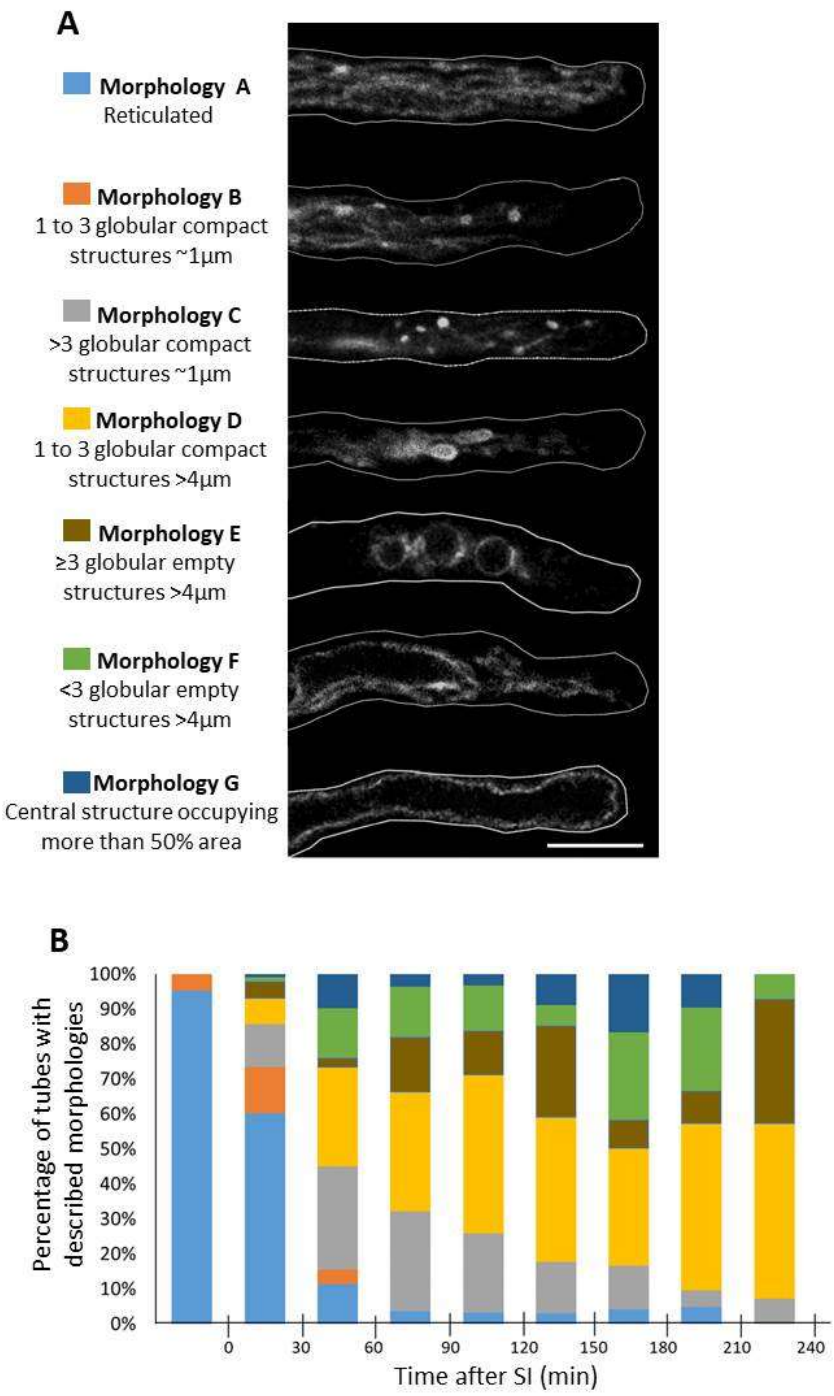

Figure 2.9. Vacuolar morphologies during SI response. The seven morphologies correspond to A: Reticular, B: 1 to 3 globular compact structures ~1 µm, C: more than 3 globular compact structures ~1 µl, D: 1 to 3 globular compact structures bigger than 4 µm, E: more than 3 globular empty structures bigger than 4 µm, F: more than 3 globular empty structures bigger than 4 µm, G: a central structure occupies more than 50% of the tube. Grayscale emphasizes the values from white (minimum) to dark grey (maximum) for each period. As a control, untreated (UT) pollen tubes were observed 3 h after germination. (A) Morphologies defined according to their appearance observed in *Arabidopsis* coexpressing $PrpS_1$ and the tonoplast marker WAVE9R. Pollen tube plasma membrane represented with a white line. Expression of mCherry in greyscale. Bar = 10 µm. (B) The presence of the different

morphologies described expressed as relative percentages, in 30 min periods before and after SI induction at 0 min.

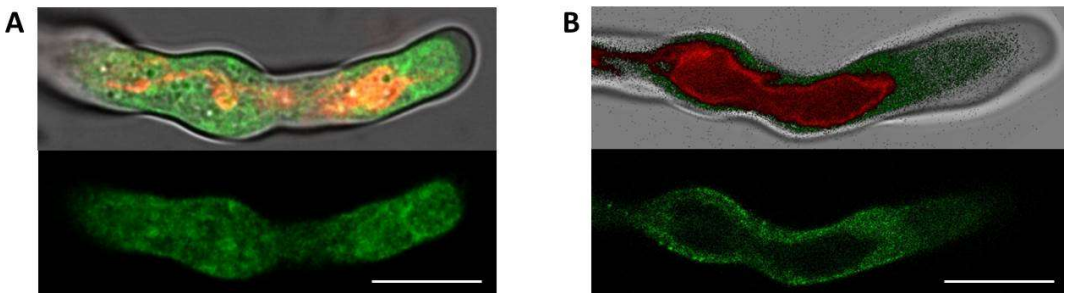

Figure 2.10. Differences between described phenotypes. The three channels showing the emission of $PrpS_1$-GFP signal (green) and VAMP711-mCherry (red) together with the bright field (greyscale) are merged in the top images while only $PrpS_1$-GFP signal is shown in the bottom ones. (A) Compact structures: The shape of the structures defined by the emission of VAMP711-mCherry is not observed when isolated the GFP signal. (B) Empty structures: When observed alone in the channel that captures $PrpS_1$-GFP emission, there is no GFP signal in areas where the structures delimited by VAMP711-mCherry signal are located. Bar = 10 µm.

2.3.4. Mitochondria

In this chapter, we also focussed on the changes that the SI response may eventually produce in mitochondrial morphology. We observed pollen tubes coexpressing the male S-determinant and a mitochondria-targeted fluorescent protein mTFP.

Before the addition of $PrsS_1$ and also 1 hour after addition, a uniform brightness is observed showing the presence of intact mitochondria throughout the cytoplasm of the tube (Figure 2.11 and 2.12). However, the images shown are preliminary data, as we do not have the confirmation of mTFP targeting only the mitochondria or of the expression levels of the probe. According to the signal captured, it is from 2 h after induction when aggregations can be observed. There is also a dramatic loss of intensity, even if mTFP has been described as resilient to changes in pH (Ai *et al.*, 2006). From this time point on, the signal stops being uniform and the formation of punctate aggregations starts. The aggregates are present all over the tube with a slight accumulation in the tip compared with the shank area. In subsequent hours, the aggregation areas seem to be reduced presenting bigger spaces without signal (Figure 2.12). Assuming that mTFP is exclusively accumulated in mitochondria, this data would suggest the loss of the original disposition and the formation of aggregates as a late response after the SI induction.

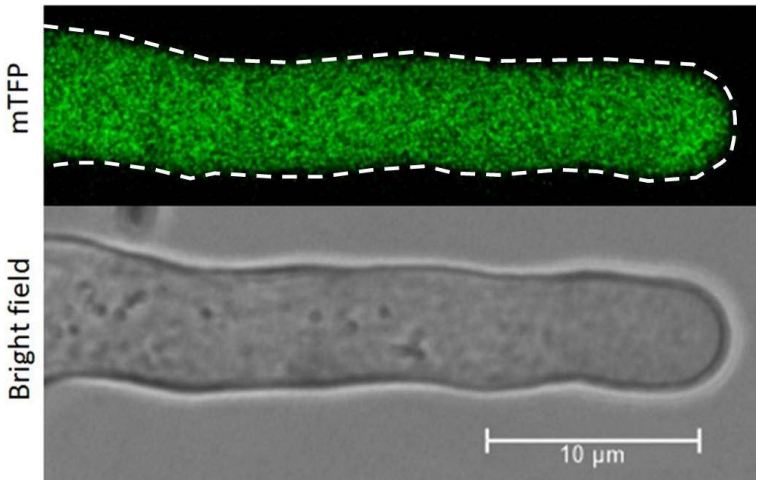

Figure 2.11. Emission of mTFP tagged to mitochondria in normal conditions. Before adding $PrpS_1$ the signal captured is uniform all along the tube.

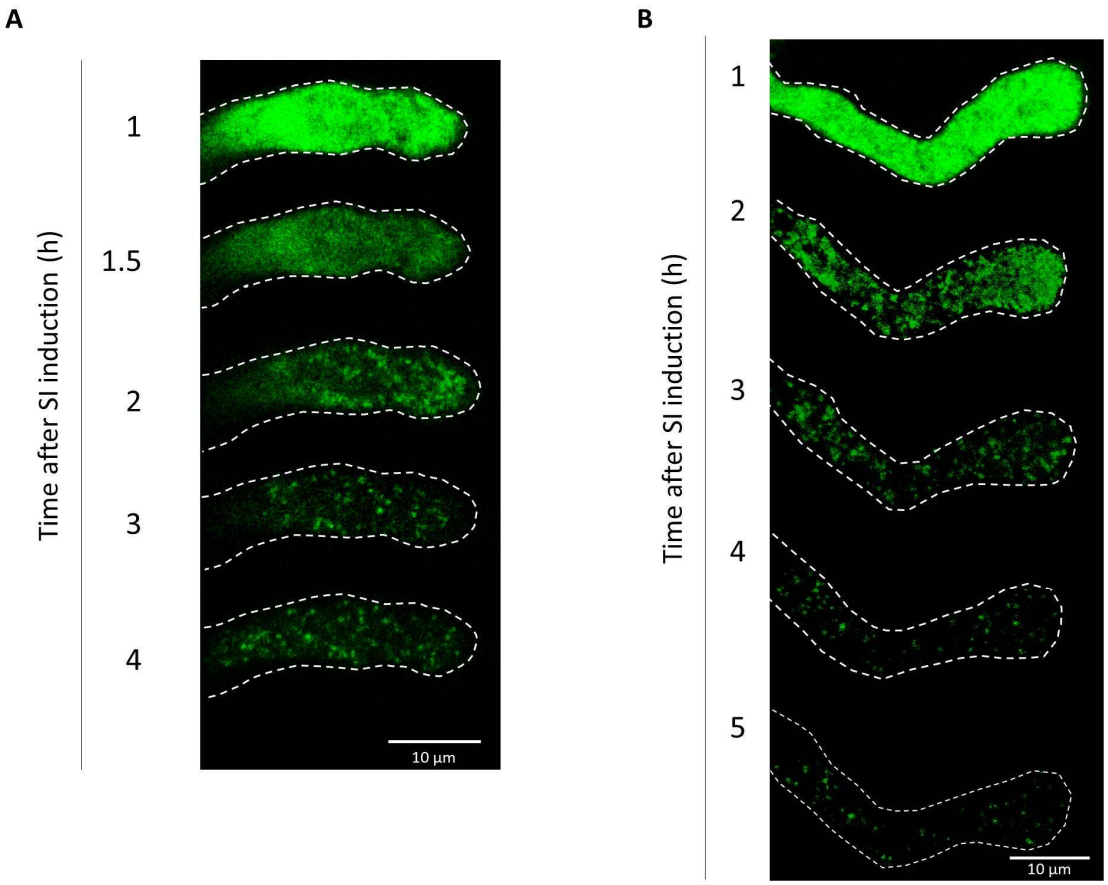

Figure 2.12. Mitochondria phenotype after SI induction in *Arabidopsis* pollen tubes. In those two typical examples, the pollen tube is defined with a dotted white line. Mitochondria tag mito-mTFP signal (green) at five different time points after induction. (A) The timepoint 1.5 shows that there is an intermediate stage between the uniform appearance and the mitochondria aggregations. (B) After 5 h the mTFP signal still indicates the presence of aggregations.

2.3.5. Nuclear disruption

The degradation of the nuclear envelope is one of the two events related to PCD that were tested in this thesis. The information we have related to changes in the nucleus during the *Papaver* SI response is about DNA integrity. In this case, to observe when the nuclear membrane loses its integrity, observations were performed with *Arabidopsis* pollen grains coexpressing PrpS and tdTomato with a nuclear-localised signal. After triggering SI with the cognate PrsS the images were captured every 20 minutes.

According to the observations presented here, the number of intact nuclei starts to decrease slightly by 10 % 1h after SI inductions. There is a steady progression of the percentage of nuclei disrupted, reaching 30% after 3h and it takes 5 h before more than 50 % of the nuclei are disrupted. The standard deviations for the measurements where rather large from 4h and onwards (Figure 2.13), reflecting big differences between the observations of different samples. Note that there is no control date (untreated pollen) since in absence of the cognate PrsS the pollen grains germinate and the pollen tubes can elongate *in vitro* for hours (Lin *et al.*, 2015).

These data suggest that in the PCD pathway that occurs in incompatible *Arabidopsis* tubes, nuclear envelope disruption is one of the late responses, and is not tightly linked to other SI-PCD hallmarks. As there is no comparable information in *Papaver* so far, the use of probes to combine in *Arabidopsis* the time points for DNA fragmentation to the presence or absence of the nuclear envelope would be an interesting further analysis.

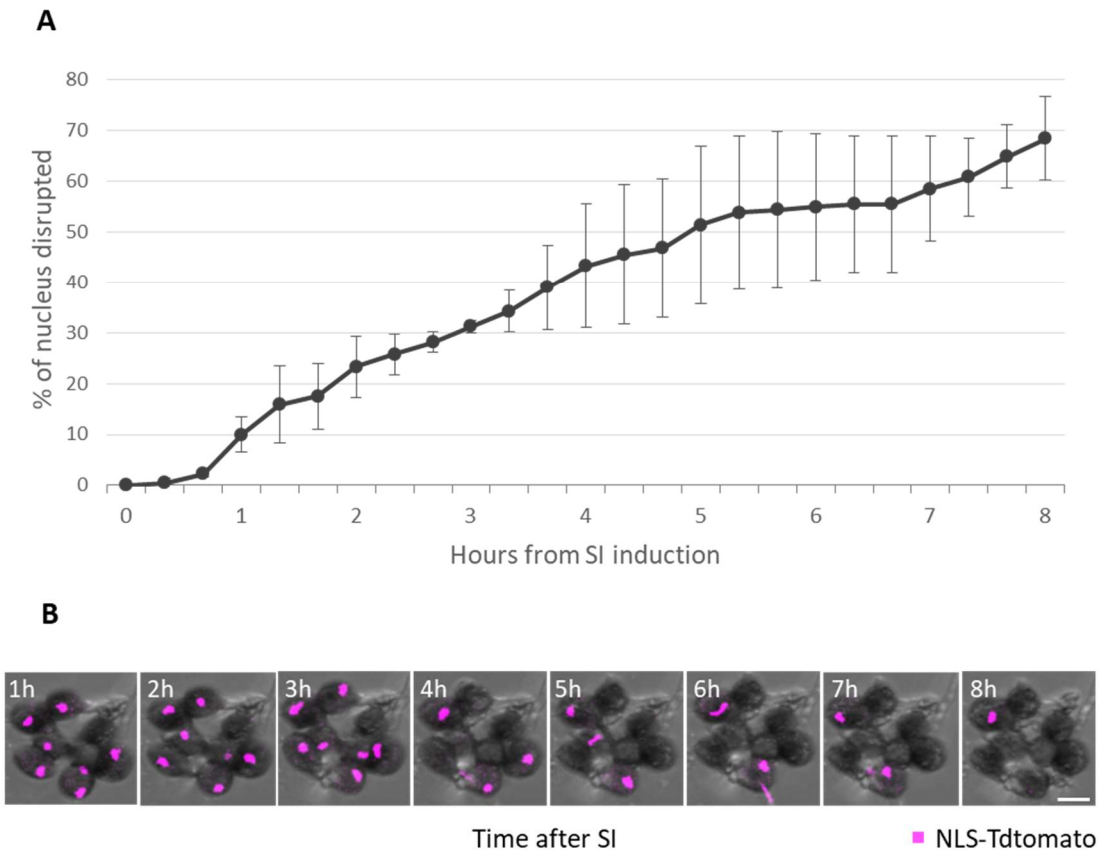

Figure 2.13. Nuclear disruption in *Arabidopsis* pollen. (A) Percentage of male germ units disrupted every 20 minutes (8 rep, n total = 170). Bars represent the standard deviation. (B) Example of time-lapse images, showing nuclear disruption after SI induction, indicated by the loss of NLS–tdTomato signal. Superposition of PMT Trans Bright field channel (greyscale) and NLS-tdTomato signal (magenta). Scale bar = 20 µm.

2.3.6. Caspase-3 like activity

In plants, there are enzymes that display caspase-like activity, as defined by the action of caspase-indicator probes and inhibitors (Sueldo and van der Hoorn, 2017). The presence of caspase-3 like enzymatic activities, which is a hallmark of PCD, was identified in *Papaver* SI (Thomas and Franklin-Tong, 2004; Bosch and Franklin-Tong, 2007).

To test the occurrence of caspase-3 like activity in the heterologous SI response in *Arabidopsis*, the fluorescent probe Ac-DEVD-AMC was used, as its emission can be captured in the presence of caspase-3/DEVDase activity. As a control, the caspase-3 inhibitor Ac-DEVD-CHO blocked the caspase-3-like activity, confirming that the emission observed resulted from the action of this kind of enzyme.

Here we show the results from capturing the emission of AMC up to 8 h after SI induction. From our observation, a significant increase in AMC signal compared with the respective control (pollen pre-treated with the inhibitor Ac-DEVD-CHO) was observed at 4 hours and onwards after SI induction (*P*-values of $1.538 \cdot 10^{-5}$, $< 2.2 \cdot 10^{-16}$, $1.16 \cdot 10^{-10}$, $< 2.2 \cdot 10^{-16}$ and $< 2.2 \cdot 10^{-16}$, for 4h, 5h, 6h, 7h, and 8h, respectively). After 7 h, the activity reaches the maximum value for the mean of the fluorescent AMC signal values. However, for every time point a wide range of fluorescence values was obtained due to the diversity of the temporal SI-PCD profiles when observing different pollen (Figure 2.14A), which can be seen when a bunch of pollen was imaged over time (Figure 2.14B).

From this data, we can confirm that, similar to *Papaver* SI, the incompatible response triggers PCD in *Arabidopsis* pollen grains, involving enzymes that exhibit a caspase-3-like activity.

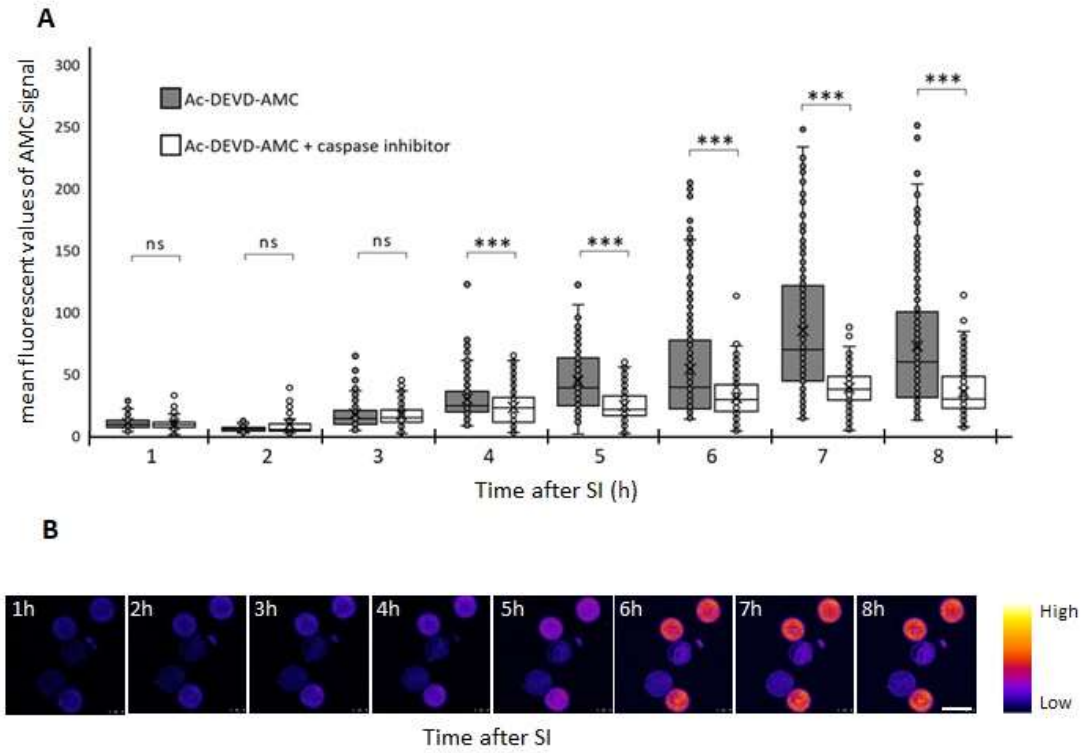

Figure 2.14. DEVDase/Caspase-3-like activity observed after SI induction of incompatible *Arabidopsis* pollen. (A) DEVDase/Caspase-3-like activity quantification from the measurement of AMC fluorescence in pollen grains during the SI response in the absence and presence of the caspase-3 inhibitor Ac-DEVD-CHO (n = 100–350). The error bars indicate the standard deviation. ns = $p>0.05$, *** = $p<0.001$. (B) Example of time-lapse images, showing the presence of DEVDase/caspase-3 activity in pollen grains after SI induction, indicated by the AMC fluorescent signal. Scale bar = 20 µm.

2.4. Discussion

Studies on *Papaver* SI have uncovered a complex and elaborate network of events triggered by SI leading to pollen tube growth arrest and PCD and have established it as one of the best understood SI systems in the plant kingdom. However, its limited genetic resources represent a bottleneck in advancing this model system further. The functional transfer of the *Papaver* SI module (PrpS and PrsS) in *Arabidopsis* pollen and pistil, respectively, prevents self-seed set, effectively rendering *Arabidopsis* self-incompatible (Lin *et al.*, 2015). The availability of *Arabidopsis* plants expressing PrpS provides opportunities to further advance our knowledge on SI-induced signalling networks leading to PCD using genetic approaches that are currently not possible in *Papaver*. The engineered *Arabidopsis* SI lines, expressing the male determinant $PrpS_1$ and genetically encoded fluorescent probes, provide a robust system to monitor SI-induced cellular alterations over time when cognate $PrsS_1$ is added to *in vitro* growing pollen (Wang *et al.*, 2020).

According to their distance in time relative to the SI induction, events can be classified as early or late. The only early event analysed in this chapter is related to the changes in the $[Ca^{2+}]_{cyt}$ after cognate $PrpS_1$-$PrsS_1$ interaction. The line used for this experiment is defined as a "fast" line due to its high $PrpS_1$ expression level that makes this line to have a fast SI response when compared with some of the other *Arabidopsis* SI lines (Wang *et al.*, 2020). Setting aside the specific time points after SI-induction, a rapid increase of the cytoplasmic Ca^{2+} concentration was observed after the tube elongation stopped, although growth arrest appeared to be preceded by a small Ca^{2+} spike. Similar to *Papaver*, results in *Arabidopsis* show the presence of a rapid increase in Ca^{2+} that seems to present differences between the tip and shank region. Like reported for *Papaver* SI (Franklin-Tong *et al.*, 1997), we observed that the increase in Ca^{2+} in the tip region was higher, especially at the beginning of the response. It sustains the role of Ca^{2+} as a second messenger in SI (Franklin-Tong *et al.*, 1993). In addition, for further analysis, it would be interesting to use the line with the genetically encoded Ca^{2+} indicator GECI that can be used to estimate local steady-state $[Ca^{2+}]_{cyt}$ (Waadt *et al.*, 2017). However, the calcium reporter Arabidiopsis SI line presented in this chapter is still a powerful tool, that can be further used to elucidate if there is a causative relation

between the highlighted changes in $[Ca^{2+}]_{cyt}$ and other events taking place during the SI response.

Alterations in vacuolar morphology and integrity, observed in *Papaver* (Wilkins *et al.*, 2015), could possibly contribute to the pH drop observed early after SI. Analysis of the vacuoles after SI induction in the *Arabidopsis* system revealed a set of different morphologies and mapped their temporal progression, providing new details about vacuolar changes during the SI response. However, it remains unclear if these vacuolar alterations play a role in the SI-induced pH drop.

Interested in organelles that may be involved in the SI-PCD response, we looked at the organization of vacuoles and mitochondria. Vacuoles presented seven types of morphologies including the reticular distribution previously observed in *Arabidopsis* pollen tubes when growing in normal conditions (Hicks *et al.*, 2004). In contrast, the signal obtained with the genetically encoded mitochondrial marker was homogeneous, with a considerable reduction of the intensity from 2 h after SI induction and the presence of aggregations that may well deserve further analysis. However, here we used mito-mTFP and its specificity in detecting mitochondria first needs to be confirmed by using other genetically encoded probes or fluorescent dyes (Liu et al., 2017; Gökerküçük et al., 2020)

Two late events related to PCD were followed, nuclear disruption and caspase-3-like activity. In both cases, results obtained confirm that pollen tubes ultimately undergo PCD after the cognate PrpS and PrsS interaction. The last late event analysed, which is also one of the hallmarks related to PCD, is the caspase-like activity. It was previously established that a caspase-3-like activity is critical for the PCD process in *Papaver* after SI induction of incompatible pollen tubes. An increase of caspase-3-like activity was also observed in *Arabidopsis* pollen grains, albeit the increase was a little slower than results obtained in *Papaver* (Bosch and Franklin-Tong, 2007). It would be interesting to eventually correlate the data obtained about the caspase-3-like activity with the nuclear envelope breakdown, using the line with the genetically encoded $PrpS_1$ _TdTomato-NLS treated with the probe Ac-DEVD-AMC.

2.4.1. Cytosolic calcium increase

In the *Papaver* SI system, the modulation of cytoplasmic calcium in the SI response has been widely confirmed. Initially, it was established by microinjections of the calcium indicator Calcium Green-1 dye in *Papaver* pollen tubes. The data obtained from this indicator suggests that calcium may have a second messenger role in the SI response and being closely associated with the process involved in stopping the pollen tube growth. This arrest of the pollen tube growth was also obtained when the $[Ca^{2+}]_{cyt}$ was increased artificially with caged Ca^{2+} (Franklin-Tong *et al.*, 1993). The use of Calcium Green-1 dye also allowed to confirm that the presence of the cognate PrsS is enough to trigger an increase in Ca^{2+} signal in *Papaver* SI pollen (Franklin - Tong *et al.*, 1995). To obtain further information about it, the dye fura-2 dextran was used to microinject *Papaver* pollen tubes and the $[Ca^{2+}]_{cyt}$ distribution during the SI response was observed using microscopy. It showed that the tip area concentrates the higher gradient of the $[Ca^{2+}]_{cyt}$ compared with other areas in the tube (Franklin-Tong *et al.*, 1997) suggesting that calcium channels present in the apical area are especially activated in this response.

In this chapter, using the genetically encoded YC3.6 sensor, we could also monitor the changes in $[Ca^{2+}]_{cyt}$ during the SI response in *Arabidopsis* pollen tubes expressing PrpS. From this data, we confirm that SI induction also triggers $[Ca^{2+}]_{cyt}$ increase in the *Arabidopsis* SI system. However, even if the pattern observed is constant, we found heterogeneity in the timing for some of the hallmark events (elongation stop, maximum $[Ca^{2+}]_{cyt}$ and cytoplasmic streaming stop). This heterogeneity may be due to variations in the expression level of $PrpS_1$ in different pollen tubes, which is directly proportional to the speed of the SI response (Wang *et al.*, 2020). Also, in growing root hairs, there are differences in the pattern of $[Ca^{2+}]_{cyt}$ fluctuations. This was considered to be due to the variability in the growth rate of individual cells (Wymer *et al.*, 1997).

There are increments and decreases in [Ca2+]cyt during the first three minutes after SI induction in the tip of both Arabidopsis and Papaver pollen tubes. Related to these $[Ca^{2+}]_{cyt}$ changes, there is an interesting aspect observed in the *Papaver* SI response, that occurs also in the heterologous *Arabidopsis* system. The presence of a transient rise in [Ca2+]cyt is followed by a second more pronounced and long-lasting

increase. When this was observed in *Papaver*, the number of cases was considered too little to consider this event as a fact (Franklin-Tong *et al.*, 1993). However, it is remarkable that this phenomenon was observed in all of the tubes analysed for SI-induced calcium modulations in this chapter. In the *Arabidopsis* system, this spike in $[Ca^{2+}]_{cyt}$ is immediately reduced before the $[Ca^{2+}]_{cyt}$ begins constantly increasing, defining a curve that reaches its maximum after 6.5 minutes on average after SI induction. The $[Ca^{2+}]_{cyt}$ presents a uniform increase in the shank region in *Arabidopsis*, similar to *Papaver* (Franklin-Tong *et al.*, 1997).

Related to external perturbations, here we show that the $[Ca^{2+}]_{cyt}$ is not affected by the addition of an external liquid medium, even when it has a temperature 20 ^{o}C lower than the AtGM in which the tubes are growing. It reinforces the data obtained from this *in vitro* SI induction since the $PrpS_1$ added to trigger SI is kept at 4 ^{o}C in order to maintain the storage conditions. Not only the temperature but the motion in the growth medium when adding a new component was suspected of causing variation in $[Ca^{2+}]_{cyt}$ as a defence response of these stresses. It was observed that *Arabidopsis* leaves present Ca^{2+} increase that is spread across the organ when wounded (Toyota *et al.*, 2018) but pollen tubes do not show any calcium-related response.

In addition, our data give information about changes in the cytoplasmic streaming. The cytoplasmic streaming is in charge of transporting nutrients and metabolites and positioning of organelles. It presents a bidirectional transport in normal conditions, often referred to as reverse fountain-like streaming, and leads the male germ unit forward in the tube (Chebli *et al.*, 2013). Disruption of the actin microfilaments causes an irreversible change and the streaming completely stops (Justus *et al.*, 2004). It is already known that calcium has an important role in controlling the cytoskeleton structure and activity (Hepler, 2016). Our data suggest that the $[Ca^{2+}]_{cyt}$ increase as a consequence of the SI response may cause the disruption of the microfilaments.

The data presented in this chapter introduce further information about calcium participating as a second messenger in the *Arabidopsis* SI system. However, in contrast with the use of dye microinjections, we did not quantitatively measure the changes in Ca^{2+} since we were not able to perform pollen tube observations with known $[Ca^{2+}]_{cyt}$

for generating a standard curve to compare the samples with. To obtain absolute measures for SI-induced changes in $[Ca^{2+}]_{cyt}$, as opposed to relative differences in ratios, the inclusion of a standard curve should be considered in future experiments, taking into account the complexity of being accurate, as certain changes in $[Ca^{2+}]_{cyt}$ immediately trigger PCD. In addition, the YC6.3 indicator expressed together with a fluorescent protein-tagged to actin filaments would give us interesting information about the relationship between changes in $[Ca^{2+}]_{cyt}$ and actin dynamics and architecture. The co-expression of the YC6.3 indicator with a pH indicator may give us interesting temporal and spatial information about a possible relationship between changes in $[Ca^{2+}]_{cyt}$ and pH, since these are amongst the earliest observed physiological changes in the *Papaver* and *Arabidopsis* SI response (Behera *et al.*, 2018; Wang *et al.*, 2020). Fortunately, the *Arabidopsis* SI system would let us address this in the future.

2.4.2. Vacuolar disorganisation

Here we evaluated the SI-induced changes in vacuolar morphology. Untreated *Arabidopsis* pollen tubes growing *in vitro* coexpressing $PrpS_1$-GFP and VAMP711-mCherry showed a reticulate vascular structure similar as observed previously in *Arabidopsis* with the genetically encoded tonoplast-specific marker, δ-TIP-GFP (Hicks *et al.*, 2004). As previously observed in *Papaver* (Wilkins *et al.*, 2015), also in the heterologous *Arabidopsis* SI model, this reticulate morphology is lost after SI induction.

Labelling of vacuoles of *Papaver* pollen tubes with Carboxy-DCFDA showed small aggregations from 15 min after SI, similar but not the same to the ones described in this chapter for *Arabidopsis* as globular and compact. In *Papaver,* these structures are present but with an appearance of aggregate instead of compact. Those punctate signals appear to decrease in size in SI *Papaver* tubes and most of the signal was lost between 1 and 2 h after SI (Wilkins *et al.*, 2015). This is different from what we observed in *Arabidopsis*, where vacuolar morphologies changed throughout the 4h monitoring period after SI induction but there was no apparent loss of the VAMP711-mCherry signal. This difference is most likely since carboxy-DCFDA labels the vacuolar lumen and hints of increasing levels of background fluorescence at later time-points in *Papaver* pollen tubes, perhaps due to the low pKa of 4.8 of this pH-sensitive dye. Labelling the vacuolar membrane by the transient expression of δ-TIP-GFP in *Papaver* pollen, showed

a similar reticulate pattern as seen with carboxy-DCFDA 90 min after SI induction. However, vacuolar changes were not evaluated beyond ~90 min after *Papaver* SI (Wilkins *et al.*, 2015). Next to the data presented here, it would be interesting to combine the genetically encoded WAMP711-mCherry indicator with the Carboxy-DCFDA probe to obtain images to elucidate the morphology of the vacuoles having information simultaneously of both lumen and tonoplast.

Furthermore, due to the acidic content of the vacuoles (Shen *et al.*, 2013), testing the relation between the changes in cytosolic pH and vacuolar integrity would provide us with valuable information to better understand the SI-PCD response. This observation could be made by triggering SI in incompatible *Arabidopsis* pollen tubes coexpressing the pH reporter pHGFP and the tonoplast indicator WAVE9R. This line could be followed under the confocal microscope to capture live-cell images before and during the SI-PCD response.

2.4.3. Mitochondria

The implication of mitochondria in cell death pathways has been evidenced in animals and plants (Bras *et al.*, 2005), especially in plants during the hypersensitive response (Lam *et al.*, 2001). One hypothesis is that plant mitochondria increase the concentration of reactive oxygen species (ROS) (Lam *et al.*, 2001; Wang *et al.*, 2008). However, the increase in ROS in the *Papaver* SI response is observed in the first minutes after Si induction (Franklin-Tong, 2014), while the mitochondrial morphology alterations were observed with transmission electron microscopy 1 h after SI induction. This alteration related to the mitochondrial morphology was defined as “swollen”. The swelling or condensation of mitochondria has been reported in the morphological changes frequently associated with PCD (Geitmann *et al.*, 2004). In addition, it was also observed in *Papaver* that the release of cytochrome c, produced by the loss of mitochondrial integrity, has its maximum 2 h after SI (Thomas and Franklin-Tong, 2004).

In order to observe if changes in the mitochondrial distribution are also found in *Arabidopsis*, we used the genetically encoded mitochondrial tag mito-mTFP. The results obtained do not resemble what is observed in *Papaver* with the MT-CMXRos probe (Bosch *et al.*, 2010), as the mito-mTFP signal does not present the punctate structures

indicating the location of the individual mitochondria previously observed with MT-CMXRos in *Papaver*. According to the results in *Papaver*, when observed with a transmission electron microscope, the cytoplasm of At-SI pollen grains and tubes should present a cytoplasm densely filled with mitochondria in normal conditions (Geitmann *et al.*, 2004). That can be the reason why the signal appears uniformly distributed for all the tubes under the confocal microscope. However, our observations are quite different to the ones obtained from *Papaver* and also *Arabidopsis* when using the commercially available probes for mitochondria such as the JC-1 dye, which is a mitochondrial membrane potential probe, and Mitotracker Red CMXRos (MT-CMXRos) respectively (Bosch *et al.*, 2010; Colaço *et al.*, 2012). In our case, the signal is more homogeneously distributed in the pollen tube cytoplasm, indicating that the emission we captured was not specific for the mitochondria. Another hypothesis is that the extra signal observed when compared with the images previously published could also be due to the emission of non-functional mitochondria, as they do not accumulate MT-CMXRos. In addition, the images obtained for At-SI pollen tubes in this chapter report dramatic changes in mitochondria 2 h after induction. However, it is required to consider that the images shown are preliminary data, as we do not have the confirmation of mTFP targeting only the mitochondria or the expression level. Further analysis with higher magnification images would be interesting and double labelling with MT-CMXRos or JC-1 not only in pollen tubes but also in other plant cells since this SI system was recently shown to be fully functional when expressed in vegetative cells (Lin *et al.*, 2020).

We captured the signal of the genetically encoded fluorescent protein mTFP (pNTP303::Mito-mTFP) that reports the mitochondrial location in the tube. The images obtained were so different from those published in Papaver pollen when using the mitochondrial probe Mitotracker MT-CMXRos® that we consider hardly comparable (Figure 2.15). The mitochondrial signal observed in *Papaver* showed a considerable co-localization to caspase-1-like/YVADase signal suggesting that in normal growing pollen there is an association between them (Bosch *et al.*, 2010). In addition, when the tubes were treated with PrsS, the YVADase signal became more diffuse after 75 min even if the YVADase activity in pollen tube extracts did not present changes after SI induction (Bosch *et al.*, 2010).

In *Arabidopsis* we observed a progressive change and some loss in the signal of Mito-mTFP, however, remaining bright with certain dots being observed that may be indicative of the location of intact mitochondria. More observations with this and also other mitochondrial probes are necessary to confirm that the structures observed are indeed mitochondria. If so, the mitochondria would be arranged throughout the tube during normal growth and would form aggregations as time passes from the SI induction.

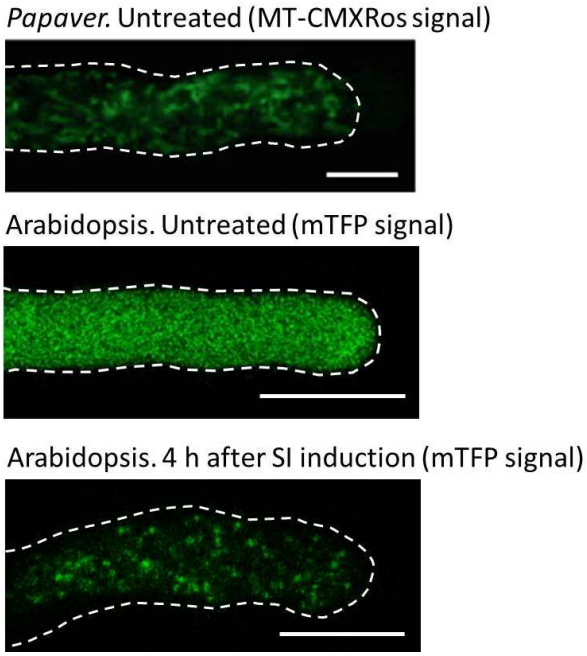

Figure 2.15 Different phenotypes observed when detecting the mitochondria location. The images are described as "Untreated" when SI was not induced. Signal captured (green), plasma membrane (discontinuous white line). The untreated Papaver pollen tube incubated with MT-CMXRos was adapted from (Bosch et al., 2010). Bar = 10µm.

2.4.4. Nuclear disruption

The dismantling of the nuclear envelope and the fragmentation of DNA is part of the cell death process described in plants and in animal apoptosis (Taylor and Hepler, 1997; Gunawardena and McCabe, 2015). Since the nuclear integrity loss is one of the main pathways taking place during apoptosis (reviewed in Reape *et al.*, 2008), we assessed SI-induced changes in nuclear integrity by inducing SI to *Arabidopsis* pollen grains coexpressing $PrpS_1$ and the fluorescent protein TdTomato with NLS. Monitoring the samples for 8 h allowed us to obtain temporal information about the disruption of the nuclear envelope after SI induction.

Related to nuclear integrity, the timepoints of DNA fragmentation have been studied in *Papaver* SI response using the *in situ* fragment end labelling (FragEL) technique. The disruption of the nuclear envelope in Papaver SI pollen has not been shown to date. Besides, instead of pollen grains, the published data shows the evidence for nuclear DNA fragmentation in incompatible *Papaver* pollen tubes. The presence of DNA fragmentation starts to differ from the untreated pollen grains from 4 h after SI and it continues up to 14 h after induction. It takes 8 h from SI induction to observe 50 % of the samples with the nuclear DNA fragmented (Jordan *et al.*, 2000). In *Arabidopsis*, we observed the absence of TdTomato signal from 1 h after SI, suggesting that the nucleus envelope integrity loss is quick. In our case, the 50 % average of the grains with the nucleus disrupted is observed after 5 h of induction, which is also faster than the time point of 50% DNA fragmentation in *Papaver*.

In addition to DNA fragmentation, *Papaver* pollen tubes were stained with DAPI to test plasma membrane permeability. It showed a constant increase of DAPI-stained nuclei, suggesting the permeability of the plasma membrane, reaching 75% after 4 h which coincides in time with the first detection of DNA fragmentation (Jordan *et al.*, 2000). It would be interesting for further studies to evaluate the relation between the membrane permeability, DNA fragmentation and nuclear envelope disruption in *Arabidopsis*. Also, the combination of the *in situ* technique transferase UTP-nick end labelling (TUNEL) in the NLS-TdTomato pollen grains to check if the DNA fragmentation and nuclear envelope rupture are correlated, or if one happens before or after the other may be of interest. As a starting point, the data presented here show that in *Arabidopsis* the response is considerably faster compared with *Papaver*, although in both cases it is confirmed that nuclear disintegration is part of the SI response and also in both cases it triggers PCD.

2.4.5. Caspase activity

In plants, there are several proteases that display caspase-like activities (Sueldo and van der Hoorn, 2017). In this thesis we focussed on DEVDase/caspase-3-activity, which had been confirmed to be present in the SI response in *Papaver* (Thomas and Franklin-Tong, 2004; Bosch and Franklin-Tong, 2007).

Here we provide evidence that heterologous SI in *Arabidopsis* likewise induces DEVDase/Caspase-3-like enzymatic activity using the Ac-DEVD-AMC probe, which can be inhibited by pre-treatment of the caspase-3 inhibitor Ac-DEVD-CHO. These results confirm that PCD is taking place after SI induction in incompatible *Arabidopsis* pollen tubes. In Papaver SI, the caspase-3/DEVDase activity peaked 5 h after SI-induction (Bosch *et al.*, 2007), while in the At-SI system peak activity was reached 2 h later, 7 h after SI induction. There are several possible explanations for the temporal delay in DEVDase activity observed in At-SI when compared to observations in *Papaver*. Firstly, the temporal profiles in *Papaver* were monitored using the Ac-DEVD-AMC probe in pollen tube protein extracts for plate reader assays. In our case, the probe was used for imaging fluorescence in *Arabidopsis* pollen grains expressing $PrpS_1$. This line expressing $PrpS_1$ without any fluorescent tag, is a so-called "slow" line (Wang *et al.*, 2020) which may therefore have a slower SI-response then observed in *Papaver*. However, the overall tendency observed in both cases is similar, showing an increase of the DEVDase activity that, even if in the slow *Arabidopsis* line the maximum was observed with 2 hours delay comparing with *Papaver*. These data confirm that a cognate $PrpS_1$-$PrsS_1$ interaction triggers DEVDase/caspase3-like activity in At-SI, and therefore, programmed cell death.

2.5. Experimental design and preliminary work in further investigating the cellular characterization of this system

Combining two or more fluorescent protein markers in a single tube allows us to better understand the relation between different events (Figure 2.16). As mentioned in chapter two, the genetically encoded tonoplast marker WAVE9R combined with a pH indicator would give us interesting information about the relation between the vacuolar organization and the changes on pH. We already have preliminary data with the genetically encoded cytosolic pH sensor pHGFP (Moseyko and Feldman, 2001). This sensor is excited with 405 nm and 488 nm. Its emission is collected separately between 500 nm and 530 nm. To obtain the pH value, the fluorescent intensity ratios from the 405 nm and 488 nm excitation channels (R405/488) were quantified and compared with a standard curve defining pH values relative to the R405/488 with known pHs using propionic acid. The WAVE9R signal was captured as explained in chapter two. Lines like

WAVE9R and the treatment of pollen grains or tubes with commercial probes, such as Lysotracker dyes that allow us to potentially obtain the information about the pH in the lumen of the vacuole (Johnson *et al.*, 2016), opens new research horizons in this SI system.

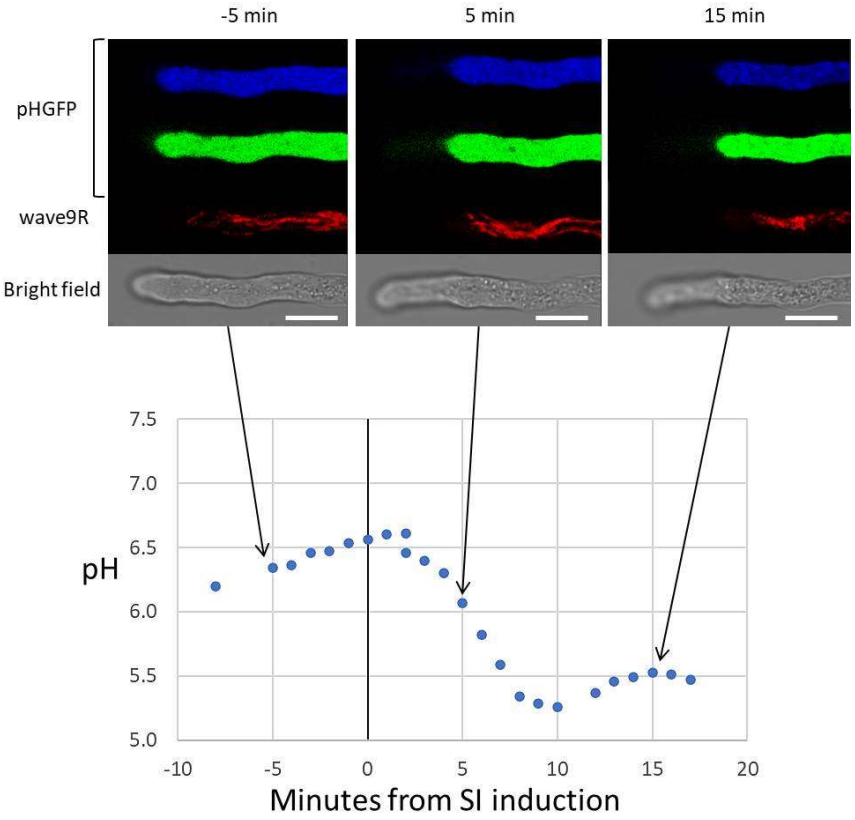

Figure 2.16. Example of the preliminary data obtained when combining two genetically encoded sensors. The cytosolic pH could be measured using the pHGFP sensor (blue and green) obtaining a pH drop after SI induction from ~6.5 to ~5.5. The vacuolar structure is observed with the signal of WAVE9R that contains mCherry attached to the tonoplast (red). The vacuolar structure presents the reticular morphology A described in wild-type or non SI-induced pollen tubes. However, after induction, it appears disorganized presenting globular structures.

2.6. Conclusion

Using genetically encoded fluorescent probes, the results in this chapter confirmed and evaluated a range of different events known to be induced in *Papaver* SI and confirm the robustness of this heterologous system to study key events involved in *Papaver* SI. The use of these genetically encoded markers allows us to compare it with the *Papaver* SI response, and to contribute to a more complete understanding of the *Papaver* SI system.

Chapter three. SI-PCD transcriptome profiling

3.1. Introduction

Although chapter two characterised some of the cellular and subcellular events that occur during the self-incompatibility (SI) response-induced programmed cell death (PCD), there are knowledge gaps related to the molecular mechanisms involved in this response. The transcriptome analysis can be a useful tool to identify genes involved in the *Papaver* SI response. It was previously shown that treatment of *Papaver* pollen with the transcription inhibitor actinomycin D (RNA polymerase II inhibitor) partially alleviated the SI response. This suggested that the SI response involves the induction of gene expression (Franklin-Tong *et al.*, 1990). With the limited genetic resources available for *Papaver*, the availability of the heterologous *Arabidopsis* SI system that exhibits all of the hallmark features of *Papaver* SI (Lin *et al.*, 2015; Wang *et al.*, 2020) provides us with the opportunity to follow a transcriptome profiling approach aimed at identifying genes involved in SI-PCD.

Before, genes associated to cell death in plants were successfully identified by analysing the transcriptome data. For example, in the lateral root cap, specific nucleases were found to be controlled transcriptionally by ANAC033/SOMBRERO (Fendrych *et al.*, 2014). Analysing the transcriptome of pollinated *Arabidopsis* pistils by RNA sequencing (RNAseq), we obtained quantitative information of the mRNA molecules in this part of the flower, regardless of whether they are translated into protein or not (Blumenberg, 2019).

Transcript profiling of pollinated pistils utilizing the heterologous *Arabidopsis* SI system offers the advantage of more reliably mimicking the *in vivo* situation of *Papaver* SI, as compared to utilizing the *in vitro* pollen tube SI assays. However, a big challenge of using pollinated pistils for transcript profiling is to distinguish between transcripts originating from pollen and the pistil.

The ecotypes Landsberg and Columbia were selected for transcript profiling and the time points 0.5 and 2 HAP were considered the most appropriated to investigate the early and late stages of the SI response. The experimental design of the transcriptome profiling experiment presented in this chapter should allow us to obtain information about the transcriptome in diverse cases to identify differentially expressed genes

during SI and SC pollinations. There are three main comparisons carried out: firstly the variances in the transcriptome when SI compared to SC situations, secondly the differences between the early and late SI response proximal to PCD, furthermore an attempt to identify differences in expression levels between pollen and stigma. Here we present the differences between SI and SC scenarios and the transcripts identified that might be related to the early and late response without distinguishing between stigma and pollen. The database generated will be used in the future to address the third question, the identification of tissue-specific candidate genes.

3.2. Materials and methods

To increment the differences between the transcriptome of pistil and pollen cells after pollination, two natural *Arabidopsis* variants (ecotypes) were used. Three ecotypes represent the most commonly used lines for research: Landsberg *erecta* (L*er*), Columbia (Col), and Wassilewskija (Ws). The phenotypic differences between them are the consequence of their genetic variability. When a set of morphological traits were analysed between these three ecotypes, it was found that aspects such as seed shape, root structure and rosette morphology were more similar between Ler and Ws than Ler compared to Col (Passardi *et al.*, 2007). L*er* and Col are the most different ecotypes when analyzing morphological, cellular and molecular attributes. More importantly, genome sequence analysis of different *Arabidopsis* ecotypes revealed that Ler is one of the lines showing highest SNPs density with Col-0, therefore, these two ecotypes were used for our transcriptome studies in order to maximize the likelihood of identifying candidate pollen genes involved in the SI-PCD response.

Col and Ler, either wild type or expressing PrpS1 or PrsS1 in pollen or stigma respectively, were used to perform four different crosses. Thus, the parental lines combined to perform the four pollination scenarios are Ler wild type (Ler_0), Ler expressing PrsS1 (Ler_PrsS1), Col wild type (Col_0) and Col expressing PrpS1 (Col_PrpS1). Ler plants were emasculated and pollinated with Col pollen (Figure 3.1).

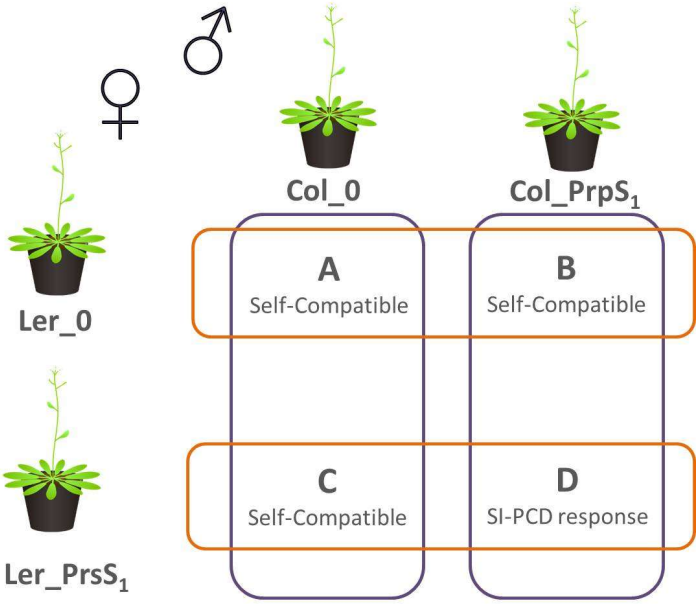

Figure 3.1. Pollinations performed. Stigmas of Arabidopsis plants ecotype Landsberg (Ler) were pollinated with the pollen of ecotype Columbia (Col). The pollination type A is carried out with Ler wild type sigmas and Col wild type pollen. For the pollination type B, the stigma is Ler wild type but the pollen grains are Col expressing $PrpS_1$. In the pollination type C, the stigma is Ler expressing $PrsS_1$ and the pollen grains are Col wild type. The only self-incompatible case is the pollination type D as both determinants are present, in which Ler stigmas expressing $PrsS_1$ are pollinated with Col pollen grains expressing $PrpS_1$.

The four types of pollinated stigmas shown in Figure 3.1 were collected at 0,5 and 2 hours after pollination (HAP). Both time points were selected taking into account the information we already have about the pollen tube development in combination with the result from a set of pollination assays described below. It has been well described that the SI response in *Papaver* triggers a signalling cascade that arrests pollen tube elongation and leads to PCD (Thomas and Franklin-Tong, 2004; Wilkins *et al.*, 2014). The pollen tube growth inhibition was also observed in SI *Arabidopsis* plants (Lin *et al.*, 2015) and we showed that this response triggers PCD too in the previous chapter of this thesis. However, it takes hours from one event to the other. The pollen tube growth inhibition rapidly occurs after the cognate PrpS-PrsS interaction, while PCD is only detected hours later.

3.2.1. Selection of the best timepoints to compare transcriptomes

A set of pollination assays were performed to identify the best possible time-points to collect pollinated pistils for transcriptome profiling. For this, Ler_PrsS$_1$ stigmas were pollinated with Col_0 and Col_PrpS$_1$ and harvested at 0.5, 1, 2 and 3 HAP. The samples were fixed and stained with aniline blue and observed with a fluorescence microscope. The images obtained did not show differences between SI and SC pollinations at 0.5 HAP, which suggests that pollen adhesion, hydration and germination in SI and SC pollinations are similar (Figure 3.2). However, at 1 HAP longer pollen tubes are observed after a SC pollination as some tubes are observed to penetrate through the stigma and reach the style, while in SI cases none of the tubes reach the style at that time point. The differences between SI and SC are bigger at 2 and 3 HAP, since the SI pollen tubes are never found further than the upper region of the style, but Col_0 pollen tubes show rapid progress through the transmitting tract.

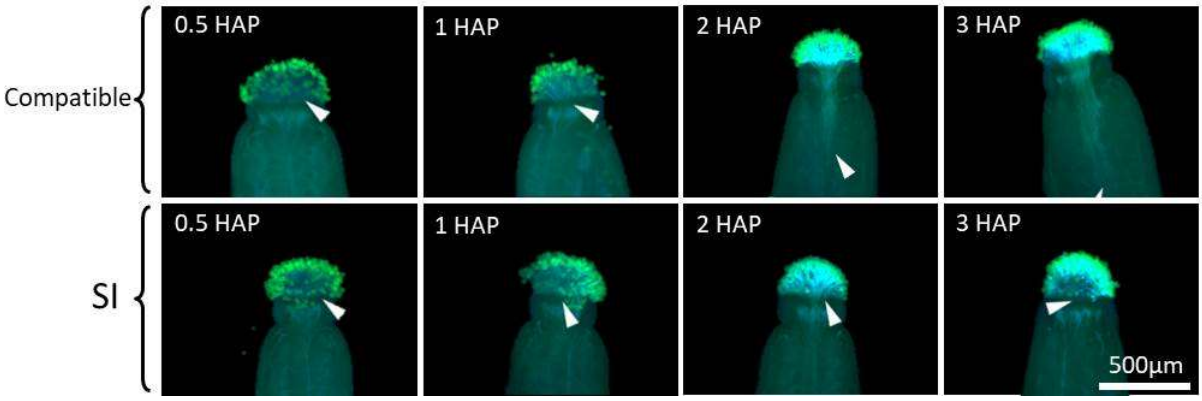

Figure 3.2. The pollen tube growth is inhibited when SI. Images of representative fixed and aniline blue-stained Ler_PrsS$_1$ pistils. The top four were pollinated with Col_0 which is a compatible line. The bottom four samples were pollinated with Col_PrsS$_1$ pollen in which a self-incompatible (SI) reaction is triggered. Samples were pollinated in vivo and harvested at different hours after pollination (HAP). The tip of pollen tubes is indicated with white arrowheads. The experiment was done together with Dr Zongcheng Lin.

These results confirm that in *Arabidopsis* SI the pollen tube growth stops between 0.5 to 1 HAP. Since at 0.5 h after SI induction the cytosolic pH of incompatible pollen drops from ~pH7 to ~pH6 and the actin filaments start transitioning from filaments to small punctate foci in both *Papaver* and *Arabidopsis* (Geitmann *et al.*, 2000b; Poulter, Staiger, *et al.*, 2010; Wang *et al.*, 2019), the 0.5 HAP time point was selected to investigate the early SI response.

On the other hand, 2 HAP was selected as we are interested in a time point in which PCD is initiating in most pollen tubes, but they are still alive and its RNA molecules are not degraded. We expect to have maximal differences in gene expression levels between SC and SI pollinations with this later time point. When studied in *Papaver* pollen in the presence of its cognate PrsS, it was found that after two hours, ~30% of the nuclei showed DAPI-staining, as discussed in chapter two, indicating a loss of plasma membrane integrity. This percentage increased to 55% when the data was collected three hours after exposure to PrsS. In addition, after three hours DNA fragmentation starts being detectable by using TUNEL assays (Jordan *et al.*, 2000). All this indicates that 3 HAP may be too late for a transcriptome analysis related to PCD as the pollen tubes are not alive anymore and the RNA is already being degraded. Moreover, the temporal profile of DEVDase activity in *Papaver* also supports 2 HAP as an appropriate time point for the late stage of the SI response. This caspase-3-like activity is a hallmark of PCD and starts to increase from 2 hours after SI induction (Bosch and Franklin-Tong, 2007), suggesting that transcriptional events related to the initiation and execution of PCD may be found at 2 HAP.

3.2.2. Selection of the parent lines to perform the crosses

In this experimental design, two *Arabidopsis* ecotypes background lines will interact in four different types of crosses. The two lines in the Colombia ecotype background are Col_0 and Col_PrpS$_1$. Col_0 is a Colombia wild type line, on the other hand, Col_PrpS$_1$ coexpresses PrpS$_1$-GFP with the pollen-specific promotor pNTP303. The presence of GFP attached to PrpS$_1$ allows us to verify that the male determinant is being expressed and homozygous by observing the pollen grains under a fluorescence microscope. The two lines in Landsberg background are Ler_0 and Ler_PrsS$_1$. The Ler wild type line is what we called Ler_0. Besides, the line Ler_PrsS$_1$ is expressing the female determinant PrsS$_1$ using the stigmatic papilla specific promoter SLR1.

3.2.2.1. Transformant Ler_PrsS$_1$ with a single insertion

To get Ler_PrsS$_1$ plants, Ler_0 was transformed with *Agrobacterium* carrying an expression plasmid PMS119 containing pSLR1::PrpS$_1$ and a BASTA herbicide resistance gene (BAR). After transformation, seeds from 36 T1 Ler_PrpS$_1$ lines were screened to calculate the segregation rate. We prepared 36 selective 120 mm square Petri plates

containing half Murashige and Skoog basal medium (MS) and BASTA herbicide (20 µg/mL). 100 seeds per line were sowed in each plate and germinated for selection following the defined Rapid Method (Harrison *et al.*, 2006). The plates were incubated at 4 ^{o}C in the dark for two days since these are the ideal conditions for breaking the dormancy (Dekkers *et al.*, 2016). Immediately after that, the plates were placed in a growth room with optimal conditions for the seeds to germinate: 25 ^{o}C and continuous light for 6 hours. After that, the plates were covered to be in the dark for 2 days. Before selection, the seeds were exposed to light for 24 hours moreThe percentage of resistance seeds for each line was counted. From this data, we select the single insertion transformants who segregated 3:1 in the T2 generation. In this case, we got 21 lines with this condition.

3.2.2.2. Functionality of $PrsS_1$ in Landsberg background

From the BASTA screening, 21 lines with a single $PrsS_1$ insertion were identified. The functionality of $PrsS_1$ was checked in all of these 21 plants by the observation of their aniline blue stained stigmas after pollination with Col_$PrpS_1$ pollen.

The procedure was similar to the one described before for *Arabidopsis* pollen tubes (Śnieżko, 2000; Schoenaers *et al.*, 2017) with some modifications. We used 12 well culture plates in which 1.5 mL Agarose 1% was added in each well. When the Agarose medium was solidified at room temperature, one emasculated Ler_$PrsS_1$ flower was placed vertically in each well, placing in each plate a total of 8 stigmas per line (Figure 3.3). Using a dissection microscope 4 stigmas per line were pollinated with Col_0 pollen and 4 with Col_$PrpS_1$ pollen. The plate was placed in a bigger box to create a wet chamber condition for 2 hours. In order to facilitate greater accessibility of the stain to internal tissues, the wells were filled with 1 M NaOH until completely covering the stigmas and incubated for 6 to 10 hours (5 M NaOH was used when it was required to reduce the incubation period to 4 h). After that, the NaOH was removed and replaced by ~2 mL aniline blue. To obtain a proper stain, the plate was placed in the dark overnight.

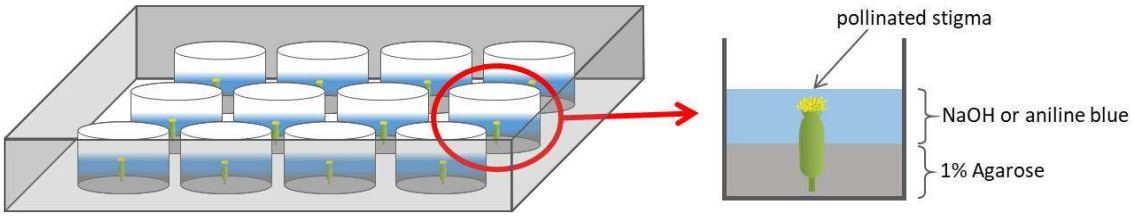

Figure 3.3. Aniline blue staining of pollinated pistils. Eight pistils per Ler_PrsS$_1$ line were placed in 12 well plates. The top four were pollinated with Col_0 pollen (SC) and the bottom 4 with Col_PrpS$_1$ (SI). Two hours after pollination NaOH was added for 6-10 hours and it was substituted by aniline blue. The stigmas were incubated in the dark with this stain overnight.

In total, 8 stigmas per line (4 SC and 4 SI pollinations) were placed on a glass microscope slide and covered with ~100 µl of 60 % glycerol before placing the coverslip. To observe the samples stained with aniline blue we used a fluorescent microscope equipped with an ultraviolet filter. The Ler_PrsS$_1$ line that showed the best SI response (pollen tube growth inhibition) was pollinated in vivo with Col_0 and Col_PrpS$_1$ pollen to double-check the results obtained from this assay.

3.2.3. Pollinations and sampling for RNAseq

For this experiment, the four types of cross-pollinations previously described (Figure 3.1) were carried out. To do this, Ler flowers were emasculated before anthesis (Alvarez-Buylla *et al.*, 2010) at the end of the day. These emasculations were performed under a dissecting microscope and after that, each plant with emasculated flowers was protected with an arasheet developed by the ARAGORN system and left to mature under normal conditions overnight. The arasheet kept the stigmas well protected and avoided cross-pollination.

The stigmas were pollinated with Col_0 or Col_PrpS$_1$ pollen also using dissecting microscopes. A total of 300 pistils were collected for each of the four types of cross-pollinations (Figure 3.4), in each case doing three repetitions of 100 pollinations (representing 3 biological replicates). After pollination, the pistils from each pollination were cut, pooled, and placed together in a 1.5 mL Eppendorf tubes that were immediately immersed in liquid nitrogen.

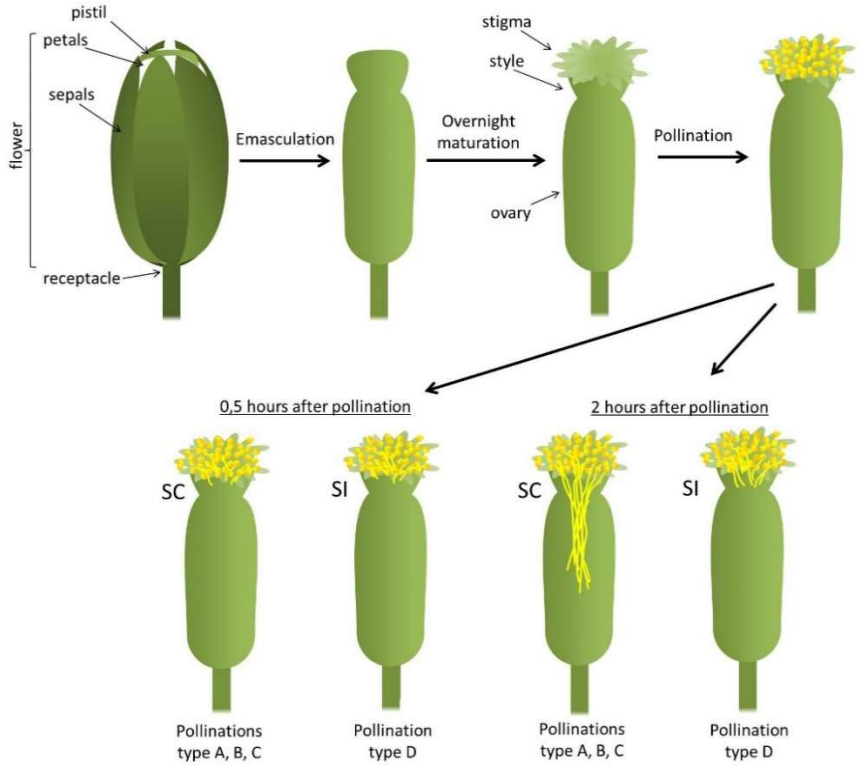

Figure 3.4. States of the pistil at key steps in the procedure. Ler stigmas were pollinated (Ler_0 for pollinations type A and B, Ler_PrsS_1 for type C and D) with Col pollen (Col_0 for pollinations type A and C) or Col_PrpS_1 (type B and D). Pollination A: Ler_0xCol_0, pollination B: Ler_0xCol_PrpS_1, pollination C: Ler_PrsS_1xCol_0, and pollination D: Ler_PrsS_1xCol_PrpS_1. From each cross, 300 samples were collected at 0,5 and 2 h after pollination for RNA sequencing.

3.2.4. Data analysis

The stigmas were harvested at both time points of interest. The RNA of the 24 samples (4 experimental crosses x 2 time points x 3 biological replicates) was extracted using Qiagen RNeasy mini kit according to manufacture's instructions and sent for RNAseq in the VIB-UGent Center for Plant Systems Biology department. The RNAseq was performed at Illumina NEXT-seq platform, aiming at 20 million reads per sample. The library preparation was performed using a standard RNA library kit. The Illumina instrument NEXT-seq 550 System High Output v2 Kit was set to perform 300 cycles, paired-end (2 x 150 bp, 1.2 pM + 1.89 % PhiX) 320 M clusters passing filter, with a quality score that predicts the probability of an error in base calling > 75% bases higher than Q30 (The percentage of bases > Q30 is averaged across the entire run). The RNAseq analysis resulted in an initial list of genes close to 20,000 for each group of comparisons made:

- Pollination type A 0.5 HAP *vs*. pollination type A 2 HAP
- Pollination type B 0.5 HAP *vs*. pollination type B 2 HAP
- Pollination type C 0.5 HAP *vs*. pollination type C 2 HAP
- Pollination type D 0.5 HAP *vs*. pollination type D 2 HAP

- Pollination type A 0.5 HAP *vs*. pollination type D 0.5 HAP
- Pollination type B 0.5 HAP *vs*. pollination type D 0.5 HAP
- Pollination type C 0.5 HAP *vs*. pollination type D 0.5 HAP

- Pollination type A 2 HAP *vs*. pollination type D 2 HAP
- Pollination type B 2 HAP *vs*. pollination type D 2 HAP
- Pollination type C 2 HAP *vs*. pollination type D 2 HAP

This chapter presents a broad overview of the transcriptome profiling results obtained. In addition to the annotations from the standard RNA library, we include further analysis about the molecular function of the genes using the PANTHER classification system (Mi *et al.*, 2019) and The Gene Ontology knowledgebase (http://pantherdb.org/).

3.2.4.1. Candidate genes involved in SI

This analysis was firstly sorted, creating two groups to separate the genes either upregulated or downregulated at least two-fold at the time point 2 hours compared with 0.5 hours after pollination. To create those groups the transcripts were segregated according to their log fold change (logFC) equal or greater than 1 and equal or smaller than -1 (from now on logFC≥1 and logFC≤-1from respectively). In both groups, we considered only the elements with a p-value smaller than 0.05 ($p<0.05$). With those two final two groups obtained, two Venn Diagrams per group were drawn using one of the web tools provided by the VIB-UGent Center for Plant Systems Biology department (http://bioinformatics.psb.ugent.be/webtools/Venn/) (Figure 3.5).

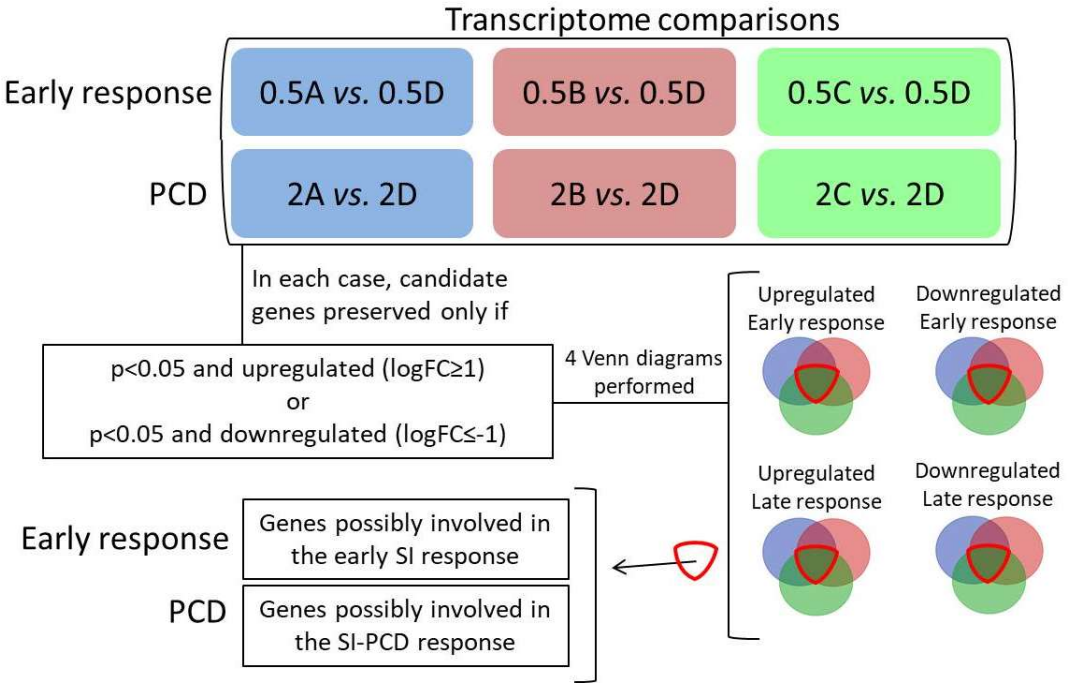

Figure 3.5. Steps to analyze the data obtained from the RNAseq. 0.5 is referred to 0.5 hours after pollination and number 2 indicates the time point 2 hours after pollination. The letters A, B, C and D are related to the type of cross (A: Ler_0xCol_0, B: Ler_0xCol_PrpS$_1$, C: Ler_PrsS$_1$xCol_0, and D: Ler_PrsS$_1$xCol_PrpS$_1$)

3.2.4.2. Genes possibly involved in SI-triggered PCD

Firstly, the differences in the genes regulation was analyzed, comparing its logFC values at the late and early time point for all the four pollination types. Firstly only the transcripts with p-value and false discovery rate (FDR) smaller than 0.05 ($p<0.05$ and $FDR<0.05$ respectively) were considered. The genes with a logFC between -1 and 1 were discarded. The upregulated genes ($LogFC\geq1$) and downregulated ($logFC\leq-1$) were analyzed separately in Venn Diagrams (Figure 3.6).

From the Venn Diagram, we obtained information about the list of up or downregulated genes in all four cases, which allowed us to compare them. In this case, A, B and C can be used as a control as in all three cases, pollen tube growth is not interrupted. The average of the logFC (comparing 2 HAP with 0.5 HAP) in the three controls was calculated and this value subtracted from the corresponding LogFC in D. From this subtraction, we can identify the genes with a higher difference in expression comparing the case in which PCD takes place and when it does not.

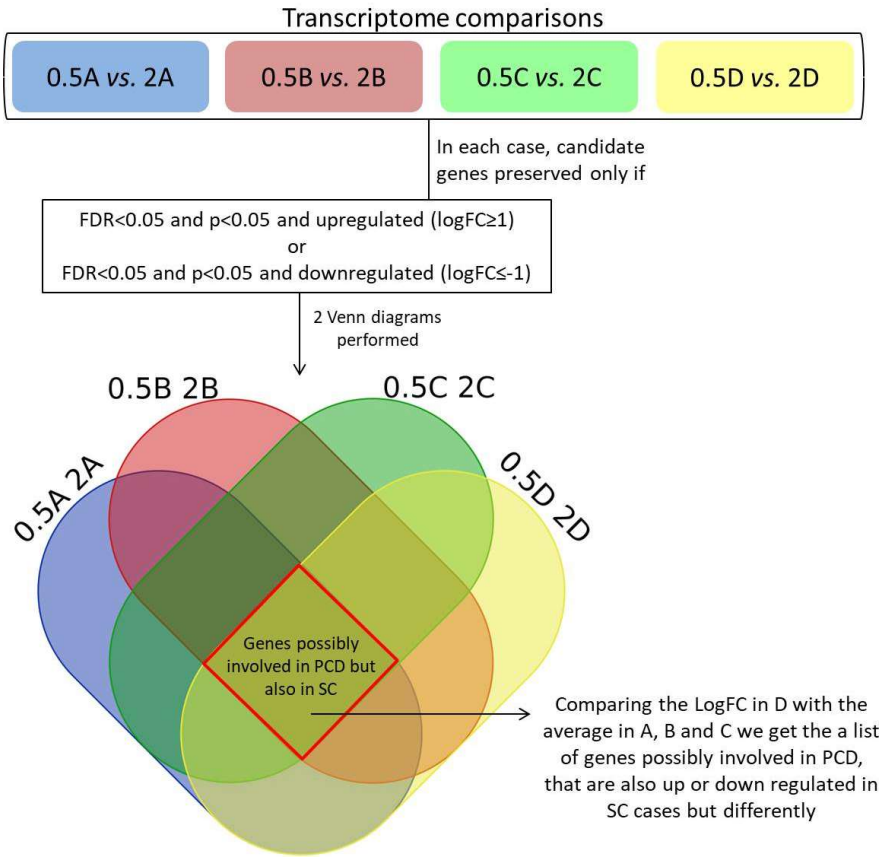

Figure 3.6. Obtention of a pool of down and up-regulated genes in all scenarios. The time points compared are 0.5 and 2 h after pollination. The type of crosses performed were A: Ler_0xCol_0, B: Ler_0xCol_PrpS_1, C: Ler_PrsS_1xCol_0, and D: Ler_PrsS_1xCol_PrpS_1. The convergent area is highlighted in red.

In addition, the logFC values in the SC cases (pollinations A, B and C) were subtracted from the logFC in the SI case (pollination D) for all the genes that presented up or downregulation in D when comparing 0.5 HAP to 2 HAP. In the three resultant lists, the genes with a result between -1 and 1 were discarded. Representing the final pool in a Venn diagram, the common genes were selected as SI-PCD candidate genes (Figure 3.7).

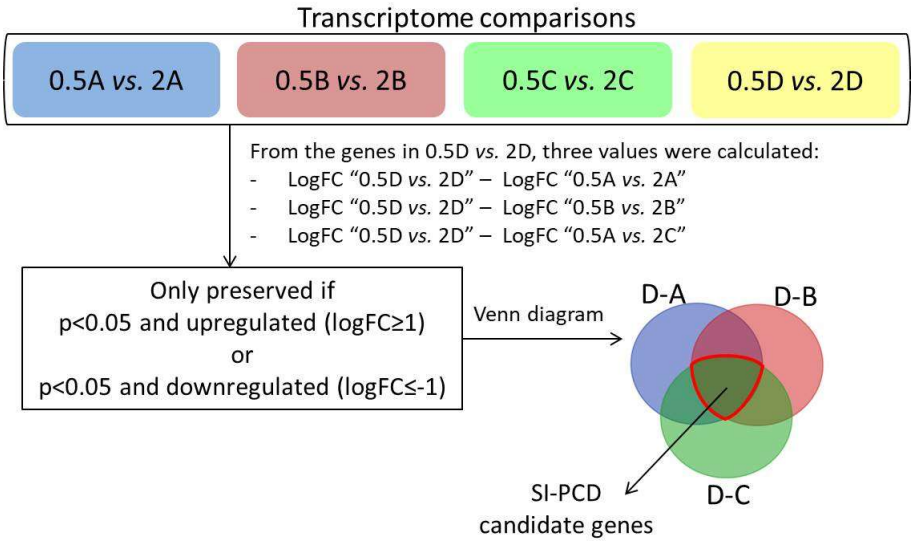

Figure 3.7. Analysis to obtain SI-PCD candidate genes. 0.5 and 2 indicate the h after pollination. A: Ler_0xCol_0, B: Ler_0xCol_PrpS$_1$, C: Ler_PrsS$_1$xCol_0, and D: Ler_PrsS$_1$xCol_PrpS$_1$. The convergence area for the three comparisons is highlighted in red.

In order to obtain the list of genes whose up or down-regulation is possible to be directly related to SI-PCD, we considered the pool of genes obtained when comparing 0.5 HAP to 2 HAP in the pollination type D. In addition, to be more specific, the ones also up or down-regulated in SC cases were discarded. As final candidates, only the ones presenting a p-value smaller than 0.05 were considered (Figure 3.8).

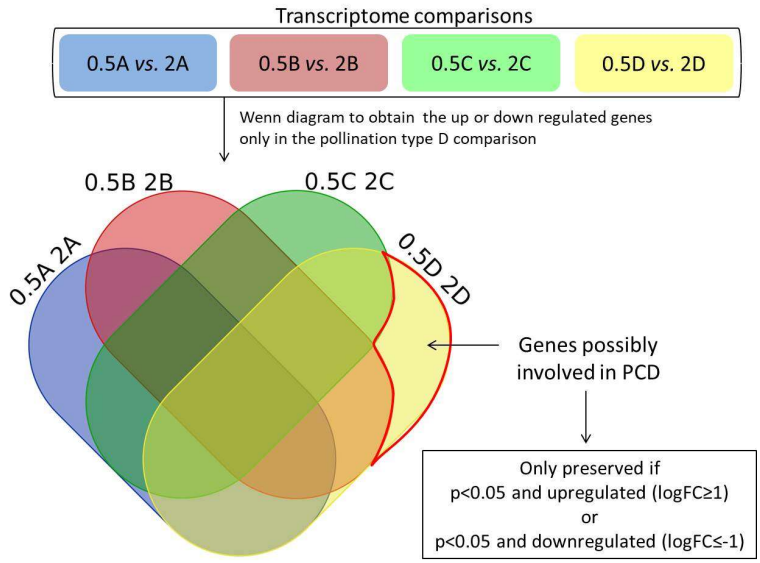

Figure 3.8. Selection of genes only up or downregulated in SI-triggered PCD. The numbers 0.5 and 2 indicate the hours from the pollination when the samples were collected. A, B, C and D indicate the type of pollination. A: Ler_0xCol_0, B: Ler_0xCol_PrpS$_1$, C: Ler_PrsS$_1$xCol_0, and D: Ler_PrsS$_1$xCol_PrpS$_1$. The area representing the transcripts exclusive for the pollination type D is highlighted in red.

3.3. Results

3.3.1. Functionality of $PrsS_1$ in *Arabidopsis* Landsberg background

In order to select the most appropriate Ler_$PrsS_1$ line to be used in this research, stigmas of 21 T1 lines that had a single insertion were *in vitro* pollinated (a total of 8 stigmas per line; 4 SC and 4 SI cross) and stained with aniline blue 2 HAP. When observed under the microscope, the Col_$PrpS_1$ pollen tubes were in all cases shorter than Col_0 (Figure 3.9A). Upon SC pollinations, the location of the pollen tubes tip could be observed deep in the ovary, while when SI the tubes did not grow far from the style. This indicates that when $PrsS_1$ is expressed in Ler lines it can trigger SI-PCD and inhibit the growth of Col_$PrpS_1$ pollen tubes. From the 21 lines, Ler_$PrsS_1$ line-3 presented the best inhibition capability. In addition, in vivo pollination followed by seedset analysis showed that Ler_$PrsS_1$ line-3 pollinated with Col_$PrpS_1$ resulted in short siliques with almost no seed formation, while normal siliques were observed when Ler_$PrsS_1$ line-3 was pollinated with Col_0 pollen (Figure 3.9B). The results from both the *in vitro* and *in vivo* pollinations defined line-3 as an adequate line to be used in this RNAseq assay.

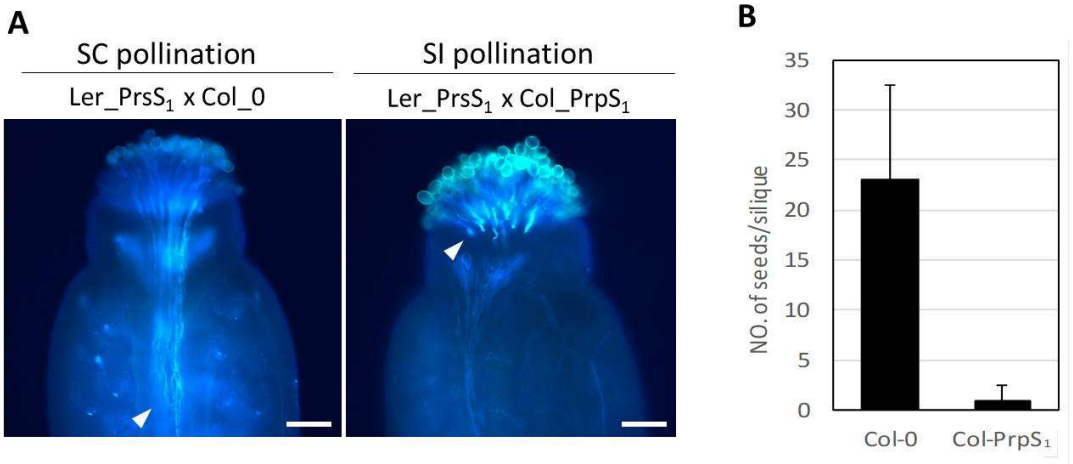

Figure 3.9. Representative observations when pollinating Ler_$PrsS_1$ stigmas. This figure shows the results using Ler_$PrsS_1$ line-3. (A) When observed two hours after pollination, the pollen tube tips of Col_0 pollen are deep in the ovary. However, Col_$PrpS_1$ presents an SI phenotype. Bar=100µm (B) Seedset analysis 5 days after cross-pollination. Results= mean±SD. The experiment was done together with Dr. Zongcheng Lin.

3.3.2. Candidate genes to have a role in SI

Once we got the four parent lines Ler_0, Ler_PrsS$_1$, Col_0 and Col_PrpS$_1$ (Col_PrpS$_1$ was established in a previously published study (Lin *et al.*, 2015), the four types of crosses defined in the experimental design (Figure 3.1) were carried out. For each case, we obtained three repetitions of 100 pollinations. The pistils were collected at the two selected time points (0.5 and 2 HAP), total RNA was extracted and sent for RNAseq with the Illumina NEXT-seq system to the VIB Nucleomics core facility.

The result of the RNAseq with the Illumina NEXT-seq system generated a list of genes with its correspondent LogFC, logCPM, p-value, FDR and annotations for each of them. We compared the three SC cases to the pollination type D (SI) at the same time point (Figure 3.10). From this comparison, we want to see the differences between them in terms of the number of genes up and down-regulated and its values. Transcripts identified as being differentially expressed when comparing SI with SC at 0.5 HAP may be related to events taking place during the early response like pollen tube growth arrest, while the ones showing differences 2 HAP may be related to PCD.

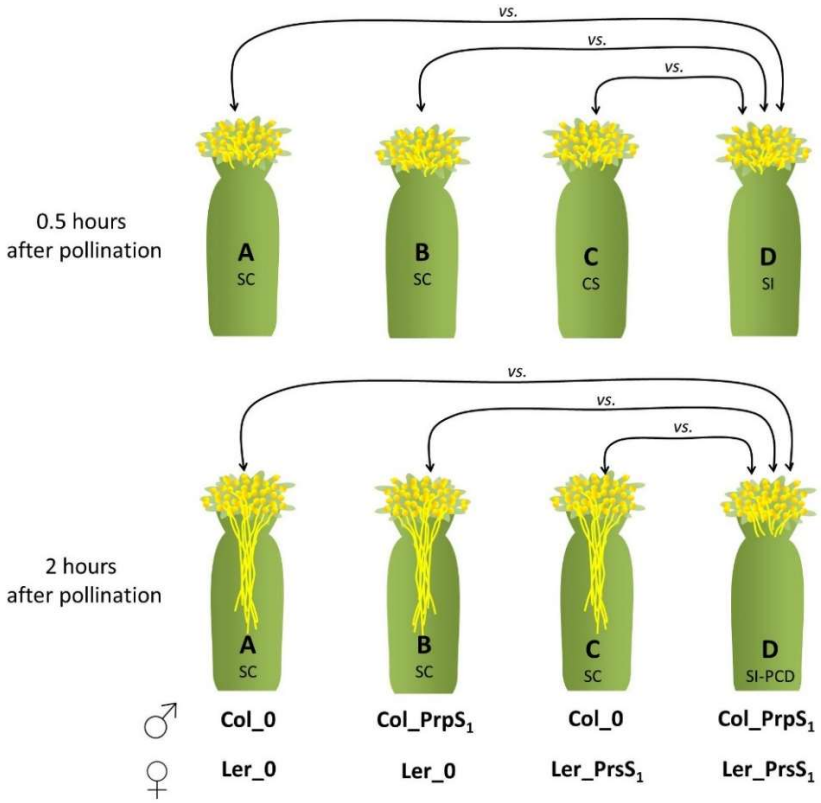

Figure 3.10. Scheme of the analysis presented in this section. Results of comparing the SC crosses (A: Ler_0 x Col_0, B: Ler_0 x Col_PrpS$_1$, C: Ler_PrsS$_1$ x Col_0) with the SI cross (D: Ler_PrsS$_1$ x Col_PrpS$_1$) at 0.5 and 2 hours after pollination.

Firstly the total list of genes obtained when comparing A, B and C *vs.* D was split into two groups: upregulated (logFC≥1) and downregulated (logFC≤-1) genes. Applying this requirement, more than 99% of transcripts were discarded. Secondly, we discarded the genes with a P-value greater than 0.05 (Table 3.1) producing in some cases a dramatic reduction of the elements.

With the resultant list, we drew a Venn Diagram to check the overlap between them (Figure 3.11). Somewhat surprisingly, none of the transcripts identified as being either up- or down-regulated following a SI pollination when compared to the individual SC pollinations was consistently differentially expressed when comparing SI with SC in the analysis of 0.5 HAP pollinated stigmas. This indicates that there are no significative regulations to highlight at this early time point. On the other hand, a total of 67 genes presented an overlap in the three comparisons when analyzing 2 HAP, 8 of them upregulated, 59 downregulated.

Table 3.1. Elements in each group, when compared the SC crosses with D at both time points. A, B, C and D represent the pollinations performed: Wt, Wt x At-PrpS_1, At-PrsS_1 x Wt and At-SI respectively. The comparisons made at 0.5 hours after pollinations are represented in pale grey, the ones at 2 hours after pollination where PCD is starting are presented in dark grey.

	0.5 HAP			2 HAP		
	A *vs.* D	B *vs.* D	C *vs.* D	A *vs.* D	B *vs.* D	C *vs.* D
Total	18948	18841	18847	19571	19490	19554
logFC≥1	37	35	21	144	97	40
logFC≥1 p<0.05	34	25	7	95	62	25
logFC≤-1	116	201	11	151	248	237
logFC≤-1 p<0.05	29	38	2	125	213	189

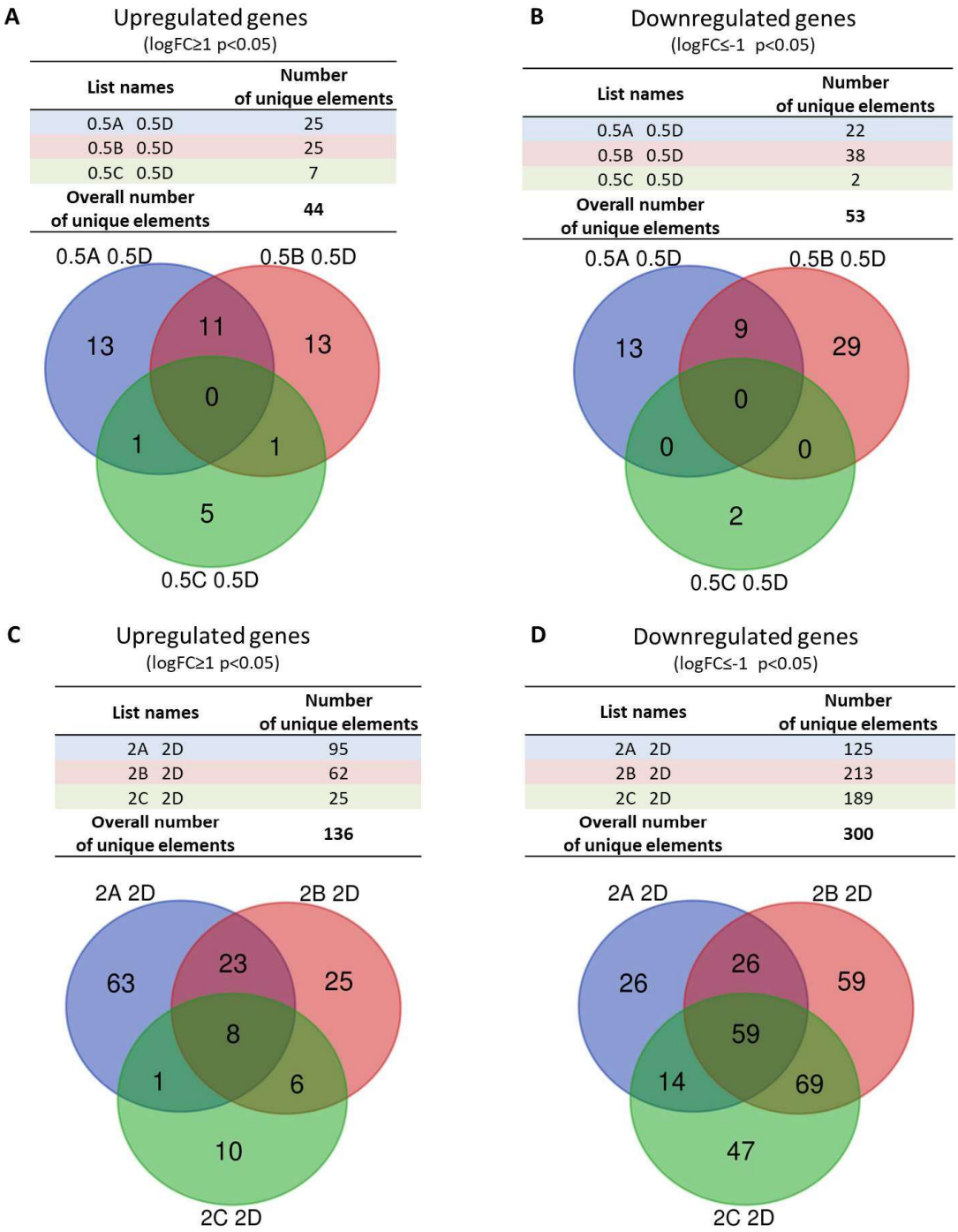

Figure 3.11. Overlap of genes comparing the transcriptome of SC crosses with the SI cross at early and late time point. The three SC crosses: A (Wt pollination) vs. D (At-SI) in blue, B (Wt x At-PrpS$_1$) vs. D in red and C (At-PrsS$_1$ x Wt) vs. D in green. Unique elements in each group and a Venn Diagram. (A) There is no overlap when comparing upregulated genes or (B) downregulated genes at 0.5 hours after pollination suggesting that SC and SI transcriptome are quite similar at this time point. Some genes are found to overlap when comparing (C) upregulated and (D) downregulated genes, at the beginning of the PCD process, 2 hours after pollination.

3.3.3. The function of candidates Hestia genes

The final list of 67 genes that overlapped in all three cases when comparing SC situations (A, B and C) with D (SI) was used for further analysis. The code Hestia (HTA) was assigned, in reference to the eldest daughter Cronus, the mythologic god of time. This nomenclature is used and the identity of the genes is not available due to intellectual property reasons. A number was assigned sorting them from smallest logFC when comparing A *vs.* D 2HAP to the highest value, since A is the Wt situation (Appendix table 3.2). HTA67 represents the gene that showed the highest upregulation in SI, in all three cases (logFC -6.81, -8.65 and -8.49 when comparing A, B and C respectively to D). The annotation from the standard RNA library kit in the Illumina NEXT-seq system identifies the function of this gene as a "domain-containing disease resistance protein", which may represent an interesting gene for further analysis.

Looking for the molecular function of those genes in the PANTHER Go-Slim, the *hestia* genes selected with a logFC≥1 (HTA1 to HTA8) were not in the database, so we did not get any description related to its possible role. However, we could obtain some information about 46 of the 59 *hestias* with a LogFC≤-1 (HTA9 to HTA67), hitting 25 functions. Thay can be grouped in six big groups: Catalytic activity is the main one, followed by Binding, Transcription regulator activity, Molecular function regulator and Molecular transducer activity (Figure 3.12).

It suggests that there is a group of genes upregulated at the beginning of the SI-induced PCD, presenting catalytic activity (40% of the 46 described genes), predominantly with oxidoreductase, hydrolase and transferase activity.

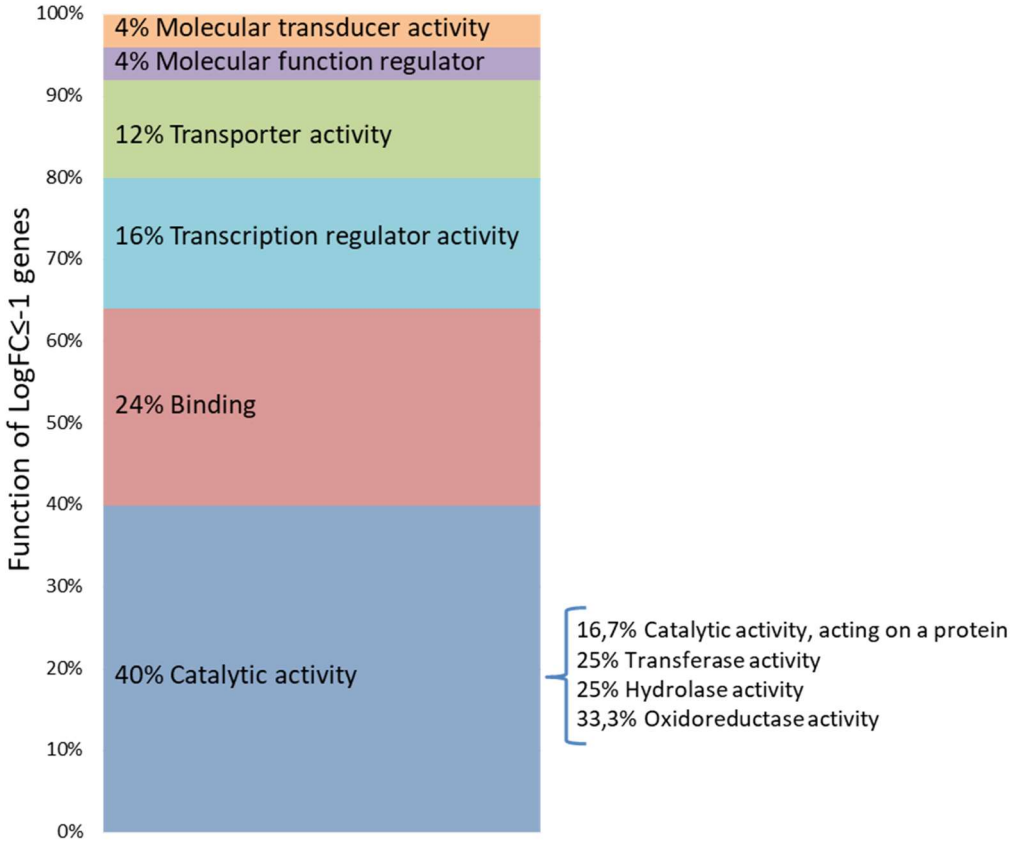

Figure 3.12. The molecular function of *hestia* genes according to the PANTHER Go-Slim genes database.

3.3.4. Candidate genes possibly involved in SI-induced PCD

Another type of comparison was carried out with the transcriptomes obtained. In this case, there were analysed the results of comparing the four types of crosses at the early and late time points without distinguishing the Col or Ler origin (Figure 3.13). Analysis in which Col or Ler derived transcripts were separated by making use of the SNPs between Col and Ler will be presented elsewhere by my colleague Dr. Zongcheng Lin.

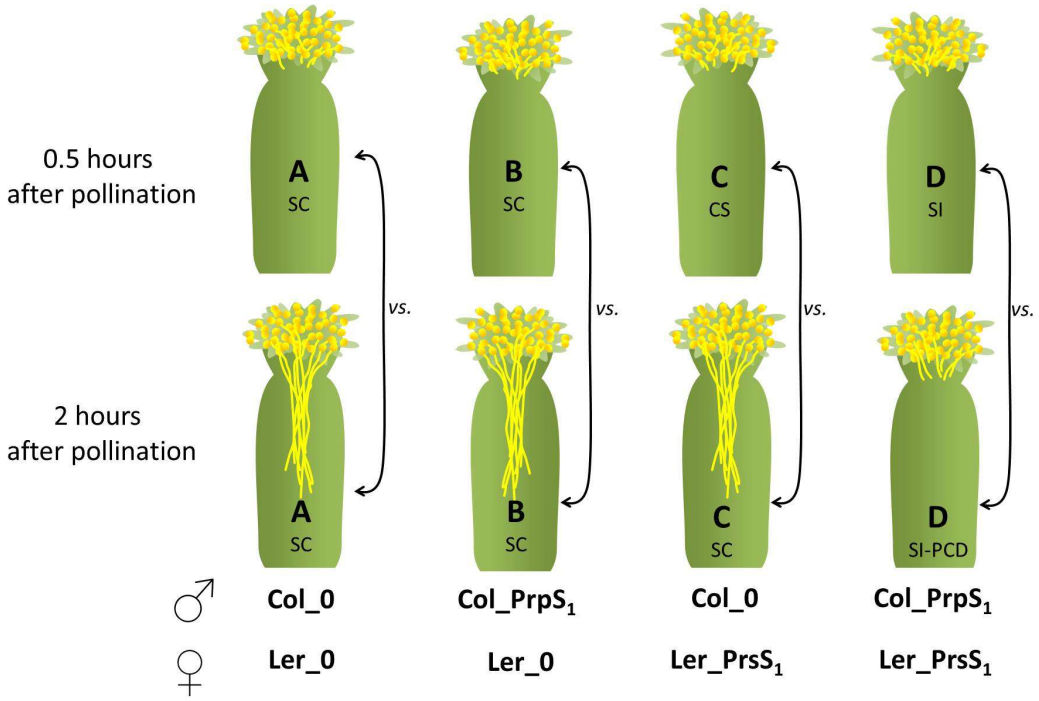

Figure 3.13. Scheme of the analysis presented in this section. Results comparing each type of pollination (A: Ler_0 x Col_0, B: Ler_0 x Col_PrpS$_1$, C: Ler_PrsS$_1$ x Col_0, D: Ler_PrsS$_1$ x Col_PrpS$_1$) at early and late time point.

To obtain information for this raw data, the first step carried out was to separate them into two groups: upregulated (logFC≥1) and downregulated (logFC≤-1) genes. In both groups, we considered only the elements with a p-Value and FDR smaller than 0.05 ($p<0.05$ and FDR<0.05 respectively) which reduced the final number of transcripts per group around ten times (Table 3.2).

All the elements meeting the requirements applied were used to draw a Venn Diagram. The Venn diagram shows that 568 transcripts were upregulated in all four groups while 1399 transcrips were downregulated in all the four groups (Figure 3.14).

Table 3.2. Elements in each group when comparing the early and late response. A, B, C and D represent the pollinations performed: Wt, Wt x At-PrpS$_1$, At-PrsS$_1$ x Wt and At-SI respectively. A, B and C in pale grey and D is presented in darker grey as this is the only self-incompatible case which means PCD is triggered.

	Self-compatible samples			SI-PCD
	0.5A 2A	0.5B 2B	0.5C 2C	0.5D 2D
Total	19624	19534	19559	18999
logFC≥1	1886	1647	1893	1009
logFC≥1 p<0.05	1830	1552	1775	960
logFC≥1 p<0.05 FDR<0.05	1764	1448	1692	877
logFC≤-1	2236	2043	2019	1874
logFC≤-1 p<0.05	2128	1944	1991	1817
logFC≤-1 p<0.05 FDR<0.05	2065	1888	1958	1718

A Upregulated genes
(logFC≥1 p<0.05 FDR<0.05)

List names	Number of unique elements
0.5A 2A	1764
0.5B 2B	1448
0.5C 2C	1692
0.5D 2D	877
Overall number of unique elements	**2372**

B Downregulated genes
(logFC≤-1 p<0.05 FDR<0.05)

List names	Number of unique elements
0.5A 2A	2065
0.5B 2B	1888
0.5C 2C	1958
0.5D 2D	1718
Overall number of unique elements	**2470**

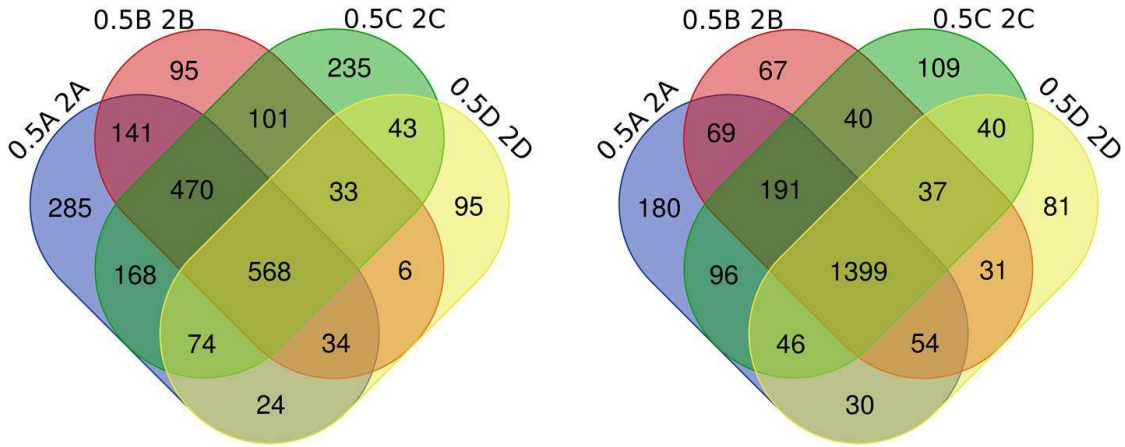

Figure 3.14. Overlap of genes comparing the transcriptome at the time point 0.5 h and 2 h after pollinations. The four types of pollinations performed in this experiment are represented with the names A: Ler_0 x Col_0, B: Ler_0 x Col_PrpS$_1$, C: Ler_PrsS$_1$ x Col_0, D: Ler_PrsS$_1$ x Col_PrpS$_1$. (A) The unique elements in each group and a Venn Diagram showing upregulated genes and (B) the downregulated ones.

On the other hand, we selected the genes with a >1 or <-1 value when subtracted from the LogFC in D the values of LogFC in A, B and C. After applying the criteria of having a p-value smaller than 0.05, a final number of 526 genes was obtained. The analysis with a Venn diagram showed that 47 of those genes were present in all three comparisons. In this group, 28 presented upregulation in 0.5 HAP *vs.* 2 HAP and 19 are downregulated. To focus on the ones presenting remarkable changes, 18 of them have a logFC bigger than 1 and 14 of them were already defined as *degoya* genes, which means its relevance is spotted in both analyses. On the other hand, 9 of them have a logFC smaller than -1, and 6 of them are *degoya* genes (Figure 3.15).

List names	Number of unique elements
D-A	255
D-B	216
D-C	256
Overall number of unique elements	**526**

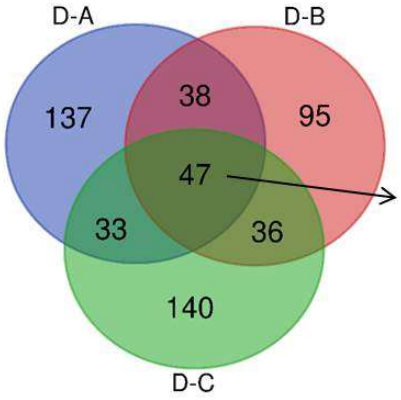

Number of genes	
Upregulated (LogFC>0)	28
Downregulated (LogFC<0)	19
Upregulated (LogFC>1)	18
Downregulated (LogFC<-1)	9

Figure 3.15. Genes convergent when compared the SI situation with the SC. LogFC obtained in 0.5 vs. 2 hours after pollination D (SI), substracting the values in A, B and C (SC).

To conclude, the up or downregulated genes only when SI were clustered. Again in this case, the ones with a p-value and FDR < 0.05 were discarded. We obtained a list of 95 upregulated and 81 downregulated genes (Figure 3.14). This is the result of comparing D 0.5 HAP *vs.* 2 HAP. Interestingly, there are 12 genes presenting a LogFC < -2 or > 2 (Table 3.3) and three candidate genes with a LogFC < -3 or > 3 which means its regulation is highly different when comparing those two time points in SI.

Table 3.3. Differences in regulation when compared 0.5 HAP vs. 2 HAP only when SI. In 12 case, candidate genes presented a LogFC < -2 or > 2. Five of them are downregulated at the late stage of SI, close to PCD. The other seven are upregulated at 2 HAP comparing with the early stage, presenting the biggest difference a gene codifying for a protein member of the peroxidase superfamily.

	LogFC	Annotation
Upregulated	3.20	ATSEN1_DIN1_SEN1_SEN1__Rhodanese/Cell cycle control phosphatase superfamily protein
	2.73	AtDRM2_DRM2__Dormancy/auxin associated family protein
	2.56	ASN1_AT-ASN1_DIN6__glutamine-dependent asparagine synthase 1
	2.14	AtPUB22_PUB22__plant U-box 22
	2.08	AtDRM1_DRM1_DYL1__dormancy-associated protein-like 1
Downregulated	-2.05	Oleosin family protein
	-2.36	AtLARP6c_LARP6c__RNA-binding protein
	-2.40	-
	-2.73	-
	-2.79	HKL3__hexokinase-like 3
	-3.52	-
	-5.62	Peroxidase superfamily protein

3.3.5. Function of candidates related to SI-triggered PCD

From the overlap analysis, we obtained a total of 1967 genes that were either up- or down-regulated in all 4 groups. The elements in this group of genes were named "degoya" (DGY), in reference to the author of the masterpiece "God of Time devouring his son". Also on this occasion, the identity of the genes is not available due to intellectual property reasons, which is why this nomenclature is used instead. A number was assigned to each DGY that allowed to organise them according to the absolute value obtained for the difference of the logFC for the type D and the average logFC for A, B and C (Appendix table 3.1). The enumeration was assigned starting from the upregulated (DGY1 to DGY568) followed by the downregulated ones (DGY569 to DGY1967) when comparing 2 HAP with 0.5 HAP.

Next we interrogated the top 50 genes for both lists using the information provided in annotations from the standard RNA library kit in the Illumina NEXT-seq system. Three top-50 genes were defined as "Plant self-incompatibility protein S1 family": DGY33, DGY47 and DGY572. In all three cases, the logFC is smaller in D

comparing with A, B and C. The highest difference is found for DGY572 since its logFC for D is 1.425 smaller than the A, B and C average. Published analysis of DGY47 included it in the fifth position on the top five genes that are functionally related to DGY33 and DGY572 (Hansen *et al.*, 2017). In both cases, its relation is due to the highest Gene Ontology Jaccard Index value. However, apart from this connection, there is no more published information about them so far.

The candidates DGY3, DGY6 and DGY603 are are also worth to be highlighted due to their function being described as “Disease resistance protein (TIR-NBS class)”, “Calcium-binding EF-hand family protein” and “alpha/beta-Hydrolases superfamily protein”, respectively. In these three cases the logFC was also smaller in D comparing with A, B and C. It suggests that the disease resistance provided by DGY3 is reduced during the SI-PCD response. Related to DGY6 and DGY603, in this thesis, we discuss the role that calcium (Chapter two) and certain hydrolases (Chapter four) may have in the SI response. In addition, there were spotted a group of genes related to acting, specially ADF, even if the logFC in SI cases is similar to the obtained when SC. Those are DGY894, DGY1063 and DGY1514 (actin-depolymerizing factor 11, 7 and 10 respectively), also DGY1613 related to actin 4 and DYG463 codifying for an actin-binding FH2 (formin homology 2) family protein.

The PANTHER classification system was used to cluster the 1967 DGY genes according to their function. When analyzing the 568 upregulated genes, 24 genes could not be mapped. The 544 remaining genes mapped to 194 functions, initially grouped in six categories (Figure 3.16A). ”Catalytic activity” was the main category covering 54,1% of the genes, followed by “Binding” with 21.1% of them. The four other categories were transporter activity (10,8%), transcription regulator activity (6,7%), molecular function regulator (6,7%) and molecular transducer activity (0,5%). When analyzed the 1399 downregulated DGY genes with the same tool, the function of 1319 genes was found in the database hitting 474 functions (Figure 3.16B). All the functions can be grouped into eight categories. The 53.8% of the genes present catalytic activity (predominantly hydrolase and transferase activity) and the second most predominant category is “Binding” with 21,9% of the total.

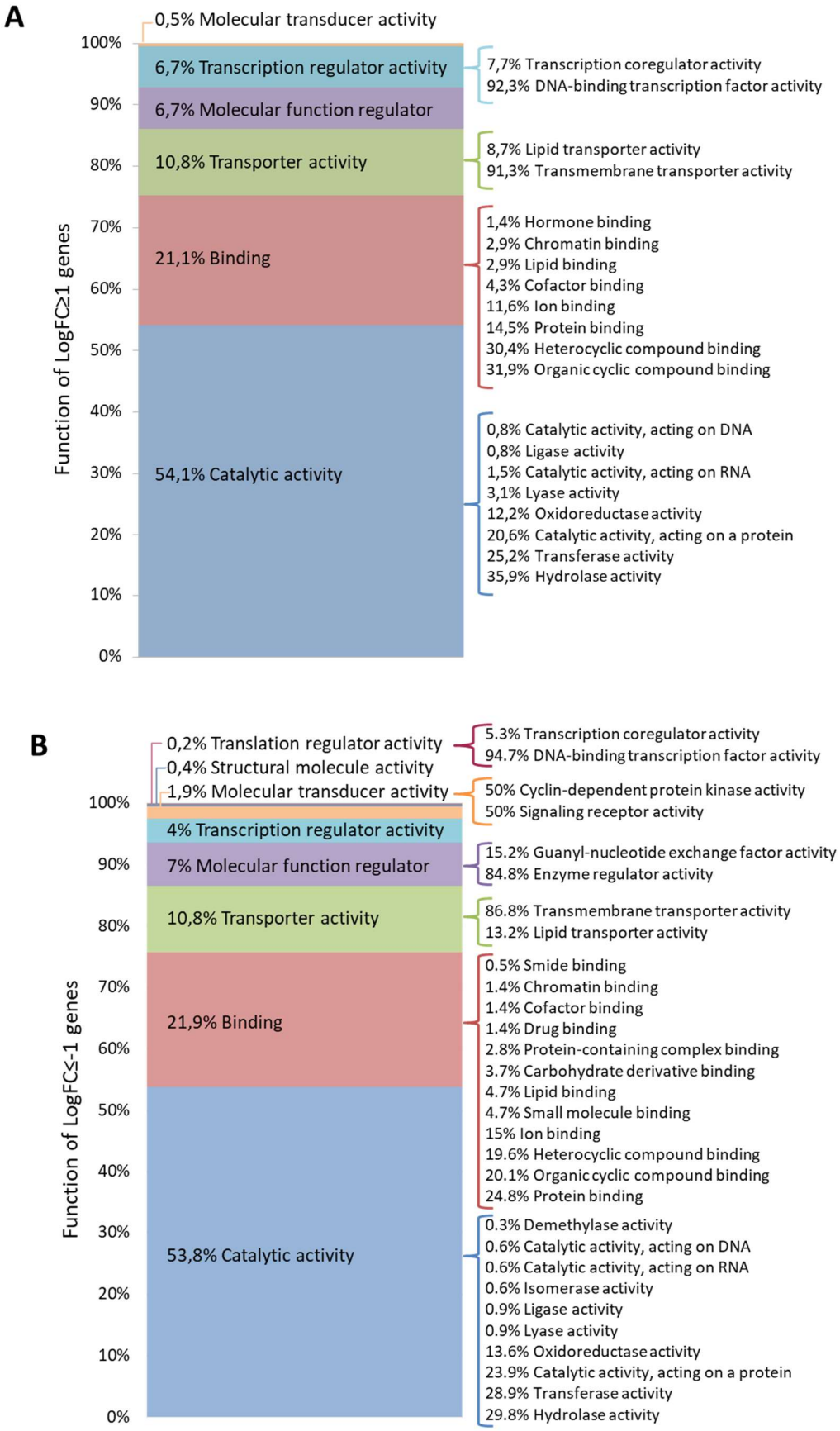

Figure 3.16. The function of genes up and down-regulated for all pollinations performed when comparing 0.5 vs. 2 hours after pollination.

In addition, when grouped the genes according to the result obtained when substracted the logFC in A, B and C to D, we got 18 and 9 up and downregulated respectively. The one presenting a bigger difference has been already described in the previous analysis as DGY572, it has a logFC of -4.06 when comparing 0.5 HAP *vs.* 2 HAP during SI, which indicates that it is upregulated in the late response. According to its annotation, as described before, this gene is a "plant self-incompatibility protein S1 family". In the opposite point with a logFC of 3.80, the gene DGY7 that codifies for a DNA-binding protein member of the WRKY transcription factor family, shows to be the more upregulated during the early response.

From the analysis of the genes only up or downregulated when SI we got three leading candidates with a logFC < -3 or > 3. One of them presents 3.2 logFC, which means is downregulated at the late stage of the SI-PCD response, and its annotation indicates to be related to the cell cycle control phosphatase. The other two have a negative logFC, -3.52 and an unknown function, and -5.62, whose annotation indicates it is a member of the peroxidase superfamily protein. Those two genes have a remarkable upregulation only present when SI.

The pool of genes obtained from this analysis should be considered for further analysis. The *degoya* but especially the 27 genes detected to have a distinct behaviour in SI crosses are potent candidates to have a role in this response. Even if from this examination, we are not able to distinguish if the differences in its expression are occurring in the pistil or the pollen tube.

3.4. Discussion

Little is known about the genetic mechanisms that intervene in the SI response and how it triggers PCD. With the study of the RNA molecules present at different time points in SC and SI scenarios, we aimed to identify genes that could play a role in the SI-PCD. In this chapter, two types of associations were presented: firstly comparing expression levels of all individual SC pollinations *vs.* SI for both the early and late time point (resulting in *hestia* candidates), secondly the differential expression values of the two time points (0.5 HAP and 2 HAP) were compared between SC and SI pollinations (obtaining *degoya* candidates). When comparing the results obtained in both analysis,

only 10 genes were found to be present in both lists, containing the DGY and HTA code (Table 3.4). Only DGY31/HTA6 coincides being upregulated in all the cases compared. In all the other 9 cases the response is reversed. DGY1/HTA53 is less upregulated going from 0.5 HAP to 2 HAP after SI when compared to SC but with a higher downregulation 2HAP in in SC cases when compared to SI. The gene that codifies for this phospholipase-like protein has also been named Polarized growth Chromatin-associated Controller 1 (PCC1 gene) when studied in yeast and Arabidopsis (Kisseleva-Romanova *et al.*, 2006; Shimada, 2010). It has been shown that this gene is induced by pathogen infections and the data suggest it is also regulated by the circadian clock (Sauerbrunn and Schlaich, 2004). We obtained negative logFC values when comparing A, B and C *vs*. D 2 HAP, which means this gene is more upregulated when the pollination is self-incompatible. It insinuates that the mechanisms for the SI-triggered PCD may be comparable or possibly presents some similitude to the process in plants for reacting to pathogen infections.

Table 3.4. Duplicated genes comparing transcriptomes analysis.

Max logFC

Min logFC

Annotation	Degoya	0.5A 2A	0.5B 2B	0.5C 2C	0.5D 2D	Hestia	2A 2D	2B 2D	2C 2D
AtPP2-B15_PP2-B15__phloem protein 2-B15	DGY575	-5.48	-5.09	-5.35	-3.99	HTA3	1.50	1.29	1.26
AMP-dependent synthetase and ligase family protein	DGY31	1.09	1.35	1.39	2.31	HTA6	1.28	1.46	1.28
	DGY609	-2.25	-2.29	-2.49	-1.49	HTA7	1.17	1.10	1.11
ASG4_REV3__Homeodomain-like superfamily protein	DGY577	-3.08	-2.92	-3.33	-1.86	HTA8	1.13	1.25	1.29
Protein kinase superfamily protein	DGY25	2.64	2.67	2.66	1.56	HTA11	-1.02	-1.18	-1.15
ATWRKY53_WRKY53__WRKY family transcription factor	DGY7	4.96	4.82	6.02	3.80	HTA18	-1.10	-1.56	-1.56
Peroxidase superfamily protein	DGY2	4.43	5.05	9.04	4.44	HTA30	-1.21	-1.75	-1.81
ATR4_CYP83B1_RED1_RNT1_SUR2__cytochrome P450, family 83, subfamily B, polypeptide 1	DGY4	3.37	3.50	4.63	2.21	HTA32	-1.24	-1.73	-1.52
ATLOX5_LOX5__PLAT/LH2 domain-containing lipoxygenase family protein	DGY10	2.69	2.86	3.13	1.59	HTA42	-1.38	-1.47	-1.60
Arabidopsis phospholipase-like protein (PEARLI 4) family	DGY1	4.78	4.59	6.75	3.07	HTA53	-1.85	-2.29	-2.40

As presented in the functional category of the candidate genes, most of these genes fall into the category of Catalytic activity. Hydrolysis is the main specific function in the catalytic activity group. Hydrolases play an important role in PCD (Stael *et al.*, 2019). For example, they are involved in the differentiation to tracheary elements that require PCD in procambium cells (Fukuda, 2000). Its differences at the gene expression level suggest that hydrolases may also be key instruments in SI to trigger PCD. This activity was the majority in both up and downregulated DGY genes, representing 35.9%

and 29.8% of the genes with catalytic activity. Even if the oxidoreductase activity was the principal catalytic activity observed in the downregulated HTA genes with catalytic activity, the next major characteristic is the hydrolase activity defining the 25% of them. It will be further discussed in chapter four since a specific hydrolase is also spotted to have a direct relation to SI.

The candidate HTA67 presents a dramatic upregulation when comparing SI *vs.* SC at a late time point (Appendix table 3.2). This gene is described as a "domain-containing disease resistance protein" in the UniProt database. According to the STRING database, this protein with a disease resistance domain was tested and recognised the AvrRpt2 type III effector avirulence protein from *Pseudomonas syringae*. It is considered that this resistance can be activated via an indirect interaction with the avirulence protein, that triggers a defence system, including the hypersensitive response, which restricts the pathogen growth (Szklarczyk *et al.*, 2019).

In order to better understand the role that HTA67 may have in the SI response, the interaction of HTA67 with other *Arabidopsis* genes was analyzed using the BAR *Arabidopsis* Interactions Viewer database (Waese *et al.*, 2017). It surprisingly predicts that the protein encoded by HTA67 interacts with four *degoya* genes: DGY39, DGY56, DGY79 and DGY1410. Both DGY39 and DGY79 encode proteins that belong to the protein kinase family and are upregulated when comparing 0.5 HAP *vs*. 2 HAP but in a lower rate in D when compared with A, B and C. It means that the upregulation decrease in the late stage of SI-PCD. DGY56 and DGY1410 encoded for a protein containing a prohibitin homology (PHB) domain associated with the membrane and plasma membrane intrinsic protein respectively. The gene DGY56 downregulated in the late timepoint but in a lower level when SI. On the other hand, DGY1410 is upregulated in all cases at 2 HAP comparing to 0.5 HAP but when SI its upregulation is lower.

When analyzed the genes only up or downregulated in the pollination type D, a member of the peroxidase family was spotted with a LogFC of -5.62 comparing early *vs.* late time point in SI. This gene was also previously identified in *Arabidopsis* seedlings having a large increase when growing them on K^+-deficient medium (Kang *et al.*, 2004). It suggested its possible implication to defence cells against harmful conditions since the

peroxiredoxins reduce hydrogen peroxide (H_2O_2) and alkyl hydroperoxides, which means they could have a crucial function in anti-oxidant defence and redox regulation (Horling *et al.*, 2003). Additionally, the abundance of this peroxidase also increased when the *Arabidopsis* roots were exposed to NaCl, supporting the theory of its possible relation to stress response (Jiang *et al.*, 2007).

From the experiment presented in this chapter, the transcriptomes of the early and late stages of the SI response were started to being elucidated. We obtained some interesting genes that could serve as candidates to test their involvement in the SI—PCD response. The data suggested a close relationship between SI and the response to pathogens. In addition, further analysis should be done to check if any mutant plants of these *degoya* and/or *hestia* genes and/or the pool of genes obtained only when SI could be enough to obtain a compatible response in *Arabidopsis* expressing cognate PrpS and PrsS.

Chapter four. Reverse genetics approaches to analyse candidate genes to be suppressors of SI-PCD

4.1. Introduction

Previous research on the *Papaver rhoeas* self-incompatibility (SI) system that controls the rejection of self-pollen in *Papaver* highlighted some of the key events involved in this response (Wilkins *et al.*, 2014). According to their time point of occurrence after SI, these events can be categorised into early and late responses. The main early responses observed in *Papaver* SI pollen are: the arrest of pollen tube growth, an increase of potassium and calcium concentration, and a dramatic cytosolic pH drop. The depolymerization of actin filaments is also observed in the early SI response. The F-actin morphology changes from bundles to small punctate foci with some actin-binding proteins (ABPs) colocalizing with these foci (Wang *et al.*, 2019). At a later stage after SI induction, an increase in caspase-like activities which are related to programmed cell death (PCD) has been observed (Bosch and Franklin-Tong, 2007). The analysis of these phenomena has led to a better understanding of how pollen tube destruction is regulated after SI.

As mentioned, one of the earliest events upon SI induction is an increase in cytosolic K^+ and Ca^{2+} ($[Ca^{2+}]_{cyt}$) in incompatible pollen. In particular, the increase in $[Ca^{2+}]_{cyt}$ plays an essential second messenger role in the SI-induced signalling pathway. Elevated Ca^{2+} levels cause rapid phosphorylation of the soluble inorganic pyrophosphatases Pr-p26.1a and Pr-p26.1b (De Graaf *et al.*, 2006). Characterization of these pyrophosphatases revealed a functional role in pollen tube growth, as their activity was associated with driving the biosynthesis of the membrane and cell wall components, required to sustain the rapid growth of these cells (Rudd and Franklin-Tong, 2003; De Graaf *et al.*, 2012; Wilkins *et al.*, 2014). The increase of $[Ca^{2+}]_{cyt}$ also triggers rapid actin depolymerization, contributing to the arrest of incompatible pollen tube growth (Snowman *et al.*, 2002). Strikingly, even after the pollen tube stops growing, actin depolymerization continues and actin-binding proteins (ABPs) are implicated in the formation of large punctate F-actin foci (Geitmann *et al.*, 2000; Poulter *et al.*, 2010). It was observed that SI also triggers transient increases in reactive oxygen species (ROS) and nitric oxide (NO), downstream of changes in $[Ca^{2+}]_{cyt}$ (Franklin-Tong *et al.*, 1993; Wilkins *et al.*, 2014). After the SI-induced inhibition of pollen tube growth, the putative mitogen-activated protein kinase (MAPK) p52 is activated, presenting its maximum

activation ~10 min after SI (Rudd *et al.*, 2003). This belated activity suggests a possible role of MAPK signalling in the induction of PCD as MAPK activation was sufficient to induce cell death in tobacco leaves and *Arabidopsis* (Rudd and Franklin-Tong, 2003). Thus, the activation of MAPK p56 is thought to signal to PCD and also DNA fragmentation and several caspase-like activities are triggered as late events in the SI response (Poulter *et al.*, 2010).

As already mentioned in chapter one, the functional transfer of the *Papaver* SI to *Arabidopsis* (Lin *et al.*, 2015) opened up new horizons to research the molecular mechanism of *Papaver* SI. *Arabidopsis* is a model plant with a short generation time, numerous seed production through self-pollination and small plant size, so it does not require special facilities for growing (Koornneef and Meinke, 2010). *Arabidopsis* became the first plant species with a sequenced genome in 1998 (Meinke *et al.*, 1998). Besides, genes of interest can be transferred to *Arabidopsis*, using *Agrobacterium* cells carrying the genes to be transferred, by dipping its inflorescences (Zhang *et al.*, 2006). Because of these characteristics, *Arabidopsis* emerged as a powerful tool for understanding gene functions and a large number of genetic engineering techniques can be applied to it.

For the data presented in this chapter, reverse and forward methods developed for genetic analysis were used to identify suppressors of the self-incompatible response. We performed reverse genetic experiments in the heterologous *Arabidopsis* SI system (At-SI) to mutate candidate genes derived from earlier research into the *Papaver* SI process, followed by seed set analysis, to investigate their role in this response. On the other hand, forward genetics approaches were carried out by inducing random mutations into seeds from At-SI plants, followed by the analysis of the SNPs in each mutant presenting a self-compatible phenotype in contrast to the self-incompatible phenotype of the parent line (Figure 4.1).

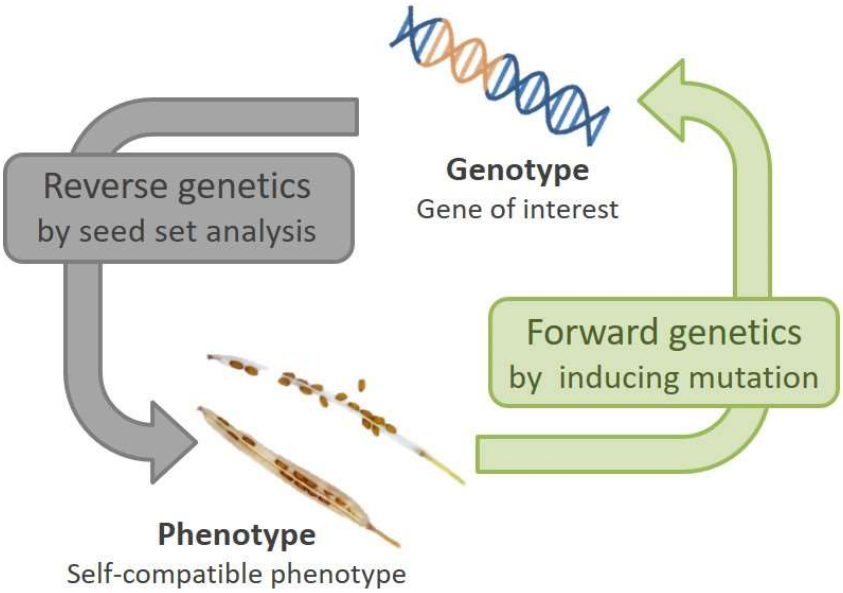

Figure 4.1 Reverse and forward genetic. Strategies used to identify suppressors of SI-PCD response can operate in two directions: Investigating candidate mutants for phenotypes (reverse genetics), or screening for phenotypes in a randomly mutagenized population to identify causative gene mutations (forward genetics).

To investigate the putative role of candidate genes during the SI response, we crossed *Arabidopsis* lines expressing PrpS in the pollen (At-PrpS lines) with T-DNA mutants of candidate genes. We selected the candidates defined as "genes of interest" based on earlier research in the *Papaver* SI-PCD model system.

Actin plays a crucial role during pollen tube elongation (Vidali *et al.*, 2001; Qu *et al.*, 2017). The SI-induced disruption and disorganization of actin filaments leads to the inhibition of the cytoplasmic streaming inside incompatible pollen tubes and it was shown that a 50% depolymerization of the actin cytoskeleton is enough to induce PCD in *Papaver* pollen tubes (Thomas *et al.*, 2006). Ultimately, the actin begins to form accumulations identified as punctate F-actin foci that keep increasing in size over time (Snowman *et al.*, 2002; Poulter *et al.*, 2010). When investigating the involvement of known regulators of actin dynamics with those F-actin foci, two ABPs have been identified as relevant due to their colocalization after the SI response with the F-actin foci. These two ABPs are Actin-Depolymerizing Factor (ADF) and Cyclase-Associated Protein (CAP) (Poulter *et al.*, 2010). Among the ADF gene family in *Arabidopsis*, which contains 11 functional protein isovariants (Ruzicka *et al.*, 2007), ADF7 was chosen as the

most promising candidate gene because of its specific expression in pollen and direct relation with the pollen tube growth. The ADF7 protein mainly localizes in young pollen tubes in the apical region and when knocked out, the pollen tube elongation rate decreased significantly compared with that of wild type (Wt) pollen (Daher and Geitmann, 2012; Zheng *et al.*, 2013), which makes it especially interesting as a potential SI regulator.

On the other hand, even if both CAP1 and CAP2 are considered as regulator proteins that control actin dynamics, in this chapter we focus on CAP1 that has been studied more extensively related to the SI response. In *Papaver* pollen, a strong presence of CAP1 was observed when total pollen protein extracts were analyzed by western blot (Poulter, Staiger, *et al.*, 2010). CAP2 presents a more restricted expression compared with CAP1 that is more widely expressed in most cells and tissues (Wang *et al.*, 2008; Zhou *et al.*, 2014) and it has been shown to interact with ADF7 in controlling actin dynamics in *Arabidopsis* pollen tubes (Jiang *et al.*, 2019). It was observed that CAP1 mutant pollen tubes could not penetrate the stigma as well as Wt pollen tubes do and their growth rate was drastically slower as well. This growth slowdown directly decreased the chances of CAP1 mutant pollen tubes reaching unfertilized ovules when in competition with wild-type pollen (Deeks *et al.*, 2007; Zhou *et al.*, 2014; Jiang *et al.*, 2019). These results showed that ADF7 and CAP1 are crucial for regulating actin dynamics during normal pollen tube growth. However, it is still unknown if they also play roles by affecting the actin dynamics in pollen tubes during the SI response. Therefore, both of them were selected as candidate genes for reversed genetics analysis using the heterologous *Arabidopsis* SI system.

Another genetic target to include in the reverse genetics approach was eukaryotic translation elongation factor 1α (eEF1α). Previous experiments had identified EF1α as an F-actin-associated target of SI-induced ROS (unpublished data). EF1α is an abundant component of the actin cytoskeleton-associated translational apparatus in eukaryotic protein synthesis. It is a very conserved family with more than 70% of sequence identity among the orthologs in eukaryotes. The binding of EF1α to F-actin in animal cells is pH-sensitive. The cytosolic acidification results in EF1α being actin-associated, which sequesters it from interaction with aminoacyl-tRNA, inhibiting protein

biosynthesis (Liu *et al.*, 1996; Gross and Kinzy, 2005). Its role in S-RNAse-based SI was studied in the Solanaceae family using *Solanum chacoense*. For this species, it was identified as a potential binding protein with the female determinant and key for the rejection mechanisms of the self-incompatible tubes (Soulard *et al.*, 2014). However, if EF1α has a role in *Papaver* SI remains elucidated. In *Arabidopsis*, four different genes are responsible for encoding EF1α with identical amino acid sequences: At1g07920 named A3 EF1α-3, At1g07930 or A2 EF1α-2, At1g07940 or A1 EF1α-1 and At5g60390 or A4 EF1α-4 (Wang *et al.*, 2012). However, differences between them were reported based on their physical separation and a comparison of their genomic sequences. Those differences suggested that the A4 gene and the A1, A2, and A3 genes could constitute two distinct subfamilies. Because, even if there are no differences in codon usage in the four *Arabidopsis* EF1α genes, and all four contain an intron at an identical position within the coding sequences (462 bp downstream of the initiating ATG codon), this intron is identical in A1 and A3, nearly homologous in A2 but completely divergent in A4 (Axelos *et al.*, 1989). Nevertheless, the final proteins obtained from those four genes are identical.

Related to PCD, we further focused on peptidases with caspase-like activity, as it is well established that caspases are essential proteases that are activated rapidly during apoptosis in animal cells (Riedl and Shi, 2004), and that caspase-like activity has been implicated in many types of plant cell death (Reape *et al.*, 2008). Its role is not to degrade enzymes as cathepsins or digestives enzymes do, but intervene as signalling peptidases. There are 12 caspases defined so far in humans with a well-conserved structure. These family members can be grouped according to their role in the activation cascade being executioners, initiators or inflammatory. This cascade starts with the initiator caspases (caspases 8, 9 and 10), leading to the activation of executioner caspases (caspases 3 and 7) by cleaving them. In a section of this chapter, I am focused on the SI-triggered caspase-3-like activity.

In contrast to animals, there are no caspase genes encoded in plant genomes, although caspase-like activities can be biochemically detected in association with many types of plant cell death (Reape *et al.*, 2008). Eight different caspase-like activities have been described in plants until now, including YVADase (caspase-1-like activity), DEVDase

(caspase-3-like activity), VEIDase (caspase-6-like activity), IETDase (caspase-8-like activity), VKMDase (caspase-6-like activity), LEHDase, TATDase and LEVDase (caspase-9-like activity) (Xu and Zhang, 2009). Considering that the detection of caspase-like activities in plants correlating with PCD induction would not demonstrate a regulatory role in the process, it suggests that they are involved in the PCD responses. To date, it has already been confirmed that caspase-like activities such as YVADase, DEVEase and VEIDase mediates different plant PCD processes (Cai and Gallois, 2015).

When analysing the *Papaver* SI system, it was observed that SI induced a caspase-3-like activity, showing maximum substrate cleavage at pH 5 (*in vitro*), with peak activity 5 h after SI induction *in vivo* (Bosch and Franklin-Tong, 2007). Caspase-like activity related to PCD is a chemically induced response in tomato (*Lycopersicon esculentum*) suspension cells (Woltering *et al.*, 2002). When tomato cells were treated with caspase 1 and caspase 3 inhibitors, it showed that apoptotic features such as nuclear and DNA fragmentation were inhibited. Indeed, nuclear DNA fragmentation, which is one of the most characteristic features of PCD, has been detected in both animals and plants and was also found in *Papaver* during SI in an S-specific manner (Jordan *et al.*, 2000). It was observed that there was DNA fragmentation in incompatible pollen and it can be inhibited by pretreatment with the caspase-3 inhibitor peptide, Ac-DEVD-CHO. In addition, pretreatment with the caspase-3 inhibitor alleviated the SI-induced pollen tube growth inhibition. The growth of incompatible pollen tubes was arrested within 5 minutes after SI induction, but caspase-3 inhibitor pretreatment resulted in the growth reinitiation after SI-induced inhibition. However, this recovery of growth does not happen when treated with a caspase-1 inhibitor (Thomas and Franklin-Tong, 2004). In human cells, caspase 3 activates an endonuclease called caspase-activated DNase, responsible for DNA fragmentation. It has been reported that caspase 3 is essential for the activation of components required for DNA fragmentation and morphological changes during apoptosis. Furthermore, caspase 3 is considered to cleave structural proteins involved in preserving the cytoplasmic and nuclear architecture and integrity (see Jänicke *et al.*, 1998). Thus, these findings indicated a relevance of the SI-induced caspase-3-like activity for SI-PCD.

We were also interested in cathepsin B (CathB), which is a cysteine protease that presents both endopeptidase and exopeptidase activity (Cavallo-Medved *et al.*, 2011), as a genetic target. This protease was found to possess caspase-3-like activity *in vitro* when purified from *Arabidopsis* seedlings. It was tested and confirmed using the synthetic caspase-3 substrate DEVD and synthetic caspase-3 inhibitors, obtaining a reduction in PCD when CathB was targeted with a caspase-3 inhibitor. Even though in normal conditions, the ultraviolet (UV) light induces apoptotic-like changes in *Arabidopsis* (Rotari *et al.*, 2005; Rotari, He and Gallois, 2005), when using a CathB1-2-3 mutant, a reduction of PCD was observed when treated with UV light (Ge *et al.*, 2016). Results suggested that these proteases may regulate the PCD pathway activated by UV light. This pathway may have evolved before the plant and animal kingdoms diverged. The main difference between its role in plants and animals, is that in plants CathB maintains its regulatory activity in the PCD process, however in animals their role is more restricted (Ge *et al.*, 2016). They also differ in their site of action, presenting in humans an exopeptidase activity (Illy *et al.*, 1997) but endopeptidase activity in plants (Iglesias-Fernández *et al.*, 2014). Due to this, CathB represented an interesting candidate to be related to SI-PCD and suitable for further analysis with reverse genetics approaches.

4.2. Material and methods

4.2.1. Actin-binding proteins in SI-PCD

To test the ABPs ADF7 and CAP1, new lines were obtained expressing $PrpS_1$-GFP and having one of those two ABPs knocked out by a T-DNA insertion. The T-DNA lines SALK_024576.47.05.x and SALK_112802.30.55.x were used as they presented an insertion in AT4G25590 encoding ADF7 and At4g34490.1 coding for CAP1, respectively (Figure 4.2A). According to the Salk Genotyping Project, Mutant adf7 and cap1 homozygous lines for the insertion were selected (Table 4.1).

Plant DNA was extracted by the Quick plant DNA extraction protocol for PCR genotyping. Leaf discs were collected separately in 500 µl tubes with alcohol-cleaned forceps. In each tube, 50 µL of extraction buffer were added (0.1 M Tris-HCl pH 9.5; 0.25 M KCl; 0.01 M EDTA). The leaf tissue was ground in a Mixer Mill (20 Hz, 1 min) with the addition of two 2.8 mm steel beads. The samples were incubated at 95 °C on a

thermoblock for 10 min and cooled on ice for 5 min. Bovine Serum Albumin (BSA) was added for stabilization (50 µL 3% (w/v)) and the mixtures were vortexed and centrifuged (13,200 rpm, 1 min). Supernatants were collected and subjected to PCR analysis. For each PCR analysis, 1 µL of extracted DNA was used as the template in a 20 µL PCR reaction with REDTaq® ReadyMix.

To obtain *adf7* and *cap1* lines coexpressing $PrpS_1$-GFP, mutant lines were pollinated with At-$PrpS_1$ pollen having GFP as a tag. The same procedure for DNA extraction was carried out. The presence of $PrpS_1$-GFP was confirmed with both microscopy observation of pollen grains and PCR analysis of DNA extracted by Quick plant DNA extraction protocol.

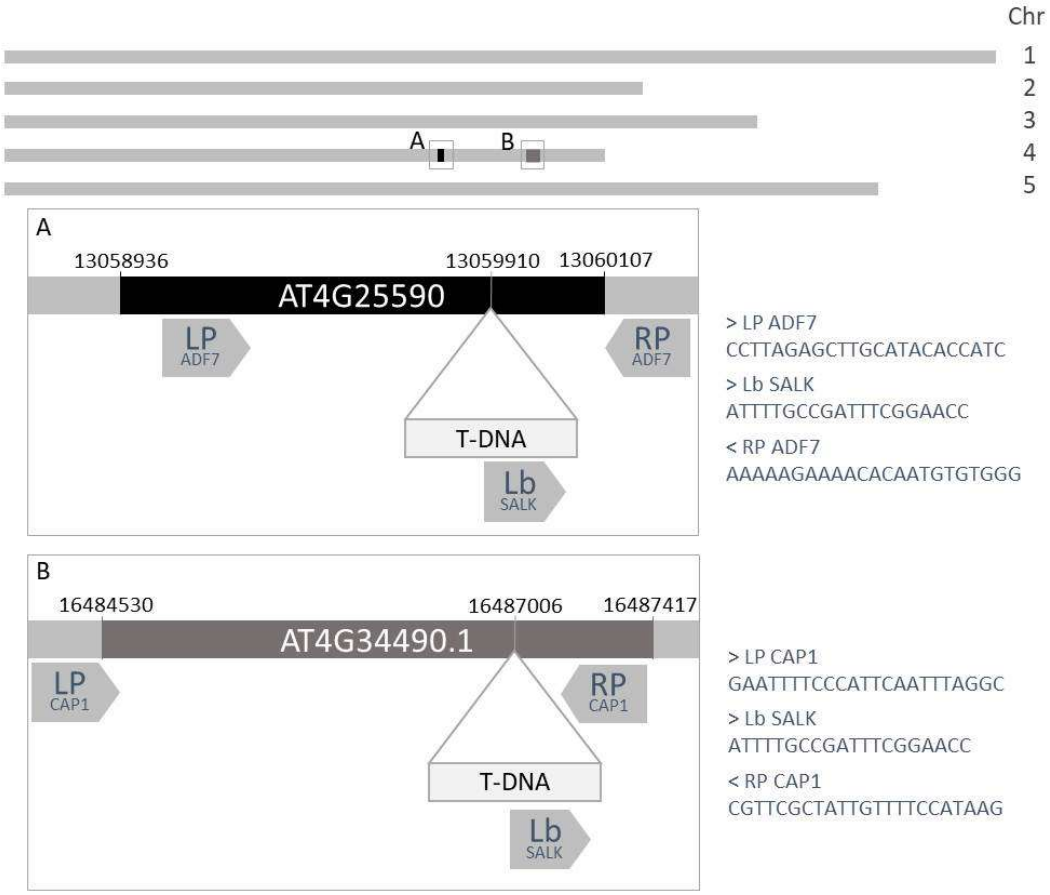

Figure 4.2. Map detail representation of lines used for reverse genetic analysis of actin-binding proteins. At4g25590, coding for ADF7, is located on chromosome 4 with SALK_024576.47.05.x having a T-DNA insertion in this gene located at 13059910 bps (A). At4g34490.1, coding for CAP1, is as well located on chromosome 4 with SALK_112802.30.55.x having a T-DNA insertion in this gene located at 16487006 bps (B). Details of the primers used for genotyping are indicated.

Table 4.1. Genotyping of ADF7 and CAP1 T-DNA mutants. Wild type (WT) lines do not have any insertion. Therefore a PCR product is obtained when using the specific left primer (LP) and right primer (RP). The homozygous (HM) lines present insertions in both chromosomes, so they generate a PCR product when running with the left border (Lb) and RP primers. Since the heterozygous (HZ) lines have one of the pair chromosomes with insertion, PCR products are obtained with both primer pairs.

				Bands observed when running the PCR products on agarose gel		
ABP	T-DNA Line	Primers	Product size (bp)	WT	HZ	HM
ADF7	SALK_024576.47.05.x	LP-RP	1015			
		Lb-RP	449-749			
CAP1	SALK_112802.30.55.x	LP-RP	1184			
		Lb-RP	550-850			

4.2.2. Caspase activity in SI-PCD

To analyse the effects of CathB on SI-PCD, two mutant lines, generated and received from the Gallois lab, Faculty of Life Sciences at the University of Manchester, were used. Those lines were a double mutant homozygous for CathB1-3 and a triple CathB1-2-3 mutant. To generate the double mutant, homozygous lines for the insertion after crossing SALK_151526 and SALK_019630 were obtained as they have an insertion in At1g02300 and At4g01610 respectively. On the other hand, it was not possible for them to obtain a triple mutant by crossing, so an RNAi hairpin silencing construct was cloned for CathB2 using a two-step nested PCR and Cathb1-3 double mutants were transformed with the CathB2:RNAi construct by floral dipping (McLellan *et al.*, 2009; Ge *et al.*, 2016). When tested, they were homozygous for the insertions (Table 4.2), both lines were pollinated with pollen expressing $PrpS_1$-GFP for them to have the male S determinant and proceed with SI-PCD tests.

Table 4.2. Genotyping CathB mutants. The primers used for genotyping SALK_151526 were left primer (LP) TGCTTTTGTTTACTTGGAAGGTC and right primer (RP) GAATGTTTCCTTATCTGCCAATG. For genotyping SALK_019630 we used LP TGGTGCTGTTGAATCACTATCAG and RP TTGCCATCAACTAAACACAAGAG. Lines analyzed: Wild type (WT), homozygous (HM) and heterozygous (HZ).

				Bands observed when running the PCR products on agarose gel		
CathB	T-DNA Line	Primers	Product size (bp)	WT	HZ	HM
1	SALK_151526	LP-RP	795			
		Lb-RP	382-582			
3	SALK_019630	LP-RP	868			
		Lb-RP	441-641			

4.2.3. Elongation factor 1α in SI-PCD

The high identity of the four *Arabidopsis* genes encoding EF1α (the EF1α Affymetrix probe recognises them all) made this a potentially interesting target for using a CRISPR/Cas9 genome editing approach to silence the four EF1α genes.

To proceed with the silencing of At1g07920, At1g07930, At1g07940 and At5g60390, four target sequences were defined for designing the guide RNA (gRNA) using the CRISPOR online tool (Haeussler *et al.*, 2016). To those sequences, BbsI sites were included on both sides with specific primers and inserted in a guide RNA vector (Table 4.3). The vector pMR2017 was used for gRNA1 and gRNA2 and pMR2018 for gRNA3 and gRNA4. With this procedure, two strategies are followed. For the "strategy g1-g4", the sequences g1 and g4 were present in the destination vector Cas9 to cause the deletion of the fragment between them. For the "strategy g2-g3" the fragment between g2 and g3 was the one removed as a product (Figure 4.3, Appendix figure 4.1).

Table 4.3. Primers used for constructing the gRNA designed. F corresponds to forward and R to reverse primers.

EF1α-g1-F	ATTGAGGCTGCTGAGATGAACAAG
EF1α -g1-R	AAACCTTGTTCATCTCAGCAGCCT
EF1α -g2-F	ATTGGAGGTCCTTCAAGTACGCAT
EF1α -g2-R	AAACATGCGTACTTGAAGGACCTC
EF1α-g3-F	ATTGATCATTGACTCCACCACTGG
EF1α-g3-R	AAACCCAGTGGTGGAGTCAATGAT
EF1α-g4-F	ATTGGTACGATGAAATCATCAAGG
EF1α-g4-R	AAACCCTTGATGATTTCATCGTAC

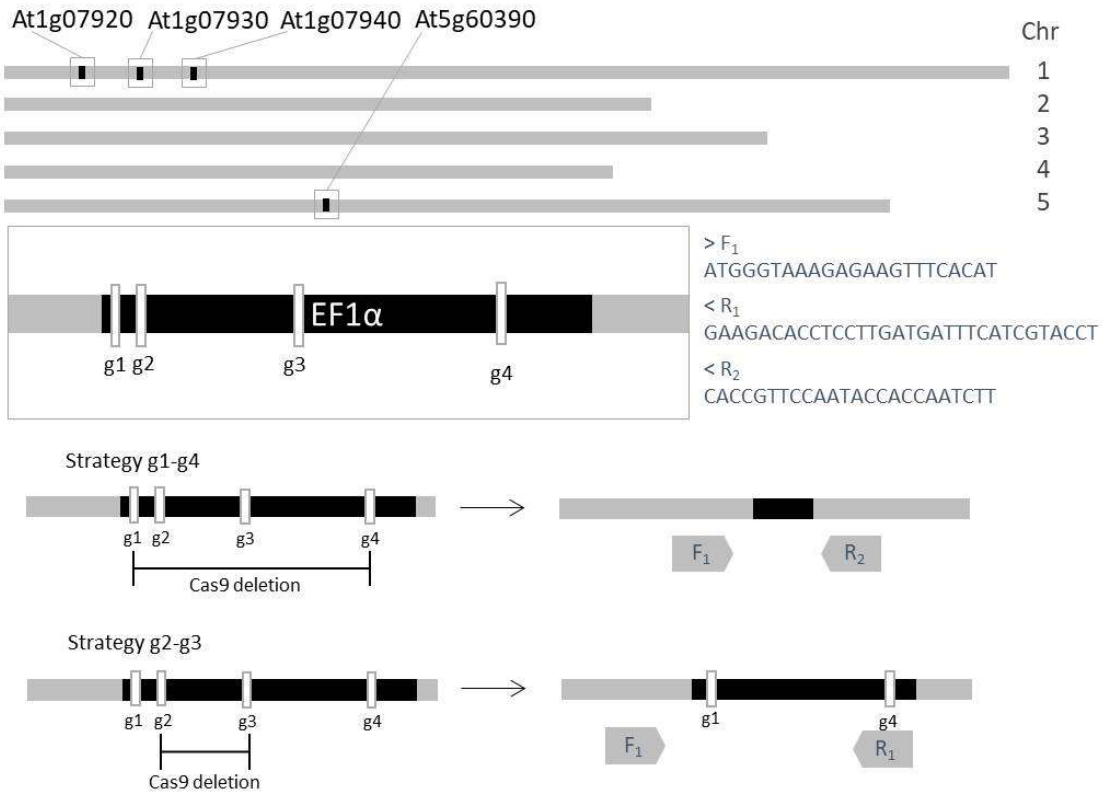

Figure 4.3. Scheme of the two strategies planned to knock out EF1α. Location in Arabidopsis genome of the four genes encoding EF1α. The location of the gRNA sites in the EF1α genes are indicated as g1, g2, g3 and g4. F and R correspond to forward and reverse primers.

When both vectors were ready, *Escherichia coli* (strain DH5α) was used for cloning. The final destination vector was included in *Agrobacterium* by electroporation (Appendix protocol 4.1). For selecting the colonies used for the plant transformation (Appendix protocol 4.2. Plant), colonies were grown on plates with LB, rifampicin, gentamycin and spectinomycin. The floral dipping was performed as explained below in section 5.2.3. When ready, the seeds were sterilised for 6 hours in a desiccator with 150 mL bleach + 8 mL concentrated HCl (37 %; 12 M). After that, seeds were grown on plates under controlled conditions of 22-25 ^{o}C and continuous light.

4.2.4. Evaluation of the phenotypes after pollinations with pollen expressing PrpS1 and mutant for candidate genes potentially involved in SI-PCD

To test the engineered lines selected, the first step is the emasculation of flowers whose stigmas would be pollinated. Stigmas from two lines were required, being wild type (Wt or Col-0) and *Arabidopsis* lines expressing PrsS (At-PrsS_1). As a control for all

the individual cases, both types of stigmas were manually pollinated with Col-0 pollen and pollen expressing $PrpS_1$-GFP separately (Table 4.4).

Table 4.4. Controls for SI-PCD Reverse genetic analysis. Stigmas Wt and expressing $PrsS_1$ were pollinated with Wt pollen (yellow) and pollen expressing $PrpS_1$-GFP (green).

Pollen	Col-0	$PrpS_1$-GFP	Col-0	$PrpS_1$-GFP
Stigma	Col-0	Col-0	$PrsS_1$	$PrsS_1$
Diagram	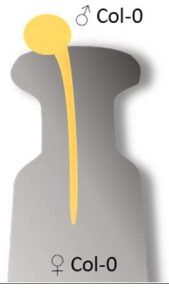	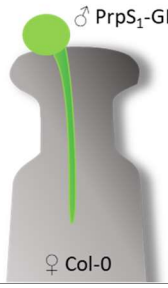		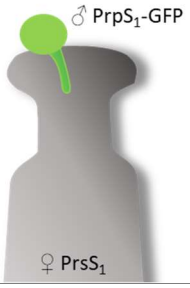
Seed-set	SC	SC	SC	SI

When all the mutant lines of interest were ready, ~5 pollinations were performed for each of them (Table 4.5). Each stigma was labelled and all plants were protected with the aratube component of the Arasystem, which is a 40 cm high transparent and fully antistatic plastic tube. Three weeks after pollination, the siliques were measured and the number of seeds per siliques counted.

Table 4.5. Lines used as male lines for manual pollinations.

Code	*Arabidopsis* thaliana Line
Wt or Col-0	Columbia-0
At-SI	pNTP303::$PrpS_1$-GFP_pSLR1::$PrsS_1$ (Lin *et al.*, 2015)
At-$PrpS_1$	pNTP303::$PrpS_1$-GFP (De Graaf *et al.*, 2012)
***CathB1-3*_$PrpS_1$**	SALK_151526 and SALK_019630 (Ge *et al.*, 2016)
***CathB1-2-3*_$PrpS_1$**	SALK_151526 and SALK_019630 plus a RNAi line (Ge *et al.*, 2016)
ADF7$^-$	SALK_024576.47.05.x (Zheng *et al.*, 2013)
ADF7$^-$_$PrpS_1$	SALK_024576.47.05.x_pNTP303::$PrpS_1$-GFP
CAP1$^-$	SALK_112802 (Deeks *et al.*, 2007)
CAP1$^-$_$PrpS_1$	SALK_112802_pNTP303::$PrpS_1$-GFP

4.3. Results

As described before, candidate genes were selected based on published results in *Papaver* that implicated specific pathways or gene functions in SI-PCD. Pollen from selected candidate mutants expressing $PrpS_1$ was used to pollinate self-incompatible *Arabidopsis*. We evaluated the phenotype of the siliques obtained and the seed set from these crosses. A self-compatible phenotype would indicate the involvement of the genes of interest in the SI-PCD response. On the other hand, the presence of more seeds when compared to those obtained in the SI control pollinations, would indicate a potential partial recovery of seed set and suggest a minor role of the genes of interest.

4.3.1. Actin-binding proteins in SI-PCD

In *Papaver*, SI triggers a rapid reorganization and depolymerization of actin filaments in incompatible pollen tubes which are defined as early events (Snowman *et al.*, 2002). The co-localization of the actin-binding proteins ADF and CAP with the F-actin foci formed after SI (Poulter *et al.*, 2010), led us to analyze their role in this response. Using reverse genetics approaches, the T-DNA mutants *adf7* and *cap1* were obtained and introduced into At-$PrpS_1$ background by crossing.

Self-compatible pollinations resulted in siliques ranging from 12.5 mm to 17 mm in length containing 28-48 seeds (Figure 4.4). Pollinations of stigmas expressing $PrsS_1$ with either *cap1* pollen or *adf7* pollen (not expressing $PrpS_1$) led to silique lengths and seed numbers typical for SC pollinations (Figure 4.4). Although Wt stigmas pollinated with *adf7/PrpS₁* had normal siliques, their seed count was significantly lower (~30) than other SC pollinations. Wt stigmas pollinated with *cap1/PrpS₁* showed both shorter siliques (average 8.3 mm) and reduced number of seeds (average 9.8 seeds). This could suggest that the combination of knocking out either CAP1 or ADF7 in combination with expressing $PrpS_1$ in pollen reduces their fitness.

Most importantly however, were the observations that none of the SI pollinations involving CAP1 or ADF7 mutant pollen could restore or even partially recover silique length or seed numbers (Figure 4.4). Stigmas expressing $PrsS_1$ pollinated with either *adf7*/$PrpS_1$ or *cap1*/$PrpS_1$ pollen exhibited similar siliques and seed numbers to the SI control pollination (stigmas expressing *PrsS₁* pollinated with pollen expressing

$PrpS_1$) (Figure 4.4). Together these results indicate that the knock-out of the ABPs ADF7 and CAP1 does not overcome the SI response.

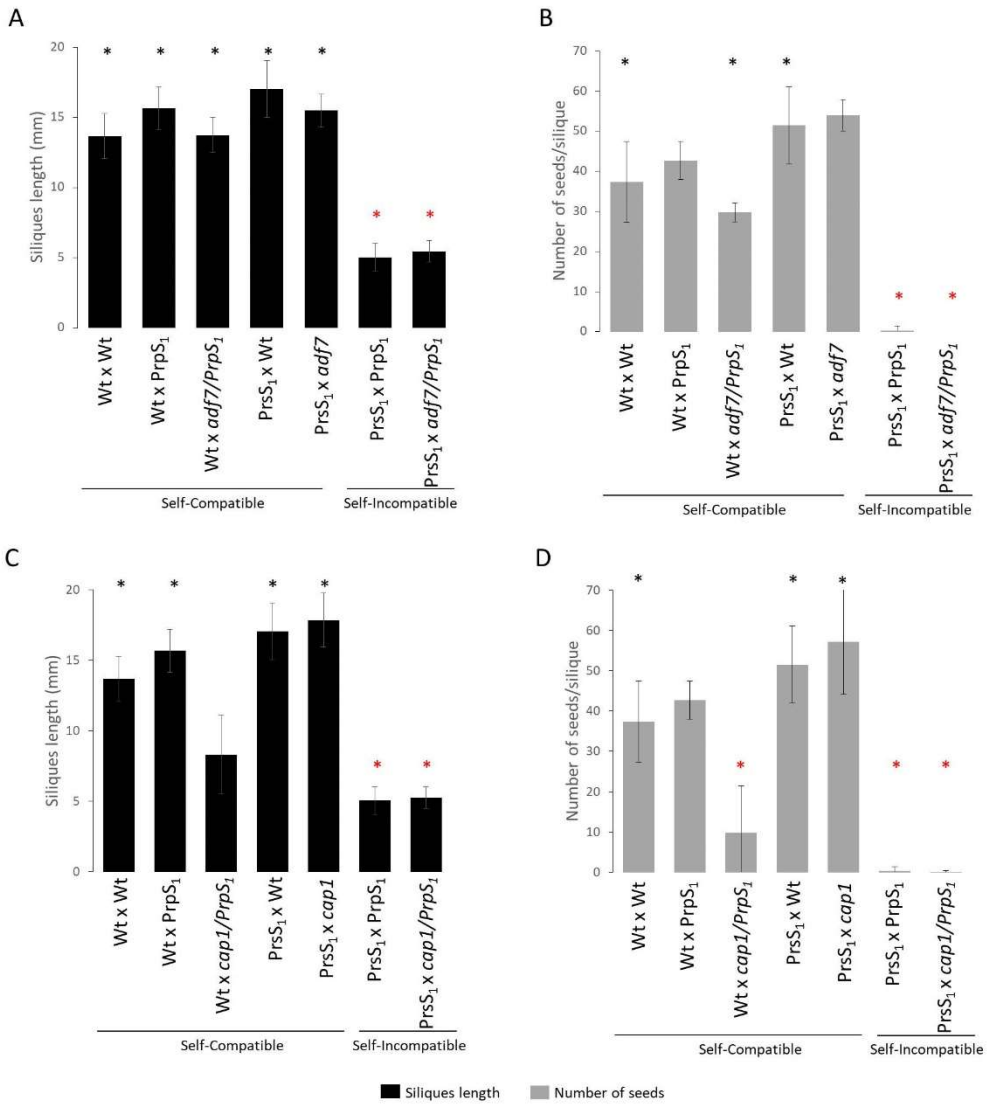

Figure 4.4. Seed set for compatible and incompatible pollinations with ADF7 and CAP1 mutant pollen. Data obtained to analyse ADF7 (siliques length A and number of seeds B) and CAP1 (siliques length C and number of seeds D). Pollinated Wt stigmas produced siliques with an SC phenotype, although in particular pollination with *cap1*/$PrpS_1$ pollen resulted in shorter siliques and lower number of seeds (C, D). The siliques produced from At-$PrsS_1$ stigmas always presented a SC phenotype when the pollen used did not express $PrpS_1$. On the other hand, for *adf7*/$PrpS_1$ and *cap1*/$PrpS_1$ pollen, siliques and seed set were found typical of SI and were statistically similar to At-SI control. Result = mean±SD (n=3 to 5). Black * when $p<0.05$ comparing with $PrsS_1$x$PrpS_1$ by Kruskal-Wallis test; Red * when $p<0.05$ comparing with WtxWt by Kruskal-Wallis test.

4.3.2. Caspase activity in SI-PCD

The detection of caspase-like activity during the SI response is a powerful indicator of PCD. Since CathB exhibits caspase-3-like activity (Ge *et al.*, 2016), the caspase-3-like activity present during the SI-PCD response may be associated with CathB. Using CathB mutants (*CathB*), we therefore tested if the absence of CathB could affect the SI-PCD response. We analyzed the seed-set of $PrpS_1$-GFP expressing pollen in the *CathB1-3* double mutant (*CathB1-3*/$PrpS_1$) and the *CatB1-2-3* triple mutant (*CathB1-2-3*/$PrpS_1$) when pollinating At-$PrsS_1$ stigmas. The seed-set obtained for these pollinations was not different from SI (Figure 4.5). Although the obtained silique phenotypes suggest that CathB is not involved in the SI-PCD response, it should be noted that some seed was formed when pollinating At-$PrsS_1$ stigmas with *CathB1-3*/$PrpS_1$ and *CathB1-2-3*/$PrpS_1$ pollen. The formation up to 3 seeds in some cases, means that a few pollen tubes reached the ovule despite both SI determinants being present. These results do not let us discard entirely CathB as a participant in the SI-PCD response.

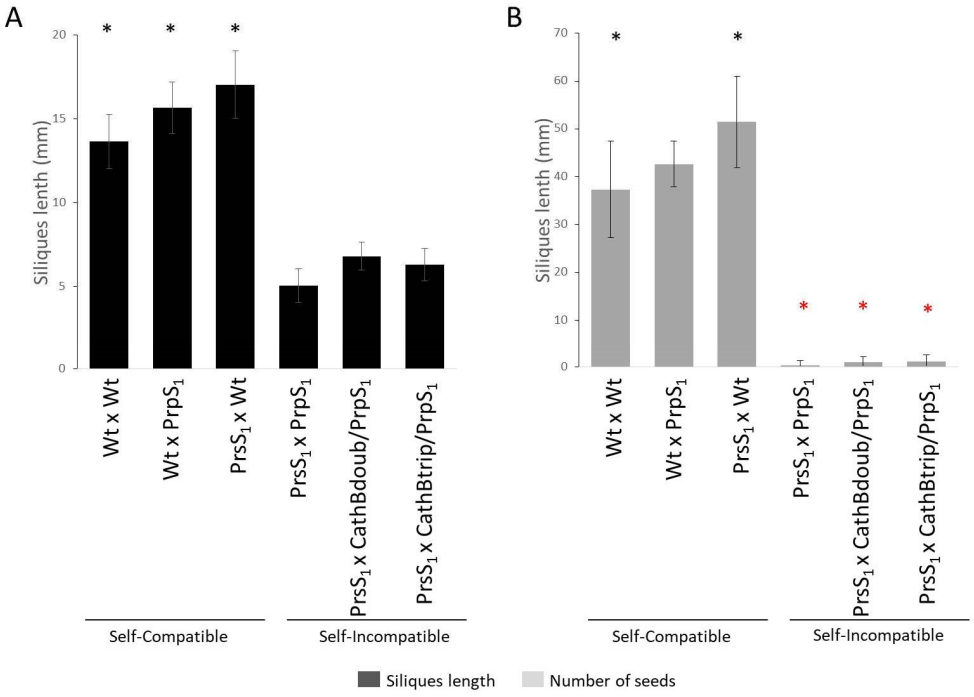

Figure 4.5. Seed set for compatible and incompatible pollinations with CathB mutant pollen. All three SC pollinations performed resulted in a large number of seeds. Little to no seed was formed for the three SI pollinations. The absence of CathB1-3 and CathB1-2-3 expression did not show differences with At-SI self-pollination, indicating that CathB is not directly involved in the SI response. Result = mean±SD (n=5). Black * when $p<0.05$ comparing with $PrsS_1$x$PrpS_1$ by Kruskal-Wallis test; Red * when $p<0.05$ comparing with WtxWt by Kruskal-Wallis test.

4.3.3. Elongation factor 1α in SI-PCD

One of the earliest events in the SI response is cytosolic acidification. EF1α has been found in association with F-actin under low pH (Liu *et al.*, 1996). To observe the possible implication of EF1α in the SI-PCD response, EF1α mutant pollen was generated. The idea of obtaining a quadruple mutant using T-DNA lines was discarded as At1g07920, At1g07930, and At1g07940 are genetically highly linked. Therefore, a CRISPR-Cas9 approach was adopted to generate EF1α mutants. However, when those CRISPR-Cas9 generated EF1α knockouts were sown, mutant seedlings were obtained, but they were not healthy and never reached to be adult plants. Thus, knocking out the four EF1α genes with CRISPR-Cas9, suggested that this approach might be lethal for the plant development. Because of that, it was not possible to use reverse genetic approaches for researching the role of EF1α in SI-PCD. However, EF1α is still an interesting highly conserved protein worthy of further analysis in the future.

4.4. Discussion

The newly established heterologous SI system expressed in *Arabidopsis* allowed us to carry out experiments difficult to perform in *Papaver* plants. Reverse and forward genetic analysis provided new information about the SI-PCD pathway and the possible implication of certain genes in this process.

These reverse genetic analyses aimed to investigate the involvement of ADF7, CAP1, CathB and EF1α in the execution of the SI-PCD response in $PrpS_1$-expressing *Arabidopsis* pollen. The results obtained for ADF7, CAP1 and CathB indicate that knocking out these genes is not enough to revert the SI response and recover seedset, while the analysis of EF1α was complicated by the high identity of the different isoforms and the lethality of its absence.

The close association that ADF7 and CAP1 have with the F-actin foci formed during the SI response is well described in *Papaver*. It suggests they have a possible role during the later stages in the SI response, in the formation and/or maintenance of the F-actin foci (Poulter *et al.*, 2010). The changes in actin filaments were confirmed to be triggered, directly or indirectly, by the cytosol acidification early in the SI response and the colocalization of ADF7 and CAP1 with the F-actin foci was always observed under

the condition of low cytosolic pH (Wilkins *et al.*, 2015; Wang *et al.*, 2020). The dynamic properties and explanations for the F-actin foci formation and its specific role are still unclear. Likewise, the importance of ADF7 and CAP1 for the process of the F-actin foci formation and consequently, its implication in the SI response is unknown. Their role may be similar to Villin which is a calcium-responsive ABP. Villins mediate actin alterations when $[Ca^{2+}]_{cyt}$ increases in the pollen tube (Zhao *et al.*, 2020). This was observed in *Arabidopsis* by fixing and staining pollen tubes to visualize F-actin at different time points, when treated with the Ca^{2+} ionophore A23187 (Zhao *et al.*, 2020) that mimics de SI response in *Papaver* (Snowman *et al.*, 2002). Therefore, a possible role that ADF7 and CAP1 may have is to be involved in the actin reorganization process generating and enlarging fragmented actin filament structures to form foci. However, the physiological function of the foci and whether they have a specific role in the SI-PCD process is still unknown.

The results from SI pollinations with ADF7 or CAP1 mutant pollen grains shown in this chapter did not result in reversion of SI. This indicates that even if both ABPs take part in the SI response, the absence of ADF7 or CAP1 is not enough to block the SI-PCD response. In order to confirm this statement, it is necessary to keep investigating these two ABPs in further experiments, including life cell imaging of these mutant At-SI lines that also express a marker for actin to determine if any change is observed structurally in the formation of F-actin foci comparing with At-SI.

Our results partially agree with the fertilization handicaps observed in previous experiments with *Arabidopsis cap1* mutant plants. These mutant pollen grains presented a reduction in the pollen germination rate comparing with Wt and a dramatic reduction in the pollen tube mean growth speed. However, after a sufficient growth period, mutant pollen tubes could fertilize the ovules (Deeks *et al.*, 2007). However, the SC pollinations we performed produced a number of seeds and silique lengths that were significantly higher when CAP1 mutant pollinated stigmas expressing $PrsS_1$ compared with Wt. On the other hand, a significant dramatic reduction in both parameters is obtained in the scenario Wtx*cap1*/$PrpS_1$ even if it is also a SC cross. The success of more than 20 pollen tubes achieving fertilization in some samples indicates that some individual pollen tubes can occasionally overcome the biological response avoiding

fertilization, but it well deserves further analysis to elucidate the reason behind. Nevertheless, cap1/$PrpS_1$ pollen triggered a self-incompatible reaction in $PrsS_1$ stigmas. On the contrary, the experiment with ADF7 using *adf7*/$PrpS_1$ pollen to perform CS crosses in Wt stigmas resulted in slightly reduced siliques and the number of seeds contrasted to Wt, but in this case, they are not significantly different when compared statistically.

Likewise associated with SI-PCD, the elongation factor 1α (EF1α) was included in this analysis with a reverse genetics approach. This component is abundant in the cytoplasm of all cells, including the pollen tubes (Liu *et al.*, 1996; Gross and Kinzy, 2005) and is considered an important factor in the cytoskeleton organization in eukaryotic cells with evolutionarily conserved importance in *Arabidopsis* (Ndamukong *et al.*, 2011). In incompatible *Solanum chacoense* the presence of S ribonuclease (S-RNase) encoded by the multiallelic S-locus, creates an S-RNase-EF1α complex that may be linked to actin cytoskeleton reorganization during the SI reaction (reviewed in Soulard *et al.*, 2014) similar as EF1α binding actin monomers in the phagotrophic bacteriovivores *Dictyostelium* (Dharmawardhane *et al.*, 1991). In *S. chacoense* SI two hypotheses relate actin with EF1A: the S-RNase-EF1α complex binding actin or EF1α mediating the binding of S-RNase with actin (Soulard *et al.*, 2014). Since there are four nearly identical genes encoding this protein in *Arabidopsis*, we attempted to knock out all 4 EF1α paralogs using CRISPR-Cas9 technology. The resulting mutant plants were heavily affected in growth and development and did not reproduce. Even if the F-actin association of this factor is important for SI, which remains to be established, it is noteworthy mentioning that EF1α is called a moonlighting protein due to the multiple roles that it may assume. For example, EF1α has been shown to interact not only with actin but also with valyl-tRNA synthetase complex, tubulin, ubiquitin and calmodulin. In addition, it is involved in signal transduction, virus infection mechanism, nuclear export of proteins and mitochondrial tRNA import (reviewed in Suhandono *et al.*, 2014). Due to this, further experiments should be defined differently preserving the plant life while analyzing the function of EF1α in the SI response. For example, testing the four genes independently or in pairs could give us some more information. The use of the tissue-specific knockout techniques based on CRISPR (CRISPR-TSKO) would be a powerful tool to address the

severe defects of knocking out the 4 EF1α genes (Decaestecker *et al.*, 2019). Due to its capacity of specifically silencing genes in particular plant cell types, it would allow us to get the four genes coding for EF1α knocked out but only in the pollen specifically.

In direct relation to PCD, we have focussed on CathB as it was evidenced to have a role in PCD and it is possibly implicated in triggering an ancestral PCD pathway that existed before the divergence of the plant and animal kingdom (Ge *et al.*, 2016). In *Arabidopsis*, CathB presents DEVDase-like/caspase-3-like activity, similar to the well-established cathepsin activity in animals (Ge *et al.*, 2016). In *Papaver* pollen tubes, an increase in DEVDase activity was observed from 1 h after SI induction, even if the maximum was only reached after 5 h (Bosch and Franklin-Tong, 2007). Since Cathepsins represent one of the few plant proteases identified thus far with DEVDase-like/caspase-3-like activity, the aim was to test if the absence of cathepsin could alleviate the SI-induced PCD process and restore fertilization, even if PCD is a late event in the SI response. However, when SI pollinations were performed with CathB mutants, there was no difference observed in the silique lengths and seed number per silique comparing with At-SI pollination. However, this does not discard CathB as playing a role in the SI-PCD process. Pollen tube growth is quickly arrested by SI so even if CathB is involved in the PCD process, knocking them out may not lead to a recovery of pollen tube growth and thus seedset. Additional experiments are needed to elucidate if CathB is involved in the SI-induced PCD process. For instance, measurements of caspase-3-like activity with probes in *cathB1-3* and *cathB1-2-3* double- and triple-mutant At-SI pollen *in vitro* would give us the information if these cathepsins are responsible for the caspase-3-like activity during SI-PCD.

Chapter five. Forward genetics analysis: Mutant screen for SI-PCD suppressors

5.1. Introduction

As mentioned in chapter one, PCD plays a vital role during the plants' life cycle. However, in comparison with animal PCD, the molecular mechanisms of plant PCD are

still largely unknown. For instance, as explained in chapter four, there are no clear homologs of animal caspases in plants, which renders knowledge transfer from animal to plant systems ineffective. In particular, we have very limited genetic knowledge, especially related to the PCD aspect triggered in *Papaver* pollen tubes after the SI response. Even if several events important for signalling to PCD have been already described (detailed in chapter two) we hardly have any information about the specific genes involved.

Hence, an unbiased ethyl methanesulfonate (EMS) based forward genetics approach to identify SI-regulators has the power to uncover entirely novel genes and mechanisms involved in PCD regulation.

By screening mutated populations for phenotypes of interest, novel gene candidates and functions can be determined using forward genetics (Ülker and Weisshaar, 2011). The more noteworthy feature of this approach is that it does not require a preconceived idea about the nature of the gene involved, representing an absolutely unbiased gene discovery process (Alonso and Ecker, 2006). EMS has high reliability as a mutagen so it was selected for this assay (McCallum et al., 2000). It is an alkylating agent that induces chemical modifications of nucleotides. Those modifications result in base changes and mispairing. The alkylation of guanine (G) residues forms O^6-ethylguanine, which can pair with thymine (T) but not with cytosine (C). Due to this, the original G/C pair can then be replaced with A (adenine)/T in the subsequent DNA repair (Greene *et al.*, 2003).

With the functional heterologous SI-PCD system in *Arabidopsis*, we now have a unique opportunity to perform a forward genetics mutant screen at high efficiency. In contrast to other tissues undergoing PCD, the SI-PCD system has several striking advantages. Firstly, pollen cells are haploid and short-lived. Hence, they can reveal phenotypes even of essential genes, which are impossible to detect in conventional screens due to the lethality of homozygous mutant plants. Secondly, the pollen transcriptome comprises only a fraction of the plant's transcriptome, which reduces the chance that gene functions are masked by redundancy. And thirdly, screening heterozygous M1 plants in a single line screen for the restoration of fertility allows a

high-throughput visual screening without the need of microscopy, which is challenging in other PCD systems.

In this case, the mutant screen was designed to detect mutations having an effect on pollen. This implies that our experimental design differs from the regular EMS mutagenesis setup which is designed to identify sporophytic mutations. In a self-incompatible line, siliques with very little or no seed-set and minimal elongation after pollination (around 5 mm) are expected (Lin *et al.*, 2015). SI-PCD suppressor mutants were identified by looking for plants with longer siliques. A heterozygous mutation in the M1 plants would already lead to the breakdown of SI for half the pollen population, resulting in full seed set and restored silique length (~17 mm). Therefore, we screened for PCD modulators in the M1 generation by selecting those plants with restored silique length and seed production. In addition, wild-type pollen is killed as a consequence of the SI-PCD reaction, so only the mutant pollen grains will reach the ovules and produce seeds (Figure 5.1).

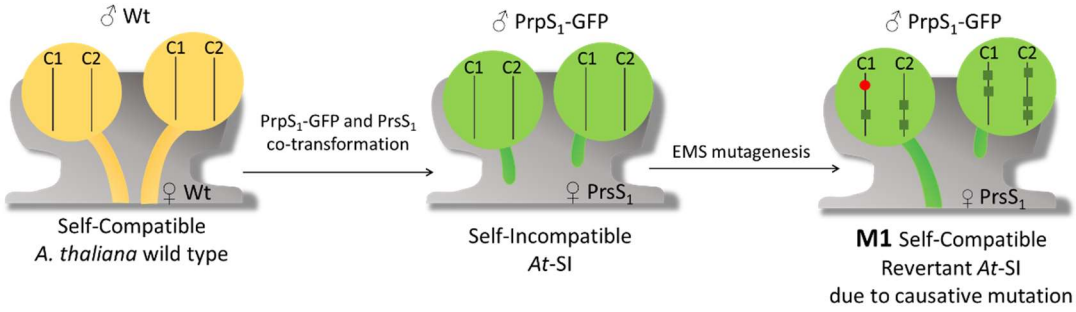

Figure 5.1. EMS mutagenesis screen to identify SI-PCD repressors from self-pollinated plants. Wild type and $PrsS_1$ stigmas (stigma, style and valves top part) represented in grey. Wild type pollen (yellow) and pollen grains expressing $PrpS_1$-GFP (green). Two kinds of tubes represented: short tubes as a consequence of an SI response, long tubes continuing to the ovule to fertilize it. In each pollen grain, chromosome 1 (C1) and chromosome 2 (C2) as an example are illustrated. EMS-induced non-causative SNPs are represented with a green square and a red circle when causative.

By Next-Generation sequencing (NGS) the whole genome can be sequenced in a shorter time than traditional map-based cloning (James *et al.*, 2013). In this chapter, the mapping method is slightly different from the conventional procedure. Our genes of interest are expressed in the pollen, and they will lead the pollen tube to PCD when expressed but to effective fertilization when mutated. This means the candidate plants will always be heterozygous after the backcrosses but after pollination, only the tubes

from grains with the causative SNPs reach the ovules. This allows us to identify the causal SNPs from the DNA pool of heterozygous mutant individuals after backcrossing twice with the non-mutagenized parent. As the non-causative SNPs caused by EMS segregate 1:3, but causative segregate in a 1:1 proportion, the causative SNPs can be identified by calculating the SNP/non-SNP segregation ratio. (Lindner *et al.*, 2012; James *et al.*, 2013).

5.2. Material and methods

5.2.1. Ethyl methanesulfonate (EMS) mutagenesis of SI *Arabidopsis*

The experimental procedure to identify suppressors for SI-PCD using EMS mutagenesis as a forward genetics approach contained some differences compared with the normal EMS mutagenesis setup. In this case, since the genetic material present in the pollen grain is haploid, a mutation in a single allele would be able to breakdown the SI response for half the pollen population. The M1 population size was estimated based on previous experiments that worked in *Arabidopsis* diploid cells, and calculated according to the number of M2 plants needed to be screened to have a high probability of recovering a recessive loss-of-function mutation (Haughn and Somerville, 1987). From this value, M1 population size is calculated taking into account the genetically effective cell number corresponding to the germline or number of meristem cells contributing to the formation of seed (Li and Rédei, 1969) and the ploidy factor, counting the number of chromosomes in a single plant cell (Haughn and Somerville, 1987). For *Arabidopsis*, in a normal EMS mutagenesis set up, about 125,000 seeds (~2.5 g) are required to obtain every possible EMS-induced homozygous mutation. This pool saturates the genome with mutations and provides a 95% chance of finding a mutation in any given base pair that can be mutated by EMS (Haughn and Somerville, 1987; Jander *et al.*, 2003). Although each plant will have dozens of point mutations caused by EMS, so only 5,000 F_2 plants are enough to find a mutation in a given gene (reviewed in Jander *et al.*, 2002). In this case, it was considered that ~40,000 is the more suitable size, resembling the protocol followed to identify genes involved in organelle integrity and other similar experiments (Von Malek *et al.*, 2002; Stefano *et al.*, 2012). With this population size, we pretend to cover the entire genome and be able to find causative mutations that prevent a normal SI response. One At-SI line (line61, expressing a single copy of both S determinants) was selected as the parent line of the EMS mutagenesis experiment. Due

to its reduced fertility, around 200 seeds could be produced from each individual homozygous plant of this line. Seeds from homozygous plants were harvested to obtain enough seeds (~10,000) for each EMS mutagenesis round. At-SI seeds were mutated in four consecutive rounds of EMS mutagenesis experiments in total. The EMS mutagenesis was carried out following a well-developed protocol of the VIB-UGent Center for Plant Systems Biology department, for a batch of 8,000 to 10,000 seeds. The equipment and solutions needed are detailed in Appendix protocol 5.1.

Because EMS is a potent carcinogen, it was crucial to strictly follow safety regulations related to the waste collection during this procedure (Amberg *et al.*, 2006). Even though, when tested in mammals, the dose-response relations data is insufficient for a risk extrapolation to humans, teratogenicity and carcinogenic effects are considered (Gocke *et al.*, 2009). All the waste upfront of EMS usage was treated as conventional waste. Whatever equipment/waste that could have been in contact with EMS needed to be rinsed with 5 M NaOH, by means of soaking in NaOH solution for 2 days. After this, solid EMS waste was separated from liquid EMS waste using a plastic funnel. All liquid waste needed to be collected in a 'basic' solutions container, while all solid waste was gathered in a garbage bag and then discarded in a solid chemical waste barrel.

It was required to prepare the fume hood and greenhouse beforehand following specific procedures. Firstly, the EMS treatment was announced on the door of the room containing the fume hood in which the process took place. All the working surfaces, as well as the back and side panels, were covered with absorbent paper to protect against possible spills. The shaker was installed wrapped in a garbage bag. All equipment was wrapped in parafilm (e.g., pipettes, caps and falcon tubes). All solutions were prepared in advance and aliquoted in desired amounts to avoid the usage of pipettes as much as possible. Two PVC bottles were cut to use as temporary waste barrels in a fume hood (one for solids, one for liquids), the cut lid of the bottles was used in combination with parafilm as a funnel to separate liquid waste from solid waste.

The two PVC bottles previously cut were filled with 0.5 L of 5 M NaOH each. A rack was put in to hold all the aliquots. A Tyvek coat, double gloves, mask, and safety

glasses were worn during the work. Care was taken for interrupting the experiment immediately if the airflow in the fume hood was insufficient (which never happened).

Having this all prepared, the complete procedure of the protocol took five days:

Day 1. The fumehood was prepared and EMS treatment was announced. 175 mg of seed stock, corresponding to ~10,000 seeds (Jako *et al.*, 2001), was prepared for EMS treatment and control (no treatment). They were divided into four 15 mL tubes, having three of them with 56 mg of seeds and one with 7 mg of seeds to be used as a control. Water was added to each of the four tubes (volume of water = twice the volume of seeds) and tubes were incubated overnight at room temperature while shaking at low speed ~50 rpm.

Day 2. In the EMS room, wearing the required protection during the process, the cut open PVC bottles were filled with 0.5 L NaOH solution each. Seeds were let to sediment and as much liquid as possible was removed. After that, Triton-X was added until it reached the 15 mL mark, to obtain a 15 mL seed suspension in the three tubes for the treatment (2 mL Triton-X was added to the control tube) and mixed by shaking. The seed-Triton mixture was incubated for 5 min. Then, after letting the seeds sediment, the Triton-X was removed with a pipet and the seeds were washed with water. This step was repeated twice. Then, 90 µL of 9.7 M EMS stock solution was diluted with 30 mL 0.1 M phosphate buffer to obtain a solution with a final concentration of ~30 mM EMS. 10 mL of the 30 mM EMS solution was added to each of the three tubes containing the seed stock for EMS treatment. For control, 10 mL of only phosphate buffer was added. The four tubes were mixed in a shaker for 6 to 7.5 hours in the fume hood. Later on, the seeds were let to sediment, and as much liquid as possible was removed. Afterward, 15 mL 0.1 M $Na_2S_2O_3$ were added to the seeds (5 mL for control) and, after vortexing, they were incubated for 5 min. The seeds were let to sediment before removing as much liquid as possible, and this incubation and washing step with $Na_2S_2O_3$ was repeated once again. After that, the seeds were rinsed four times with water and mixing by shaking, letting the seeds sediment before removing as much liquid as possible every time. Finally, the seeds were transferred with a minimal volume of water to a new falcon tube and shaken overnight at 4°C in the cold room.

Meanwhile, 2500 pots with soil (50 pots per tray, 50 trays) were arranged in the greenhouse.

Day 3. Seeds were prepared to be sown, mixing them with 0.1% agarose solution in two empty 500 mL bottles. From this suspension, 400 µl were pipetted in each one of the pots placed in the greenhouse the day before. Those pots were covered with cling film as soon as possible after sowing.

At the end of the day, it was recommended to check if all solid waste was properly immersed in the NaOH solution in the EMS room.

Day 5. All the EMS liquid and solid waste were cleaned up.

Five days after seeds were sown, the pots were checked to ensure that ~3 seedlings were germinating per pot. Extra seedlings were removed and transferred to pots with less than three seedlings.

5.2.2. Screening of adult plants for recovery of seedset

Three weeks after seeds were sown, the effect of EMS was observed on the plants before forming a complete rosette (Figure 5.2). Later on, when the first flowering stem appeared, those were cut once (for higher yield harvest) and each group of 50 trays was fenced surrounding them with plastic sheets with holes to avoid condensation designed by the aratube components of the Arasystem. Each round of EMS mutagenesis was screened twice. The first screen was carried out one month after the seeds were sown when the plants started to flower. Mutants with longer siliques were selected by looking for siliques longer than 0.5 cm which is the size of the SI siliques (Figure 5.3).

For those plants from which no obvious longer siliques were observed, the main stems were cut back and subjected to a second screen ten days after the first screening.

Figure 5.2. Phenotypes observed as the result of chlorophyll gene mutations produced by EMS. The red arrows point to white areas produced as a result of chlorophyll mutation. Mutants with this phenotype were defined in Delphinium malabaricum as type alba-green (Kolar et al., 2011). Bar = 1 cm.

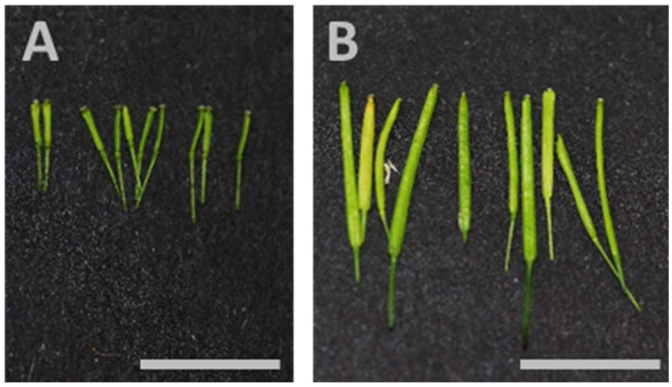

Figure 5.3. Differences between the length of siliques. Siliques formed in a self-incompatible plant (A). Siliques observed in selected mutants after EMS mutagenesis (B). Bar = 1 cm.

To eliminate false positives, PrpS/PrsS was amplified from DNA extracted from candidate mutants, and subjected to sequencing to check if there was any mutation in the PrpS/PrsS coding region. Candidate mutants with mutated PrpS/PrsS were eliminated from further analysis. The expression level of PrpS was checked by examination of the GFP signal in the pollen.

5.2.3. Test of candidate genes

In order to identify the causative mutations of the self-compatibility SHOREmap deep sequencing was carried out by the VIB-UGent Center for Plant system Biology experts, to perform the SNPs ratio mapping. This tool permits the analysis of a mapping population generated by backcrossing to the non-mutagenised progenitor, by calculating the SNP/non-SNP segregation (Nordström *et al.*, 2012).

To screen the candidates, we selected all the nonsynonymous mutations with an allele frequency over 0.4, obtaining a list of genes of interest. Those genes with SNPs located in the centromere or an apparently not causal region were discarded from this list. A "Position Match" analysis was carried out and to conclude, "Gene match" showed us the primary candidate, as six different nonsynonymous mutations were present in six different lines that were identified as having reverted from being self-incompatible to self-compatible.

This main candidate of interest from this mutant screen for a suppressor for SI-PCD was HLD1. We wanted to test if only the absence of HLD1 could block the SI response in the presence of both S determinants. In order to test if the loss of function of this gene affects the SI response, two corresponding T-DNA lines, both homozygous for the insertion, were used. Those lines mutants for the *highlander* gene coexpressing $PrpS_1$ (*hld1*-$PrpS_1$) were obtained by transformation with *Agrobacterium* with the plasmid pNTP303::$PrpS_1$-GFP. To do that, the bacteria were inoculated in a 50 mL falcon tube containing 1 mL LB without antibiotics and incubated 8-9 hours shaking at 28 ^oC. A further 10 mL of LB without antibiotics was added and it was incubated overnight (28 ^oC and 230 rpm) until the OD600 was around 2.0. When ready, 40 mL of MilliQ (MQ) water containing 10% (w/v) sucrose and 0.05% (v/v) Silwet was added to the *Agrobacterium* culture and the floral dipping was carried out immediately, having in each pot at least 5 inflorescences of 10-15 cm high. Inflorescences from *hld*-$PrpS_1$ plants were gathered and dipped in the *Agrobacterium* culture, agitating gently for 2-3 seconds. Each plant was wrapped with cling-film straight away and kept, lying down on a tray, in the dark for 24 hours. After that, plants were covered by a bag and returned to their normal position in the growth chamber.

When ready for harvesting, the seeds were collected and sterilised with bleach. *Arabidopsis* T1 seeds obtained after floral dip transformation with the plasmid pNTP303::$PrpS_1$-GFP were sown on culture plates with Glufosinate-ammonium, also known as phosphinothricin (PPT) or BASTA. The plates contained 0.5 MS (2.15 g/L), 0.8% (w/v) Agar, 50 µg/mL PPT, adjusted to pH 5.8 with KOH).

After two weeks on selective plates, the resistant seedlings were transferred to soil in individual pots and protected with a bag. At the rosette stage, leaf samples were taken for DNA extraction. DNA samples were used for PCR genotyping to check if the plants were homozygous for the T-DNA insertion. Equally, the presence of $PrpS_1$ was tested by PCR and sequencing the fragment to confirm that the male determinant did not present any error on its sequence that may affect the PrpS-PrsS interaction. The plants with negative results were discarded and the positively tested plants were protected with bags to collect their seeds. The T2 *hld*-$PrpS_1$-GFP seeds harvested were sown in soil pots. Checking them under the fluorescent microscope when adults, only the plants presenting GFP homozygous pollen were preserved.

Stigmas from At-SI and *hld1*-$PrpS_1$-GFP T2 lines (as a control) were pollinated with *hld1*-$PrpS_1$-GFP pollen as follows. Wt self-crosses were used as a SC control. To test the behaviour of *hld1*-$PrpS_1$ pollen in SC conditions, self-crosses of this line were also performed (as the female determinant is not expressed in this line). In order to test if the SI response is affected by the absence of this hld gene, At-SI stigmas were pollinated with *hld1*-$PrpS_1$-GFP T2 lines. In each case, 9 to 20 repetitions were performed.

5.3. Results

A forward genetic screen was executed to identify molecular suppressors of SI-induced PCD. To this end, a total of more than 40,000 At-SI seeds were mutated using EMS. In total, our screen produced 40 M1 plants with fully or partially restored fertility. We dubbed these mutants "*highlander" (hld)*, in reference to the immortal warriors in the movie "Highlander". Five of the *hld* mutants were discarded for being GFP-negative when examined with a fluorescence binocular microscope. In the At-SI line, GFP is fused to $PrpS_1$. Consequently, the absence of a GFP signal indicated that these plants were self-compatible because PrpS-GFP was not expressed anymore, or because they were wild-type pollen contaminations.

To validate the SC phenotype, pollen from the remaining 35 *highlanders* was used to pollinate the self-incompatible parent line (backcross1 generation, BC1 hereafter) and vice versa (Figure 5.4). Even if the M1 plant genotype was heterozygous, only the pollen tubes with a mutant hld allele should be able to develop a pollen tube

and reach the ovule without activating an SI response. Hence, the seeds resulting from BC1 should all be hld heterozygous, except for very few cases in which pollen escapes the SI response (Figure 5.7).

The consistency of having the revertant phenotype was checked (long siliques similar to wild type). Plants presenting siliques with SI phenotype after this backcross were discarded. From these backcrosses, pollen from 9 *highlanders* resulted in long siliques comparable with those of the wild type (Table 5.1). A screen of BC1 plants was carried out when at least 10 siliques were formed in each plant. Therefore, we expected all of these 9 BC1 lines to be self-compatible. Indeed, all the BC1 lines formed long siliques containing seeds, indicating that genuine revertant mutant lines were identified.

It is well known that the SI response relies on the proper interaction between $PrpS_1$ localised in the pollen plasma membrane and $PrsS_1$ secreted by the stigmatic papilla. A downregulation or coding frame mutation of either gene could lead to a breakdown of $PrpS_1$-$PrsS_1$ interaction, resulting in the failure of the SI response, and thus long siliques and normal seed set. Therefore, a series of experiments were carried out to exclude mutations leading to loss of function or low expression of either $PrpS_1$ or $PrsS_1$.

To test if the stigma-expressed $PrsS_1$ remained functional in the *hld* mutants identified, at least 10 stigmas from at least two BC1 plants from each hld line were emasculated, and pollinated with non-mutated At-SI pollen. At-SI stigmas were used as the control. Both the silique length and the number of seeds per silique were comparable with those of At-SI stigma pollinated with At-SI pollen (Figure 5.4), demonstrating that $PrsS_1$ was functional in all the 9 *hld* lines, and able to interact with $PrpS_1$ to trigger the SI response.

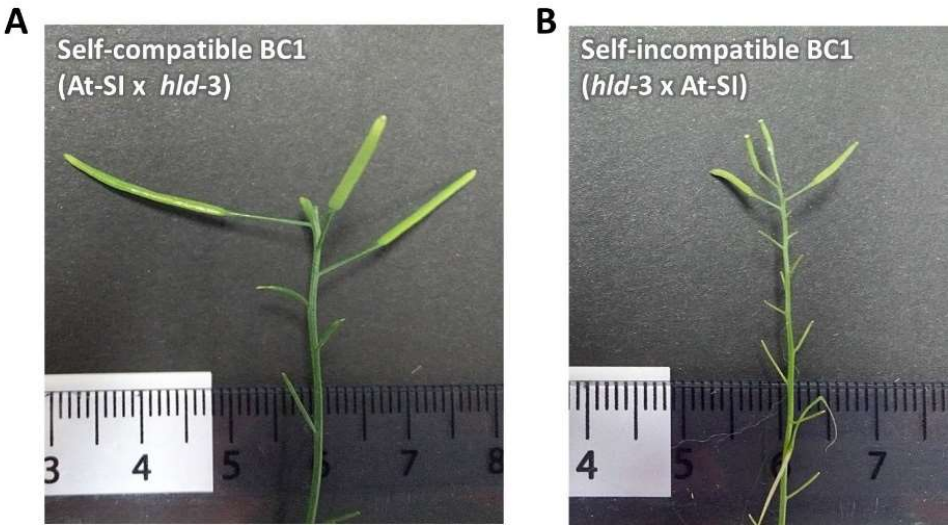

Figure 5.4. Silique phenotypes were obtained after BC1. (A) $PrsS_1$ expressing stigmas resulted in SC phenotype when pollinated with highlander pollen (*hld-3* shown in this example). (B) The siliques presented a SI phenotype as a result of pollinating highlander stigmas (*hld-3* in the image) with At-$PrpS_1$ pollen; seeds were not developed as a SI response was triggered.

Table 5.1. Screening of the HLD mutant lines resulting from the first backcross (BC1).

Mutant line	Total BC1 plants checked	SC	SC/Total x100%
***hld*-3**	28	28	100%
***hld*-5**	21	21	100%
***hld*-7**	32	32	100%
***hld*-17**	23	23	100%
***hld*-19**	24	24	100%
***hld*-22**	30	30	100%
***hld*-24**	35	35	100%
***hld*-25**	27	27	100%
***hld*-40**	20	20	100%

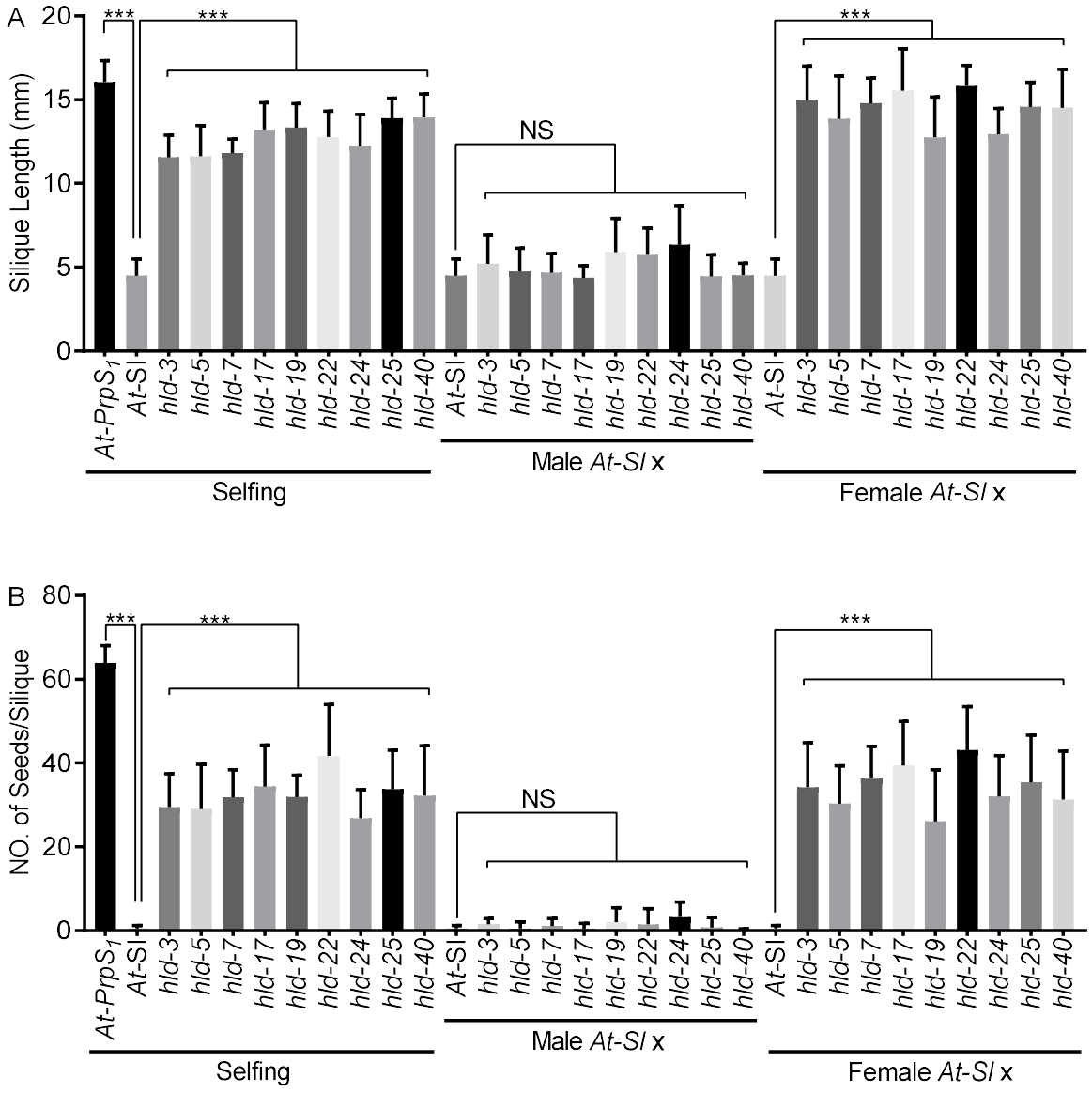

Figure 5.5. Examination of PrpS1 and PrsS1 functionality in hld mutants. The functionality of $PrpS_1$ and $PrsS_1$ of hld mutants was examined by three different sets of pollinations: 1) the hld mutants were selfed; 2) Hld stigmas were pollinated with At-SI pollen; 3) Hld pollen was used to pollinate At-SI stigmas (BC1). For all the pollinations the silique length (A) and the number of seeds/silique (B) were documented. For each cross, 9-12 pollinations were done. One-way ANOVA was performed for statistical analysis. Result = mean±SD; NS, non-significant ($p>0.05$); ***, $p<0.001$. Experiments were done together with Dr Zongcheng Lin.

Conversely, to exclude unaltered expression levels in the pollen-expressed $PrpS_1$, pollen was collected from individual M2 plants of each line and investigated using a fluorescence binocular microscope for $PrpS_1$-GFP fluorescence, with pollen from the background *At*-SI line as control. There was no significant difference observed regarding the GFP fluorescence intensity between the *At*-SI pollen and the pollen of M2 plants of

hld lines (data not shown). This demonstrated that, compared with the non-mutagenized *At*-SI lines, there was no alteration in the $PrpS_1$ expression level in the 9 *hld* lines. As mutations in the $PrpS_1$ coding sequence might also affect the $PrpS_1$-$PrsS_1$ function or interaction, we also checked the $PrpS_1$ DNA sequence in every individual *hld* line. Based on sequencing results, two of the 9 HLD mutant lines, *hld*-22 and *hld*-40, were discarded as they presented a mutation in $PrpS_1$, considering it the cause of their SC phenotype. These results also demonstrated that the $PrpS_1$ DNA sequence of the remaining seven *hld* lines was not affected during the EMS mutagenesis (Figure 5.6).

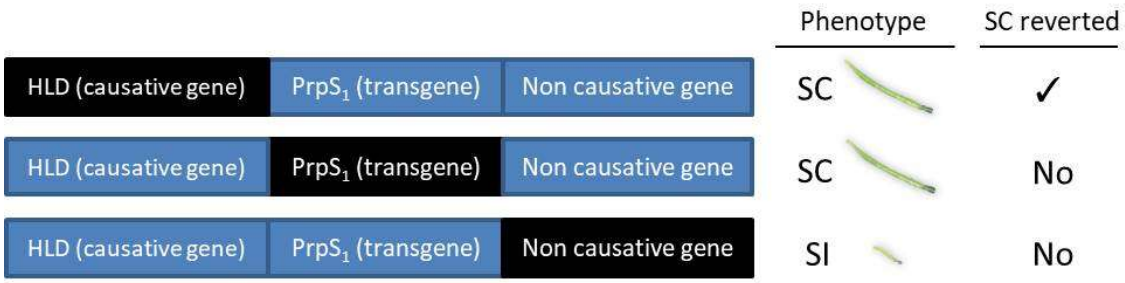

Figure 5.6. Resulting phenotypes according to the location of the mutation. The genes are represented in black when knocked out. Only when a HLD gene is mutated the self-compatible phenotype obtained will be due to a failure in the SI response.

These results suggest that the causal genes of the *hld* lines are functional downstream of $PrpS_1$-$PrsS_1$ interaction, either in the SI-induced signalling pathway or in the downstream PCD response.

5.3.1. Single-Nucleotide Polymorphisms-Ratio Mapping

Single-Nucleotide Polymorphisms (SNP)-Ratio Mapping (SRM) was carried out for identifying causal mutations in regions of interest of the 7 *hld* mutants (Lindner *et al.*, 2012). After backcrossing with the non-mutagenized SI parent line, any unlinked SNP generated by the EMS mutagenesis segregates 1:3 in the pool of mutant individuals of the F1 population of the BC2, whereas the causative SNP segregates 1:1 (Figure 5.7). Within the context of this experimental setup, we do not need to select for the mutant individuals among the F1 population of BC2, as all the progenies of BC2 will be heterozygous mutants producing long siliques.

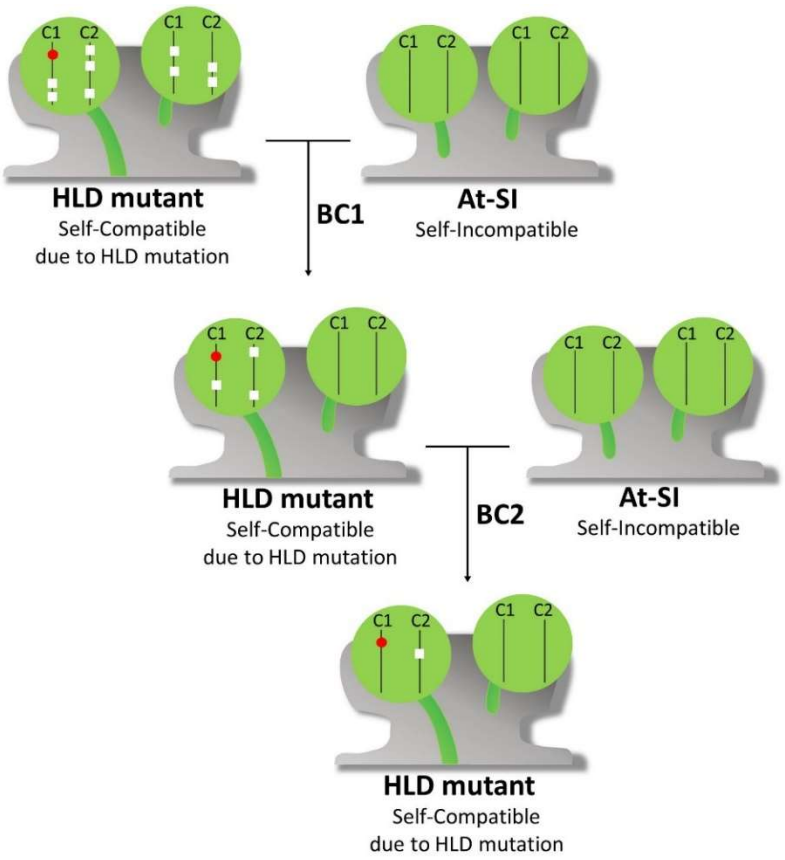

Figure 5.7. Schematic representation of the experimental design to reduce the number of non-causative SNPs in HLD mutants. Stigmas expressing $PrsS_1$ (stigma, style and ovary top part represented in grey). Pollen grains express $PrpS_1$-GFP (green). Two kinds of tubes represented: short tubes as a consequence of an SI response and SC long tubes continuing to the ovule to fertilize the ovule. In each pollen grain, chromosome 1 (C1) and chromosome 2 (C2) are illustrated. EMS induces causative SNPs (red circle) and non-causative SNPs (white square). In this example, the causative mutation is on C1. Only pollen tubes from pollen grains with causative mutations will be able to fertilize the ovule in $PrsS_1$ expressing stigmas. Backcrosses with the parent line result in a reduction in the number of non-causative SNPs.The final cross produces a ratio of 1:1 EMS-causative SNP and 1:3 non-causative.

To reduce non-causative background mutations, a second back-cross (BC2) was performed. For this, the pollen of *hld* M2 plants was used to pollinate its *At*-SI parent line stigmas. The resulting M3 seeds were sown and for each *hld* line, 50 individual M3 seedlings were pooled together for DNA extraction. Additionally, the DNA of 50 non-mutagenized seedlings was extracted as the unmutagenized control.

In six of the seven *hld* mutants (*hld* 3, 5, 7, 19, 24 and 25), different nonsynonymous mutations of a single gene that we designated HLD1, were identified (Table 5.2). Those SNPs were all located in the "bell-shaped" region and it made this gene an interesting and promising gene for subsequent analysis (Figure 5.8). From the other *hld* mutant, hld17, due to the low sequencing coverage, further sequencing is still needed to identify the causal gene of this mutant.

Table 5.2. Features of the SNPs located in HLD1. Different nonsynonymous amino acid change mutations were found in HLD1, located on chromosome 3, in six different EMS-mutated At-SI plants from the forward genetic screening.

HLD mutant	3	5	7	19	24	25
Position	10099918	10100835	10096445	10098797	10101497	10100048
Allele Frequency	0.49	0.48	0.60	0.36	0.55	0.39
Reference Base	G	G	G	G	C	G
Mutation Base	A	A	A	A	T	A
Number of mutation reads	18	23	18	12	29	16
Base quality	40	40	40	32	40	38
Type of sequence	CDS	CDS	CDS	CDS	CDS	Splice site change
The numerical order of the codon having the mutation	2037	2538	222	1425	2845	
Site of mutation in codon	3	3	3	3	1	
Reference Amino acid	W	W	W	W	Q	
The numerical order of the amino acid having the mutation	679	846	74	475	949	
Mutation Amino acid	*	*	*	*	*	

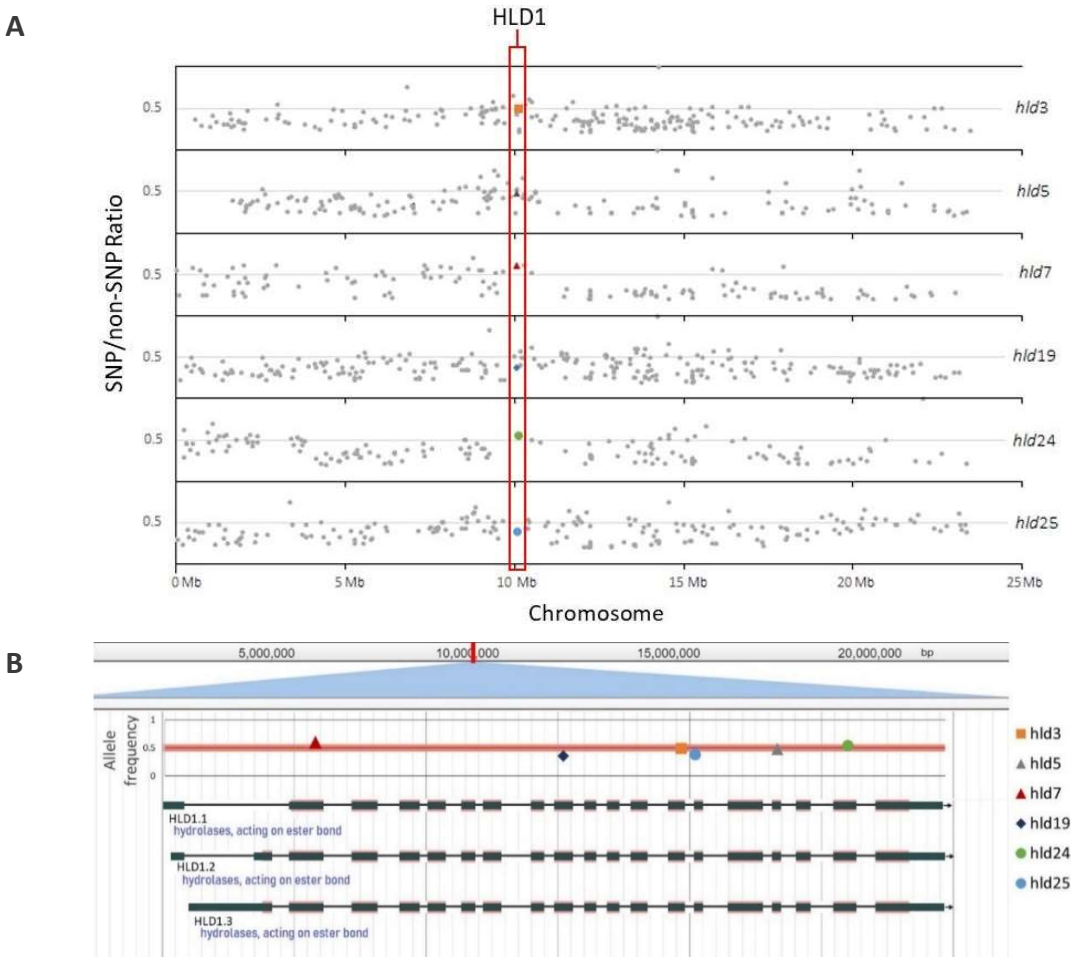

Figure 5.8. Ratio SNP/non-SNP ratio plots highlighting causative SNPs located in HLD1. (A) SNP/non-SNP ratio in chromosome 3. In the region containing HLD1 (red rectangle) the coloured symbols represent the causative SNPs in this gene found in the six hld mutants. (B) Location in chromosome 3 of HLD1 (protein-coding genes HLD1.1, HLD1.2 and HLD1.3) and the six SNPs spotted in the six mutants within the gene.

5.3.2. Testing HLD1 involvement in the SI-PCD response

From the screening of At-SI plants that were subjected to mutations induced by EMS, one causative gene was identified. HLD1 was the main candidate from this screen. Therefore further analyses were carried out to elucidate its implication on the SI-PCD response with the correspondent T-DNA lines coexpressing $PrpS_1$.

Crosses between At-SI stigmas and *hld1*-$PrpS_1$ pollen resulted in longer siliques (~12 mm) and higher seed number (~18) when compared to incompatible control crosses (At-SI x At-SI), indicating that loss of function of HLD1 can at least partly overcome the SI induced pollen tube growth arrest. However, the large error bars for the measurements following At-SI x *hld1*-$Prps_1$ crosses indicate the wide range of outcomes obtained (for instance, the seedset ranged between 0 and 47 seeds for individual crosses). Statistical analysis grouped this cross together with Wt x *hld1*-$PrpS_1$, as their seed-set was significantly different from SC and SI controls. One set of SC control pollinations (Wt stigma x *hld1*-$PrpS_1$ pollen) resulted in significantly lower seedset measures when compared with Wt x Wt pollinations while SC controls through self-cross of the *hld1*-$PrpS_1$ line developed siliques with a phenotype similar to Wt. These inconsistencies indicate that a human error and/or environmental factor may have contributed to some of the observed low silique sizes and seed numbers for some of the SC pollinations (Figure 5.9).

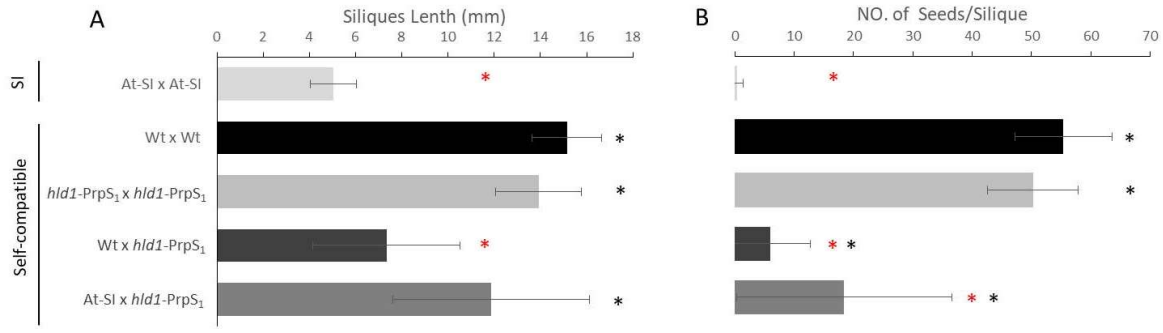

Figure 5.9. Examination of T-DNA hld-PrpS1 line. The functionality of the SALK T-DNA hld-$PrpS_1$ pollen was examined. Pollinations were performed of Wt, At-SI and hld-$PrpS_1$ stigmas with hld-$PrpS_1$ pollen. Self Wt and self At-SI pollinations were included as controls. (A) Silique length. (B) The number of seeds per silique. Result = mean±SD (n=9-20). Black * when $p<0.05$ comparing with $PrsS_1xPrpS_1$ by Kruskal-Wallis test; Red * when $p<0.05$ comparing with WtxWt by Kruskal-Wallis test.

5.3.3. Predicted protein structure

Little has been published so far, related to this gene that codes for a 120 kD predicted molecular weight hydrolase (Figure 5.10). As shown in Figure 5.8, it can contain three splice variants resulting in different mRNAs with similar length: HLD1.1, HLD1.2 and HLD1.3 (7389 bp, 7335 bp and 7163 bp respectively). In all three cases, the encoded protein is predicted to present hydrolase activity.

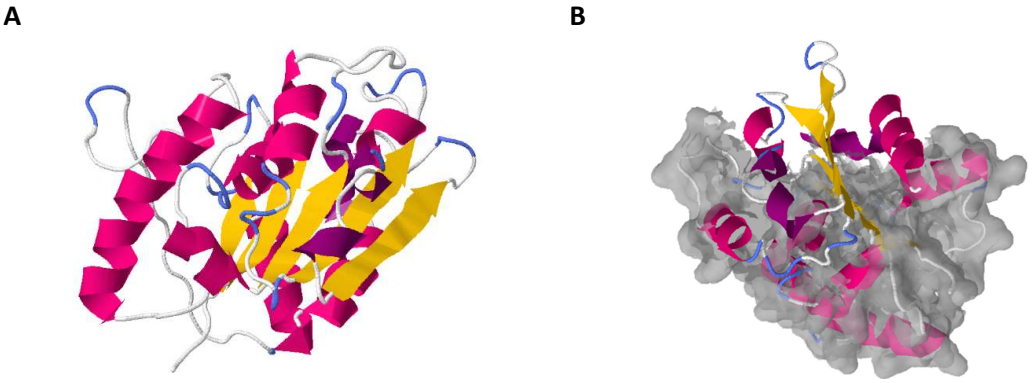

Figure 5.10. Tertiary structure 3D model of the protein encoded by HLD1. (A) Model of the protein sequence encoded by this hld gene. Colour code: alpha-helix = fuchsia, 3/10 helix and pi helix = purple, beta-strand = yellow, beta-turn = blue, coil = white. (B) Prototype including the molecular surface (grey). Its topology is predicted to have eight transmembrane helical structures. (Sources: http://bar.utoronto.ca/eplant/, https://www.uniprot.org/uniprot)

5.4. Discussion

From the mutation of 40,000 At-SI seeds with EMS, a single candidate was identified, which mutation suppresses the heterologous SI-PCD response in *Arabidopsis* plants. Even if the data obtained from the WGS data will probably provide some others in the future, in this chapter HLD1 is the *highlander* candidate analyzed, because of the presence of SNPs in this gene, in six of the highlander mutant plants selected from the screening.

From the expression level data, we know that HLD1 is expressed in a wide variety of tissues including the flower with a uniform expression level in stigma and stamens (Figure 5.11A). Focussing on male structures, HLD1 appears to be expressed in pollen grains and pollen tubes, reaching maximum expression levels when tested 30 minutes after *in vitro* incubation (Figure 5.11B). As expected from the predicted eight transmembrane domains (Figure 5.10), the plasma membrane and the endoplasmatic reticulum are the organelles presenting the highest expression level (Figure 5.11C).

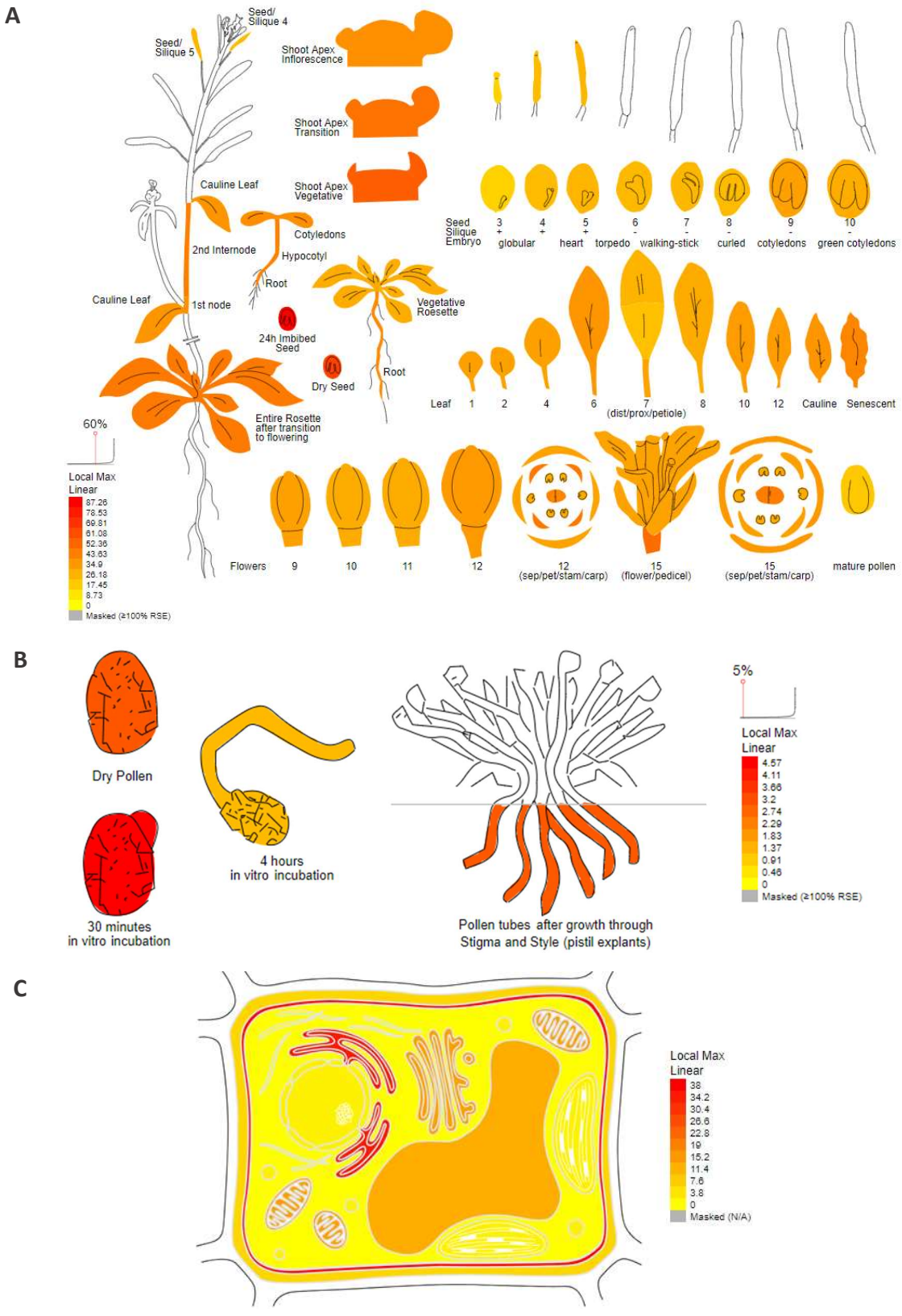

Figure 5.11. Electronic fluorescent pictograph of HLD1 expression data. (A) Visualization from the transcriptome data of Arabidopsis showing that HLD1 is widely expressed including in the reproductive tissues. (B) Examining expression levels in the pollen grains and pollen tubes indicates that HLD1 is higher expressed in pollen grains after 30 minutes of *in vitro* incubation. (C) At the cellular level, the highest expression levels were found in the plasma membrane (Localization Score: 38) and the endoplasmic reticulum (Localization Score: 34). Source: bar.utoronto.ca/eplant based on (Qin et al., 2009).

Although little is known about HLD1 in *Arabidopsis*, a homolog identified in *Cryptomerica japonica* was described as a participant in intracellular trafficking, secretion, and vesicular transport, having a specific role as a negative regulator of COPII vesicle formation (Yoshida *et al.*, 2012). The COPII protein Secretory31B (SEC31B) was found to be required for pollen wall development in *Arabidopsis*. Pollen tubes of *sec31b* mutant pollen grew significantly slower compared with wild type, even if growth was not completely arrested as we observe in SI plants (Zhao *et al.*, 2016). HLD1 was also described as a homologous gene to Gab1p/PIG-U, which are respectively yeast and mammalian protein subunits of glycosyl-phosphatidylinositol (GPI) membrane anchor. This component is also required for the integrity of the pollen grain and pollen tube growth (Ellis *et al.*, 2010; Bundy *et al.*, 2016). Its closer homologs in humans and yeast are PGAP1 and Bst1p respectively, both being also components of the GPI lipid anchor biosynthetic pathway (Luschnig and Seifert, 2010). The biosynthesis of GPI is well conserved in animals, yeast and plants (Murphy *et al.*, 2011) with a close homolog for every human GPI anchor biosynthesis and remodelling component expressed in *Arabidopsis*.

Our results have revealed HLD1 as a component of the SI-PCD pathway related to pollen tube growth, which opens a new route in this process to be explored. As its absence let some pollen tubes reach the ovule despite the $PrpS_1$-$PrsS_1$ interaction, it indicates that HLD1 may be an important intermediary in triggering SI-PCD. Although, when using *hld1*-$PrpS_1$ pollen to pollinate both Wt and At-SI stigmas to test the implication of the HLD1 gene in the SI response, the results obtained differed from the SC and SI scenarios due to the inconsistency in the number of seeds per silique. One factor that may have influenced this is that the stigmas used to perform these crosses were probably not at their optimal maturation point, so may be in a too advanced stage in maturation. This would make stigmas less receptive and the pollen germination rate slower. Therefore, to confirm HLD1 as a gene implicated in SI-PCD, it would be required to repeat the pollination assays and increase the number of repetitions for each, as well as to carry out other experimental approaches to investigate the function of HLD1 in the SI-PCD process.

Chapter six. General discussion

6.1. Introduction

The expression of the male *Papaver* S-determinants, PrpS, in the pollen of self-compatible *Arabidopsis* results in a successful self-incompatible response when challenged with PrsS proteins *in vitro,* and also triggered a SI response *in vivo* in transgenic *Arabidopsis* plants with stigmas expressing cognate PrsS (De Graaf *et al.*, 2012; Lin *et al.*, 2015). These results cleared a path that allows us to better understand the Papaver SI system by working with SI Arabidopsis lines and using advanced technologies available for this plant model organism. With life cell imaging using genetically encoded probes or specific dyes, it is possible to characterize time events of interest and compare them with those observed in *Papaver.* The similitude of those two systems let us use *Arabidopsis* as a model plant and not only to compare phenotypes in time but also to identify which genes may be involved in the SI response. So far, only the *Papaver* S genes, PrpS and PrsS, have been characterised genetically (Foote *et al.*, 1994; Poulter *et al.*, 2010). However downstream genes involved in this response and how they trigger PCD are still unknown. Both, a forward screening of erratically mutated SI *Arabidopsis* plants looking for revertants of the SI-PCD response and profiling the SI transcriptome, gave us chances to find more genes playing a role in this chain of reactions.

6.2. Cellular characterization of SI-PCD in incompatible *Arabidopsis* PrpS-expressing pollen

The changes in time were captured during the SI response by imaging pollen tubes or pollen grains. *Arabidopsis* pollen grains can be hydrated and germinated *in vitro* to facilitate the observations. It was confirmed in *Papaver* that the SI response can be followed in pollen and pollen tubes. For example, the typical punctate actin foci observed in *Papaver* pollen tubes during SI response are also present in *Arabidopsis* PrpS-expressing pollen grains 3 h after SI induction by the addition of the cognate PrsS (De Graaf *et al.*, 2012). In this thesis, five events were studied using *Arabidopsis* pollen expressing PrpS: *in vitro* germinated pollen tubes to test the cytosolic calcium increase, vacuolar disorganisation and mitochondria morphology, whereas pollen grains *hydrated in vitro* were used to follow the nuclear disruption and caspase-3 like activity.

The images obtained with the confocal microscope and its further statistical analysis showed that, similar to *Papaver*, also in *Arabidopsis*, the cytosolic calcium increase is an early event since it promptly occurs after the addition of $PrsS_1$ to $PrpS_1$ expressing pollen tubes. The time range coincides with the cytosolic calcium increase already described in *Papaver* where it takes place during the first ~10 minutes after SI induction (Franklin-Tong *et al.*, 1993; Franklin-Tong *et al.*, 1997; Wilkins *et al.*, 2015). However, using the *Arabidopsis* system and the genetically encoded calcium marker YC3.6, we could additionally observe that there is a calcium peak always present immediately before the elongation stops. It takes on average ~4.5 min from the arrest of pollen tube elongation until the maximum $[Ca^{2+}]_{cyt}$ was reached. We observed that shortly after the $[Ca^{2+}]_{cyt}$ starts slowly to decrease, the cytoplasm stream completely stops. The three main functions of the pollen tube cytoplasmic streaming are all blocked or dramatically affected when the streaming stops: the transport of nutrients and metabolites stops, the organelles cannot be relocated in response to changes in environmental conditions and the generation of convection stops which block the continuous mixing of the cytosolic content required for chemical and enzymatic reactions (Reviewed in Chebli *et al.*, 2013). It has also been known for decades that *Lilium longiflorum* pollen tubes incubated with the calcium ionophore A23187 present cytoplasmic streaming inhibition, suggesting the calcium may be a physiological regulator of the streaming (Kohno and Shimmen, 1988). Not only the cytoplasmic streaming but also the pollen tube growth itself seems to be related to calcium, since the cytoplasm of wild type growing pollen tubes show oscillations in the $[Ca^{2+}]_{cyt}$ in a coordinate pattern with the tube growth (Cárdenas *et al.*, 2008).

Another early key event described in incompatible *Papaver* pollen tubes is a dramatic pH decrease (Bosch and Franklin-Tong, 2007; Wilkins *et al.*, 2015). It is still unknown how this pH drop is produced and if it is directly related to the mechanisms that the SI system has for triggering PCD. However, this was hypothesized since it was shown that a pH drop can regulate signalling pathways and trigger developmental PCD in plants, for example, the turnover of *Arabidopsis* lateral rootcap (Fendrych *et al.*, 2014). In this thesis, the *in vitro* observations of phenotypical changes in the vacuoles were presented, to follow their behaviour and analyse if a possible rupture of this

organelle could be the consequence of the pH drop. In normal conditions, the structure that the vacuole forms is a reticulate net all over the tube (Bosch *et al.*, 2010). This structure was also observed in *Arabidopsis* pollen tubes before the SI induction, by observing the genetically encoded tonoplast marker WAVE9R (Geldner *et al.*, 2009). However, when the cognate PrsS is added, their disposition stops being reticular and changes to the six other types of morphologies described in chapter two. Although SI induced evident changes in vacuole phenotype, there was still a strong WAVE9R signal present 4 h after SI induction. To test if the vacuolar content leak to the cytoplasm contributing to its acidification, it would be interesting to observe the combination of WAVE9R with a pH marker such as pHGFP and test if there is any correlation between the pH changes and the vacuolar morphologies described. In addition, utilizing a marker specifically expressed in the vacuolar lumen could provide a more direct strategy to test for SI-induced changes to vacuolar integrity rather than morphology.

Three events that occur late in the SI response, close to PCD, were analyzed. We used *in vitro* germinated pollen tubes to observe changes in the mitochondria, and hydrated pollen grains to visualise the nuclear disruption and the caspase-3-activity.

Also related to PCD we were interested in using the transgenic self-incompatible *Arabidopsis* lines to research on the nuclear disruption and its timing in the SI response. It is well known that nuclear disruption is a hallmark of PCD observed in plants, for example, in the process required for the tracheary emblems differentiation. This differentiation involves the vacuole rupture that triggers nuclear degradation (Obara *et al.*, 2001). We examined the timing when the male germ unit (MGU: vegetative nucleus and sperm cells) is disrupted by following the signal of a genetically encoded fluorescent protein nucleo-localised. There is no data from similar experiments in *Papaver*. However, it has been published that the DNA is fragmented in *Papaver* pollen tubes 4 hours after induction (Jordan *et al.*, 2000). We observed in *Arabidopsis* a constant increment of the percentage of nuclei disrupted, taking between 4 to 5 hours to reach 50 % of the nuclei. Even 8 h after SI induction, some of the MGU are still observable; however, we did not get information about DNA integrity with this marker. Also, comparing the state of the sperm cells with the vegetative cell to figure out which suffers a faster degradation would be interesting. To address this, instead of using hydrated

pollen grains, germinating the pollen tubes would let us distinguish between the three nuclei, even if because of its continuous motion in the tube, it is quite challenging to follow them in time. Another option would be combining this SI *Arabidopsis* line expressing the fluorescent nucleo-localised tag combined with DAPI staining (Durbarry, 2004). The nuclear fragmentation is directly related to caspases since analysis in animal cells showed that caspase-3 is required for DNA fragmentation (Jänicke *et al.*, 1998). To evaluate the caspase-3-like activity in *Arabidopsis* pollen grains during the SI response we used the probe Ac-DEVD-AMC. In *Papaver* it takes 5 h after SI induction for the DEVDase activity to peak (Bosch and Franklin-Tong, 2007) while in *Arabidopsis* we observed the peak activity later, 7 h after SI. This difference in time may be related to the variation in speed in which different *Arabidopsis* SI lines respond, which makes it difficult for the comparisons. Performing semi-quantitative RT–PCR it was shown that different expression levels of $PrpS_1$ in *Arabidopsis* were associated with the 'slow' or 'rapid' speed of the SI response (Wang *et al.*, 2020). The probe Ac-DEVD-AMC was used with a slow line since there was no faster transgenic SI *Arabidopsis* line not expressing GFP available. The green fluorescent protein coincides with the Ac-DEVD-AMC probe wave range of excitation and emission. Nevertheless, we can confirm that there is caspase-3-like activity late in the SI response which reinforces the theory of SI-induced PCD in the pollen tube.

6.3. From comparing gene expression levels

In order to identify new genes for further investigations, the transcriptome of self-compatible and self-incompatible pollinated stigmas with self-compatible and self-incompatible pollen were compared and we also made comparisons between the early and late stage of the pollinations. A wide number of genes were identified as possible participants in the SI response.

When comparing the SC *vs.* SI cases, 64 *hestia* genes were described for presenting differences at 2 hours after pollination. 56 of these genes are upregulated when SI at 2 HAP suggesting its expression may be linked to PCD. This pool could be further investigated using SI *Arabidopsis* lines mutant for the *hestia* genes to elucidate

if its absence can stop PCD in incompatible pollen tubes. The tissue-specific CRISPR-TSKO technique (Decaestecker *et al.*, 2019) could be used to elucidate the consequences of their absence specifically in the pollen tube. The gene that showed the highest upregulation 2 HAP was HTA67 which encodes a disease resistance protein according to the *Arabidopsis* information resource (TAIR) (Berardini *et al.*, 2015). It suggests that entrance of an SI pollen tube in the stigma may be understood as disease and trigger PCD to protect the plant. On the contrary, the overexpression of the 8 genes downregulated following SI may give us also some information about its role in this response. The gene presenting a higher downregulation 2 HAP in SI is HTA1 involved in lipid transport (Berardini *et al.*, 2015). Additionally, more than 1,000 *degoya* genes present differences in their expression when comparing SC and SI cases 0.5 HAP *vs.* 2 HAP transcriptomes. However, we found some of them much up or downregulated when SI which indicates that the SI response is responsible for those differences in their expression level. Further from this comparison, we isolated the genes that are more up or downregulated when SI comparing to the SC cases, obtaining a shortlist of 12 genes. In this group, a gene stands out that encodes for a peroxidase superfamily protein with a LogFC 5.62 when comparing 2 HAP *vs.* 0.5 HAP, indicating that its presence highly increases late in the SI-PCD response. However, we need to take into account that we cannot distinguish so far if it is overexpressed in the stigma, where the level of peroxidase activity is always high related to its maturity (McInnis *et al.*, 2006). The peroxidase activity was measured in *Petunia hybrida* fixed stigmas after SC and SI pollinations. It was found that the peroxidase activity is present in stigmas pollinated with SI pollen but this activity is not responsible for the tube growth inhibition (Carraro *et al.*, 1989). In SI *Arabidopsis* we could assume the same since the upregulation of this gene is observed far from the early response when the pollen tube is stopped.

In this study, we have identified possible new SI-PCD elements. Using this pool, the future research topic should be to experimentally investigate whether changing one of these elements will affect the response and how they are involved.

6.4. Identification of possible suppressors of SI-PCD

Other approaches carried out to find genes that could participate in the SI response were reverse and forward screenings. We analysed the seed set of selected genes with the reverse genetic screening according to previous publications in *Papaver.* This approach did not highlight any of them as strong interactor in the SI response. However, the detailed phenotypical differences that ADF7, CAP1, CathB1-3, CathB1-2-3 and EF1α mutant pollen tubes may have during SI are still unknown. The use of genetically encoded fluorescence proteins tagged to these proteins and/or treatment with organelle or activity-specific probes would possibly reveal the role these proteins may have, even if not decisive enough to block the SI response completely.

In addition, we performed a forward screen for plants presenting a SC phenotype after inducing random mutations on SI seeds. From this essay, one candidate has been identified. The *highlander* gene HLD1 encoding according to TAIR a protein predicted to present hydrolase activity (Berardini *et al.*, 2015). We showed that HLD1 mutant *Arabidopsis* SI plants do not present a SI phenotype when their seed-set was analysed. Only the absence of HLD1 as identified in the screen reduced the SI response significantly, reinforcing its candidacy as a suppressor of SI-PCD.

6.5. Summary

Using the tools now available with the *Arabidopsis* SI system, five main physiological changes in the pollen tube during the SI response were investigated. With this phenotypical analysis of SI *Arabidopsis* pollen tubes using confocal microscopy for live-cell imaging, we followed early and late events to characterize the cellular and subcellular processes occurring during the SI-PCD response. These *in vitro* observations confirmed that the cytosolic calcium concentration increases in incompatible pollen tubes immediately after SI induction. This increase is followed by the arrest of pollen tube elongation. Besides, we observed diverse morphologies in vacuolar disorganisation suffering continuous changes for hours. The mitochondria morphology was analyzed, observing a signal that decreases its intensity in time and late in the response, some dots appears even if we currently cannot confirm if these represent mitochondria. In addition, using pollen grains hydrated *in vitro* the disruption of the male germ unit was monitored confirming this hallmark of PCD also to occur in *Arabidopsis* SI. To conclude, also using pollen grains hydrated *in vitro*, we could measure an increment of caspase-3 like activity late after SI induction, manifesting the predicted PCD reaction. Furthermore, in this collaborative project, we successfully identified novel genes possibly involved in SI-PCD. The pool of genes obtained represents promising targets to further investigate the future for a role in SI-PCD. This thesis was predominantly aimed at exploring the availability of the heterologous Arabidopsis SI system and our findings have demonstrated that it is suitable for a better understanding of SI-PCD in *Papaver* and to further investigate the molecular mechanisms with the advanced genetic approaches available for *Arabidopsis*.

Appendix

Appendix table 3.1. List of the first 100 up and downregulated *degoya* genes with its logFC and annotations

Results of logFC≥1 comparing the timepoints 0.5 *vs.* 2 h after pollination						
Code	**A**	**B**	**C**	**D**	**Annotation**	**Average ABC - D**
DGY1	4.78	4.59	6.75	3.07	*Arabidopsis* phospholipase-like protein (PEARLI 4) family	-2.305
DGY2	4.43	5.05	9.04	4.44	Peroxidase superfamily protein	-1.732
DGY3	3.34	4.36	3.77	2.12	Disease resistance protein (TIR-NBS class)	-1.701
DGY4	3.37	3.50	4.63	2.21	ATR4_CYP83B1_RED1_RNT1_SUR2__cytochrome P450, family 83, subfamily B, polypeptide 1	-1.619
DGY5	4.14	4.08	3.68	2.45	NET2B__Kinase interacting (KIP1-like) family protein	-1.515
DGY6	3.12	3.49	2.99	1.70	Calcium-binding EF-hand family protein	-1.498
DGY7	4.96	4.82	6.02	3.80	ATWRKY53_WRKY53__WRKY family transcription factor	-1.464
DGY8	2.57	2.72	3.22	1.53	Leucine-rich repeat (LRR) family protein	-1.305
DGY9	3.18	2.80	3.52	1.87	AtCAF1a_CAF1a__Polynucleotidyl transferase, ribonuclease H-like superfamily protein	-1.302
DGY10	2.69	2.86	3.13	1.59	ATLOX5_LOX5__PLAT/LH2 domain-containing lipoxygenase family protein	-1.300
DGY11	3.75	3.55	6.02	3.15	AtPAE4_PAE4__Pectinacetylesterase family protein	-1.288
DGY12	2.14	2.17	2.74	1.07	Domain of unknown function (DUF966)	-1.275
DGY13	2.78	2.92	3.63	1.84	ATSOT17_ATST5C_SOT17__sulfotransferase 17	-1.269
DGY14	2.90	3.24	4.36	2.26	Glycoprotein membrane precursor GPI-anchored	-1.244
DGY15	2.72	2.90	3.02	1.66	CRK5_RLK6__cysteine-rich RLK (RECEPTOR-like protein kinase) 5	-1.217
DGY16	2.67	2.66	2.80	1.52	Protein of unknown function (DUF1195)	-1.189
DGY17	2.57	2.14	2.66	1.27	PIF6_PIL2__phytochrome interacting factor 3-like 2	-1.183
DGY18	4.37	4.27	4.51	3.22	LTPG3__Bifunctional inhibitor/lipid-transfer protein/seed storage 2S albumin superfamily protein	-1.161
DGY19	2.49	2.36	2.87	1.42	ATWRKY40_WRKY40__WRKY DNA-binding protein 40	-1.160
DGY20	2.14	2.38	2.48	1.18	ARA8_ATPCS1_CAD1_PCS1__phytochelatin synthase 1 (PCS1)	-1.158
DGY21	3.21	3.51	3.58	2.29	ATCAL4_CML12_TCH3__Calcium-binding EF hand family protein	-1.138
DGY22	2.45	2.81	3.10	1.67	EVR_SOBIR1__Leucine-rich repeat protein kinase family protein	-1.119
DGY23	2.46	2.99	2.79	1.64		-1.108
DGY24	3.24	2.98	3.07	1.99	RHS17__root hair specific 17	-1.108
DGY25	2.64	2.67	2.66	1.56	Protein kinase superfamily protein	-1.098
DGY26	2.22	2.04	2.48	1.16	ATH5_ATTRX5_LIV1_TRX-h5_TRX5__thioredoxin H-type 5	-1.089
DGY27	3.25	3.47	3.16	2.24	AtRAV1_EDF4_RAV1__related to ABI3/VP1 1	-1.059
DGY28	2.56	3.12	2.67	1.73		-1.058

DGY29	1.91	2.38	2.65	1.26	S-adenosyl-L-methionine-dependent methyltransferases superfamily protein	-1.055
DGY30	2.72	2.71	2.75	1.69	AtTN10_TIR_TN10__toll/interleukin-1 receptor-like	-1.044
DGY31	1.09	1.35	1.39	2.31	AMP-dependent synthetase and ligase family protein	1.030
DGY32	3.87	4.47	3.99	3.08	Ankyrin repeat family protein	-1.026
DGY33	2.42	2.64	2.67	1.56	Plant self-incompatibility protein S1 family	-1.019
DGY34	2.78	2.99	3.62	2.12	ATMPK11_MPK11__MAP kinase 11	-1.010
DGY35	2.56	2.88	3.01	1.81	MCU4__Protein of unknown function (DUF607)	-1.007
DGY36	2.06	1.90	2.65	3.21	ATERF#011_CEJ1_DEAR1__cooperatively regulated by ethylene and jasmonate 1	1.003
DGY37	2.50	2.74	2.84	1.69	ATERF11_ERF11__ERF domain protein 11	-1.001
DGY38	2.41	2.52	1.88	1.28	ATPEP1_PEP1_PROPEP1__precursor of peptide 1	-0.993
DGY39	2.54	2.80	3.28	1.88	FLS2__Leucine-rich receptor-like protein kinase family protein	-0.990
DGY40	1.98	2.17	1.83	1.01	ATSERK5_BAK8_SERK5__somatic embryogenesis receptor-like kinase 5	-0.980
DGY41	1.83	2.01	3.15	1.36	Leucine-rich repeat (LRR) family protein	-0.974
DGY42	2.52	2.44	3.02	1.70	AKN2_APK2__APS-kinase 2	-0.961
DGY43	2.09	2.24	2.66	1.38	S-locus lectin protein kinase family protein	-0.955
DGY44	3.88	3.58	3.07	2.56	Plant thionin family protein	-0.951
DGY45	2.76	2.73	4.03	2.23	ABCG36_ATABCG36_ATPDR8_PDR8_PEN3__ABC-2 and Plant PDR ABC-type transporter family protein	-0.942
DGY46	2.74	2.95	3.83	2.25	PGSIP7__Nucleotide-diphospho-sugar transferases superfamily protein	-0.921
DGY47	3.36	3.71	3.48	2.60	Plant self-incompatibility protein S1 family	-0.916
DGY48	1.89	2.06	1.90	1.03	Leucine-rich repeat family protein	-0.914
DGY49	2.58	2.33	1.63	1.27	ATMYBL2_MYBL2__MYB-like 2	-0.908
DGY50	2.74	2.06	1.66	1.25	Protein of unknown function (DUF962)	-0.907
DGY51	1.97	2.06	2.89	1.41	BGLU26_PEN2__Glycosyl hydrolase superfamily protein	-0.901
DGY52	2.35	2.44	3.38	1.83	ATCCR2_CCR2__cinnamoyl coa reductase	-0.897
DGY53	1.21	1.43	1.49	2.27	ASY2__DNA-binding HORMA family protein	0.896
DGY54	2.39	2.52	2.19	1.48	NIP4;2_NLM5__NOD26-like intrinsic protein 4;2	-0.885
DGY55	3.09	2.94	3.38	2.26	glycine-rich protein	-0.877
DGY56	2.45	2.70	2.30	1.61	AtHIR1__SPFH/Band 7/PHB domain-containing membrane-associated protein family	-0.874
DGY57	2.77	2.86	2.96	2.00	AtPCR2_PCR2__PLANT CADMIUM RESISTANCE 2	-0.864
DGY58	2.25	1.77	2.18	1.21	NDR1__Late embryogenesis abundant (LEA) hydroxyproline-rich glycoprotein family	-0.857
DGY59	2.36	2.31	2.32	1.48	Defensin-like (DEFL) family protein	-0.854
DGY60	3.44	3.23	4.59	2.90	S-adenosyl-L-methionine-dependent methyltransferases superfamily protein	-0.848
DGY61	2.27	2.45	2.19	1.46		-0.844
DGY62	1.73	1.71	2.13	1.03	ATEXO70B2_EXO70B2__exocyst subunit exo70 family protein B2	-0.825
DGY63	2.33	2.09	2.45	1.48	Protein of unknown function (DUF784)	-0.811
DGY64	1.82	2.00	1.97	1.13	S-locus lectin protein kinase family protein	-0.800
DGY65	2.48	1.72	2.28	1.37	Integrase-type DNA-binding superfamily protein	-0.794

DGY66	1.89	1.58	2.00	1.03	ATERF-5_ATERF5_AtMACD1_ERF102_ERF5__ethylene responsive element binding factor 5	-0.792
DGY67	2.09	2.46	2.30	1.49	ATEXLA3_ATEXPL3_ATHEXP BETA 2.3_EXLA3_EXPL3__expansin-like A3	-0.792
DGY68	2.90	2.68	2.72	1.98		-0.787
DGY69	2.60	2.32	2.60	1.72	AtSTS_RS4_STS__stachyose synthase	-0.785
DGY70	1.95	1.46	2.19	1.09	CYP94C1__cytochrome P450, family 94, subfamily C, polypeptide 1	-0.774
DGY71	3.99	3.88	4.01	3.19	BGLU12__beta glucosidase 12	-0.772
DGY72	1.92	2.19	2.21	1.35	ATOPR1_OPR1__12-oxophytodienoate reductase 1	-0.760
DGY73	3.56	3.75	3.55	2.87	AthCYSTM3	-0.746
DGY74	2.53	2.66	2.97	1.98	GGT1__gamma-glutamyl transpeptidase 1	-0.742
DGY75	2.55	1.86	1.82	1.34		-0.734
DGY76	1.72	2.04	2.23	1.28	Disease resistance protein (TIR-NBS-LRR class) family	-0.719
DGY77	2.12	1.89	2.46	1.44	ANNAT8__annexin 8	-0.714
DGY78	1.92	1.80	2.09	1.22	transmembrane receptors	-0.712
DGY79	1.45	1.64	2.12	1.03	MIK2__Leucine-rich repeat receptor-like protein kinase family protein	-0.707
DGY80	4.05	3.94	4.42	3.43	AOC3__allene oxide cyclase 3	-0.706
DGY81	1.90	2.37	2.32	1.49	CAR2__Calcium-dependent lipid-binding (CaLB domain) family protein	-0.705
DGY82	2.05	2.38	2.08	1.48		-0.690
DGY83	1.96	1.98	2.39	1.42	FUM2__FUMARASE 2	-0.687
DGY84	1.78	1.77	2.23	1.25	Calcium-dependent phosphotriesterase superfamily protein	-0.678
DGY85	2.25	1.59	1.95	1.26	CEP3__Cysteine proteinases superfamily protein	-0.668
DGY86	2.40	2.01	2.23	1.56	Protein of unknown function (DUF784)	-0.653
DGY87	2.47	2.15	2.69	1.79	Protein of unknown function (DUF784)	-0.647
DGY88	1.41	1.37	1.59	2.10	Plant invertase/pectin methylesterase inhibitor superfamily protein	0.638
DGY89	1.85	1.96	2.34	1.41	Eukaryotic aspartyl protease family protein	-0.638
DGY90	1.77	1.88	1.69	1.15	ATSERK4_BAK7_BKK1_SERK4__somatic embryogenesis receptor-like kinase 4	-0.632
DGY91	2.99	3.31	2.91	2.44	Ankyrin repeat family protein	-0.630
DGY92	4.10	4.38	3.95	3.52	Protein kinase protein with adenine nucleotide alpha hydrolases-like domain	-0.628
DGY93	1.88	1.90	1.79	1.23	SAG101__senescence-associated gene 101	-0.627
DGY94	2.14	1.58	2.00	1.28	ATWRKY34_MSP3_WRK34_WRKY34__WRKY DNA-binding protein 34	-0.622
DGY95	2.03	1.72	1.26	1.05	AtTT8_BHLH42_TT8__basic helix-loop-helix (bHLH) DNA-binding superfamily protein	-0.620
DGY96	2.76	2.66	2.80	2.12	Protein kinase superfamily protein	-0.617
DGY97	3.03	3.06	2.99	2.42	BGLU13__beta glucosidase 13	-0.614
DGY98	1.07	1.09	1.51	1.83	DELTA-TIP2_TIP2;2__tonoplast intrinsic protein 2;2	0.610
DGY99	2.16	2.34	2.59	1.76	AtBBE17__FAD-binding Berberine family protein	-0.603
DGY100	1.96	1.77	1.44	1.13	SAUR66__SAUR-like auxin-responsive protein family	-0.596

Final logFC≤-1 comparing the timepoints 0.5 *vs.* 2 h after pollination						
	A	**B**	**C**	**D**	**Annotation**	**Average ABC - D**
DGY569	-6.87	-5.23	-4.98	-3.00	DVL5_RTFL15__ROTUNDIFOLIA like 15	2.697
DGY570	-5.65	-3.92	-3.59	-2.67	Cysteine/Histidine-rich C1 domain family protein	1.716
DGY571	-4.62	-4.75	-4.80	-3.17	CYP79A3P__cytochrome P450, family 79, subfamily A, polypeptide 3 pseudogene	1.553
DGY572	-2.40	-2.87	-2.63	-4.06	Plant self-incompatibility protein S1 family	-1.425
DGY573	-3.01	-3.26	-3.81	-4.78	Integrase-type DNA-binding superfamily protein	-1.417
DGY574	-3.60	-3.44	-2.73	-1.94	AMT1;3_ATAMT1;3__ammonium transporter 1;3	1.318
DGY575	-5.48	-5.09	-5.35	-3.99	AtPP2-B15_PP2-B15__phloem protein 2-B15	1.314
DGY576	-2.57	-2.87	-3.47	-1.70	other RNA	1.267
DGY577	-3.08	-2.92	-3.33	-1.86	ASG4_REV3__Homeodomain-like superfamily protein	1.254
DGY578	-5.12	-3.79	-3.53	-2.93	Cytochrome P450 superfamily protein	1.222
DGY579	-8.15	-6.26	-6.94	-8.26		-1.148
DGY580	-2.96	-2.81	-2.62	-1.66	F-box and associated interaction domains-containing protein	1.134
DGY581	-3.22	-2.62	-2.68	-1.71	ABCB13_PGP13__P-glycoprotein 13	1.132
DGY582	-3.44	-2.71	-3.13	-1.97	ATFLS2_FLS2__flavonol synthase 2	1.124
DGY583	-3.24	-3.35	-3.03	-2.11	ATEXP24_ATEXPA24_ATHEXP ALPHA 1.19_EXP24_EXPA24__expansin A24	1.095
DGY584	-2.39	-2.45	-2.45	-1.34		1.095
DGY585	-3.09	-2.79	-2.60	-1.73	AITR2	1.094
DGY586	-2.73	-3.42	-3.03	-1.98	RNA-binding KH domain-containing protein	1.077
DGY587	-3.22	-2.51	-2.66	-1.73	Cellulase (glycosyl hydrolase family 5) protein	1.069
DGY588	-1.34	-1.84	-1.34	-2.56	Late embryogenesis abundant protein (LEA) family protein	-1.054
DGY589	-3.46	-3.42	-2.58	-2.11		1.042
DGY590	-2.56	-3.24	-2.47	-1.74	Putative methyltransferase family protein	1.018
DGY591	-2.70	-1.91	-2.24	-1.27	Subtilase family protein	1.013
DGY592	-1.77	-1.62	-1.47	-2.63	HSP20-like chaperones superfamily protein	-1.010
DGY593	-2.95	-3.60	-3.33	-2.29	ATSFL61_CEG_SFL61__F-box and associated interaction domains-containing protein	1.006
DGY594	-2.24	-3.06	-2.73	-1.67	transposable element gene	1.001
DGY595	-3.37	-2.79	-2.90	-2.02	AHL24__Predicted AT-hook DNA-binding family protein	1.001
DGY596	-2.91	-3.20	-2.92	-2.01		1.000
DGY597	-3.63	-2.74	-3.82	-2.43	HXXXD-type acyl-transferase family protein	0.965
DGY598	-1.34	-1.49	-2.29	-2.66	pfkB-like carbohydrate kinase family protein	-0.956
DGY599	-2.81	-3.58	-3.34	-2.29	EDA2__Serine carboxypeptidase S28 family protein	0.950
DGY600	-3.13	-3.33	-3.11	-2.25	GDSL-like Lipase/Acylhydrolase superfamily protein	0.939
DGY601	-3.55	-3.28	-3.29	-2.45	AtUGT85A3_UGT85A3__UDP-glucosyl transferase 85A3	0.928
DGY602	-3.04	-3.14	-2.90	-2.12	Polyketide cyclase/dehydrase and lipid transport superfamily protein	0.907
DGY603	-3.14	-2.86	-3.53	-2.27	alpha/beta-Hydrolases superfamily protein	0.902
DGY604	-2.96	-2.99	-3.70	-2.32		0.894
DGY605	-2.83	-3.19	-2.92	-2.11		0.870

DGY606	-2.75	-2.92	-2.75	-1.94		0.869
DGY607	-2.60	-2.14	-2.53	-1.57	F-box family protein with a domain of unknown function (DUF295)	0.857
DGY608	-2.36	-1.74	-1.78	-1.11	UDP-Glycosyltransferase superfamily protein	0.857
DGY609	-2.25	-2.29	-2.49	-1.49		0.853
DGY610	-2.57	-1.68	-2.28	-1.34		0.831
DGY611	-2.36	-3.06	-3.00	-1.98		0.826
DGY612	-2.33	-2.42	-1.92	-1.41	ARR6__response regulator 6	0.812
DGY613	-2.18	-2.12	-2.24	-1.38		0.798
DGY614	-2.78	-3.20	-2.67	-2.09		0.797
DGY615	-1.61	-1.51	-2.22	-2.57		-0.791
DGY616	-3.97	-2.79	-2.49	-2.30	other RNA	0.790
DGY617	-2.49	-2.38	-2.26	-1.60		0.781
DGY618	-2.38	-2.32	-2.73	-1.70	*Arabidopsis* protein of unknown function (DUF241)	0.780
DGY619	-2.47	-3.54	-1.88	-1.85	AGL54__AGAMOUS-like 54	0.778
DGY620	-2.82	-2.53	-2.70	-1.90	LYK2__Protein kinase superfamily protein	0.777
DGY621	-2.20	-1.48	-1.88	-1.08	Integrase-type DNA-binding superfamily protein	0.777
DGY622	-2.85	-2.84	-2.57	-1.98	CPK20__calcium-dependent protein kinase 20	0.772
DGY623	-3.35	-2.78	-2.76	-2.20	SRF5__STRUBBELIG-receptor family 5	0.769
DGY624	-3.13	-2.48	-2.42	-3.44	ERF109_RRTF1__redox responsive transcription factor 1	-0.763
DGY625	-3.90	-3.65	-3.76	-3.01	ATEXP11_ATEXPA11_ATHEXP ALPHA 1.14_EXP11_EXPA11__expansin 11	0.762
DGY626	-2.68	-2.75	-2.74	-1.96	SAUR35__SAUR-like auxin-responsive protein family	0.761
DGY627	-2.60	-2.60	-2.08	-1.67	Plant self-incompatibility protein S1 family	0.759
DGY628	-1.96	-1.70	-2.55	-2.82		-0.752
DGY629	-4.11	-3.97	-4.00	-3.29	HMS_PME6__Plant invertase/pectin methylesterase inhibitor superfamily	0.743
DGY630	-3.01	-2.38	-2.29	-1.84	Zinc-binding dehydrogenase family protein	0.723
DGY631	-2.20	-1.68	-1.65	-1.12		0.721
DGY632	-2.63	-2.50	-2.09	-1.69	Regulator of chromosome condensation (RCC1) family with FYVE zinc finger domain	0.720
DGY633	-1.96	-1.74	-1.93	-1.16		0.720
DGY634	-2.69	-2.63	-2.83	-2.00	Cytochrome P450 superfamily protein	0.717
DGY635	-3.19	-2.55	-3.49	-2.36	ELIP_ELIP1__Chlorophyll A-B binding family protein	0.715
DGY636	-2.72	-2.38	-2.68	-1.88	alpha/beta-Hydrolases superfamily protein	0.713
DGY637	-2.22	-2.10	-1.97	-1.40	ATGATL1_GATL1_GLZ1_PARVUS__Nucleotide-diphospho-sugar transferases superfamily protein	0.695
DGY638	-2.56	-2.10	-2.74	-1.77	Protein of unknown function (DUF1264)	0.695
DGY639	-1.53	-1.68	-1.17	-2.15		-0.694
DGY640	-2.63	-2.62	-2.84	-2.00		0.694
DGY641	-2.44	-2.26	-2.33	-1.65		0.692
DGY642	-2.18	-2.35	-2.36	-1.61	Bifunctional inhibitor/lipid-transfer protein/seed storage 2S albumin superfamily protein	0.692
DGY643	-1.54	-1.42	-2.67	-1.19	NGA4__AP2/B3-like transcriptional factor family protein	0.690
DGY644	-3.30	-3.31	-3.13	-2.57	Plant invertase/pectin methylesterase inhibitor superfamily	0.685
DGY645	-3.00	-3.25	-3.24	-2.48		0.685

DGY646	-1.41	-1.45	-1.47	-2.13		-0.683
DGY647	-2.77	-2.48	-2.30	-1.84	ATTIP1.3_GAMMA-TIP3_TIP1;3__tonoplast intrinsic protein 1;3	0.678
DGY648	-2.94	-2.55	-2.45	-1.98	GDSL-like Lipase/Acylhydrolase superfamily protein	0.672
DGY649	-1.87	-1.75	-1.92	-1.18		0.666
DGY650	-1.76	-1.44	-2.09	-1.10	Fasciclin-like arabinogalactan family protein	0.661
DGY651	-2.72	-1.78	-2.13	-1.56	CPK18__calcium-dependent protein kinase 18	0.656
DGY652	-2.40	-1.97	-2.97	-3.10	Polyketide cyclase/dehydrase and lipid transport superfamily protein	-0.656
DGY653	-2.81	-2.42	-2.87	-2.05	Exostosin family protein	0.654
DGY654	-1.87	-1.56	-2.61	-2.66	GRX480_GRXC9_roxy19__Thioredoxin superfamily protein	-0.651
DGY655	-3.13	-1.71	-1.64	-1.52	TPX2 (targeting protein for Xklp2) protein family	0.645
DGY656	-3.30	-2.59	-2.87	-2.28	Peroxidase superfamily protein	0.642
DGY657	-3.73	-3.44	-3.68	-2.97	Peroxidase superfamily protein	0.641
DGY658	-1.70	-1.82	-2.16	-1.25	Legume lectin family protein	0.637
DGY659	-2.97	-2.89	-2.40	-2.11	Protein kinase family protein	0.637
DGY660	-3.21	-3.09	-2.76	-2.39	GNL2__GNOM-like 2	0.630
DGY661	-1.87	-2.10	-1.51	-1.20	GCS1_HAP2__hapless 2	0.630
DGY662	-2.80	-3.09	-2.81	-2.27	Regulator of chromosome condensation (RCC1) family protein	0.629
DGY663	-1.77	-1.69	-1.66	-1.08	alpha 1,4-glycosyltransferase family protein	0.629
DGY664	-1.68	-1.70	-1.84	-1.12	Acyl-CoA N-acyltransferases (NAT) superfamily protein	0.627
DGY665	-2.88	-3.32	-3.11	-2.48	PRA1.C__prenylated RAB acceptor 1.C	0.626
DGY666	-2.70	-2.80	-2.68	-2.10	RALFL25__ralf-like 25	0.626
DGY667	-1.80	-1.68	-1.43	-1.01	AtGulLO6_GulLO6__D-arabinono-1,4-lactone oxidase family protein	0.624
DGY668	-2.08	-2.61	-2.48	-1.77	S-adenosyl-L-methionine-dependent methyltransferases superfamily protein	0.623

Appendix table 3.2. List of *hestia* genes with its logFC and annotations.

Results of logFC when comparing A, B and C crosses *vs*. D 2 h after pollination				
Code	**A**	**B**	**C**	**Annotation**
HTA1	2.18	1.86	1.26	Bifunctional inhibitor/lipid-transfer protein/seed storage 2S albumin superfamily protein
HTA2	1.71	1.55	1.14	Galactosyltransferase family protein
HTA3	1.50	1.29	1.26	AtPP2-B15_PP2-B15__phloem protein 2-B15
HTA4	1.36	1.54	1.05	CYP86A4__cytochrome P450, family 86, subfamily A, polypeptide 4
HTA5	1.29	1.21	1.14	CCT motif family protein
HTA6	1.28	1.46	1.28	AMP-dependent synthetase and ligase family protein
HTA7	1.17	1.10	1.11	
HTA8	1.13	1.25	1.29	ASG4_REV3__Homeodomain-like superfamily protein
HTA9	-1.02	-1.22	-1.14	SAUR48__SAUR-like auxin-responsive protein family
HTA10	-1.02	-1.84	-1.49	Curculin-like (mannose-binding) lectin family protein
HTA11	-1.02	-1.18	-1.15	Protein kinase superfamily protein
HTA12	-1.04	-1.57	-1.30	UGT87A2__UDP-Glycosyltransferase superfamily protein
HTA13	-1.04	-1.11	-1.69	Protein kinase superfamily protein
HTA14	-1.04	-1.72	-1.71	AtBBE10__FAD-binding Berberine family protein
HTA15	-1.05	-1.15	-1.45	ARACIN1
HTA16	-1.07	-1.81	-1.35	tolB protein-related
HTA17	-1.09	-1.64	-1.34	FAD/NAD(P)-binding oxidoreductase family protein
HTA18	-1.10	-1.56	-1.56	ATWRKY53_WRKY53__WRKY family transcription factor
HTA19	-1.14	-1.63	-1.66	AtPRX71_PRX71__Peroxidase superfamily protein
HTA20	-1.14	-1.15	-1.39	Glycoprotein membrane precursor GPI-anchored
HTA21	-1.14	-1.36	-1.39	Major facilitator superfamily protein
HTA22	-1.15	-1.79	-1.52	alpha/beta-Hydrolases superfamily protein
HTA23	-1.15	-1.36	-1.28	PIRL2__plant intracellular ras group-related LRR 2
HTA24	-1.16	-1.24	-1.77	ATMYB15_ATY19_MYB15__myb domain protein 15
HTA25	-1.16	-1.12	-1.28	*Arabidopsis* phospholipase-like protein (PEARLI 4) family
HTA26	-1.17	-1.12	-1.03	
HTA27	-1.17	-1.47	-1.54	CRK19__cysteine-rich RLK (RECEPTOR-like protein kinase) 19
HTA28	-1.18	-1.58	-1.67	ACO4_EAT1_EFE__ethylene-forming enzyme
HTA29	-1.20	-1.35	-1.71	Plant invertase/pectin methylesterase inhibitor superfamily protein
HTA30	-1.21	-1.75	-1.81	Peroxidase superfamily protein
HTA31	-1.22	-1.33	-1.06	U3D__U3D; snoRNA
HTA32	-1.24	-1.73	-1.52	ATR4_CYP83B1_RED1_RNT1_SUR2__cytochrome P450, family 83, subfamily B, polypeptide 1
HTA33	-1.26	-1.67	-1.71	VQ12__VQ motif-containing protein
HTA34	-1.30	-1.66	-1.71	Chitinase family protein
HTA35	-1.30	-2.02	-1.83	AtBBE11__FAD-binding Berberine family protein
HTA36	-1.31	-1.64	-1.81	ATGLR2.5_GLR2.5__glutamate receptor 2.5
HTA37	-1.31	-1.56	-1.71	Leucine-rich repeat (LRR) family protein
HTA38	-1.32	-1.52	-1.66	
HTA39	-1.32	-1.25	-1.48	
HTA40	-1.34	-1.31	-1.97	ATWRKY30_WRKY30__WRKY DNA-binding protein 30

HTA41	-1.38	-1.42	-1.41	ATCML9_CAM9_CML9__calmodulin 9
HTA42	-1.38	-1.47	-1.60	ATLOX5_LOX5__PLAT/LH2 domain-containing lipoxygenase family protein
HTA43	-1.39	-1.43	-1.48	AtWRKY22_WRKY22__WRKY family transcription factor
HTA44	-1.47	-1.66	-1.92	ATCHX3_CHX3__cation/H+ exchanger 3
HTA45	-1.48	-2.00	-1.97	defense protein-related
HTA46	-1.50	-1.70	-1.67	AGL37_PHE1__MADS-box transcription factor family protein
HTA47	-1.54	-2.40	-2.00	ATRBOHC_RBOHC_RHD2__NADPH/respiratory burst oxidase protein D
HTA48	-1.67	-2.46	-2.27	ATSUC7_SUC7__sucrose-proton symporter 7
HTA49	-1.70	-2.29	-2.18	ATNHL10_NHL10_YLS9__Late embryogenesis abundant (LEA) hydroxyproline-rich glycoprotein family
HTA50	-1.76	-1.95	-2.04	Protein kinase superfamily protein
HTA51	-1.77	-1.25	-1.23	
HTA52	-1.82	-2.47	-2.47	Legume lectin family protein
HTA53	-1.85	-2.29	-2.40	*Arabidopsis* phospholipase-like protein (PEARLI 4) family
HTA54	-1.86	-2.32	-1.92	ATGSTF2_ATPM24_ATPM24.1_GST2_GSTF2__glutathione S-transferase PHI 2
HTA55	-1.89	-2.49	-2.43	IOS1__Leucine-rich repeat protein kinase family protein
HTA56	-1.94	-1.45	-1.85	ATMLO12_MLO12__Seven transmembrane MLO family protein
HTA57	-2.02	-1.80	-1.87	
HTA58	-2.04	-2.53	-2.32	Legume lectin family protein
HTA59	-2.06	-1.71	-1.64	CRK18__cysteine-rich RLK (RECEPTOR-like protein kinase) 18
HTA60	-2.43	-2.28	-2.22	ATEXT1_ATEXT4_EXT1_EXT4_ORG5__extensin 4
HTA61	-2.52	-2.39	-2.04	
HTA62	-2.54	-2.83	-2.78	Cysteine/Histidine-rich C1 domain family protein
HTA63	-2.73	-2.66	-2.52	Leucine-rich repeat protein kinase family protein
HTA64	-2.82	-3.34	-3.28	transposable element gene
HTA65	-3.36	-3.95	-4.14	ATSUC6_SUC6__sucrose-proton symporter 6
HTA66	-5.23	-5.03	-5.21	serine-type endopeptidase inhibitors
HTA67	-6.81	-8.65	-8.49	RPS2__NB-ARC domain-containing disease resistance protein

Appendix figure 4.1. Four genes encoding EF1α proteins aligned by MUSCLE (3.8). Highlighted areas described in this thesis as gRNA1 (grey background), gRNA2 (orange font), gRNA3 (blue background) and gRNA4 (yellow background).

```
AT5G60390      -------------------CAAAGAGAAAGCGAAAACCCTAGA-------------CACC
AT1G07930      GTAAAATTGTCATTACGCTAAGGAGATTATCTTAAACCCTAAC------TTTTTTCCGCT
AT1G07920      --------------------------------TAAACCCTAAC----ATTGGTTTCGGAT
AT1G07940      --------------------CGATGTTATGTTAAACCCTAACTTATTATTTCTTTCGAT
                                              ********

AT5G60390      TCGTAGCTATAAGTACCCTCGAGTCGACCAGGATTAGGGTGCGCTCTCATATTTCTCACA
AT1G07930      TCACCACTATAAATACAAACTTGTTTACC---CTTCCAATTTATTTCTCTACTTGTCCAC
AT1G07920      TCAACGCTATAAATAAA---------ACCACTCTCGTTGCTGATTCC---ATTTATC-GT
AT1G07940      TCACCACTATAAATAAACTCGA----ATCCCAAACATAGCTTTATTCCTTGCTTC---AT
               **    ****** **           * *               *       **

AT5G60390      TTTTCG------TAGCCGCAAGA-----CTCCTT------------------TCAGATTC
AT1G07930      TTTTCT-----ACAGCCGCATCATCCTTCTCCCTTGTGCGATATCGTTTGCGTGAGAT--
AT1G07920      TCTTATTGACCCTAGCCGCTACA-----CACTTTTCTGCGATATCTC-----TGAGAT--
AT1G07940      TTTTCGTCACCCTAGCCGCTTTA-----CTCTCT--TGCGATATCTC-----TGAGAT--
               * **         ******   *     * *  *                  * ****

AT5G60390      TTACTTG---------CAGCTATGGGTAAAGAGAAGTTTCACATTAACATTGTGGTCATT
AT1G07930      TTGTCTGAAAAGTAGCTAACCATGGGTAAAGAGAAGTTTCACATCAACATTGTGGTCATT
AT1G07920      TTGTTGA--CAGTCTCTAACCATGGGTAAAGAGAAGTTTCACATCAACATTGTGGTCATT
AT1G07940      TTGTTTG-ACAGTCTCTAACCATGGGTAAAGAGAAGTTTCACATCAACATTGTGGTCATT
               **              * * ********************** ***************

AT5G60390      GGTCATGTTGATTCTGGAAAATCGACCACAACTGGTCACTTGATCTATAAGCTTGGTGGT
AT1G07930      GGCCACGTCGATTCTGGAAAGTCGACAACCACTGGACACTTGATCTACAAGTTGGGTGGT
AT1G07920      GGCCACGTCGATTCTGGAAAGTCGACCACCACTGGGCACTTGATCTACAAGTTGGGTGGT
AT1G07940      GGCCACGTCGATTCTGGAAAGTCGACCACCACTGGACACTTGATCTACAAGTTGGGTGGT
               ** ** ** ************ ***** ** ***** ************ *** * ******

AT5G60390      ATTGACAAGCGTGTCATCGAGAGGTTCGAGAAGGAGGCTGCTGAGATGAACAAGAGGTCC
AT1G07930      ATTGACAAGCGTGTGATCGAGAGGTTCGAGAAGGAGGCTGCTGAGATGAACAAGAGGTCC
AT1G07920      ATTGACAAGCGTGTCATTGAGAGGTTCGAGAAGGAGGCTGCTGAGATGAACAAGAGGTCC
AT1G07940      ATTGACAAGCGTGTCATTGAGAGGTTCGAGAAGGAGGCTGCTGAGATGAACAAGAGGTCC
               ************** ** ****************************************

AT5G60390      TTCAAGTACGCATGGGTGTTGGACAAACTTAAGGCCGAGCGTGAGCGTGGTATTACCATC
AT1G07930      TTCAAGTACGCATGGGTGTTGGACAAACTTAAGGCTGAGCGTGAGCGTGGTATCACCATT
AT1G07920      TTCAAGTACGCATGGGTTTTGGACAAACTTAAGGCTGAGCGTGAGCGTGGTATCACCATT
AT1G07940      TTCAAGTACGCATGGGTTTTGGACAAACTTAAGGCTGAGCGTGAGCGTGGTATCACCATT
               ***************** ***************** ***************** *****

AT5G60390      GATATTGCTCTATGGAAGTTCGAGACCACCAAGTACTACTGCACAGTCATTGATGCCCCA
AT1G07930      GACATTGCTCTCTGGAAGTTCGAGACCACCAAGTACTACTGCACTGTCATTGATGCTCCT
AT1G07920      GACATTGCTCTCTGGAAGTTCGAGACCACCAAGTACTACTGCACTGTCATTGATGCTCCT
AT1G07940      GACATTGCTCTCTGGAAGTTCGAGACCACCAAGTACTACTGCACTGTCATTGATGCTCCT
               ** ******** ******************************** *********** **

AT5G60390      GGACATCGTGATTTCATCAAGAACATGATTACTGGTACCTCCCAGGCTGATTGTGCTGTT
AT1G07930      GGTCATCGTGATTTCATCAAGAACATGATCACTGGTACCTCCCAGGCTGATTGTGCTGTC
AT1G07920      GGCCATCGTGATTTCATCAAGAACATGATCACTGGTACCTCCCAGGCTGATTGTGCTGTC
AT1G07940      GGCCATCGTGATTTCATCAAGAACATGATCACTGGTACCTCCCAGGCTGATTGTGCTGTC
               ** ************************* ******************************

AT5G60390      CTTATCATTGACTCCACCACTGGAGGTTTTGAGGCTGGTATCTCTAAGGATGGTCAGACC
AT1G07930      CTTATCATTGACTCCACCACTGGTGGTTTTGAGGCTGGTATCTCCAAGGATGGTCAGACC
AT1G07920      CTTATCATTGACTCCACCACTGGTGGTTTTGAGGCTGGTATCTCCAAGGATGGTCAGACC
AT1G07940      CTTATCATTGACTCCACCACTGGTGGTTTTGAGGCTGGTATCTCCAAGGATGGTCAGACC
               ********************** ******************* ***************

AT5G60390      CGTGAGCACGCTCTTCTTGCTTTCACCCTTGGTGTCAAGCAGATGATTTGCTGTTGTAAC
AT1G07930      CGTGAGCACGCTCTCCTTGCTTTCACCCTTGGTGTCAAGCAGATGATCTGCTGTTGTAAC
AT1G07920      CGTGAGCACGCTCTACTTGCTTTCACCCTTGGTGTCAAGCAGATGATCTGCTGTTGTAAC
AT1G07940      CGTGAGCACGCTCTACTTGCTTTCACCCTTGGTGTCAAGCAGATGATCTGCTGTTGTAAC
               ************** ******************************** ************
```

```
AT5G60390       AAGATGGATGCCACCACCCCCAAATACTCCAAGGCTAGGTACGATGAAATCATCAAGGAG
AT1G07930       AAGATGGATGCCACTACCCCCAAGTACTCCAAGGCCAGGTACGATGAAATCATCAAGGAG
AT1G07920       AAGATGGATGCCACTACCCCCAAGTACTCCAAGGCCAGGTACGATGAAATCATCAAGGAG
AT1G07940       AAGATGGATGCCACTACCCCCAAGTACTCCAAGGCCAGGTACGATGAAATCATCAAGGAG
                ************** ******** *********** ************************

AT5G60390       GTGTCTTCATACCTGAAGAAGGTCGGATACAACCCTGACAAAATCCCATTTGTGCCAATC
AT1G07930       GTGTCTTCCTACTTGAAGAAGGTTGGTTACAACCCCGACAAAATCCCATTTGTGCCCATC
AT1G07920       GTGTCTTCCTACTTGAAGAAGGTTGGTTACAACCCCGACAAAATCCCATTTGTGCCCATC
AT1G07940       GTGTCTTCCTACTTGAAGAAGGTTGGTTACAACCCCGACAAAATCCCATTTGTGCCCATC
                ******** *** ********** ** ******** ******************** ***

AT5G60390       TCTGGATTCGAGGGAGACAACATGATTGAGAGGTCAACCAACCTTGACTGGTACAAGGGA
AT1G07930       TCTGGATTTGAGGGTGACAACATGATTGAGAGGTCCACCAACCTTGACTGGTACAAGGGA
AT1G07920       TCTGGATTTGAGGGTGACAACATGATTGAGAGGTCCACCAACCTTGACTGGTACAAGGGA
AT1G07940       TCTGGATTTGAGGGTGACAACATGATTGAGAGGTCCACCAACCTTGACTGGTACAAGGGA
                ******** ***** ******************** ************************

AT5G60390       CCAACTCTTCTTGAGGCTCTTGACCAGATCAACGAGCCCAAGAGGCCATCAGACAAGCCC
AT1G07930       CCAACTCTCCTTGAGGCTCTTGACCAGATCAACGAGCCCAAGAGGCCGTCAGACAAGCCC
AT1G07920       CCAACTCTCCTTGAGGCTCTTGACCAGATCAACGAGCCCAAGAGGCCGTCAGACAAGCCC
AT1G07940       CCAACTCTCCTTGAGGCTCTTGACCAGATCAACGAGCCCAAGAGGCCGTCAGACAAGCCC
                ******** ************************************* ************

AT5G60390       CTTCGTCTTCCACTTCAGGATGTCTACAAGATTGGTGGTATTGGAACGGTGCCAGTGGGA
AT1G07930       CTTCGTCTCCCACTTCAGGATGTCTACAAGATTGGTGGTATTGGAACGGTGCCAGTGGGA
AT1G07920       CTTCGTCTCCCACTTCAGGATGTCTACAAGATTGGTGGTATTGGAACGGTGCCAGTGGGA
AT1G07940       CTTCGTCTCCCACTTCAGGATGTCTACAAGATTGGTGGTATTGGAACGGTGCCAGTGGGA
                ******** ************************************************

AT5G60390       CGTGTTGAGACTGGTATGATCAAGCCTGGTATGGTTGTTACCTTTGCTCCCACAGGGTTG
AT1G07930       CGTGTTGAGACTGGTATGATCAAGCCTGGTATGGTTGTGACCTTTGCTCCCACAGGATTG
AT1G07920       CGTGTTGAGACTGGTATGATCAAGCCTGGTATGGTTGTGACCTTTGCTCCCACAGGATTG
AT1G07940       CGTGTTGAGACTGGTATGATCAAGCCTGGTATGGTTGTGACCTTTGCTCCCACAGGATTG
                ************************************ ***************** ***

AT5G60390       ACCACTGAGGTTAAGTCTGTTGAGATGCACCACGAGTCTCTTCTTGAGGCACTTCCCGGT
AT1G07930       ACCACTGAGGTCAAGTCTGTTGAGATGCACCACGAGTCTCTTCTTGAGGCACTTCCAGGT
AT1G07920       ACCACTGAGGTCAAGTCTGTTGAGATGCACCACGAGTCTCTTCTTGAGGCACTTCCAGGT
AT1G07940       ACCACTGAGGTCAAGTCTGTTGAGATGCACCACGAGTCTCTTCTTGAGGCACTTCCAGGT
                *********** ***************************************** ***

AT5G60390       GACAATGTTGGATTCAATGTCAAGAATGTTGCTGTCAAGGATCTTAAGAGAGGATACGTT
AT1G07930       GACAACGTTGGGTTCAATGTTAAGAATGTTGCCGTGAAGGATCTTAAGAGAGGGTACGTC
AT1G07920       GACAACGTTGGGTTCAATGTTAAGAATGTTGCTGTCAAGGATCTTAAGAGAGGGTACGTC
AT1G07940       GACAACGTTGGGTTCAATGTTAAGAATGTTGCTGTCAAGGATCTTAAGAGAGGGTACGTC
                ***** ***** ******** *********** ** ***************** *****

AT5G60390       GCCTCTAACTCCAAGGATGATCCAGCTAAGGGTGCCGCCAACTTCACCTCCCAGGTCATC
AT1G07930       GCCTCCAACTCCAAGGATGACCCTGCCAAGGGTGCTGCTAACTTCACCTCCCAGGTCATC
AT1G07920       GCATCCAACTCCAAGGATGACCCTGCCAAGGGTGCTGCTAACTTCACCTCCCAGGTCATC
AT1G07940       GCATCCAACTCCAAGGATGACCCTGCCAAGGGTGCTGCTAACTTCACCTCCCAGGTCATC
                ** ** ************** ** ** ******** ** ********************

AT5G60390       ATCATGAACCACCCTGGTCAGATTGGTAACGGTTACGCCCCAGTTCTCGATTGCCACACC
AT1G07930       ATCATGAACCACCCTGGTCAGATTGGTAACGGTTACGCCCCAGTCTTGGATTGCCACACC
AT1G07920       ATCATGAACCACCCTGGTCAGATTGGTAACGGTTACGCCCCAGTCCTGGATTGCCACACC
AT1G07940       ATCATGAACCACCCTGGTCAGATTGGTAACGGTTACGCCCCAGTCCTGGATTGCCACACC
                ****************************************  * ************

AT5G60390       TCTCACATTGCAGTCAAGTTCTCTGAGATCTTGACCAAGATTGACAGGCGTTCTGGTAAG
AT1G07930       TCTCACATTGCAGTCAAGTTCTCTGAGATCTTGACCAAGATTGACAGGCGTTCTGGTAAG
AT1G07920       TCTCACATTGCAGTCAAGTTCTCTGAGATCTTGACCAAGATTGACAGGCGTTCTGGTAAG
AT1G07940       TCTCACATTGCAGTCAAGTTCTCTGAGATCTTGACCAAGATTGACAGGCGTTCTGGTAAG
                ************************************************************
```

```
AT5G60390      GAGATTGAGAAGGAGCCCAAGTTTTTGAAGAATGGTGACGCTGGTATGGTTAAGATGACC
AT1G07930      GAGATTGAGAAGGAGCCCAAATTCTTGAAGAATGGTGATGCTGGTATGGTGAAGATGACT
AT1G07920      GAGATTGAGAAGGAGCCCAAGTTCTTGAAGAATGGTGATGCTGGTATGGTGAAGATGACT
AT1G07940      GAGATTGAGAAGGAGCCTAAATTCTTGAAGAATGGTGATGCTGGTATGGTGAAGATGACT
               ***************** ** ** ************** ************ ********

AT5G60390      CCAACCAAGCCCATGGTTGTTGAGACTTTCTCCGAGTACCCACCTTTGGGACGTTTCGCT
AT1G07930      CCAACCAAGCCCATGGTTGTGGAGACCTTCTCTGAGTACCCACCACTTGGACGTTTCGCT
AT1G07920      CCAACCAAGCCCATGGTTGTGGAGACCTTCTCTGAGTACCCACCACTTGGACGTTTCGCT
AT1G07940      CCAACCAAGCCCATGGTTGTGGAGACCTTCTCTGAGTACCCACCACTTGGACGTTTCGCT
               ******************** ***** ***** ***********  * ************

AT5G60390      GTTAGGGACATGAGGCAGACCGTTGCTGTTGGTGTTATTAAGAGCGTGGACAAGAAGGAC
AT1G07930      GTTAGGGACATGAGGCAGACTGTTGCAGTCGGTGTTATCAAGAGTGTTGACAAGAAGGAC
AT1G07920      GTGAGGGACATGAGGCAGACTGTTGCAGTCGGTGTTATCAAGAGTGTTGACAAGAAGGAC
AT1G07940      GTGAGGGACATGAGGCAGACTGTTGCAGTCGGTGTTATCAAGAGTGTTGACAAGAAGGAC
               ** ***************** ***** ** ******** ***** ** ************

AT5G60390      CCAACTGGAGCCAAGGTCACCAAGGCTGCAGTGAAGAAGGGTGCCAAATGA---------
AT1G07930      CCAACCGGAGCCAAGGTTACCAAGGCTGCAGTTAAGAAGGGTGCAAAGTGAACTCGAATC
AT1G07920      CCAACCGGAGCCAAGGTTACCAAGGCTGCCGTCAAGAAGGGTGCGAAGTGAACC---ATC
AT1G07940      CCAACTGGAGCCAAGGTTACCAAGGCTGCAGTCAAGAAGGGTGCCAAGTGAACTCTGAAC
               ***** ************ ************ ** ************ ** ***

AT5G60390      --TGAGACTTT------------CGTTATGATCGACTCTCTTATGGTTTTC---------
AT1G07930      CTCAAAACTCTAT---CCGCAGATGAATCAAAAAACAATATTAGTTTCTTTACTTTAG--
AT1G07920      CTCAAAACTCTATCTGCCGCAGGTGAATCAAAGGACAGTGTTAGTTTTATTACAATAG--
AT1G07940      ATCAAAACTCTTT---CCGCTGATGAAATGAAGGACTATTTTAGTTTCTTTACTTTAGTA
                   * *** *             *     *   **  * ***   *  *

AT5G60390      -TTTGGTTCTTAAAACTTTGATGGCGTTTGAGCCTTTTTCTTTTTTC------TCTTTAT
AT1G07930      -TTTGGTATTTGGTCGC------GTGTTATAGCTTCGTTTCTTCTCCATCGGAACTCTGT
AT1G07920      -TTTGGTATTTGGTCGCGTGTCTGTGTTCTTGTTTCGTTTTCTCCCCGTCAGAGCGTTGT
AT1G07940      GTTTGGTATTTGGTTGGTTGTTTGTGTTACCGCTTCGTTTATTCTCCGTCGGAGCTCAAT
                ******  **           * ***   *  *  **   *   *       *    *

AT5G60390      TTCTGTGACTTTCTCTCTCCCTCCTTTTTGGATATCTCTGAG---------ACTTTTTAT
AT1G07930      TCCCGGAACTGGGT-------TCTTGATCGGAGGTGGCGGAGCTACTTTGCACCTA----
AT1G07920      TCTCGTAATTGGGT-------TCTTGATCGGAGGTGGCGGATCTAC---ACACACATTCT
AT1G07940      TCTCGGAATTGGGT-------TCTTGATCGGAGGTGGCGGAGGTACTTGGCACTCGAGCT
               *   *  * *   *       ** *  * ***  *  * **          **

AT5G60390      TATGGTTTTCAATTATGCAGTTTCCGGATAATTTTGCTTGAAACTTATTTAGGAGTTGTG
AT1G07930      -------TTTTGCTTTTGAATTGTTAT-CAATTTTG-----AACCTATTTGGAGATTCGG
AT1G07920      TCCTGTTTTTTGCTTTTTATTTGTTTTCTCATTTTG-----AACTGTTTTAAAATTTCTG
AT1G07940      TCCTGTTTATTTCTTTTGTTTTGTGTTATGATTTTG-----AACCTTTTTGGATATTCGG
                      *     * *    **        ******     ***   ***     **  *

AT5G60390      TTACA--AAGTTGCTGTCTTTCTT--TGTTCTTGTTTAAACAATCATTCAGAGATCAACC
AT1G07930      TTATATGATGTGA-----TTTTCCGAGGATATTCTCT----------------------C
AT1G07920      TTATATGA-ATGAATGTTTTCCCTGCGGTTATTATCT-----------------------
AT1G07940      TTATATGATATTTGTGTCATTCCTGCGGATATTATCTTATC----------TTATCAACT
               *** *  *  *        *       * * ** * *

AT5G60390      CAACCATACTTAGCGTTTTAAGATCTATGTAAGAGATAGGGTTCTATAGTTTCGT-TAGA
AT1G07930      TTTTTTTGTTGCGTGTATCACATTCGAATTCAGT-------CTCTTGGATAACTTGTGGA
AT1G07920      ----------------TCTTTACTCTAATT-----------TTCTCTTGTTGCGT-----
AT1G07940      TAAGTCTGTTT----TTCTTCTCTAAAATTCAACGATCAGCCTCTGAAGTTTCTTACATG
                                     *  *  *           ***    *  * *

AT5G60390      ATTAACTTGTGCTT------AGTGTTTT-------CTGACAA------------------
AT1G07930      A-AAACTTATAACTTCAAGAAAAACCTTATAAACACTTACAACTTCAACAAAATATCGTA
AT1G07920      ---AAATCGTTTCC------GAAATCTT-------TTTACCTCT----------------
AT1G07940      GTAAAATTGTAATC------TAGAACTT-------TAAACAACATTGGAGAAACAAGTCT
                  ** *  *               **         **

AT5G60390      ----------
AT1G07930      A---------
AT1G07920      ----------
AT1G07940      ATATCAGTTT
```

Appendix protocol 4.1. *Agrobacterium* transformation by electroporation.

- Thaw a 100 µl aliquot of competent *Agrobacterium* cells on ice. We use GV3301 Rifampicin + Gentamycin resistant
- Add 200-500 ng of your plasmid up to 10 µl and mix gently
- Place 50 µl of the mix in the electroporation cuvette (0.1 cm)
- Apply one pulse (50 mF, load resistance 200 W, maximum power 25 W, current 25 mA and voltage 1800 V)
- Very slowly add 500 µl of LB medium
- Transfer it to an Eppendorf tube
- Incubate at 28 °C shaking 100 rpm in the dark for 3 h
- Plate 100 µl in a LB + Rif 25 mg/ml + Gen 10 mg/ml + appropriate antibiotic plate
- Incubate for 2 days at 28 °C until single colonies appear (~5 colonies are expected)
- Check for the presence of the construct by colony PCR

Appendix protocol 4.2. Plant transformation with *Agrobacterium*.

a) Sowing and growing of the parental plants

- Suspend approximately 12 mg of seeds in 27.5 ml 0.2% agar
- Incubate seeds for 2-3 days at 4 ºC
- Prepare multiplug-tray with a mixture of sand:soil (1:3)
- Dispense the seeds, 1 drop/cell, with a Pasteur pipette
- Germinate the plants for 2 weeks under standard conditions
- Prepare pots with a mixture of sand and peat (1:3)
- Transplant the seedlings to the pots
- Set temperature to 22 ºC / day and 18 ºC / night
- Set RH to 65-70%
- Set photoperiod to 12 h

b) *Agrobacterium* growth conditions and preparation

- Start procedure in the morning in a 50 ml Falcon containing 1 ml LB without antibiotic
- Shake 8-9 h at 28 ºC
- Add 10 ml of LB without antibiotic
- Shake overnight at 28 ºC (230 rpm)
- Check OD600 in the morning, should be approximately 2.0
- Add 40 ml of MQ water containing sucrose (10 %, 4 g) and Silwet (0.05 %, 20 µl)

c) Flower dip

- Inflorescences should be 10-15 cm high
- Invert the inflorescences in the Agro culture and agitate gently for 2-3 seconds
- Return the plants to normal growing conditions
- Dome the plants with cling-film and maintain in the dark.
- After 24h, remove the cling-film and protect the plant to avoid cross-contamination.

Appendix protocol 5.1 The equipment and solutions needed to carry out Arabidopsis mutagenesis with Ethyl methanesulfonate.

- Eco nitrile PF 250 gloves (cat III)
- Dupont™ Tyvek coat (cat III, type 5/6)
- 3M FFP3 Mask
- Absorbent paper
- Parafilm
- Wrapped orbital shaker
- Wrapped P200 with parafilm
- Wrapped P1000 with parafilm
- Tips 200 µL
- Tips 1 mL (some wide bore tips)
- 3 cut open PVC bottles
- 1 cut plastic funnel
- Grey garbage bag
- Petri-dish
- Whatman paper
- 500 mL glass bottle
- 12 - 50 mL falcon tubes
- 10 – 25 mL pipettes
- Water
- 2L 5M NaOH
- 100 mL 0.1 M phosphate buffer
- 300 mL 0.1 M $Na_2S_2O_3$
- 200 mL 0.05% Triton X-100
- 30 µL 9.7 M EMS
- 600 mL 0.1% Agarose
- 250 mg seed stock
- The material present in the EMS room

Extra info:

- 5 M NaOH (=200 g/L)
- 0.1 M phosphate buffer (pH 7.5)

  16.6 mL $H_2PO_4^-$ (=136.1 g/L) + 83.4 mL HPO_4^{2-} (=228.22 g/L) + 900 mL H_2O

  Potassium dihydrogen phosphate (228.2 g/mol)

  Dipotassium hydrogen phosphate trihydrate (136.1 g/mol)
- 0.1M $Na_2S_2O_3$ (=24.818 g/L)

  Disodium thiosulfate pentahydrate (248.2 g/mol)
- 0.05% Triton X-100 (=0.5 mL/L)

References

Adrain, C. and Martin, S. J. (2001) 'The mitochondrial apoptosome: A killer unleashed by the cytochrome seas', *Trends in Biochemical Sciences*. Trends Biochem Sci, pp. 390–397. doi: 10.1016/S0968-0004(01)01844-8.

Ai, H. W. *et al.* (2006) 'Directed evolution of a monomeric, bright and photostable version of Clavularia cyan fluorescent protein: Structural characterization and applications in fluorescence imaging', *Biochemical Journal*, 400(3), pp. 531–540. doi: 10.1042/BJ20060874.

Alonso, J. M. and Ecker, J. R. (2006) 'Moving forward in reverse: Genetic technologies to enable genome-wide phenomic screens in Arabidopsis', *Nature Reviews Genetics*. Nature Publishing Group, pp. 524–536. doi: 10.1038/nrg1893.

Alvarez-Buylla, E. R. *et al.* (2010) 'Flower Development'. doi: 10.1199/tab.0127.

Amberg, D. C., Burke, D. J. and Strathern, J. N. (2006) 'Ethyl Methane Sulfonate (EMS) Mutagenesis', *Cold Spring Harbor Protocols*, 2006(1), p. pdb.prot4180. doi: 10.1101/pdb.prot4180.

Axelos, M. *et al.* (1989) 'The gene family encoding the Arabidopsis thaliana translation elongation factor EF-1α: Molecular cloning, characterization and expression', *MGG Molecular & General Genetics*, 219(1–2), pp. 106–112. doi: 10.1007/BF00261164.

Baker, H. G. (1953) 'Race formation and reproductive method in flowering plants', *Symp. Society Experimental Biology*, 7, pp. 114–145.

Balk, J. *et al.* (2003) 'The intermembrane space of plant mitochondria contains a DNase activity that may be involved in programmed cell death', *The Plant Journal*, 34(5), pp. 573–583. doi: 10.1046/j.1365-313X.2003.01748.x.

Behera, S. *et al.* (2018) 'Cellular Ca 2+ signals generate defined pH signatures in plants', *Plant Cell*, 30(11), pp. 2704–2719. doi: 10.1105/tpc.18.00655.

Berardini, T. Z. *et al.* (2015) 'The arabidopsis information resource: Making and mining the "gold standard" annotated reference plant genome', *Genesis*, 53(8), pp. 474–485. doi: 10.1002/dvg.22877.

Bergelson, J. *et al.* (1998) 'Genetic variation within and among populations of Arabidopsis thaliana', *Genetics*, 148(3), pp. 1311–1323. Available at: /pmc/articles/PMC1460032/?report=abstract (Accessed: 28 August 2020).

Bittencourt Júnior, N. S. (2017) 'Evidence for post-zygotic self-incompatibility in Handroanthus impetiginosus (Bignoniaceae)', *Plant Reproduction*, 30(2), pp. 69–79. doi: 10.1007/s00497-017-0300-7.

Blumenberg, M. (2019) 'Introductory Chapter: Transcriptome Analysis', in *Transcriptome Analysis*. IntechOpen. doi: 10.5772/intechopen.85980.

Boggs, N. A., Nasrallah, J. B. and Nasrallah, M. E. (2009) 'Independent S-Locus Mutations Caused Self-Fertility in Arabidopsis thaliana', *PLoS Genetics*. Edited by G. P. Copenhaver, 5(3), p. e1000426. doi: 10.1371/journal.pgen.1000426.

Bosch, M. *et al.* (2010) 'Characterization of a legumain/vacuolar processing enzyme and YVADase activity in Papaver pollen', *Plant Molecular Biology*, 74(4), pp. 381–393. doi: 10.1007/s11103-010-9681-9.

Bosch, Maurice. and Franklin-Tong, V. E. (2007) 'Temporal and spatial activation of caspase-like enzymes induced by self-incompatibility in Papaver pollen.', *Proceedings of the National Academy of Sciences of the United States of America*, 104(46), pp. 18327–32. doi: 10.1073/pnas.0705826104.

Bosch, Maurice and Franklin-Tong, V. E. (2007a) 'Temporal and spatial activation of caspase-like enzymes induced by self-incompatibility in Papaver pollen', *Proceedings of the National Academy of Sciences of the United States of America*, 104(46), pp. 18327–18332. doi: 10.1073/pnas.0705826104.

Bosch, Maurice and Franklin-Tong, V. E. (2007b) 'Temporal and spatial activation of caspase-like enzymes induced by self-incompatibility in Papaver pollen', *Proceedings of the National Academy of Sciences of the United States of America*, 104(46), pp. 18327–18332. doi: 10.1073/pnas.0705826104.

Bosch, M. and Franklin-Tong, V. E. (2008) 'Self-incompatibility in Papaver: Signalling to trigger PCD in incompatible pollen', in *Journal of Experimental Botany*. doi: 10.1093/jxb/erm195.

Bras, M., Queenan, B. and Susin, S. A. (2005) 'Programmed cell death via mitochondria: Different modes of dying', *Biochemistry (Moscow)*, 70(2), pp. 231–239. doi: 10.1007/s10541-005-0105-4.

Britannica, T. E. of E. (2017) *List of plants in the family Papaveraceae*, *Encyclopedia Britannica*. Available at: https://www.britannica.com/topic/list-of-plants-in-the-family-Papaveraceae-2041449 (Accessed: 20 April 2021).

Bundy, M. G. R. *et al.* (2016) 'A mutation in the catalytic subunit of the glycosylphosphatidylinositol transamidase disrupts growth, fertility, and stomata formation', *Plant Physiology*. doi: 10.1104/pp.16.00339.

Cai, Y. M. and Gallois, P. (2015) 'Programmed cell death regulation by plant proteases with caspase-like activity', in *Plant Programmed Cell Death*. Springer International Publishing, pp. 191–202. doi: 10.1007/978-3-319-21033-9_8.

Cárdenas, L. *et al.* (2008) 'Pollen tube growth oscillations and intracellular calcium levels are reversibly modulated by actin polymerization', *Plant Physiology*, 146(4), pp. 1611–1621. doi: 10.1104/pp.107.113035.

Cardoso, J. C. F. *et al.* (2018) 'Towards a unified terminology for angiosperm reproductive system', *Acta Botanica Brasilica*. Sociedade Botanica do Brasil, pp. 329–348. doi: 10.1590/0102-33062018abb0124.

Carraro, L. *et al.* (1989) 'Peroxidase Activity and Gametophytic Incompatibility: Bud-Pollination in Petunia Hybrida', *Caryologia International Journal of Cytology, Cytosystematics and Cytogenetics*, 42, pp. 225–234. doi: 10.1080/00087114.1989.10796969.

Cavallo-Medved, D., Moin, K. and Sloane, B. (2011) 'Cathepsin B: Basis Sequence: Mouse.', *The AFCS-nature molecule pages*, 2011. Available at: http://www.ncbi.nlm.nih.gov/pubmed/28781583 (Accessed: 20 June 2020).

Charlesworth, D. (2010) 'Self-incompatibility', *F1000 Biology Reports*. Faculty of 1000 Ltd, p. 68. doi: 10.3410/B2-68.

Chebli, Y., Kroeger, J. and Geitmann, A. (2013) 'Transport Logistics in Pollen Tubes - ScienceDirect', *Molecular Plant*, 6(4), pp. 1037–1052. Available at: https://www.sciencedirect.com/science/article/pii/S167420521460900X?via%3Dihub (Accessed: 2 July 2020).

Chen, C. Y. *et al.* (2002) 'The regulation of actin organization by actin-depolymerizing factor in elongating pollen tubes', *Plant Cell*, 14(9), pp. 2175–2190. doi: 10.1105/tpc.003038.

Clapham, D. E. (1995) 'Calcium signaling', *Cell*, pp. 259–268. doi: 10.1016/0092-8674(95)90408-5.

Clark, F. M. (1961) 'Early Ideas on Inbreeding and Crossbreeding.', *The Canadian veterinary journal = La revue veterinaire canadienne*, 2(9), pp. 329–31. Available at: http://www.ncbi.nlm.nih.gov/pubmed/17421396 (Accessed: 17 August 2020).

Colaço, R., Moreno, N. and Feijó, J. A. (2012) 'On the fast lane: mitochondria structure, dynamics and function in growing pollen tubes', *Journal of Microscopy*, 247(1), pp. 106–118. doi: 10.1111/j.1365-2818.2012.03628.x.

Crow, J. F. (1994) 'Advantages of sexual reproduction', *Developmental Genetics*, pp. 205–213. doi: 10.1002/dvg.1020150303.

Curtis, W. C. (1900) 'Is there any distinction between sexual reproduction and asexual reproduction.', *Science*, 12(312), pp. 940–946. doi: 10.1126/science.12.312.940.

Daher, F. B. and Geitmann, A. (2012) 'Actin depolymerizing factors ADF7 and ADF10 play distinct roles during pollen development and pollen tube growth', *Plant Signaling and Behavior*, 7(7), pp. 1–3. doi: 10.4161/psb.20436.

Decaestecker, W. *et al.* (2019) 'CRISPR-Tsko: A technique for efficient mutagenesis in specific cell types, tissues, or organs in Arabidopsis', *Plant Cell*, 31(12), pp. 2868–2887. doi: 10.1105/tpc.19.00454.

Deeks, M. J. *et al.* (2007) 'Arabidopsis CAP1 - A key regulator of actin organisation and development', *Journal of Cell Science*, 120(15), pp. 2609–2618. doi: 10.1242/jcs.007302.

Dekkers, B. J. W. *et al.* (2016) 'Dormant and after-ripened Arabidopsis thaliana seeds are distinguished by early transcriptional differences in the imbibed state', *Frontiers in Plant Science*, 7(AUG2016). doi: 10.3389/fpls.2016.01323.

Dharmawardhane, S. *et al.* (1991) 'Compartmentalization and actin binding properties of ABP-50: The elongation factor-1 alpha ofDictyostelium', *Cell Motility and the Cytoskeleton*, 20(4), pp. 279–288. doi: 10.1002/cm.970200404.

Domínguez, F. and Cejudo, F. J. (2012) 'A comparison between nuclear dismantling during plant and animal programmed cell death', *Plant Science*. Elsevier, pp. 114–121. doi: 10.1016/j.plantsci.2012.09.009.

Durbarry, A. (2004) 'Genetic analysis of sperm cell formation in Arabidopsis thaliana L. Heynh', *Biology*.

Ellis, M. *et al.* (2010) 'Arabinogalactan-proteins: Key regulators at the cell surface?', *Plant Physiology*, 153(2), pp. 403–419. doi: 10.1104/pp.110.156000.

Fendrych, M. *et al.* (2014) 'Programmed cell death controlled by ANAC033/SOMBRERO determines root cap organ size in arabidopsis', *Current Biology*, 24(9), pp. 931–940. doi: 10.1016/j.cub.2014.03.025.

Feng, Q. N. *et al.* (2017) 'Adaptor protein-3-dependent vacuolar trafficking involves a subpopulation of COPII and HOPS tethering proteins', *Plant Physiology*, 174(3), pp. 1609–1620. doi: 10.1104/pp.17.00584.

Foote, H. C. *et al.* (1994) 'Cloning and expression of a distinctive class of self-incompatibility (S)

gene from Papaver rhoeas L.', *Proceedings of the National Academy of Sciences of the United States of America*, 91(6), pp. 2265–9. doi: 10.1073/pnas.91.6.2265.

Franklin-Tong, V. E., Ride, J. P., Read, N. D., Trewavas, A. J. and Christopher, F. (1993) 'The self-incompatibility response in Papaver rhoeas is mediated by cytosolic free calcium', *Plant Journal*, 4(1), pp. 163–177. doi: 10.1046/j.1365-313X.1993.04010163.x.

Franklin-Tong, V. E., Ride, J. P., Read, N. D., Trewavas, A. J. and Franklin, F. C. H. (1993) 'The self-incompatibility response in Papaver rhoeas is mediated by cytosolic free calcium', *The Plant Journal*, 4(1), pp. 163–177. doi: 10.1046/j.1365-313X.1993.04010163.x.

Franklin-Tong, V. E. *et al.* (1996) 'Growth of pollen tubes of Papaver rhoeas is regulated by a slow-moving calcium wave propagated by inositol 1,4,5-trisphosphate', *Plant Cell*, 8(8), pp. 1305–1321. doi: 10.1105/tpc.8.8.1305.

Franklin-Tong, V. E. *et al.* (2002) 'Involvement of extracellular calcium influx in the self-incompatibility response of Papaver rhoeas', *Plant Journal*, 29(3), pp. 333–345. doi: 10.1046/j.1365-313X.2002.01219.x.

Franklin-Tong, V. E. (2013) 'Self-Fertilization', in *Brenner's Encyclopedia of Genetics: Second Edition*. Elsevier Inc., pp. 379–381. doi: 10.1016/B978-0-12-374984-0.01393-0.

Franklin-Tong, V. E. (2014) 'Papaver rhoeas S-Determinants and the Signaling Networks They Trigger', in *Sexual Reproduction in Animals and Plants*. Springer Japan, pp. 273–287. doi: 10.1007/978-4-431-54589-7_23.

Franklin-Tong, V. E. and Franklin, F. C. H. (2003) 'The different mechanisms of gametophytic self-incompatibility', *The Royal Society*, 358, pp. 1025–1032. doi: 10.1098/rstb.2003.1287.

Franklin-Tong, V. E., Hackett, G. and Hepler, P. K. (1997) 'Ratio-imaging of Ca2+i in the self-incompatibility response in pollen tubes of Papaver rhoeas', *The Plant Journal*, 12(6), pp. 1375–1386. doi: 10.1046/j.1365-313x.1997.12061375.x.

Franklin-Tong, V. E., Lawrence, M. J. and Franklin, F. C. H. (1990) 'Self-Incompatibility in Papaver rhoeas L.: inhibition of incompatible pollen tube growth is dependent on pollen gene expression', *New Phytologist*, 116(2), pp. 319–324. doi: 10.1111/j.1469-8137.1990.tb04720.x.

Franklin-Tong, V. E., Ride, J. P. and Franklin, F. C. H. (1995) 'Recombinant stigmatic self-incompatibility (S-) protein elicits a Ca2+ transient in pollen of Papaver rhoeas', *The Plant Journal*, 8(2), pp. 299–307. doi: 10.1046/j.1365-313X.1995.08020299.x.

Fraser, M. S., Dauphinee, A. N. and Gunawardena, A. H. L. A. N. (2020) 'Determining the effect of calcium on cell death rate and perforation formation during leaf development in the novel model system, the lace plant (Aponogeton madagascariensis)', *Journal of Microscopy*, 278(3), pp. 132–144. doi: 10.1111/jmi.12859.

Fukuda, H. (2000) *Programmed cell death of tracheary elements as a paradigm in plants*, *Plant Molecular Biology*.

Ge, Y. *et al.* (2016) 'Inhibition of cathepsin B by caspase-3 inhibitors blocks programmed cell death in Arabidopsis', *Cell Death and Differentiation*, 23(9), pp. 1493–1501. doi: 10.1038/cdd.2016.34.

Geissbuehler, M. and Lasser, T. (2013) 'How to display data by color schemes compatible with red-green color perception deficiencies', *Optics Express*, 21(8), p. 9862. doi: 10.1364/oe.21.009862.

Geitmann, A. *et al.* (2000a) 'Alterations in the actin cytoskeleton of pollen tubes are induced by the self-Incompatibility reaction in Papaver rhoeas', *Plant Cell*, 12(7), pp. 1239–1251. doi: 10.1105/tpc.12.7.1239.

Geitmann, A. *et al.* (2000b) 'Alterations in the actin cytoskeleton of pollen tubes are induced by the self-Incompatibility reaction in Papaver rhoeas', *Plant Cell*, 12(7), pp. 1239–1251. doi: 10.1105/tpc.12.7.1239.

Geitmann, A., Franklin-Tong, V. E. and Emons, A. C. (2004) 'The self-incompatibility response in Papaver rhoeas pollen causes early and striking alterations to organelles', *Cell Death and Differentiation*, 11(8), pp. 812–822. doi: 10.1038/sj.cdd.4401424.

Geldner, N. *et al.* (2009) 'Rapid, combinatorial analysis of membrane compartments in intact plants with a multicolor marker set', *Plant Journal*, 59(1), pp. 169–178. doi: 10.1111/j.1365-313X.2009.03851.x.

Gibbs, P. E. (2014) 'Late-acting self-incompatibility - the pariah breeding system in flowering plants', *New Phytologist*, 203(3), pp. 717–734. doi: 10.1111/nph.12874.

Gocke, E. *et al.* (2009) 'Literature review on the genotoxicity, reproductive toxicity, and carcinogenicity of ethyl methanesulfonate', *Toxicology Letters*, pp. 254–265. doi: 10.1016/j.toxlet.2009.03.016.

Govindaraju, D. R. (2019) 'An elucidation of over a century old enigma in genetics—Heterosis', *PLoS Biology*, 17(4). doi: 10.1371/journal.pbio.3000215.

De Graaf, B. H. J. *et al.* (2006) 'Self-incompatibility in Papaver targets soluble inorganic pyrophosphatases in pollen', *Nature*, 444(7118), pp. 490–493. doi: 10.1038/nature05311.

De Graaf, B. H. J. *et al.* (2012) 'The Papaver self-incompatibility pollen S-determinant, PrpS, functions in Arabidopsis thaliana', *Current Biology*, 22(2), pp. 154–159. doi: 10.1016/j.cub.2011.12.006.

Greene, E. A. *et al.* (2003) 'Spectrum of chemically induced mutations from a large-scale reverse-genetic screen in Arabidopsis', *Genetics*, 164(2), pp. 731–740.

Groover, A. and Jones, A. M. (1999) 'Tracheary Element Differentiation Uses a Novel Mechanism Coordinating Programmed Cell Death and Secondary Cell Wall Synthesis', *Plant Physiology*, 119, pp. 375–384. Available at: www.plantphysiol.org (Accessed: 7 August 2020).

Gross, S. R. and Kinzy, T. G. (2005) 'Translation elongation factor 1A is essential for regulation of the actin cytoskeleton and cell morphology', *Nature Structural and Molecular Biology*, 12(9), pp. 772–778. doi: 10.1038/nsmb979.

Gunawardena, A. N. and McCabe, P. F. (2015) *Plant programmed cell death*, *Plant Programmed Cell Death*. Springer International Publishing. doi: 10.1007/978-3-319-21033-9.

Haeussler, M. *et al.* (2016) 'Evaluation of off-target and on-target scoring algorithms and integration into the guide RNA selection tool CRISPOR', *Genome Biology*, 17(1), p. 148. doi: 10.1186/s13059-016-1012-2.

Hansen, B. O. *et al.* (2017) 'EnsembleNet: ensemble gene function predictions for Arabidopsis thaliana', *New Phytologist*. doi: 10.1101/181396.

Hara-Nishimura, I. and Hatsugai, N. (2011) 'The role of vacuole in plant cell death', *Cell Death and Differentiation*. Nature Publishing Group, pp. 1298–1304. doi: 10.1038/cdd.2011.70.

Harrison, S. J. *et al.* (2006) 'A rapid and robust method of identifying transformed Arabidopsis

thaliana seedlings following floral dip transformation', *Plant Methods*, 2(1), p. 19. doi: 10.1186/1746-4811-2-19.

Haughn, G. and Somerville, C. R. (1987) 'Selection for Herbicide Resistance at the Whole-Plant Level', in, pp. 98–107. doi: 10.1021/bk-1987-0334.ch007.

Hepler, P. K. (2005) 'Calcium: A central regulator of plant growth and development', *Plant Cell*. American Society of Plant Biologists, pp. 2142–2155. doi: 10.1105/tpc.105.032508.

Hepler, P. K. (2016) 'The cytoskeleton and its regulation by calcium and protons', *Plant Physiology*. American Society of Plant Biologists, pp. 3–22. doi: 10.1104/pp.15.01506.

Hepler, P. K., Vidali, L. and Cheung, A. Y. (2001) 'Polarized Cell Growth in Higher Plants', *Annual Review of Cell and Developmental Biology*, 17(1), pp. 159–187. doi: 10.1146/annurev.cellbio.17.1.159.

Heslop-Harrison, J. (1975) 'Incompatibility and the Pollen-Stigma Interaction', *Annual Review of Plant Physiology*, 26(1), pp. 403–425. doi: 10.1146/annurev.pp.26.060175.002155.

Hicks, G. R. *et al.* (2004) 'Geminating pollen has tubular vacuoles, displays highly dynamic vacuole biogenesis, and requires VACUOLESS1 for proper function', *Plant Physiology*, 134(3), pp. 1227–1239. doi: 10.1104/pp.103.037382.

Horling, F. *et al.* (2003) 'Divergent light-, ascorbate-, and oxidative stress-dependent regulation of expression of the peroxiredoxin gene family in Arabidopsis', *Plant Physiology*, 131(1), pp. 317–325. doi: 10.1104/pp.010017.

Igic, B., Lande, R. and Kohn, J. R. (2008) 'Loss of self-incompatibility and its evolutionary consequences', *International Journal of Plant Sciences*, pp. 93–104. doi: 10.1086/523362.

Iglesias-Fernández, R. *et al.* (2014) 'The AtCathB3 gene, encoding a cathepsin B-like protease, is expressed during germination of Arabidopsis thaliana and transcriptionally repressed by the basic leucine zipper protein GBF1', *Jurnal of Experimental Botany*, 65(8), pp. 2009–2021.

Illy, C. *et al.* (1997) 'Role of the Occluding Loop in Cathepsin B Activity', *Journal of Biological Chemistry*, 272(2), pp. 1197–1202. doi: 10.1074/jbc.272.2.1197.

Iwano, M. *et al.* (2009) 'Fine-Tuning of the cytoplasmic Ca2+ concentration is essential for pollen tube growth', *Plant Physiology*, 150(3), pp. 1322–1334. doi: 10.1104/pp.109.139329.

Izyumov, D. S. *et al.* (2004) '"Wages of fear": Transient threefold decrease in intracellular ATP level imposes apoptosis', *Biochimica et Biophysica Acta - Bioenergetics*. Biochim Biophys Acta, pp. 141–147. doi: 10.1016/j.bbabio.2004.05.007.

Jako, C. *et al.* (2001) 'Seed-specific over-expression of an arabidopsis cDNA encoding a diacylglycerol acyltransferase enhances seed oil content and seed weight', *Plant Physiology*, 126(2), pp. 861–874. doi: 10.1104/pp.126.2.861.

James, G. V. *et al.* (2013) 'User guide for mapping-by-sequencing in Arabidopsis', *Genome Biology*, 14(6). doi: 10.1186/gb-2013-14-6-r61.

Jander, G. *et al.* (2002) 'Arabidopsis Map-Based Cloning in the Post-Genome Era'. doi: 10.1104/pp.003533.

Jander, G. *et al.* (2003) 'Ethylmethanesulfonate saturation mutagenesis in Arabidopsis to determine frequency of herbicide resistance', *Plant Physiology*, 131(1), pp. 139–146. doi: 10.1104/pp.102.010397.

Jänicke, R. U. *et al.* (1998) 'Caspase-3 is required for DNA fragmentation and morphological changes associated with apoptosis', *Journal of Biological Chemistry*, 273(16), pp. 9357–9360. doi: 10.1074/jbc.273.16.9357.

Jiang, Y. *et al.* (2007) 'Comparative proteomic analysis of NaCl stress-responsive proteins in Arabidopsis roots', *Journal of Experimental Botany*, 58(13), pp. 3591–3607. doi: 10.1093/jxb/erm207.

Jiang, Y. *et al.* (2019) 'Mechanism of CAP1-mediated apical actin polymerization in pollen tubes', *Proceedings of the National Academy of Sciences of the United States of America*, 116(24), pp. 12084–12093. doi: 10.1073/pnas.1821639116.

Johnson, D. E. *et al.* (2016) 'The position of lysosomes within the cell determines their luminal pH', *Journal of Cell Biology*, 212(6), pp. 677–692. doi: 10.1083/jcb.201507112.

Jordan, N. D., Franklin, F. C. H. and Franklin-Tong, V. E. (2000) 'Evidence for DNA fragmentation triggered in the self-incompatibility response in pollen of Papaver rhoeas', *Plant Journal*, 23(4), pp. 471–479. doi: 10.1046/j.1365-313X.2000.00811.x.

Justus, C. D. *et al.* (2004) 'Microtubules and microfilaments coordinate to direct a fountain streaming pattern in elongating conifer pollen tube tips', *Planta*, 219(1), pp. 103–109. doi: 10.1007/s00425-003-1193-2.

Juyou Wu, J. *et al.* (2011) 'Self-Incompatibility in papaver rhoeas activates nonspecific cation conductance permeable to Ca2+ and k+', *Plant Physiology*, 155(2), pp. 963–973. doi: 10.1104/pp.110.161927.

Kachroo, A., Nasrallah, M. E. and Nasrallah, J. B. (2002) 'Self-incompatibility in the Brassicaceae: Receptor-ligand signaling and cell-to-cell communication', *Plant Cell*, 14(SUPPL.), p. s227. doi: 10.1105/tpc.010440.

Kanchiswamy, C. *et al.* (2014) 'Calcium Imaging Perspectives in Plants', *International Journal of Molecular Sciences*, 15(3), pp. 3842–3859. doi: 10.3390/ijms15033842.

Kandasamy, M. K., Nasrallah, J. B. and Nasrallah, M. E. (1994) 'Pollen-pistil interactions and developmental regulation of pollen tube growth in Arabidopsis', *Development*, 120(12).

Kang, J. G. *et al.* (2004) 'Comparative proteome analysis of differentially expressed proteins induced by K+ deficiency inArabidopsis thaliana', *PROTEOMICS*, 4(11), pp. 3549–3559. doi: 10.1002/pmic.200400898.

Kisseleva-Romanova, E. *et al.* (2006) 'Yeast homolog of a cancer-testis antigen defines a new transcription complex', *EMBO Journal*, 25(15), pp. 3576–3585. doi: 10.1038/sj.emboj.7601235.

Koch, M. A., Haubold, B. and Mitchell-Olds, T. (2000) 'Comparative Evolutionary Analysis of Chalcone Synthase and Alcohol Dehydrogenase Loci in Arabidopsis, Arabis, and Related Genera (Brassicaceae)', *Molecular Biology and Evolution*, 17(10), pp. 1483–1498. doi: 10.1093/oxfordjournals.molbev.a026248.

Kohno, T. and Shimmen, T. (1988) *Mechanism of Ca inhibition of cytoplasmic streaming in lily pollen tubes*.

Kolar, F., Pawar, N. and Dixit, G. (2011) *Induced chlorophyll mutations in Delphinium malabaricum (Huth) Munz*, *Journal of Applied Horticulture*.

Kong, J., Lau, S. and Jürgens, G. (2015) 'Twin plants from supernumerary egg cells in Arabidopsis', *Current Biology*, 25(2), pp. 225–230. doi: 10.1016/j.cub.2014.11.021.

Koornneef, M. and Meinke, D. (2010) 'The development of Arabidopsis as a model plant', *The Plant Journal*, 61(6), pp. 909–921. doi: 10.1111/j.1365-313X.2009.04086.x.

Korthout, H. A. A. J. *et al.* (2000) 'The presence and subcellular localization of caspase 3-like proteinases in plant cells', *FEBS Letters*, 475(2), pp. 139–144. doi: 10.1016/S0014-5793(00)01643-4.

Koutsogiannis, Z., Macleod, E. T. and Maciver, S. K. (2019) 'G418 induces programmed cell death in Acanthamoeba through the elevation of intracellular calcium and cytochrome c translocation', *Parasitology Research*, 118(2), pp. 641–651. doi: 10.1007/s00436-018-6192-0.

Krebs, M. *et al.* (2012) 'FRET-based genetically encoded sensors allow high-resolution live cell imaging of Ca 2+ dynamics', *Plant Journal*, 69(1), pp. 181–192. doi: 10.1111/j.1365-313X.2011.04780.x.

Kurup, S. *et al.* (1998) 'Identification and cloning of related self-incompatibility S-genes in Papaver rhoeas and Papaver nudicaule', *Sexual Plant Reproduction*, 11(4), pp. 192–198. doi: 10.1007/s004970050141.

Kusaba, M. *et al.* (2001) 'Self-incompatibility in the genus Arabidopsis: Characterization of the S locus in the outcrossing A. lyrata and its autogamous relative A. thaliana', *Plant Cell*, 13(3), pp. 627–643. doi: 10.1105/tpc.13.3.627.

Lalanne, E. and Twell, D. (2002) 'Genetic Control of Male Germ Unit Organization in Arabidopsis 1'. doi: 10.1104/pp.003301.

Lam, E. (Eric), Fukuda, H. (Hiroo) and Greenberg, J. (2000) *Programmed cell death in higher plants*. Kluwer Academic Publishers.

Lam, E., Kato, N. and Lawton, M. (2001) 'Programmed cell death, mitochondria and the plant hypersensitive response', *Nature*. Nature Publishing Group, pp. 848–853. doi: 10.1038/35081184.

Lambert, T. J. (2019) 'FPbase: a community-editable fluorescent protein database', *Nature Methods*. Nature Publishing Group, pp. 277–278. doi: 10.1038/s41592-019-0352-8.

Latrasse, D. *et al.* (2016) *Plant programmed cell death from a chromatin point of view*, *Journal of Experimental Botany*. Available at: https://academic.oup.com/jxb/article/67/20/5887/2483854 (Accessed: 29 April 2020).

Levin, D. A. (1970) 'Reinforcement of Reproductive Isolation: Plants Versus Animals', *The American Naturalist*, 104(940), pp. 571–581. doi: 10.1086/282691.

Li, S. L. and Rédei, G. P. (1969) 'Estimation of mutation rate in autogamous diploids', *Radiation Botany*, 9(2), pp. 125–131. doi: 10.1016/s0033-7560(69)80079-7.

Li, S., Šamaj, J. and Franklin-Tong, V. E. (2007) 'A mitogen-activated protein kinase signals to programmed cell death induced by self-incompatibility in Papaver pollen', *Plant Physiology*, 145(1), pp. 236–245. doi: 10.1104/pp.107.101741.

Liepman, A. H. *et al.* (2010) 'Arabidopsis - A powerful model system for plant cell wall research', *Plant Journal*, 61(6), pp. 1107–1121. doi: 10.1111/j.1365-313X.2010.04161.x.

Lin, Z. *et al.* (2015) 'The Papaver rhoeas S determinants confer self-incompatibility to Arabidopsis thaliana in planta', *Science*, 350(6261), pp. 684–687. doi: 10.1126/science.aad2983.

Lin, Z. *et al.* (2020) 'Ectopic expression of a self-incompatibility module triggers growth arrest

and cell death in vegetative cells', *Plant Physiology*, 183(4), p. pp.00292.2020. doi: 10.1104/pp.20.00292.

Lindner, H. *et al.* (2012) 'SNP-ratio mapping (SRM): Identifying lethal alleles and mutations in complex genetic backgrounds by next-generation sequencing', *Genetics*, pp. 1381–1386. doi: 10.1534/genetics.112.141341.

Liu, G. *et al.* (1996) 'F-actin sequesters elongation factor 1α from interaction with aminoacyl-tRNA in a pH-dependent reaction', *Journal of Cell Biology*, 135(4), pp. 953–963. doi: 10.1083/jcb.135.4.953.

Liu, J. and Qu, L.-J. (2008) 'Meiotic and Mitotic Cell Cycle Mutants Involved in Gametophyte Development in Arabidopsis', *Molecular Plant* •, 1. doi: 10.1093/mp/ssn033.

Löfke, C. *et al.* (2015) 'Auxin regulates SNARE-dependent vacuolar morphology restricting cell size', *eLife*, 2015(4). doi: 10.7554/eLife.05868.

Luschnig, C. and Seifert, G. J. (2010) 'Posttranslational modifications of plasma membrane proteins and their implications for plant growth and development', *Plant Cell Monographs*, 19, pp. 109–128. doi: 10.1007/978-3-642-13431-9_5.

Ma, J. F. *et al.* (2012) 'Different regulatory processes control pollen hydration and germination in Arabidopsis', *Sexual Plant Reproduction*, 25(1), pp. 77–82. doi: 10.1007/s00497-011-0173-0.

Ma, W. and Berkowitz, G. A. (2007) 'The grateful dead: Calcium and cell death in plant innate immunity', *Cellular Microbiology*. John Wiley & Sons, Ltd, pp. 2571–2585. doi: 10.1111/j.1462-5822.2007.01031.x.

Von Malek, B. *et al.* (2002) 'The Arabidopsis male-sterile mutant dde2-2 is defective in the ALLENE OXIDE SYNTHASE gene encoding one of the key enzymes of the jasmonic acid biosynthesis pathway'. doi: 10.1007/s00425-002-0906-2.

Martínez-Fábregas, J. *et al.* (2013) 'New arabidopsis thaliana cytochrome c partners: A look into the elusive role of cytochrome c in programmed cell death inplants', *Molecular and Cellular Proteomics*, 12(12), pp. 3666–3676. doi: 10.1074/mcp.M113.030692.

McCallum, C. M. *et al.* (2000) 'Targeted screening for induced mutations', *Nature Biotechnology*, 18(4), pp. 455–457. doi: 10.1038/74542.

Mccue, A. D. *et al.* (2011) 'Cytoplasmic connection of sperm cells to the pollen vegetative cell nucleus: potential roles of the male germ unit revisited', *Journal of Experimental Botany*, 62(5), pp. 1621–1631. doi: 10.1093/jxb/err032.

McInnis, S. M. *et al.* (2006) 'The role of stigma peroxidases in flowering plants: Insights from further characterization of a stigma-specific peroxidase (SSP) from Senecio squalidus (Asteraceae)', in *Journal of Experimental Botany*. Oxford Academic, pp. 1835–1846. doi: 10.1093/jxb/erj182.

McLellan, H. *et al.* (2009) 'Functional redundancy in the Arabidopsis Cathepsin B gene family contributes to basal defence, the hypersensitive response and senescence', *New Phytologist*, 183(2), pp. 408–418. doi: 10.1111/j.1469-8137.2009.02865.x.

Meinke, D. W. *et al.* (1998) *Arabidopsis thaliana: A Model Plant for Genome Analysis Author(s)*, *Source: Science, New Series*.

Mi, H. *et al.* (2019) 'Protocol Update for large-scale genome and gene function analysis with the PANTHER classification system (v.14.0)', *Nature Protocols*, 14(3), pp. 703–721. doi:

10.1038/s41596-019-0128-8.

Moseyko, N. and Feldman, L. J. (2001) 'Expression of pH-sensitive green fluorescent protein in Arabidopsis thaliana', *Plant, Cell and Environment*, 24(5), pp. 557–563. doi: 10.1046/j.1365-3040.2001.00703.x.

Muñoz-Sanz, J. V. *et al.* (2020) 'Self-(In)compatibility Systems: Target Traits for Crop-Production, Plant Breeding, and Biotechnology', *Frontiers in Plant Science*. Frontiers Media S.A., p. 1. doi: 10.3389/fpls.2020.00195.

Murphy, A., Schulz, B. and Peer, W. (2011) *The Plant Plasma Membrane*. Edited by A. Murphy, B. Schulz, and W. Peer. Available at: https://link.springer.com/book/10.1007%2F978-3-642-13431-9 (Accessed: 3 June 2020).

Nagai, T. *et al.* (2004) 'Expanded dynamic range of fluorescent indicators for Ca2+ by circularly permuted yellow fluorescent proteins', *Proceedings of the National Academy of Sciences of the United States of America*, 101(29), pp. 10554–10559. doi: 10.1073/pnas.0400417101.

Nasrallah, M. E., Liu, P. and Nasrallah, J. B. (2002) *Generation of Self-Incompatible Arabidopsis thaliana by Transfer of Two S Locus Genes from A. lyrata*. Available at: http://science.sciencemag.org/ (Accessed: 20 April 2021).

Ndamukong, I. *et al.* (2011) 'A cytoplasm-specific activity encoded by the Trithorax-like ATX1 gene.', *Nucleic acids research*, 39(11), pp. 4709–18. doi: 10.1093/nar/gkq1300.

Nicotera, P., Zhivotovsky, B. and Orrenius, S. (1994) 'Nuclear calcium transport and the role of calcium in apoptosis', *Cell Calcium*, 16(4), pp. 279–288. doi: 10.1016/0143-4160(94)90091-4.

Nordström, K. J. V *et al.* (2012) *SHOREmap Manual*.

Obara, K., Kuriyama, H. and Fukuda, H. (2001) 'Direct evidence of active and rapid nuclear degradation triggered by vacuole rupture during programmed cell death in zinnia', *Plant Physiology*, 125(2), pp. 615–626. doi: 10.1104/pp.125.2.615.

Passardi, F. *et al.* (2007) 'Morphological and physiological traits of three major Arabidopsis thaliana accessions', *Journal of Plant Physiology*, 164(8), pp. 980–992. doi: 10.1016/j.jplph.2006.06.008.

Petruzzello, M. (2020) *List of plants in the family Brassicaceae*, *Encyclopedia Britannica*. Available at: https://www.britannica.com/topic/list-of-plants-in-the-family-Brassicaceae-2004620 (Accessed: 20 April 2021).

Poulter, N. S., Staiger, C. J., *et al.* (2010) 'Actin-binding proteins implicated in the formation of the punctate actin foci stimulated by the self-incompatibility response in papaver', *Plant Physiology*, 152(3), pp. 1274–1283. doi: 10.1104/pp.109.152066.

Poulter, N. S., Wheeler, M. J., *et al.* (2010a) 'Self-incompatibility in Papaver: Identification of the pollen S-determinant PrpS', *Biochemical Society Transactions*. Biochem Soc Trans, pp. 588–592. doi: 10.1042/BST0380588.

Poulter, N. S., Wheeler, M. J., *et al.* (2010b) 'Self-incompatibility in Papaver: Identification of the pollen S-determinant PrpS', *Biochemical Society Transactions*, pp. 588–592. doi: 10.1042/BST0380588.

Prunet, N. and Duncan, K. (2020) 'Imaging flowers: a guide to current microscopy and tomography techniques to study flower development', *Journal of Experimental Botany*, 71(10), pp. 2898–2909. doi: 10.1093/jxb/eraa094.

Punwani, J. A., Rabiger, D. S. and Drews, G. N. (2007) 'MYB98 positively regulates a battery of synergid-expressed genes encoding filiform apparatus-localized proteins', *Plant Cell*, 19(8), pp. 2557–2568. doi: 10.1105/tpc.107.052076.

Qin, Y. *et al.* (2009) 'Penetration of the Stigma and Style Elicits a Novel Transcriptome in Pollen Tubes, Pointing to Genes Critical for Growth in a Pistil', *PLoS Genetics*. Edited by G. S. Barsh, 5(8), p. e1000621. doi: 10.1371/journal.pgen.1000621.

Qu, X. *et al.* (2017) 'Organizational Innovation of Apical Actin Filaments Drives Rapid Pollen Tube Growth and Turning', *Molecular Plant*, 10(7), pp. 930–947. doi: 10.1016/j.molp.2017.05.002.

Reape, T. J., Molony, E. M. and Mccabe, P. F. (2008) 'Programmed cell death in plants: distinguishing between different modes', *Journal of Experimental Botany*, 59(3), pp. 435–444. doi: 10.1093/jxb/erm258.

Riedl, S. J. and Shi, Y. (2004) 'Molecular mechanisms of caspase regulation during apoptosis.', *Nature reviews. Molecular cell biology*, 5(11), pp. 897–907. doi: 10.1038/nrm1496.

Rotari, V. *et al.* (2005) 'Caspase-like activities and UV-induced programmed cell death in Arabidopsis', *BMC Plant Biology*, 5(Suppl 1), p. S18. doi: 10.1186/1471-2229-5-s1-s18.

Rotari, V. I., He, R. and Gallois, P. (2005) 'Death by proteases in plants: Whodunit', *Physiologia Plantarum*, pp. 376–385. doi: 10.1111/j.1399-3054.2005.00465.x.

Rudd, J. J. *et al.* (2003) 'Activation of a putative MAP kinase in pollen is stimulated by the self-incompatibility (SI) response', *FEBS Letters*, 547(1–3), pp. 223–227. doi: 10.1016/S0014-5793(03)00710-5.

Rudd, J. J. and Franklin-Tong, V. E. (2003) *Signals and targets of the self-incompatibility response in pollen of Papaver rhoeas*. doi: 10.1093/jxb/erg001.

Ruzicka, D. R. *et al.* (2007) 'The ancient subclasses of Arabidopsis ACTIN DEPOLYMERIZING FACTOR genes exhibit novel and differential expression', *The Plant Journal*, 52(3), pp. 460–472. doi: 10.1111/j.1365-313X.2007.03257.x.

Saito, S. and Uozumi, N. (2020) 'Calcium-Regulated Phosphorylation Systems Controlling Uptake and Balance of Plant Nutrients', *Frontiers in Plant Science*, 11. doi: 10.3389/fpls.2020.00044.

Sauerbrunn, N. and Schlaich, N. L. (2004) 'PCC1: A merging point for pathogen defence and circadian signalling in Arabidopsis', *Planta*, 218(4), pp. 552–561. doi: 10.1007/s00425-003-1143-z.

Sawada, H., Inoue, N. and Iwano, M. (2014) *Sexual Reproduction in Animals and Plants*, *Sexual Reproduction in Animals and Plants*. Edited by H. Sawada, N. Inoue, and M. Iwano. Tokyo: Springer Japan. doi: 10.1007/978-4-431-54589-7.

Schoenaers, S. *et al.* (2017) 'The kinase ERULUS controls pollen tube targeting and growth in arabidopsis thaliana', *Frontiers in Plant Science*, 8. doi: 10.3389/fpls.2017.01942.

Schopfer, C. R., Nasrallah, M. E. and Nasrallah, J. B. (1999) 'The male determinant of self-incompatibility in Brassica', *Science*, 286(5445), pp. 1697–1700. doi: 10.1126/science.286.5445.1697.

Shen, J. *et al.* (2013a) 'Organelle pH in the arabidopsis endomembrane system', *Molecular Plant*, 6(5), pp. 1419–1437. doi: 10.1093/mp/sst079.

Shen, J. *et al.* (2013b) 'Organelle pH in the Arabidopsis Endomembrane System', *Molecular Plant*, 6(5), pp. 1419–1437. doi: 10.1093/MP/SST079.

Shimada, Y. (2010) *Sample-wise network for microarray experiments*, *Plant and Cell Physiology Advance Access*. Available at: http://pcp.oxfordjournals.org/ (Accessed: 29 July 2020).

Shin, J. J. H. and Loewen, C. J. R. (2011) 'Putting the pH into phosphatidic acid signaling', *BMC Biology*. BioMed Central, p. 85. doi: 10.1186/1741-7007-9-85.

Simpson, M. G. (2010) 'Plant Reproductive Biology', in *Plant Systematics*. Elsevier, pp. 573–584. doi: 10.1016/b978-0-12-374380-0.50013-0.

Śnieżko, R. (2000) 'Fluorescence Microscopy of Aniline Blue Stained Pistils', in *Methods in Plant Electron Microscopy and Cytochemistry*. Totowa, NJ: Humana Press, pp. 81–86. doi: 10.1007/978-1-59259-232-6_5.

Snowman, B. N. *et al.* (2002) *Signal-Mediated Depolymerization of Actin in Pollen during the Self-Incompatibility Response*, *Source: The Plant Cell*.

Soulard, J. *et al.* (2014) 'eEF1A is an S-RNase binding factor in self-incompatible Solanum chacoense', *PLoS ONE*, 9(2). doi: 10.1371/journal.pone.0090206.

Stael, S. *et al.* (2019) 'Plant proteases and programmed cell death', *Journal of Experimental Botany*, 70(7), pp. 1991–1995. doi: 10.1093/jxb/erz126.

Stefano, G., Renna, L. and Brandizzi, F. (2012) 'Fluorescence-microscopy screening and next-generation sequencing: Useful tools for the identification of genes involved in organelle integrity', *Journal of Visualized Experiments*, 62(62), p. 3809. doi: 10.3791/3809.

Stone, S. L. and Goring, D. R. (2001) 'The molecular biology of self-incompatibility systems in flowering plants', *Plant Cell, Tissue and Organ Culture*, pp. 93–114. doi: 10.1023/A:1011980210048.

Sueldo, D. J. and van der Hoorn, R. A. L. (2017) 'Plant life needs cell death, but does plant cell death need Cys proteases?', *FEBS Journal*. Blackwell Publishing Ltd, pp. 1577–1585. doi: 10.1111/febs.14034.

Suhandono, S., Apriyanto, A. and Ihsani, N. (2014) 'Isolation and characterization of three cassava elongation factor 1 alpha (MeEF1A) promoters', *PLoS ONE*. Edited by M.-J. Virolle, 9(1), p. e84692. doi: 10.1371/journal.pone.0084692.

Szklarczyk, D. *et al.* (2019) 'STRING v11: Protein-protein association networks with increased coverage, supporting functional discovery in genome-wide experimental datasets', *Nucleic Acids Research*, 47(D1), pp. D607–D613. doi: 10.1093/nar/gky1131.

Takasaki, T. *et al.* (2000) 'The S receptor kinase determines self-incompatibility in Brassica stigma', *Nature*, 403(6772), pp. 913–916. doi: 10.1038/35002628.

Takayama, S. and Isogai, A. (2005) 'SELF-INCOMPATIBILITY IN PLANTS', *Annual Review of Plant Biology*, 56(1), pp. 467–489. doi: 10.1146/annurev.arplant.56.032604.144249.

Taylor, L. P. and Hepler, P. K. (1997) 'POLLEN GERMINATION AND TUBE GROWTH', *Annual Review of Plant Physiology and Plant Molecular Biology*, 48(1), pp. 461–491. doi: 10.1146/annurev.arplant.48.1.461.

Thomas, S. G. *et al.* (2006) 'Actin depolymerization is sufficient to induce programmed cell death in self-incompatible pollen', *Journal of Cell Biology*, 174(2), pp. 221–229. doi: 10.1083/jcb.200604011.

Thomas, S. G. and Franklin-Tong, V. E. (2004a) 'Self-incompatibility triggers programmed cell death in Papaver pollen', *Nature*, 429(6989), pp. 305–309. doi: 10.1038/nature02540.

Thomas, S. G. and Franklin-Tong, V. E. (2004b) 'Self-incompatibility triggers programmed cell death in Papaver pollen', *Nature*, 429(6989), pp. 305–309. doi: 10.1038/nature02540.

Thompson, R. D. and Kirch, H. H. (1992) 'The S locus of flowering plants: when self-rejection is self-interest', *Trends in Genetics*. Elsevier Current Trends, pp. 381–387. doi: 10.1016/0168-9525(92)90299-J.

Thornberry, N. A. and Lazebnik, Y. (1998) 'Caspases: Enemies within', *Science*. American Association for the Advancement of Science, pp. 1312–1316. doi: 10.1126/science.281.5381.1312.

Toyota, M. *et al.* (2018) 'Glutamate triggers long-distance, calcium-based plant defense signaling', *Science*, 361(6407), pp. 1112–1115. doi: 10.1126/science.aat7744.

Ülker, B. and Weisshaar, B. (2011) 'Resources for Reverse Genetics Approaches in Arabidopsis thaliana', in *Genetics and Genomics of the Brassicaceae*. Springer New York, pp. 527–560. doi: 10.1007/978-1-4419-7118-0_19.

Vaz Martins, T. and Livina, V. N. (2019) 'What Drives Symbiotic Calcium Signalling in Legumes? Insights and Challenges of Imaging', *International Journal of Molecular Sciences*, 20(9), p. 2245. doi: 10.3390/ijms20092245.

Vidali, L., Mckenna, S. T. and Hepler, P. K. (2001) *Actin Polymerization Is Essential for Pollen Tube Growth □ V*, *Molecular Biology of the Cell*.

Vigano, M. A. *et al.* (2018) *DARPins recognizing mTFP1 as novel reagents for in vitro and in vivo protein manipulations*. Available at: http://bio.biologists.org/ (Accessed: 9 May 2020).

Waadt, R. *et al.* (2017) 'Multiparameter imaging of calcium and abscisic acid and high-resolution quantitative calcium measurements using R-GECO1-mTurquoise in Arabidopsis', *New Phytologist*, 216(1), pp. 303–320. doi: 10.1111/nph.14706.

Waese, J. *et al.* (2017) 'ePlant: Visualizing and exploring multiple levels of data for hypothesis generation in plant biology', *Plant Cell*, 29(8), pp. 1806–1821. doi: 10.1105/tpc.17.00073.

Walker, E. A. *et al.* (1996) 'Molecular analysis of two functional homologues of the S3 allele of the Papaver rhoeas self-incompatibility gene isolated from different populations', *Plant Molecular Biology*, 30(5), pp. 983–994. doi: 10.1007/BF00020809.

Wang, C. *et al.* (2008) 'Mitochondrial shuttling of CAP1 promotes actin- and cofilin-dependent apoptosis', *Journal of Cell Science*, 121(17), pp. 2913–2920. doi: 10.1242/jcs.023911.

Wang, H. *et al.* (2012) 'Proteomic analysis of early-responsive redox-sensitive proteins in Arabidopsis', *Journal of Proteome Research*, 11(1), pp. 412–424. doi: 10.1021/pr200918f.

Wang, L. *et al.* (2019) 'Self-incompatibility in Papaver pollen: programmed cell death in an acidic environment', *Journal of Experimental Botany*, 70(7), pp. 2113–2123. doi: 10.1093/jxb/ery406.

Wang, L. *et al.* (2020) 'New opportunities and insights into Papaver self-incompatibility by imaging engineered Arabidopsis pollen', *Journal of Experimental Botany*. doi: 10.1093/jxb/eraa092.

Weterings, K. and Russell, S. D. (2004) 'Experimental analysis of the fertilization process', *Plant Cell*. American Society of Plant Biologists, pp. S107–S118. doi: 10.1105/tpc.016873.

Wheeler, M. J. *et al.* (2009) 'Identification of the pollen self-incompatibility determinant in Papaver rhoeas', *Nature*, 459(7249), pp. 992–995. doi: 10.1038/nature08027.

White, J. G., Amos, W. B. and Fordham, M. (1987) 'An evaluation of confocal versus conventional imaging of biological structures by fluorescence light microscopy.', *The Journal of cell biology*, 105(1), pp. 41–48. doi: 10.1083/jcb.105.1.41.

Wilkins, K. A. *et al.* (2011) 'Reactive oxygen species and nitric oxide mediate actin reorganization and programmed cell death in the self-incompatibility response of papaver', *Plant Physiology*, 156(1), pp. 404–416. doi: 10.1104/pp.110.167510.

Wilkins, K. A. (2013) *Investigating pollen signalling networks triggered by the self-incompatibility response in Papaver rhoeas*, *University of Birmingham Research Archive e-theses repository*.

Wilkins, K. A. *et al.* (2015) 'Self-incompatibility-induced programmed cell death in field poppy pollen involves dramatic acidification of the incompatible pollen tube cytosol', *Plant Physiology*, 167(3), pp. 766–779. doi: 10.1104/pp.114.252742.

Wilkins, K. A., Poulter, N. S. and Franklin-Tong, V. E. (2014) 'Taking one for the team: self-recognition and cell suicide in pollen'. doi: 10.1093/jxb/ert468.

Woltering, E. J., Van der Bent, A. and Hoeberichts, F. A. (2002) 'Do plant caspases exist?', *Plant Physiology*. American Society of Plant Biologists, pp. 1764–1769. doi: 10.1104/pp.006338.

Wymer, C. L., Bibikova, T. N. and Gilroy, S. (1997) 'Cytoplasmic free calcium distributions during the development of root hairs of Arabidopsis thaliana', *The Plant Journal*, 12(2), pp. 427–439. doi: 10.1046/j.1365-313X.1997.12020427.x.

Xu, Q. and Zhang, L. (2009) 'Plant caspase-like proteases in plant programmed cell death', *Plant Signaling and Behavior*, 4(9), pp. 902–904. doi: 10.4161/psb.4.9.9531.

Yaqing, W. and Keming, C. (1998) 'Programmed cell death during the vessel element differentiation of the secondary xylem in Eucommia ulmoides shoots', *Acta Botanica Sinica*, 40(12), pp. 1102–1107. Available at: https://europepmc.org/article/cba/319608 (Accessed: 8 August 2020).

Yoshida, K., Futamura, N. and Nishiguchi, M. (2012) 'Collection of expressed genes from the transition zone of Cryptomeria japonica in the dormant season', *Journal of Wood Science*, 58(2), pp. 89–103. doi: 10.1007/s10086-011-1234-6.

Zhang, Q.-F. *et al.* (2020) 'Ceramide-Induced Cell Death Depends on Calcium and Caspase-Like Activity in Rice', *Frontiers in Plant Science*, 11, p. 145. doi: 10.3389/fpls.2020.00145.

Zhang, X. *et al.* (2006) 'Agrobacterium-mediated transformation of Arabidopsis thaliana using the floral dip method', *Nature Protocols*, 1(2), pp. 641–646. doi: 10.1038/nprot.2006.97.

Zhao, B. *et al.* (2016) 'Secretory COPII protein SEC31B is required for pollen wall development', *Plant Physiology*, 172(3), pp. 1625–1642. doi: 10.1104/pp.16.00967.

Zhao, W. *et al.* (2020) 'Villin controls the formation and enlargement of punctate actin foci in pollen tubes', *Journal of cell science*, 133(6). doi: 10.1242/jcs.237404.

Zheng, Y. *et al.* (2013) 'Arabidopsis ACTIN-DEPOLYMERIZING FACTOR7 severs actin filaments and regulates actin cable turnover to promote normal pollen tube growth', *Plant Cell*, 25(9), pp. 3405–3423. doi: 10.1105/tpc.113.117820.

Zhou, G. L. *et al.* (2014) 'Phosphorylation of the cytoskeletal protein CAP1 controls its

association with cofilin and actin', *Journal of Cell Science*, 127(23), pp. 5052–5065. doi: 10.1242/jcs.156059.

Participation in published papers

- **Ectopic expression of a self-incompatibility module triggers growth arrest and cell death in vegetative cells**. 2020. Lin Z, Xie F, **Triviño M**, Karimi M, Bosch M, Franklin-Tong VE, Nowack MK. Plant Physiology. Vol 183. Issue 2.

- **New opportunities and insights into Papaver self-incompatibility by imaging engineered Arabidopsis pollen**. 2020. Wang L, **Triviño M**, Lin Z, Carli J, Eaves DJ, Van Damme D, Nowack MK, Franklin-Tong VE, Bosch M. Journal of Experimental Botany. Volume 71, Issue 8, pp 2451–2463.

- **Self-incompatibility in Papaver pollen: programmed cell death in an acidic environment**. 2019. Wang L, Lin Z, **Triviño M**, Nowack MK, Franklin-Tong VE, Bosch M. Journal of Experimental Botany. Volume 70, Issue 7, pp 2113-2123.

Original cover: “All Around The Moon” by Jules Verne (First edition, 1876)